DEVELOPMENTS IN PETROLEUM SCIENCE 34

a practical companion to reservoir stimulation

M. J. ECONOMIDES

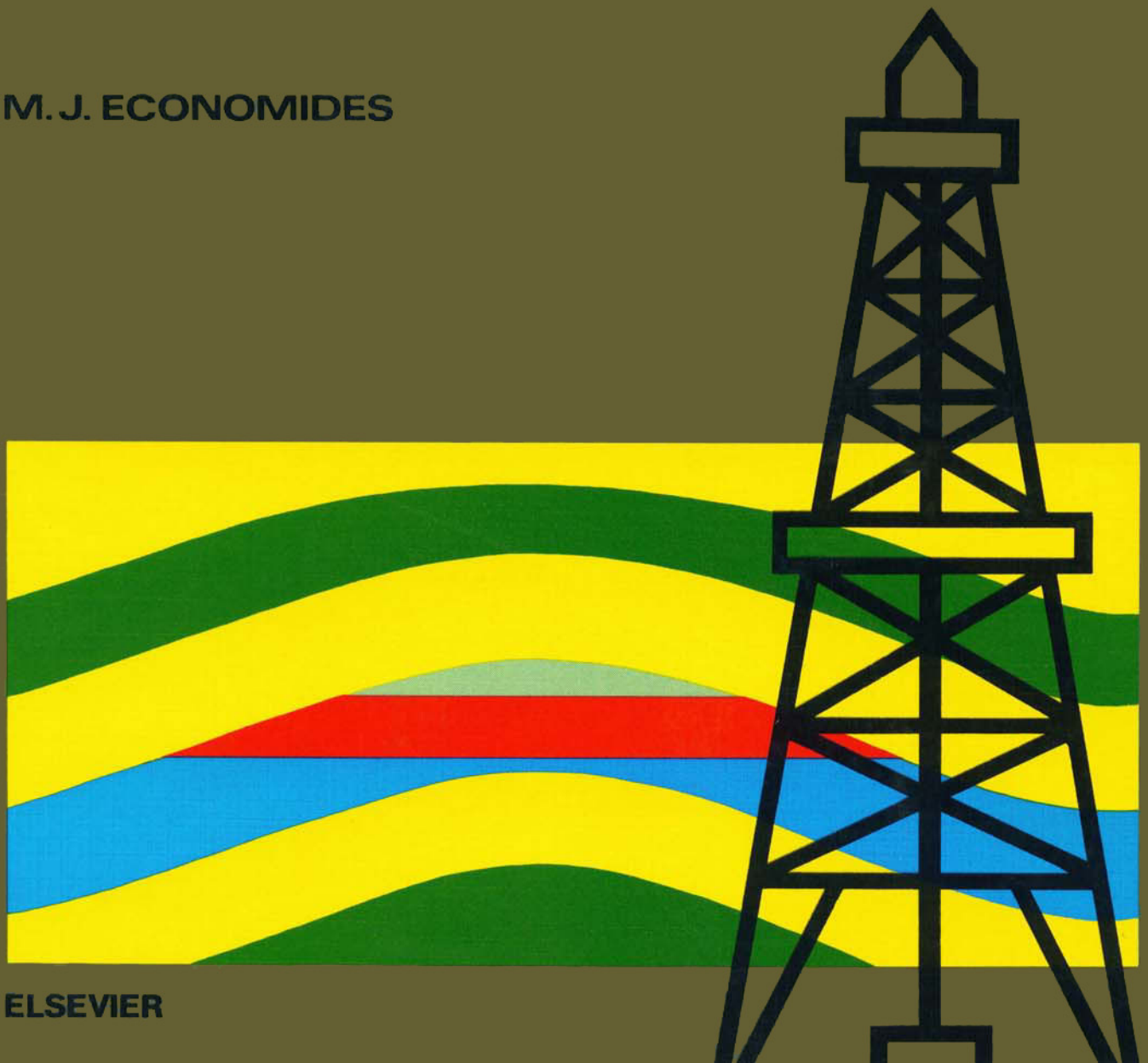

ELSEVIER

Developments in Petroleum Science, 34

a practical companion to reservoir stimulation

DEVELOPMENTS IN PETROLEUM SCIENCE

Advisory Editor: G.V. Chilingarian

Volumes 1, 3, 4, 7 and 13 are out of print.

2. W.H. FERTL - Abnormal Formation Pressures
5. T.F. YEN and G.V. CHILINGARIAN (Editors) - Oil Shale
6. D.W. PEACEMAN - Fundamentals of Numerical Reservoir Simulation
8. L.P. DAKE - Fundamentals of Reservoir Engineering
9. K. MAGARA - Compaction and Fluid Migration
10. M.T. SILVIA and E.A. ROBINSON - Deconvolution of Geophysical Time Series in the Exploration for Oil and Natural Gas
11. G.V. CHILINGARIAN and P. VORABUTR - Drilling and Drilling Fluids
12. T.D. VAN GOLF-RACHT - Fundamentals of Fractured Reservoir Engineering
14. G. MÓZES (Editor) - Paraffin Products

15A. O. SERRA - Fundamentals of Well-log Interpretation, 1. The acquisition of logging data

15B. O. SERRA - Fundamentals of Well-log Interpretation, 2. The interpretation of logging data

16. R.E. CHAPMAN - Petroleum Geology

17A. E.C. DONALDSON, G.V. CHILINGARIAN and T.F. YEN (Editors) - Enhanced Oil Recovery, I. Fundamentals and analyses

17B. E.C. DONALDSON, G.V. CHILINGARIAN and T.F. YEN (Editors) - Enhanced Oil Recovery, II. Processes and operations

18A. A.P. SZILAS - Production and Transport of Oil and Gas, A. Flow mechanics and production (second completely revised edition)

19A. G.V. CHILINGARIAN, J.O. ROBERTSON Jr. and S. KUMAR - Surface Operations in Petroleum Production, I

19B. G.V. CHILINGARIAN, J.O. ROBERTSON Jr. and S. KUMAR - Surface Operations in Petroleum Production, II

20. A.J. DIKKERS - Geology in Petroleum Production
21. F. RAMIREZ - Application of Optimal Control Theory to Enhanced Oil Recovery
22. E.C. DONALDSON, G.V. CHILINGARIAN and T.F. YEN - Microbial Enhanced Oil Recovery
23. J. HAGOORT - Fundamentals of Gas Reservoir Engineering
24. W. LITTMANN - Polymer Flooding
25. N.K. BAIBAKOV and A.R. GARUSHEV - Thermal Methods of Petroleum Production
26. D. MADER - Hydraulic Proppant Fracturing and Gravel Packing
27. G. DA PRAT - Well Test Analysis for Naturally Fractured Reservoirs
28. E.B. NELSON (Editor) - Well Cementing
29. R.W. ZIMMERMAN - Compressibility of Sandstones
30. G.V. CHILINGARIAN, S.J. MAZZULLO and H.H. RIEKE II - Carbonate Reservoir Characterization: A Geologic-Engineering Analysis, Part I
31. E.C. DONALDSON (Editor) - Microbial Enhancement of Oil Recovery - Recent Advances
32. R.M. LARSEN (Editor) - Structural and Tectonic Modelling and its Application to Petroleum Geology
33. E. FJÆR, R.M. HOLT, P. HORSRUD, A.M. RAAEN and R. RISNES - Petroleum Related Rock Mechanics

Developments in Petroleum Science, 34

a practical companion to reservoir stimulation

M. J. ECONOMIDES

Mining University Leoben, Institute of Drilling and Production, Franz-Josef- Strasse 19, Leoben, A 8700, Austria

ELSEVIER, Amsterdam — London — New york — Tokyo 1992

ELSEVIER SCIENCE PUBLISHERS B.V.
Sara Burgerhartstraat 25
P.O. Box 211, 1000 AE Amsterdam, The Netherlands

Distributors for the United States and Canada:

ELSEVIER SCIENCE PUBLISHING COMPANY INC.
655, Avenue of the Americas
New York, NY 10010, U.S.A.

ISBN 0-444-89324-5

This book is printed on acid-free paper.

Printed in The Netherlands

Contents

This Page Intentionally Left Blank

Introduction

This workbook is a "practical companion" to the second edition of *Reservoir Stimulation* (published by Prentice Hall, Englewood Cliffs, NJ in 1989), and it is my intention that the two books be used together.

I feel this new volume will be particularly useful for the training of new engineers and petroleum engineering students, as it contains approximately 100 problems and their solutions plus a lengthy chapter giving data necessary for designing a stimulation treatment.

The chapters containing practical problems are labeled with letters of the alphabet (from A to J) to distinguish them from the chapters in *Reservoir Stimulation.* Problems are stated concisely at the beginning of the chapter and are followed by a reference to the particular section(s) of the textbook containing information necessary for the solution. Equations, figures and tables from the textbook are referred to in the workbook but are not reproduced. New references used in this volume are explicitly described. All others are referred back to the textbook.

The accompanying table lists the chapters in *Reservoir Stimulation* that correspond to chapters in this volume where the practical problems arising from the technology are presented.

The assistance throughout this effort of my friend, Bill Diggons, manager of Schlumberger Wireline, Testing & Marketing Services, is greatly appreciated. Special thanks also go to Glenda DeLuna and Donna Peterson for invaluable contributions in the editing and preparation of the text.

Prof. Dr. Michael J. Economides
May 1991

Chapter in *Reservoir Stimulation*	Chapter in This Volume
1	A
2	B
3	E
4	C
5	C
7	D
8	E
9	E
10	B
11	F
12	G
13	G
14	G
15	H
16	H
17	I
18	I
19	J

This Page Intentionally Left Blank

A. Reservoir and Well Considerations

EXAMPLE A-1

Calculation of the Permeability and the Skin Effect from an Oilwell Test

An oil well was tested during a 96-hr drawdown. Measured bottomhole pressures are listed in Table A-1, and relevant well and reservoir data are shown in Table A-2. Calculate the permeability and the skin effect.

Solution (Ref. Sections 1-2, 1-2.1, 1-2.5, 1-2.7)

The first step is to plot the pressure and pressure derivative data on log-log paper. These data are shown in Fig. A-1. Several things are evident here:

1. Wellbore storage effects ended before the first point was recorded, as indicated by the separate pressure and pressure derivative.
2. The flattening of the derivative at the far right indicates infinite-acting behavior.
3. These data can be interpreted by both semilogarithmic straight-line analysis and by log-log type-curve matching.

Figure A-2 is the semilogarithmic analysis with the straight line passing through the last three points as indicated by the log-log diagnostic plot of Fig. A-1. This is a particularly critical step. As can be seen from Fig. A-2, in the absence of a diagnostic plot and especially if the test were the typical 24-hr test, a much steeper straight line could be drawn, grossly underestimating the permeability and the well skin effect.

The slope of the correct straight line is 10.5 psi/cycle. Using Eq. 1-14,

$$k = \frac{(162.6)(33)(1.05)(1.1)}{(10.5)(62)} = 9.5 \text{ md.} \qquad \text{(A-1)}$$

The p_{1hr}, on the extension of the straight line, is 1151 psi. From Eq. 1-15a,

$$s = 1.151\left[\frac{1255 - 1151}{10.5} - \log\frac{9.5}{(0.31)(1.1)(6\times 10^{-5})(0.5)} + 3.23\right]$$

$$= +8. \qquad \text{(A-2)}$$

The same data can be interpreted through type-curve matching. This is shown in Fig. A-3 where the data are matched against the Bourdet et al. (1983) solution. The match points extracted from Fig. A-3 are

$p_D = 1.02$
$\Delta p = 10$ psi
$t_D/C_D = 0.22$
$t = 0.1$ hr
and $C_D e^{2s} = 10^8$.

t (hr)	p_{wf} (psi)	t (hr)	p_{wf} (psi)
0.5	1245	10	1159
0.75	1240	12	1153
1.00	1235.5	18	1145
1.5	1228	24	1142
2.0	1221	36	1136
3.0	1207	48	1135
4.0	1197.5	72	1133
5.0	1189	96	1132
7.0	1173		

Table A-1—Bottomhole pressure data for Example A-1.

q_o	=	33 STB/d
μ_o	=	1.1 cp
B_o	=	1.05 res bbl/STB
h	=	62 ft
r_w	=	6 in.
c_t	=	6×10^{-5} psi^{-1}
ϕ	=	0.31
p_i	=	1255 psi

Table A-2—Well and reservoir data for Example A-1.

From Eq. 1-2 and the pressure match:

$$k = \frac{(1.02)\,(141.2)\,(33)\,(1.1)\,(1.05)}{(66)\,(10)} = 8.3 \text{ md.} \quad \text{(A-3)}$$

Dividing both sides of Eq. 1-3 by C_D results in

$$t_D/C_D = \frac{0.000264\,k\,t}{C_D \phi \mu c_t r_w^2}. \quad \text{(A-4)}$$

Eq. A-4 and the time match can be used to calculate C_D:

$$C_D = \frac{(0.000264)\,(8.3)\,(0.1)}{(0.22)\,(0.31)\,(1.1)\,(6\times 10^{-5})\,(0.5)^2} = 195. \quad \text{(A-5)}$$

From the value of the $C_D e^{2s}$ (obtained from the match), the skin effect can be calculated:

$$s = \frac{1}{2} \ln \frac{10^8}{195} = +6.6. \quad \text{(A-6)}$$

The two analyses are within 12% for the permeability and 17% for the skin effect, which is an excellent agreement.

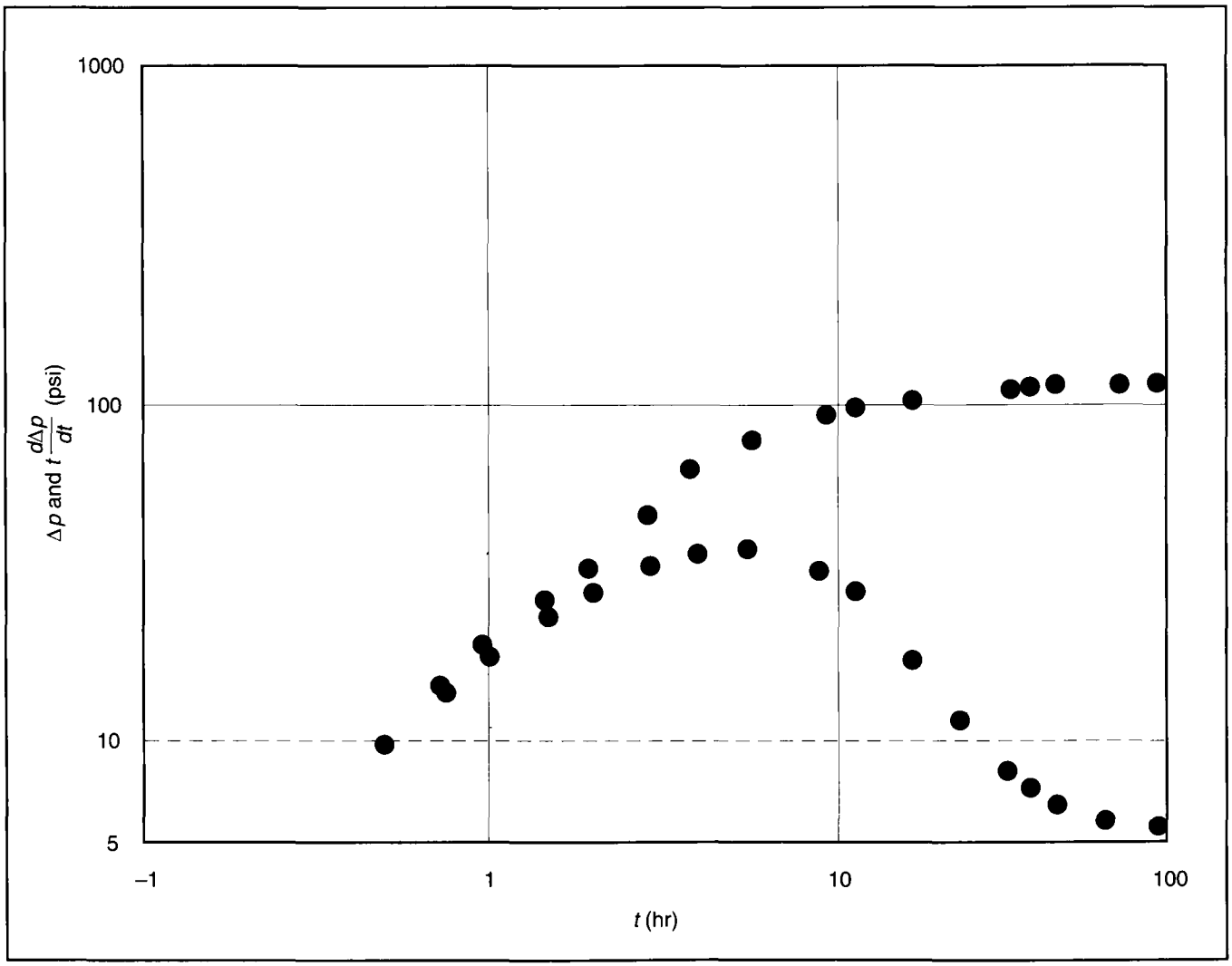

Figure A-1—Log-log diagnostic plot for Example A-1.

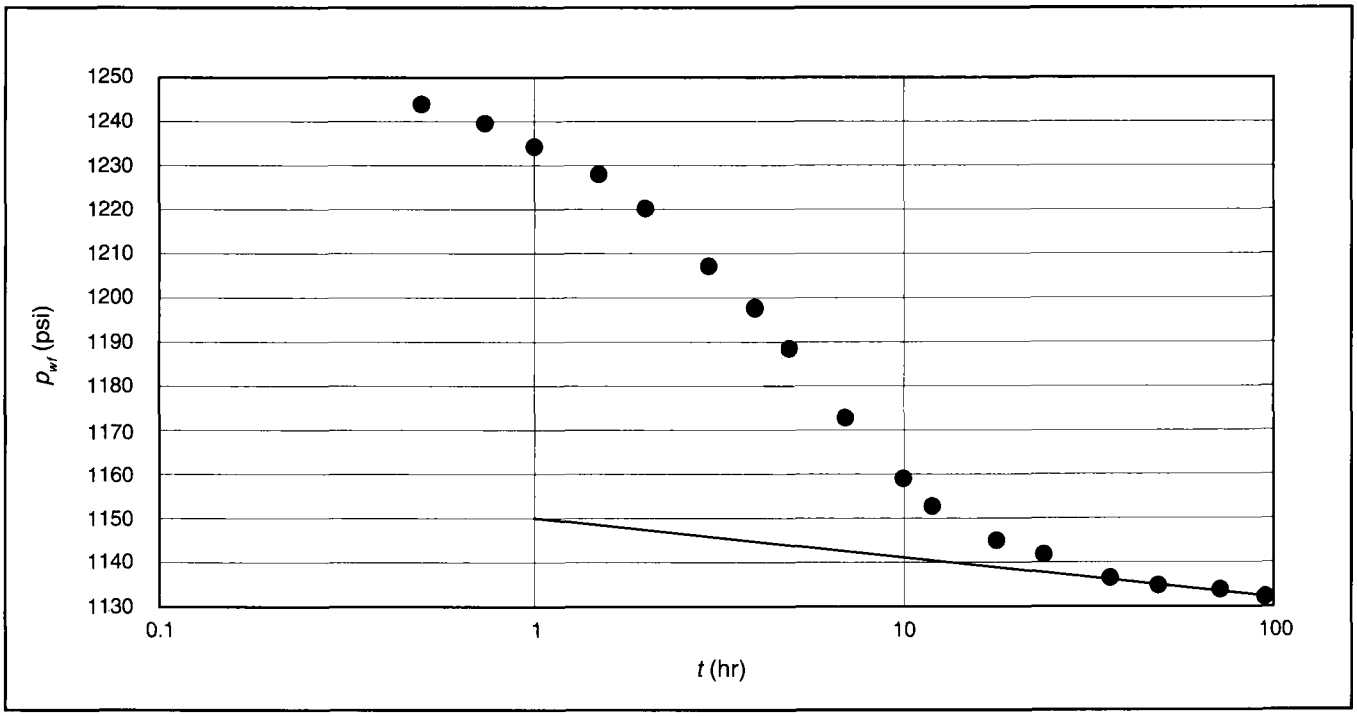

Figure A-2—Semilogarithmic straight line for Example A-1.

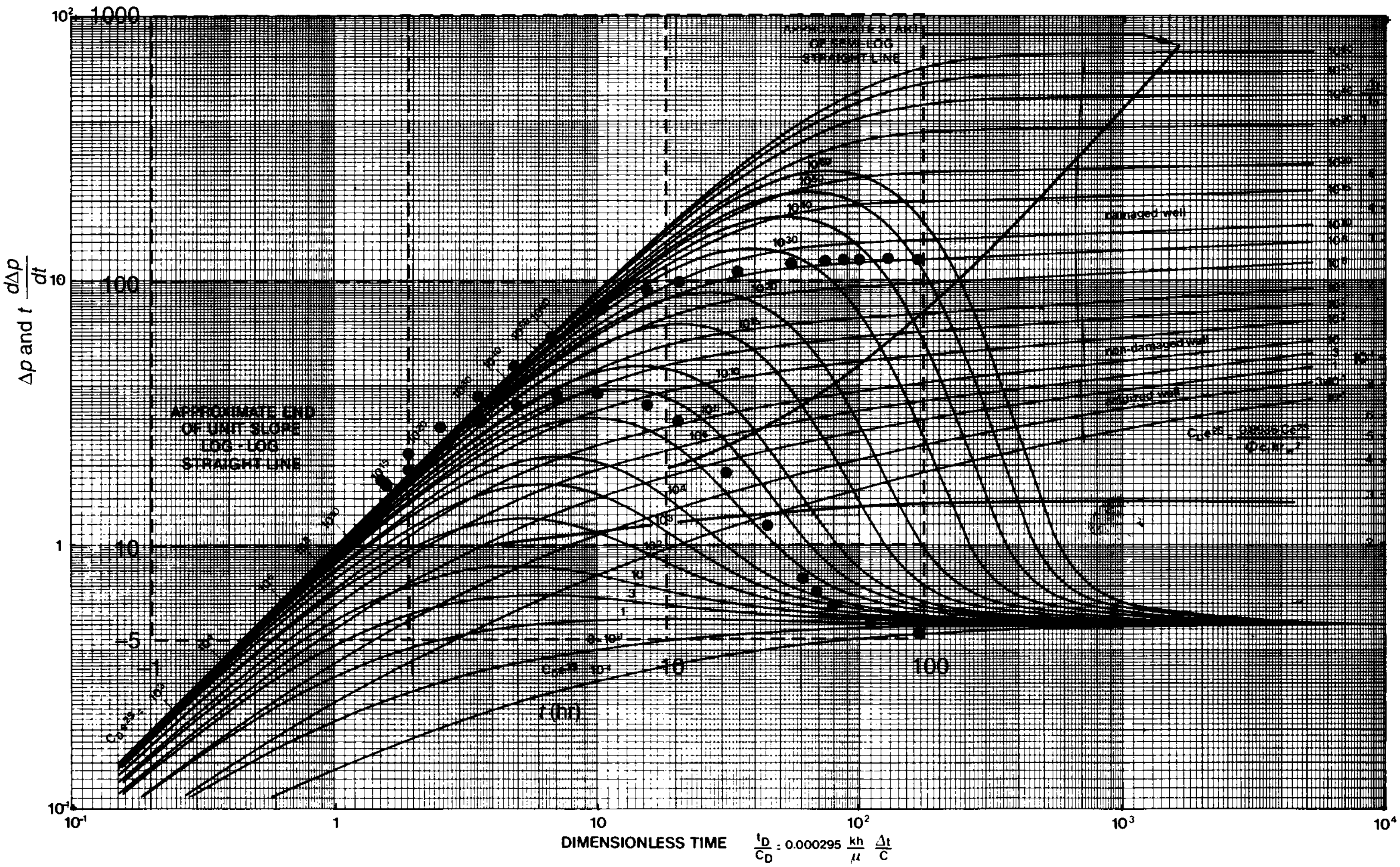

Figure A-3—Type-curve matching for Example A-1.

EXAMPLE A-2

Interpretation of a Gas Injection Test

This test was performed in a well for a gas storage reservoir. Measured bottomhole pressures are shown in Table A-3, and well and reservoir data are listed in Table A-4. Pressure-squared difference (rather than the more correct real-gas pseudopressure) is used. While pressure-squared difference can be calculated readily, the real-gas pseudopressure is now in wide use by almost all analysts.

t (hr)	p_{wf} (psi)	Δp^2 (psi^2)
0.0167	1353	48,384
0.033	1376	111,151
0.05	1396	166,591
0.083	1425	248,400
0.167	1480	408,175
0.33	1540	589,375
0.5	1565	667,000
1	1592	752,239
2	1604	790,591
5	1613	819,544
7	1615	826,000
10	1617	832,464
12	1619	838,936
15	1620	842,175
20	1622.5	850,281
24	1625	858,400
32	1626	861,651
40	1627.5	866,531
48	1629	871,416
56	1630	874,675
64	1631.5	879,567
72	1632	881,199
80	1633	884,464
168	1639	904,096

Table A-3—Bottomhole pressures for Example A-2.

Solution (Ref. Sections 1-2.3, 1-2.4)

Figure A-4 is the log-log diagnostic graph for this example, clearly identifying the infinite-acting portion (after about 3 hr) indicated by the flat pressure derivative. This leads directly to Fig. A-5, which is the semilogarithmic plot. A straight line is evident with a slope equal to 55,500 psi^2/cycle. From Eq. 1-31,

$$k = \frac{(1638)(1200)(0.023)(0.96)(540)}{(55{,}500)(120)} = 3.5 \text{ md.} \quad \text{(A-7)}$$

The Δp^2_{1hr} is 776,250 psi^2, and from Eq. 1-37,

$$s' = 1.151\left[\frac{776{,}250}{55{,}500} - \log\frac{3.5}{(0.094)(0.023)(2.5\times10^{-4})(0.229^2)} + 3.23\right]$$

$$= +11. \quad \text{(A-8)}$$

Since this is a gas well, the calculated skin effect is an effective value (s') and is rate dependent. However, for the small injection rate for this example, it can be considered as very near the actual well skin effect.

With such a developed infinite-acting behavior, there is no need for type-curve matching.

p_i	=	1335 psi
ϕ	=	0.094
μ	=	0.023 cp
c_t	=	2.5×10^{-4} psi^{-1}
Z	=	0.96
r_w	=	0.229 ft [5½ in.]
h	=	120 ft
T	=	80°F [540°R]
q_{inj}	=	1.2 MMSCF/d

Table A-4—Well and reservoir data for Example A-2.

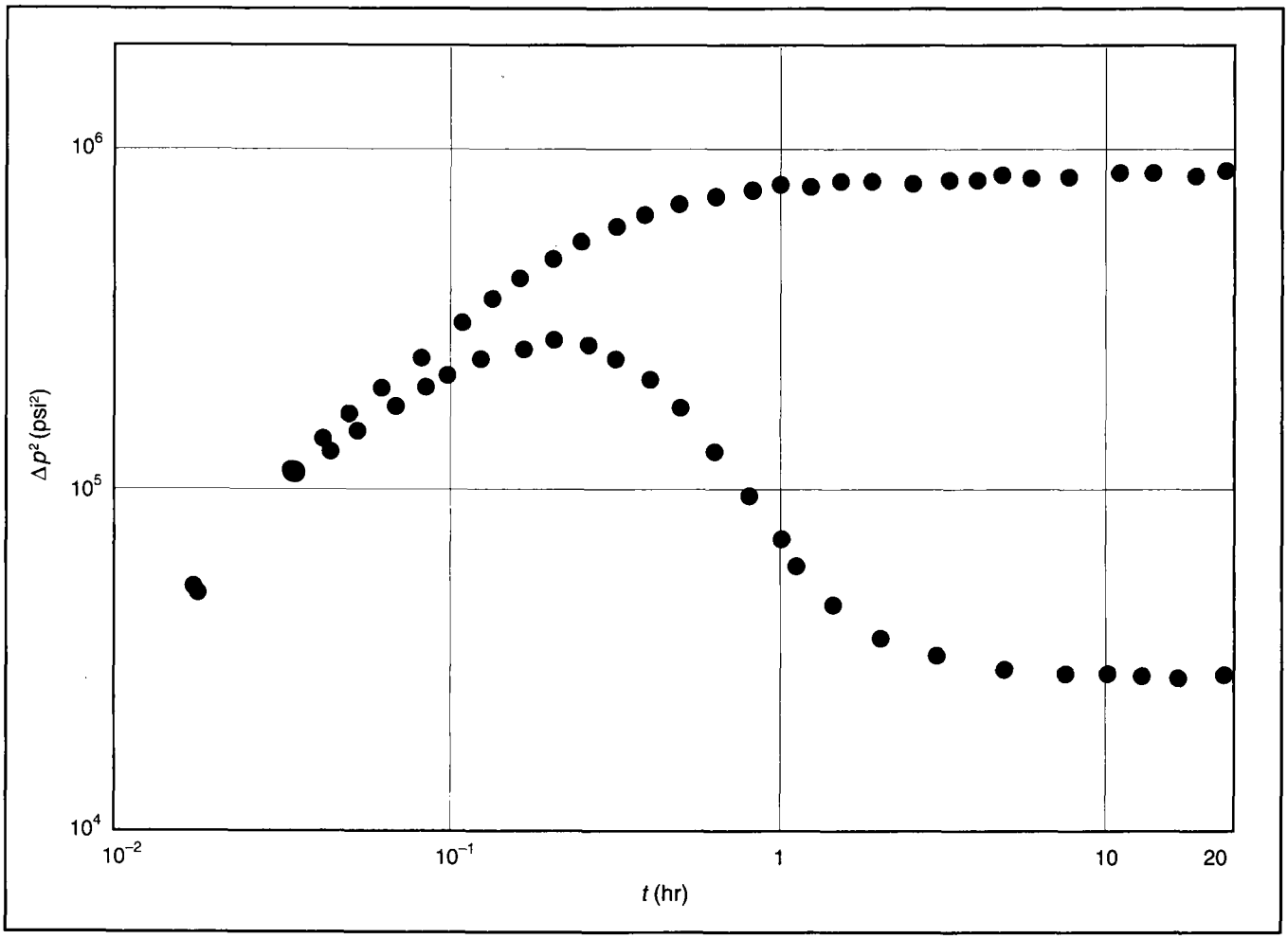

Figure A-4—Log-log diagnostic graph for Example A-2.

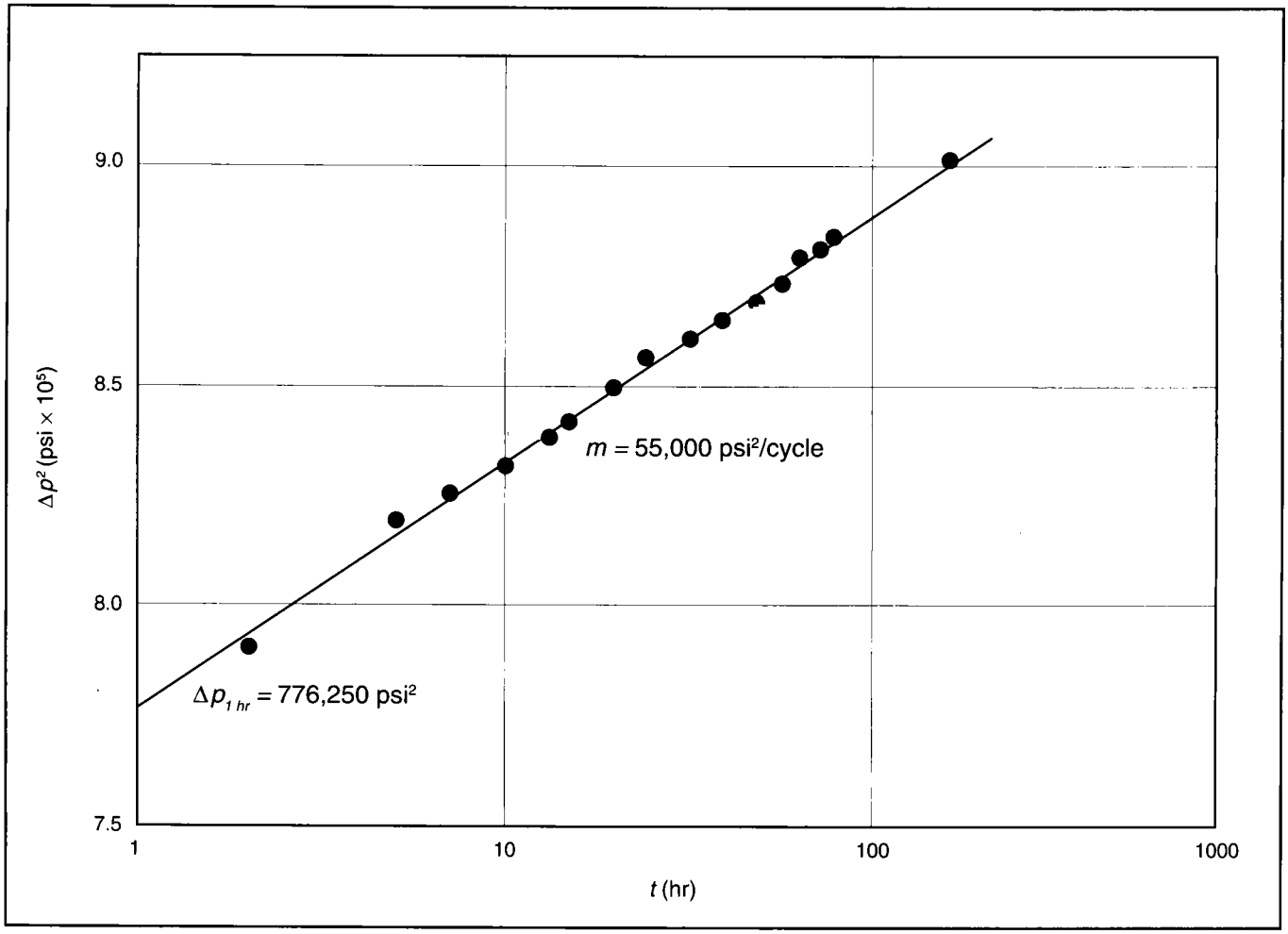

Figure A-5—Semilogarithmic graph for Example A-2.

EXAMPLE A-3

Calculation of the Permeability of a Tight Reservoir from a Short-Duration Pressure Buildup Well Test

This example demonstrates the method to *estimate* the reservoir permeability from a very short-duration pressure buildup test. Table A-5 contains the bottomhole pressures for this test, while the pertinent well and reservoir data are listed in Table A-6.

Solution (Ref. Section 1-3.6)

Figure A-6 is a log-log diagnostic plot for this problem, and it indicates clearly that this (36-hr) well test is considerably shorter than would be needed for a semilogarithmic interpretation or even for a reasonably unique type-curve matching.

Thus, the method implied by Eq. 1-101 can be employed to estimate the well permeability. At first, from Fig. A-6, the time at the end of wellbore storage effects ($t_{e.w.b.}$) can be extracted. This is equal to approximately 3 hr, as indicated by the separation of the pressure and pressure derivative.

Next, the dimensioned wellbore coefficient must be calculated. This is given approximately by:

$$C = V_{well}\, c_f, \tag{A-9}$$

and must be in barrels per pounds per square inch (divide ft^3 by 5.615). In Eq. A-9, c_f is the fluid compressibility under wellbore conditions. Thus,

$$C = \frac{(3.14)\,(3.068)^2\,(13{,}200)\,(4 \times 10^{-5})}{(4)\,(144)\,(5.615)}$$

$$= 4.8 \times 10^{-3}\ \text{bbl/psi}. \tag{A-10}$$

From Eq. 1-101,

$$k \cong \frac{(3000)\,(4.8 \times 10^{-3})\,(0.7)}{(42)\,(3)} = 0.08\ \text{md}. \tag{A-11}$$

Since the flow rate before the buildup was 9.5 STB/d, then an attempt for a "forward" match is shown in Fig. A-7. Taking any arbitrary pressure difference (e.g., 3148 psi), the dimensionless pressure is calculated from Eq. 1-2:

$$p_D = \frac{(0.08)\,(42)\,(3148)}{(141.2)\,(9.5)\,(1.08)\,(0.7)} \cong 10.5. \tag{A-12}$$

The match is made by superimposing the real data graph at $\Delta p = 3148$ psi with the type curve at $p_D = 10.5$. As can be seen, the *beginning* of the infinite-acting behavior would have started at approximately 200 hr (where the derivative begins to flatten). For an accurate calculation of the permeability, a test duration of a month or more would have been required.

No calculation of the skin effect is attempted or is necessary. First, the permeability is only an estimate (assuming zero skin effect in the development of Eq. 1-101). Furthermore, such a well is an obvious candidate for hydraulic fracturing, and the skin effect will be bypassed by such a treatment. The technique employed in this example is intended to provide only a rough estimate. It should never substitute for a properly designed and executed pressure transient test. It should be used as a last resort for wells where proper duration testing is uneconomical or impractical.

t (hr)	Δp (psi)	t (hr)	Δp (psi)
0.083	30.2	4	1209
0.167	57.9	5	1486
0.25	85.6	6	1712
0.5	171.2	8	2165
0.75	251.8	10	2520
1.0	314.8	12	2845
1.25	440.7	15	3148
1.5	478.4	20	3651
2.0	680.0	24	3903
2.5	755.4	36	4356
3.0	931.7		

Table A-5—Bottomhole pressures for Example A-3.

d_{tbg}	=	3.068 in.
r_w	=	0.406 ft
H	=	13,200
μ	=	0.7 cp
q	=	9.5 STB/d
B	=	1.08 res bbl/STB
h	=	42 ft
c_t	=	$1.2 \times 10^{-5}\ \text{psi}^{-1}$
ϕ	=	0.17
c_f (in well)	=	$4 \times 10^{-5}\ \text{psi}^{-1}$

Table A-6—Well and reservoir data for Example A-3.

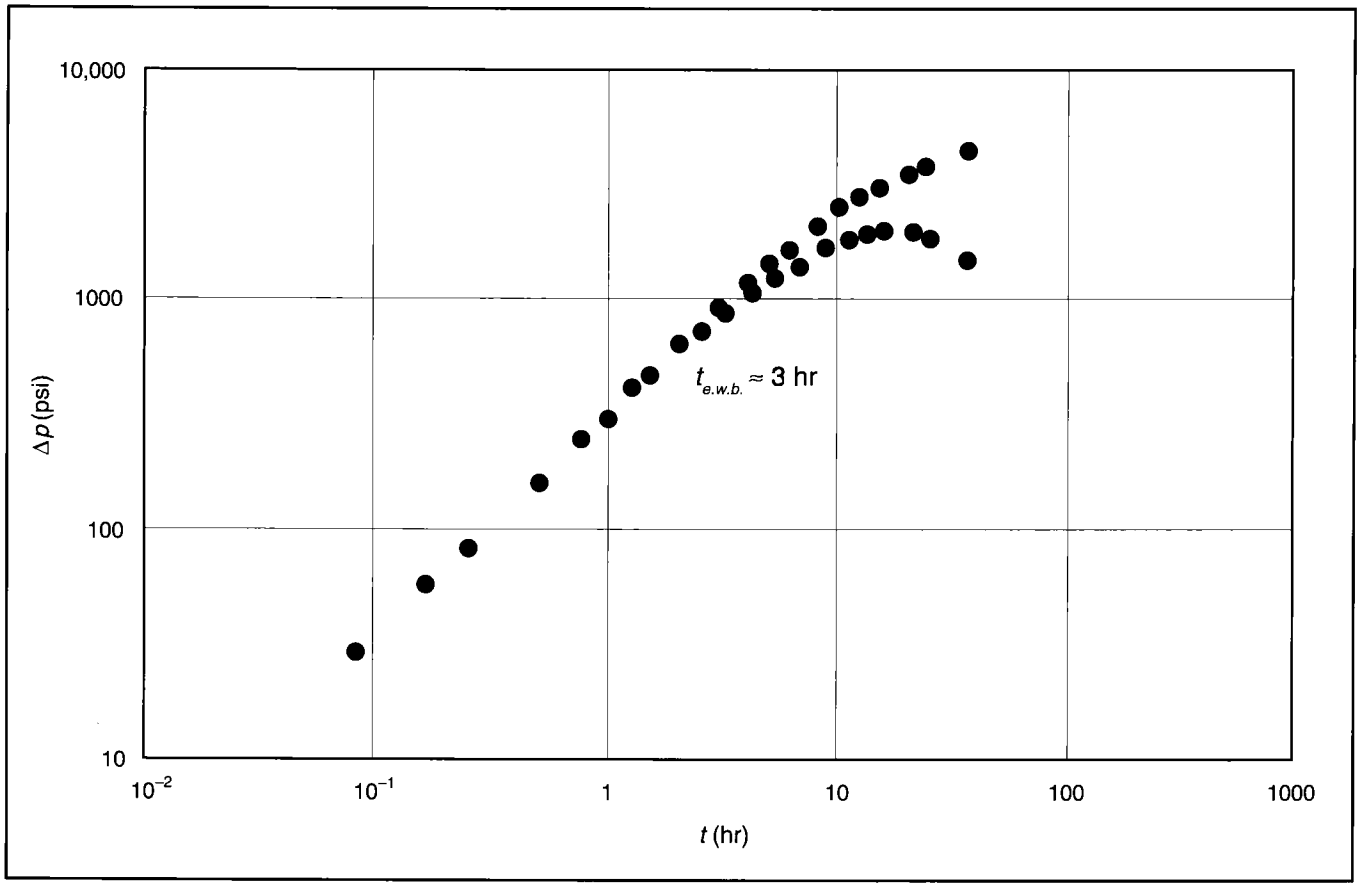

Figure A-6—Log-log diagnostic plot for Example A-3.

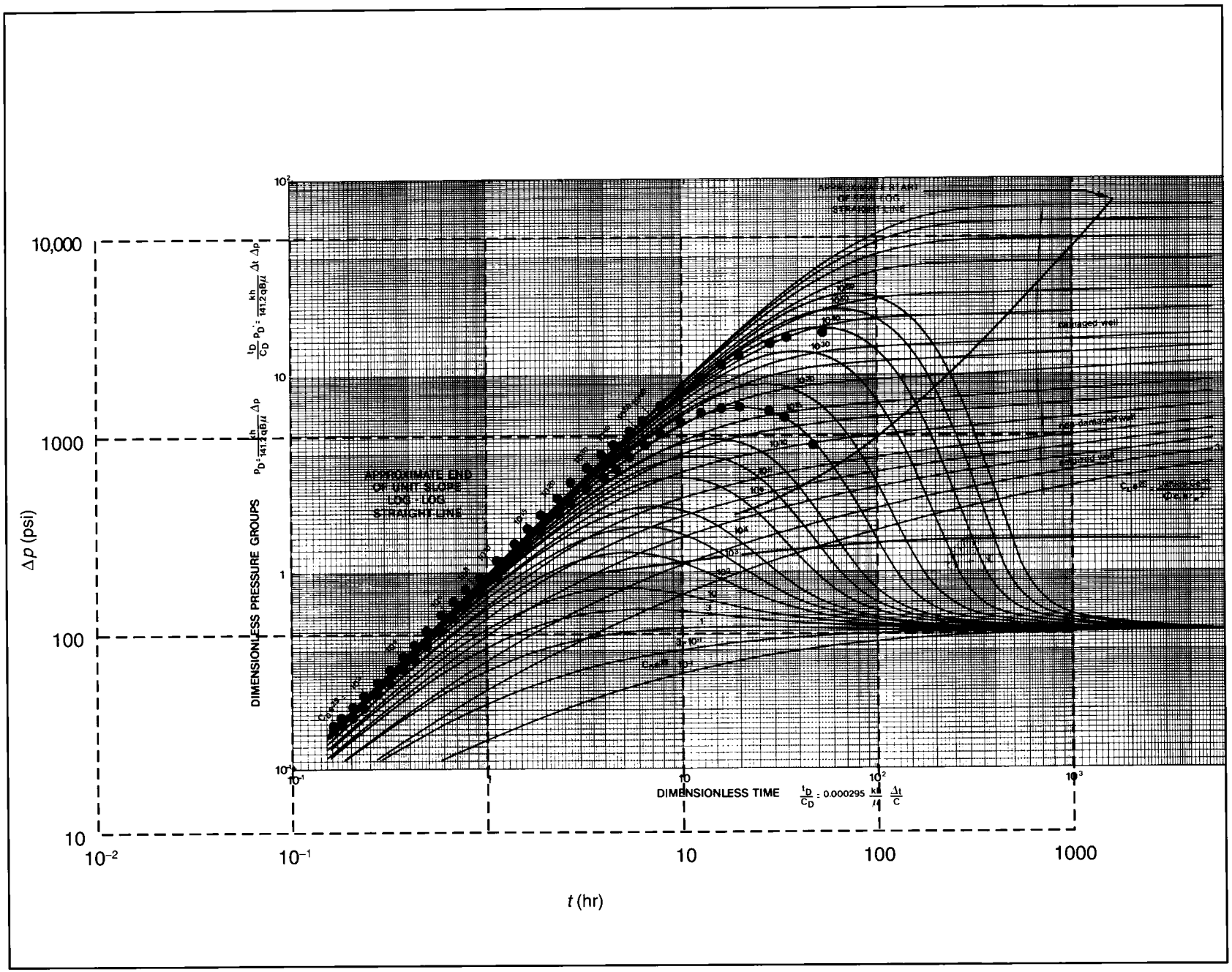

Figure A-7—Type-curve matching for Example A-3.

EXAMPLE A-4

Forecast of Transient Well Performance

Assuming that the bottomhole pressure for the well analyzed in Example A-1 is 750 psi, construct a 180-day deliverability curve both before and after acidizing (assume that $s = 0$ after stimulation).

Solution (Ref. Section 1-2.1)

Equation 1-13 can be rearranged as

$$q = \frac{kh(p_i - p_{wf})}{162.6B\mu} \left[\log t + \log \frac{k}{\phi \mu c_t r_w^2} - 3.23 + 0.87s\right]^{-1}. \quad \text{(A-13)}$$

With the variables given and calculated in Example A-1, Eq. A-13 reduces to (before stimulation)

$$q = \frac{1584}{\log t + 10.03}, \quad \text{(A-14)}$$

and (after stimulation, $s = 0$)

$$q = \frac{1584}{\log t + 3.04}. \quad \text{(A-15)}$$

(Note that in Eqs. A-14 and A-15, the time, t, must be in hours.)

Figure A-8 is a graph of expected performance assuming the 750-psi flowing bottomhole pressure before and after stimulation. The rates at the 180-day landmark are 240 STB/d and 118 STB/d, respectively.

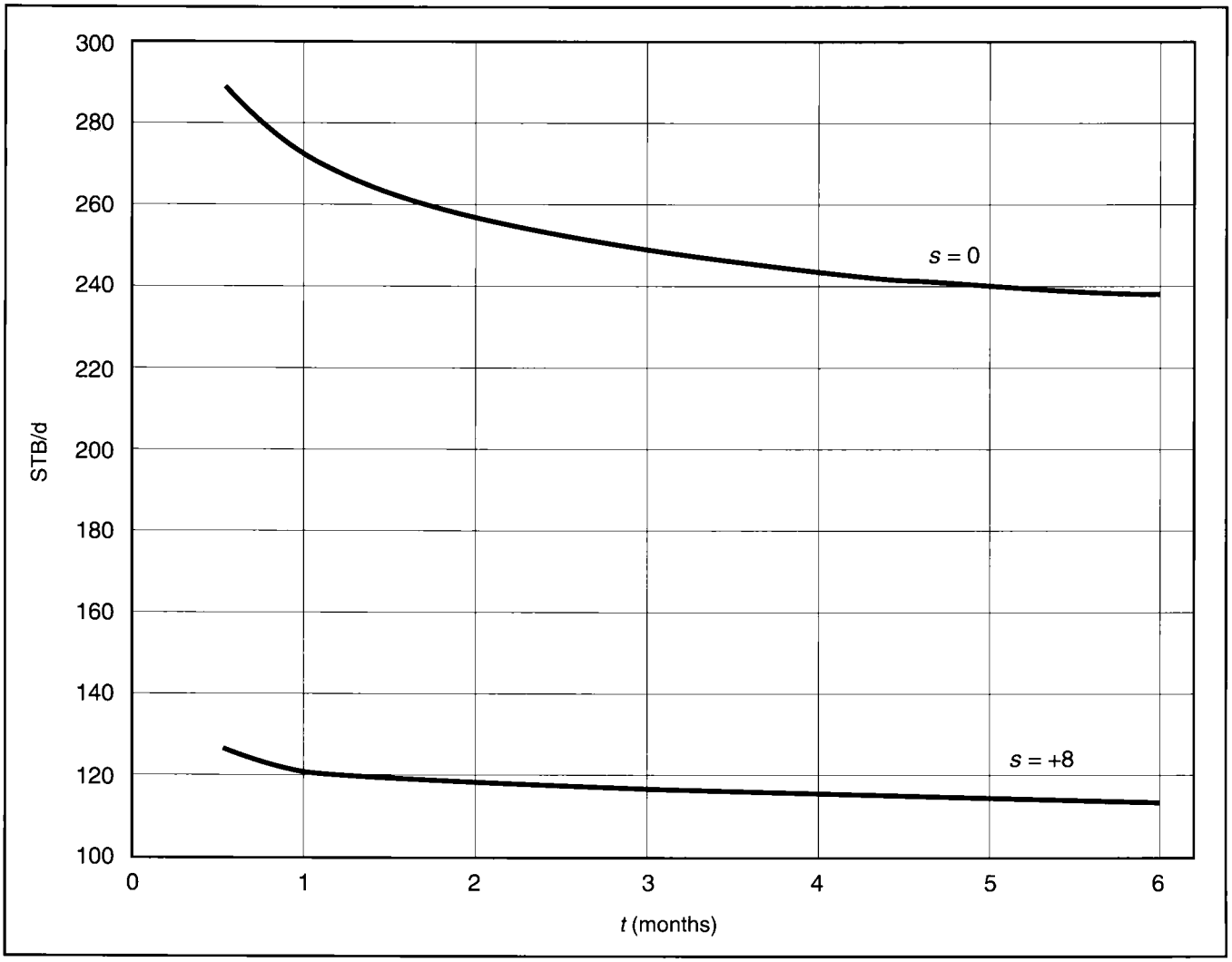

Figure A-8—Forecast of performance of well in Example A-4.

EXAMPLE A-5

Impact of Reservoir Extent on Well Performance

Calculate the difference in oilwell production rate using the simple steady-state expression for radial flow. Assume drainage areas of 40, 80, 160 and 640 acres. Table A-7 contains the necessary data for this calculation.

Solution (Ref. Section 1-3)

The relevant Eq. 1-65 can be rearranged and written in oilfield units as

$$q = \frac{kh(p_e - p_{wf})}{141.2B\mu\left[\ln(r_e/r_w) + s\right]}. \qquad \text{(A-16)}$$

Assuming that the skin effect is zero (this would result in the most pronounced difference in the production rate), then the increases in the production rate (or productivity index) at steady state are as shown in Table A-8.

These increases indicate that the drainage area assigned to a well has a small impact on the production rate. For tight reservoirs this is particularly true, because transient behavior is evident for much of the time.

For a higher permeability, closed reservoir (i.e., flowing under pseudosteady-state conditions), the rate at late time can be significantly different. In such a case, material balance and inflow performance relationships must be combined.

k	=	10 md
μ	=	0.8 cp
h	=	50 ft
B	=	1.1 res bbl/STB
p_e	=	3000 psi
r_w	=	0.328-ft [7⅞-in.] well
p_{wf}	=	1000 psi

Table A-7—Well and reservoir data for Example A-5.

A (acres)	r_e (ft)	$\ln(r_e/r_w)$	q/q_{40}
40	745	7.73	1
80	1053	8.07	1.04
160	1489	8.42	1.09
640	2980	9.11	1.18

Table A-8—Production rate increases (over a 40-acre spacing) for Example A-5.

EXAMPLE A-6

Stimulation Treatment Choice: Fracturing vs. Acidizing

Using the data given in Example A-5 for a 40-acre-spacing well, predict production rates at steady state for a range of permeabilities and for skin effects equal to 0 and 10. Comment on whether the well for these cases is a candidate for fracturing or acidizing.

Solution (Ref. Section 1-3)

Equation A-16 can be reduced to

$$q = \frac{920k}{7.73 + s}. \qquad \text{(A-17)}$$

If permeabilities range between 10 md and 0.01 md, then the rates given in Table A-9 can be expected at steady state.

If the permeability were 10 md, then elimination of the skin effect (if it were possible) from 10 to 0 would result in a production rate increase from 519 STB/d to 1190 STB/d, a substantial benefit. Thus, matrix stimulation would be indicated, whereas hydraulic fracturing would be subjected to net present value considerations (Ref. Chapter 8).

If the permeability were 0.01 md, then elimination of the skin effect from 10 to 0 would result in an increase in the production rate from 0.5 STB/d to 1.2 STB/d, an unattractive prospect. In general, reservoirs with permeabilities of 1 md or less are usually candidates for hydraulic fracturing, while those with permeabilities of 10 md and above are candidates for matrix stimulation. Reservoirs with permeabilities between 1 and 10 md require intensive study and sound design practices for the appropriate choice of stimulation treatments.

k (md)	$s = 10$ q (STB/d)	$s = 0$ q (STB/d)
10	519	1190
1	52	119
0.1	5	12
0.01	0.5	1.2

Table A-9—Production rates for the well in Examples A-5 and A-6 (at steady state).

EXAMPLE A-7

Productivity Index Ratios for Damaged and Undamaged Wells

Calculate the PI ratios (compared to zero skin) at steady state for a well where the penetration of damage ranges up to 10 ft and the permeability impairment ranges up to 95% ($k/k_s = 20$). Assume that $r_e = 745$ ft (40 acres) and $r_w = 0.328$-ft (7⅞-in.) well radius [$\ln(r_e/r_w) = 7.73$].

Solution (Ref. Sections 1-3, 1-3.1)

The productivity index ratio between the ideal case ($s = 0$) and a real case ($s \neq 0$) can be obtained from Eq. 1-69:

$$\frac{(\mathrm{PI})_{ideal}}{(\mathrm{PI})_{real}} = \frac{\ln(r_e/r_w) + s}{\ln(r_e/r_w)}. \qquad \text{(A-18)}$$

Furthermore, the skin effect, s, is given in terms of k_s and r_s by Eq. 1-77.

As an example, if $r_s = 3$ ft (the damaged ring is then 3 ft – $r_w = 2.672$ ft) and $k/k_s = 10$, then from Eq. 1-77,

$$s = (10 - 1)\ln\frac{3}{0.328} \cong 20, \qquad \text{(A-19)}$$

and

$$\frac{(\mathrm{PI})_{ideal}}{(\mathrm{PI})_{real}} = \frac{7.73 + 10}{7.73} = 2.29. \qquad \text{(A-20)}$$

At $k/k_s = 50$, the skin effect is 108 and the PI ratio is 15.

Figure A-9 is a graph summarizing the solution to this example.

The logarithmic relationship of the damage radius is evident. Increasing the damage radius from 1 ft to 3 ft (with $k/k_s = 10$) results in a ratio of PIs equal to 1.32, whereas increasing the damage from 1 ft to 10 ft results in a ratio equal to only 2.18.

On the other hand, given a damage radius, the ratio of the PI is almost directly proportional to the permeability impairment.

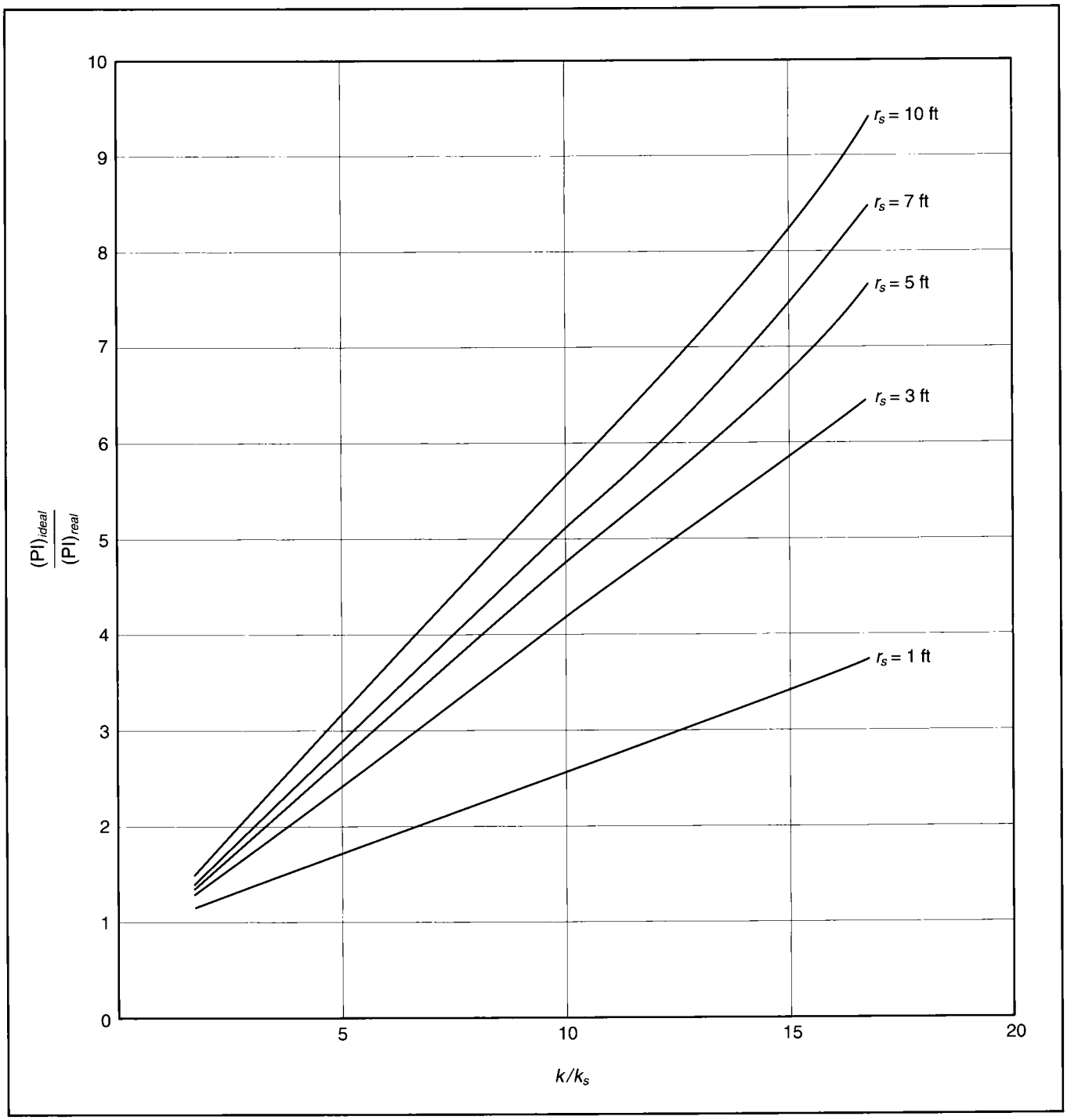

Figure A-9—Effects of damage ratio and permeability impairment on PI ratio.

EXAMPLE A-8

Pressure Drop Across Damaged Zone

It is often confusing as to what portion of the total pressure drop (from the reservoir proper and across the sandface) is caused by the near-wellbore zone. This is the zone characterized by the total skin effect. Calculate the total Δp and the ratio $\Delta p_{skin}/\Delta p$ for a range of skin effects using the well and reservoir data in Example A-5. Use the steady-state relationship for a 40-acre spacing. Assume a rate equal to 200 STB/d.

Solution (Ref. Sections 1-3 and 1-3.1)

The total pressure drop is given by Eq. 1-67, whereas the ratio $\Delta p_{skin}/\Delta p$ is

$$\frac{\Delta p_{skin}}{\Delta p_{total}} = \frac{s}{\ln(r_e/r_w) + s}. \qquad \text{(A-21)}$$

Figure A-10 contains the total pressure drop from the reservoir and into the well and the ratio $\Delta p_{skin}/\Delta p_{total}$. For skin effects larger than 10, which is a value encountered often in pressure transient analysis, the ratio is approximately 60% or more. This calculation indicates the importance of skin removal.

This calculation also demonstrates the scope of pressure transient measurements. While Eq. 1-67 is for steady-state conditions, Eq. 1-39 is for transient flow. As can be seen, the only difference is the replacement of the term $\ln r_e/r_w$ by p_D, the latter being invariably smaller. The Δp_{skin} remains constant as suggested by Van Everdingen and Hurst (1949). Thus, measurements of fractions of pounds per square inch are currently used to detect pressure transients, while the total pressure may be already penalized by hundreds of pounds per square inch as a result of the near-wellbore condition.

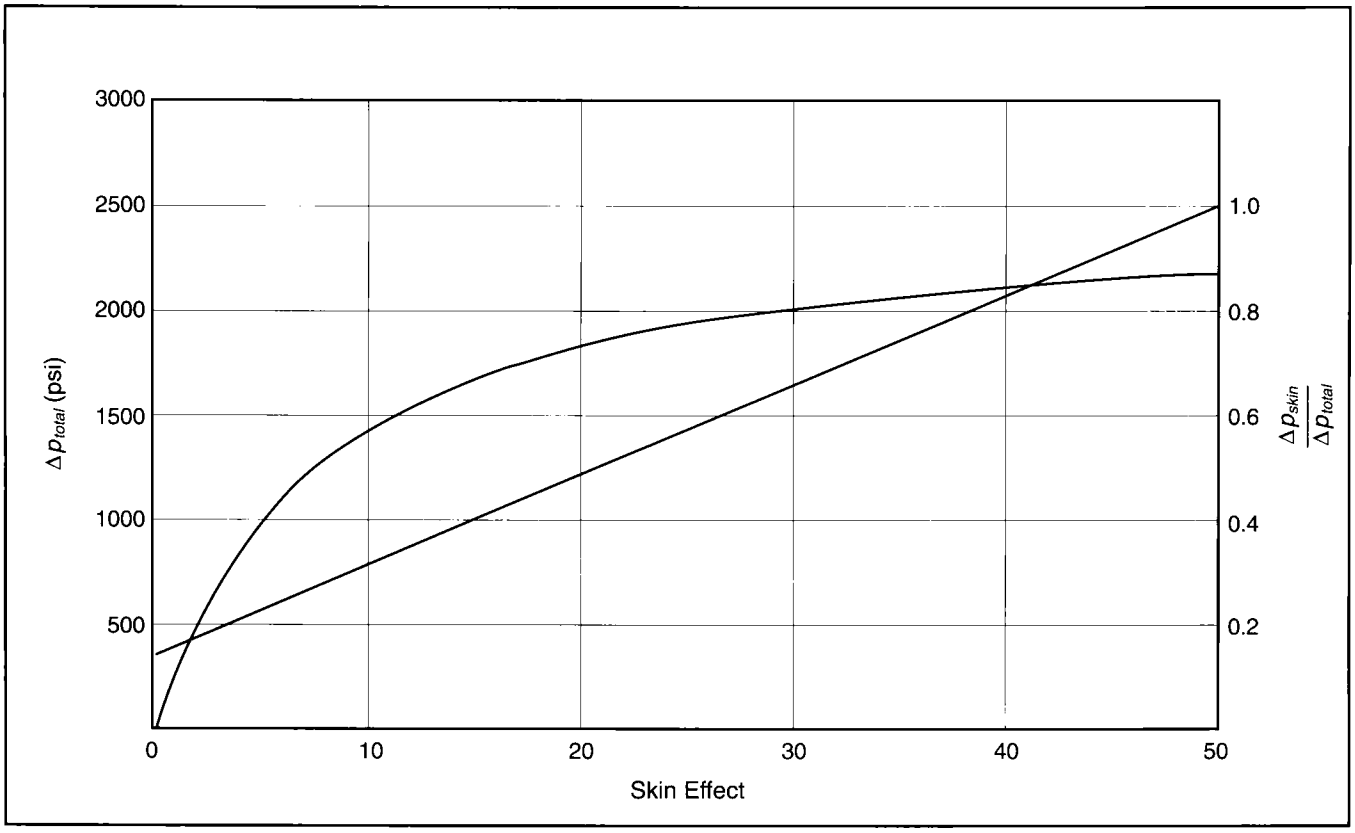

Figure A-10—Total pressure drop and ratio of pressure resulting from skin to the total pressure drop for Example A-8.

EXAMPLE A-9

Skin Effect Resulting from Partial Penetration and Slant

Calculate the skin effect resulting from partial penetration for a well described in Fig. A-11. What would the skin effect be if the well were penetrating the reservoir at a 45° slant? Well radius is 0.5 ft.

Solution (Ref. Section 1-3.3)

The dimensionless variables given by Eqs. 1-79 to 1-82 and as required for Tables 1-1a and 1-1b must be calculated:

$$h_D = \frac{50}{0.5} = 100, \tag{A-22}$$

and

$$z_{wD}/h_D = \frac{z_w/r_w}{h/r_w} = \frac{40}{50} = 0.8. \tag{A-23}$$

This is a highly off-centered well, drilled to avoid water coning. Table 1-1a uses symmetry in the flowlines; i.e., a 0.8 off-centered well would have the same behavior as a 0.2 off-centered well. (The latter may be necessary to avoid gas coning.)

$$h_{wD}/h_D = \frac{h_w/r_w}{h/r_w} = \frac{5}{50} = 0.1. \tag{A-24}$$

From Table 1-1a, the skin effect from partial completion is $s_c = +15.8$.

If the well were completed so that the midpoint of the perforations coincided with the midpoint of the reservoir, then $z_{wD}/h_D = 0.5$, reducing the skin effect (to +15.2; see Table 1-1a).

Of course, the most critical variable is the penetration ratio h_w/h; If it is larger than 0.5, then the associated skin effect becomes small (about +2 or less).

Reservoir thickness is important, too. Assuming that $h_D = 1000$ (i.e., $h = 500$ ft) and keeping $z_{wD}/h_D = 0.8$ and $h_{wD}/h_D = 0.1$, then $s_c = +35.8$. Skin effects of this magnitude can be observed in thick reservoirs, such as the Prudhoe Bay field, that also exhibit gas coning problems.

For the second configuration in Fig. A-9, all dimensionless variables remain the same (as given by Eqs. A-22 to A-24). From Table 1-1a, and since $\theta = 45°$, then $s_{c+\theta} = +12.1$. Thus, the slant contributes a negative skin effect, $s_\theta = -3.7$. A more slanting well (e.g., $\theta = 75°$) would result in a substantial negative contribution to the skin effect (–11.6).

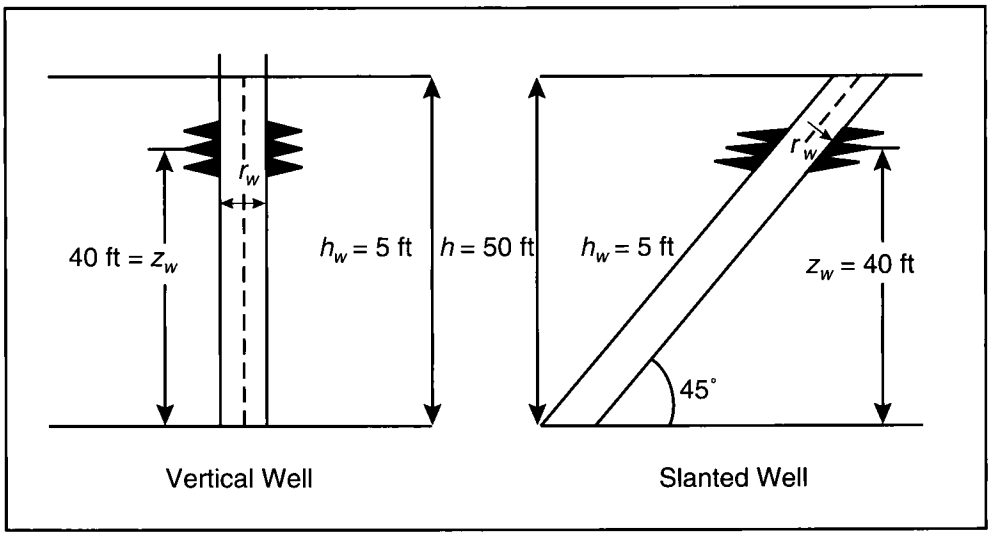

Figure A-11—Well configuration for Example A-9.

EXAMPLE A-10

Calculation of the Perforation Skin Effect

Calculate the perforation skin effect for a well described in Fig. A-12. Assume that the ratio of the horizontal to vertical permeability $k_H/k_v = 5$.

Solution (Ref. Section 1-3.4)

The total perforation skin effect, s_p, is given by Eq. 1-83. At first, the plane-flow effect, s_h, is calculated.

A. Calculation of s_h

From Table 1-2, $\alpha_\theta = 0.648$, since $\theta = 120°$. Then, from Eq. 1-85,

$$r'_w(\theta) = 0.648\,(0.328 + 0.667) = 0.645\,\text{ft}, \qquad \text{(A-25)}$$

and from Eq. 1-84,

$$s_h = \ln \frac{0.328}{0.645} = -0.676. \qquad \text{(A-26)}$$

(If $\theta = 60°$, then $s_h = -0.90$; if $\theta = 90°$, then $s_h = -0.79$. All from Table 1-2.)

The vertical conveying skin effect, s_v, is then calculated.

B. Calculation of s_v

From Eq. 1-86,

$$h_D = \frac{0.5\sqrt{5}}{0.667} = 1.67. \qquad \text{(A-27)}$$

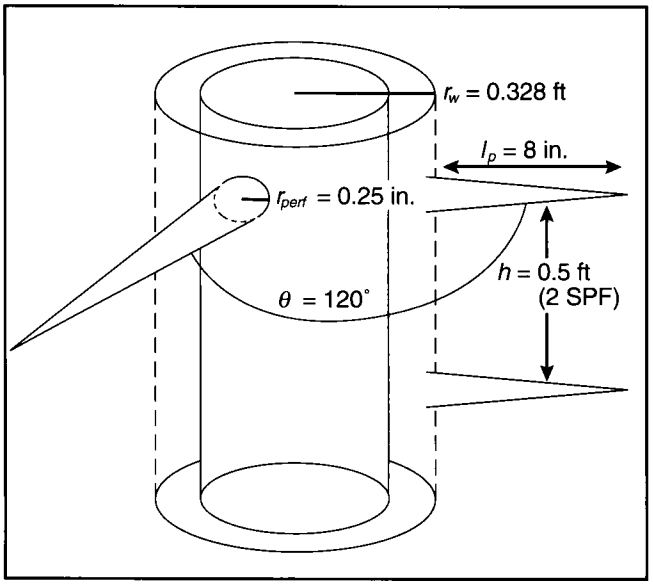

Figure A-12—Well configuration for Example A-10.

From Eq. 1-87,

$$r_{pD} = \frac{(0.25/12)}{(2)\,(0.5)}\left(1+\sqrt{0.2}\right) = 0.03. \qquad \text{(A-28)}$$

To use Eq. 1-89, the constants a and b must be calculated from Eqs. 1-90 and 1-91. The correlation coefficients a_1, a_2, b_1 and b_2 must be obtained from Table 1-3. Thus,

$$a = (-2.018)\log(0.03) + 0.0634 = 3.1, \qquad \text{(A-29)}$$

$$b = (1.6136)\,(0.03) + 1.7770 = 1.825, \qquad \text{(A-30)}$$

and, finally, from Eq. 1-89,

$$s_v = 10^{3.1}\,1.67^{0.825}\,0.03^{1.825} = +3.2. \qquad \text{(A-31)}$$

If $k_H/k_v = 1$ (i.e., if there were perfect permeability isotropy), then:

$h_D = 0.75$,
$r_{pD} = 0.42$,
$a = 2.84$,
$b = 1.84$,
and $s_v = +1.6$.

If $h = 2$ ft (1 shot/2 ft) (i.e., a job with very bad perforation density), then:

$h_D = 6.7$,
$r_{pD} = 0.0168$,
$a = 3.64$,
$b = 1.804$,
and $s_v = +12.7$.

Finally, the wellbore skin effect, s_{wb}, is calculated:

C. Calculation of s_{wb}

From Eq. 1-88,

$$r_{wD} = \frac{0.328}{0.667 + 0.328} = 0.33. \qquad \text{(A-32)}$$

From Eq. 1-92 and using Table 1-4 for the constants c_1 and c_2,

$$s_{wb} = 6.6 \times 10^{-3} e^{5.320\,(0.33)} = 0.038. \qquad \text{(A-33)}$$

From Eq. 1-83, the total perforation skin effect is

$$s_p = -0.676 + 3.2 + 0.038 = +2.6. \qquad \text{(A-34)}$$

If the perforation density were 0.5 SPF, then the skin effect would be substantial: $s_p \cong +12$.

This Page Intentionally Left Blank

B. Rock Mechanics

EXAMPLE B-1

Calculation of the Normal and Shear Stresses at any Angle from the Principal Stresses

Assuming that the principal horizontal stress components at depth are 3000 and 4000 psi, determine the normal and shear stresses on a fault at 20° from the direction of the minimum horizontal stress. At what angle would the maximum shear stress be, what would be its value and what would be the corresponding magnitude of the normal stress?

Solution (Ref. Section 2-2.1)

Figure B-1 denotes the fault and the two principal stress directions. In Eqs. 2-2 and 2-3, since σ_x and σ_y are the principal stresses, then $\tau_{xy} = 0$. (Definition of principal stress direction: shear stresses vanish.)

As a result, Eq. 2-2 gives

$$\sigma = 4000 \cos^2 20° + 3000 \sin^2 20°$$

$$= 3883 \text{ psi}, \tag{B-1}$$

and Eq. 2-3 gives

$$\tau = \frac{1}{2}(3000 - 4000) \sin(2 \times 20°)$$

$$= -321 \text{ psi}. \tag{B-2}$$

At the maximum sheer stress $\partial\tau/\partial\theta = 0$, and thus from Eq. 2-3 and remembering that $\tau_{xy} = 0$, then

$$\frac{\partial\tau}{\partial\theta} = \frac{1}{2}(\sigma_{H,min} - \sigma_{H,max})(2)(\cos 2\theta) = 0, \tag{B-3}$$

$$\longrightarrow \cos 2\theta = 0, \tag{B-4}$$

and, thus, $2\theta = 90°$ or $\theta = 45°$.

Then, from Eq. 2-3 at 45°,

$$\tau = \frac{1}{2}(3000 - 4000) \sin 90° = -500 \text{ psi}, \tag{B-5}$$

and from Eq. 2-2 at 45°,

$$\sigma = 4000 \cos^2 45° + 3000 \sin^2 45°$$

$$= 3500 \text{ psi}. \tag{B-6}$$

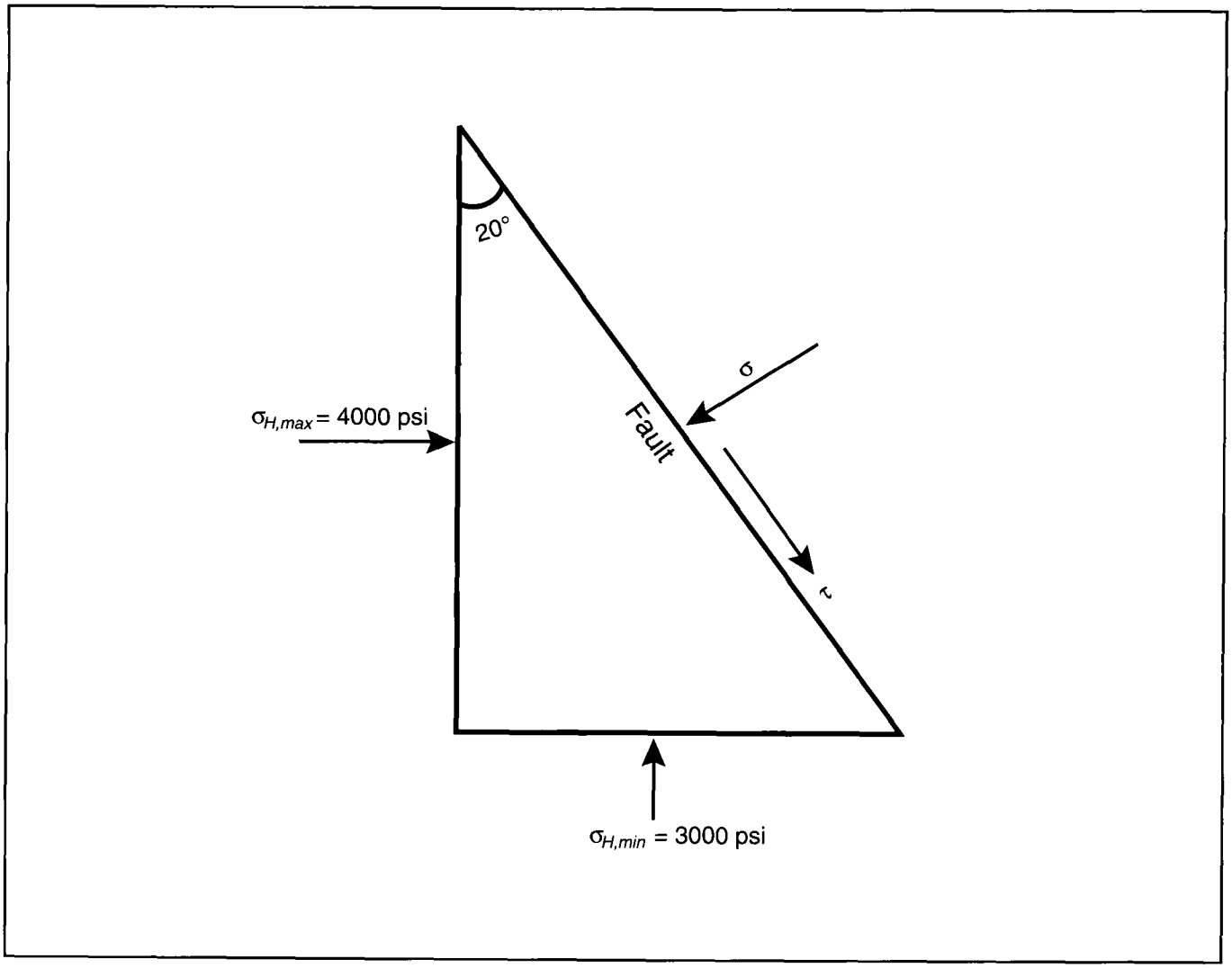

Figure B-1—Principal stress directions and fault for Example B-1.

EXAMPLE B-2

Calculation of the Effective Stress

If a reservoir is 10,000 ft deep and has a 0.70 oil saturation, calculate the effective vertical stress. Use the variables given in Table B-1.

Solution (Ref. Section 2-2.4)

The absolute vertical stress is equal to the overburden pressure, and from Eq. 2-40,

$$\sigma = \rho_f g H = \frac{\rho_f H}{144} = \frac{(165)(10{,}000)}{144}$$

$$= 11{,}483 \text{ psi}. \tag{B-7}$$

To calculate Biot's poroelastic constant, the total and bulk compressibilities are required.

$$c_t = S_o c_o + S_w c_w + c_f, \tag{B-8}$$

and

$$c_t = (0.7)(10^{-5}) + 0.3(3 \times 10^{-6}) + 3 \times 10^{-6}$$

$$= 1.09 \times 10^{-5} \text{psi}^{-1}. \tag{B-9}$$

From Eq. 2-16,

$$\alpha = 1 - \frac{3 \times 10^{-6}}{1.09 \times 10^{-5}} = 0.72. \tag{B-10}$$

Since no information was given on reservoir pressure, then

$$p \approx \frac{\rho_o H}{144} = \frac{(50.5)(10{,}000)}{144} = 3507 \text{ psi}, \tag{B-11}$$

and from Eq. 2-14,

$$\sigma' = 11{,}483 - (0.72)(3507) \cong 8960 \text{ psi}. \tag{B-12}$$

ρ_f =	2.65 g/cc [165 lb/ft^3]
ρ_o =	50.5 lb/ft^3
c_f =	3×10^{-6} psi
c_o =	10^{-5} psi
c_w =	3×10^{-6} psi

Table B-1—Formation data for Example B-2.

EXAMPLE B-3

Calculation of Horizontal Stresses

Calculate the minimum horizontal stress at 10,000 ft depth for a formation with the properties used in Example B-2. Assume that the Poisson's ratio is 0.25. Will the absolute minimum stress increase or decrease during reservoir depletion?

Solution (Ref. Section 2-4.1)

Equation 2-41a provides the absolute minimum horizontal stress as a function of the vertical stress. The vertical stress is equal to the weight of the overburden. Furthermore, the pore pressure was assumed to be the hydrostatic value. Thus, at 10,000 ft,

$$\sigma_{H,min} = \frac{0.25}{(1 - 0.25)} [11{,}483 - (0.72)(3507)] + (0.72)(3507) = 5511 \text{ psi.} \quad \text{(B-13)}$$

The effective minimum stress is then

$$\sigma'_{H,min} = 5511 - (0.72)(3507) = 2986 \text{ psi.} \quad \text{(B-14)}$$

During depletion a rearrangement of Eq. 2-41a can be instructive:

$$\sigma_{H,min} = \frac{\nu}{1 - \nu} \sigma_v + \alpha p \left(\frac{1 - 2\nu}{1 - \nu} \right). \quad \text{(B-15)}$$

As the pore pressure decreases, the $\sigma_{H,min}$ decreases. For a 1000-psi depletion in the reservoir pressure, the minimum horizontal stress for this formation will decrease by

$$\Delta\sigma_{H,min} = (0.72)(1000) \left(\frac{1 - 0.5}{1 - 0.25} \right) = 480 \text{ psi.} \quad \text{(B-16)}$$

EXAMPLE B-4

Critical Depth for Horizontal vs. Vertical Hydraulic Fractures

Assuming that the Poisson's relationship is in effect and assuming that the horizontal stresses are "locked" in place, what would be the critical depth above which horizontal fractures would be generated if 2000 ft of overburden were removed by some geologic means? Use the formation variables given in Example B-2.

Solution (Ref. Section 2-4.1)

The solution to this problem is outlined in the graphical construction shown in Fig. 2-20. Eq. 2-41a can be rewritten as a function of depth, and with substitution of the calculated variables in Example B-2, it becomes

$$\sigma_{H,min} = 0.55 H. \quad \text{(B-17)}$$

Figure B-2 is a graph of the vertical and minimum horizontal stresses. The "original" vertical stress is shown as a dashed line, whereas the current vertical stress, relieved by 2000 ft of overburden, is shown as a solid line, starting at $H = -2000$ ft. The slope of this curve is also 165/144 = 1.146, as for the "original" vertical stress.

The intercept happens at 3847 ft from the original ground surface or at 1847 ft from the current ground surface. Thus, depths shallower than this will likely develop a horizontal hydraulic fracture, and depths below this level will develop a vertical hydraulic fracture.

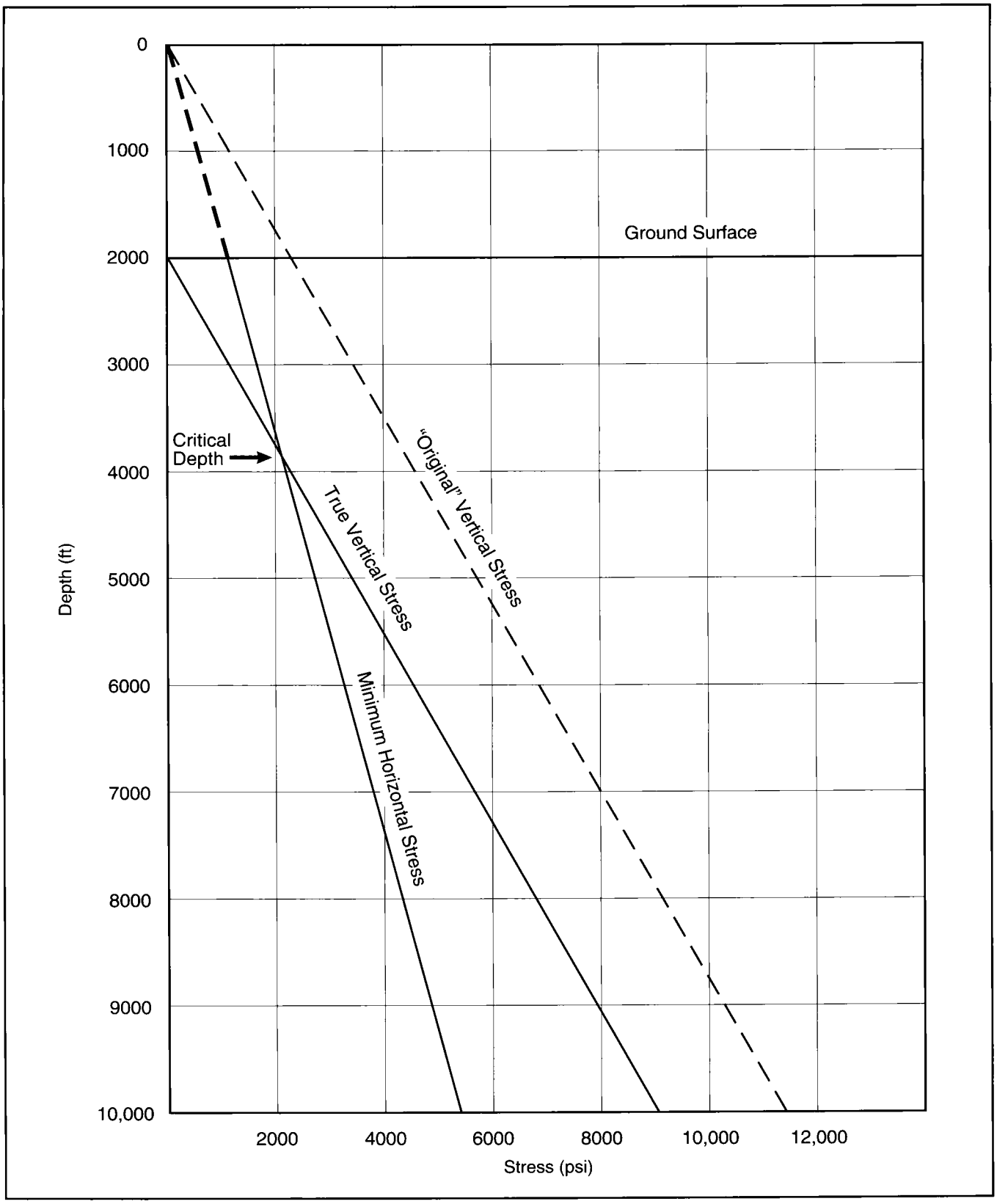

Figure B-2—Critical depth for horizontal hydraulic fractures as calculated for Example B-4.

EXAMPLE B-5

Fracture Initiation Pressure

Calculate the fracture initiation pressure for a formation with $\sigma_{H,min}$ = 5000 psi, $\sigma_{H,max}$ = 6500 psi, p = 3700 psi and T = 500 psi (tensile stress). If this well is 10,000 ft deep, and if a water-base fracturing fluid is used (assume ρ = 60 lb/ft^3), what would be the minimum wellhead pressure to initiate the fracture (i.e., assume zero friction pressure drop in the well).

Solution (Ref. Section 2-4.7)

Equation 2-50 provides the expression for the fracture initiation pressure:

$$p_{breakdown} = 3(5000) - 6500 - 3700 + 500$$
$$= 5300 \text{ psi}. \quad \text{(B-18)}$$

This value is bottomhole. Thus, the hydrostatic pressure head must be subtracted in order to calculate the wellhead pressure requirement:

$$\Delta p_{hydrostatic} = \frac{\rho H}{144} = \frac{(60)(10{,}000)}{144}$$
$$= 4167 \text{ psi}, \quad \text{(B-19)}$$

and therefore the minimum wellhead pressure should be 5300 – 4167 = 1133 psi. This pressure would require a significant addition to account for the friction pressure drop. For example, pumping a crosslinked fluid at 30 BPM down a 3.5-in. tubing may result in a friction pressure drop equal to 150 psi/1000 ft and thus add 1500 psi to the wellhead pressure requirement.

The breakdown pressure calculated from Eq. 2-50 is an upper limit. For a lower limit, Eqs. 2-52 and 2-53 can be used. Thus, assuming that Biot's constant, α, is 0.7 and the Poisson's ratio, ν, is 0.25, then from Eq. 2-53,

$$\eta = \frac{0.7(1 - 0.5)}{2(1 - 0.25)} = 0.233, \quad \text{(B-20)}$$

and

$$p_{breakdown} = \frac{3(5000) - 6500 - 2(0.233)(3700) + 500}{2(1 - 0.233)}$$
$$= 4743 \text{ psi}. \quad \text{(B-21)}$$

EXAMPLE B-6

Estimation of Fracture Height Migration

Calculate the fracture height for 300 psi and 500 psi net pressure for a formation with the confining stresses and data shown in Table B-2.

Solution (Ref. Section 10-2)

Equations 10-3 and 10-4 have the following forms if stresses are in psi, height in ft, density in lb/ft^3 and the critical stress intensity factor in psi $\sqrt{\text{in.}}$. The relevant illustration is Fig. 10-2.

$$\Delta p = \frac{0.0217}{\sqrt{h_u}}\left[K_{Ic}\left(1-\sqrt{\frac{h_u}{h}}\right) + 0.515\,(\sigma_b-\sigma_a)\sqrt{h_u}\,\cos^{-1}\left(\frac{h}{h_u}\right)\right] + 0.0069\,\rho(h_u-0.5h). \quad \text{(B-22)}$$

$$\Delta p = \frac{0.0217}{\sqrt{h_d}}\left[K_{Ic}\left(1-\sqrt{\frac{h_d}{h}}\right) + 0.515\,(\sigma_c-\sigma_a)\sqrt{h_d}\,\cos^{-1}\left(\frac{h}{h_d}\right)\right] - 0.0069\,\rho(h_d-0.5h). \quad \text{(B-23)}$$

In both Eqs. B-22 and B-23, the inverse cosine must be entered in *degrees.*

Table B-3 is a summary of fracture height migration, both upward (from the base of the reservoir) and downward (from the top of the reservoir), and the corresponding net pressures.

Finally, Fig. B-3 is a graph of net pressure, Δp, for both upward and downward fracture height migration. The quantity Δh_u implies migration above the top of the reservoir; Δh_d implies downward migration from the bottom of the reservoir.

From Fig. B-3 at 300 psi net pressure, the upward and the downward fracture migrations would be 24 ft and 12 ft, respectively. For 500 psi net pressure, the upward and the downward fracture height migrations would be 162 ft and 48 ft, respectively.

This exercise demonstrates the means to calculate the allowable net pressure for a tolerable fracture height migration.

σ_a	=	4500 psi
h	=	60 ft
σ_b	=	5100 psi
K_{Ic}	=	1000 psi $\sqrt{\text{in.}}$
σ_c	=	5900 psi
ρ	=	55 lb/ft^3

Table B-2—Confining stresses and data for formation for Example B-6.

$\Delta h_{u,d}$ (ft)	$h_{u,d}$	Δp_u (psi)	Δp_d (psi)
10	70	208	277
20	80	277	370
30	90	323	430
40	100	356	475
60	120	402	536
80	140	433	578
120	180	473	630
150	210	492	656
200	260	514	685

Table B-3—Net pressure required for upward and downward fracture height migration for Example B-6.

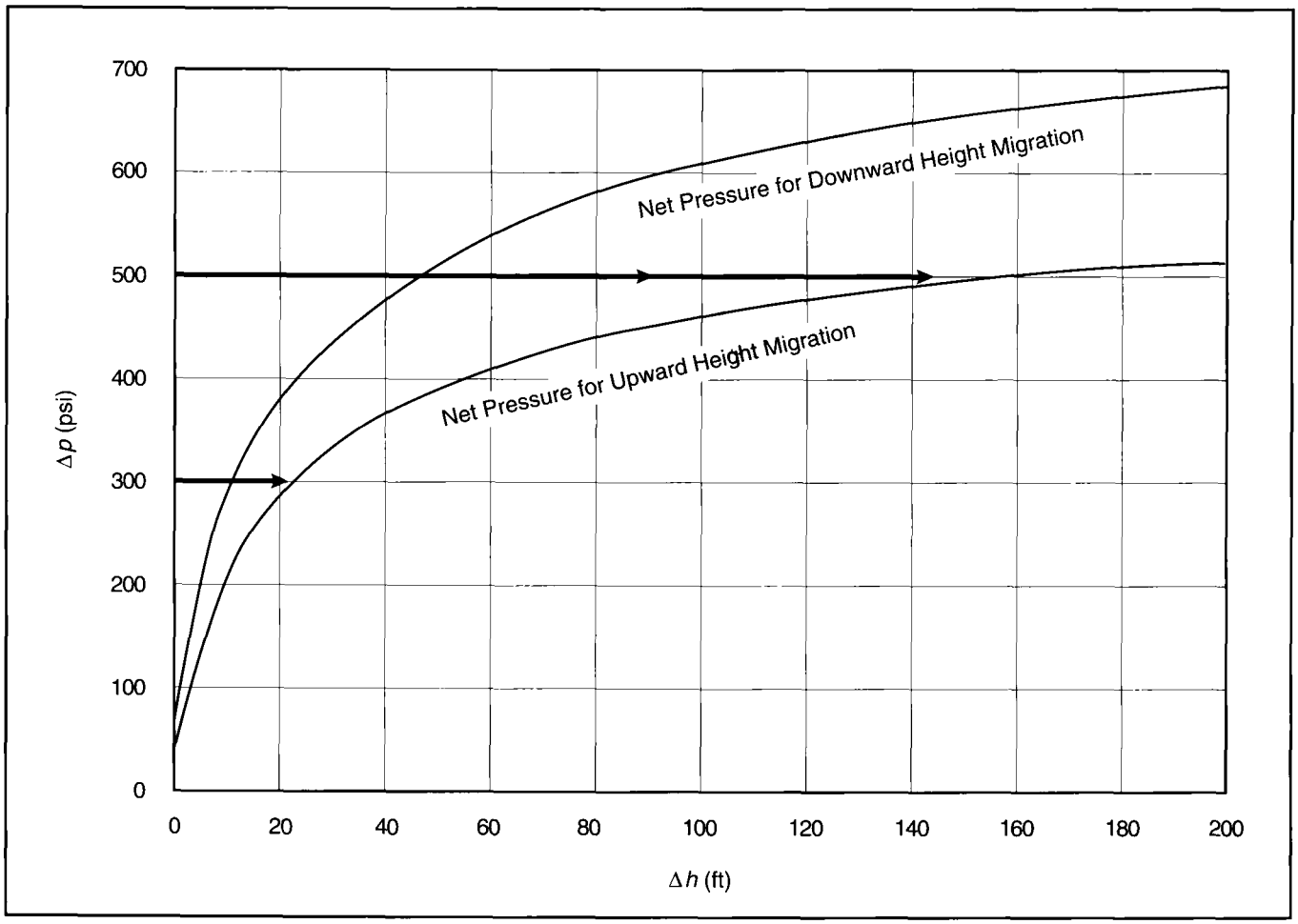

Figure B-3—Net pressure for upward and downward fracture height migration for Example B-6.

EXAMPLE B-7

Failure Envelope and Wellbore Stability

A series of laboratory tests was performed on a typical reservoir sandstone. The tests and data are shown in Table B-4.

Contemplating a completion at 10,000 ft, microhydraulic fracturing tests were conducted and revealed an in-situ stress condition described as:

$$\sigma_v = 11{,}000 \text{ psi}, \ \sigma_{H,min} = 3800 \text{ psi, and } \sigma_{H,max} = 7200 \text{ psi.}$$

Assuming this is a dry hole, will the borehole be stable? If this borehole is to be used as an "injection" well, what is the maximum injection pressure that can be tolerated? If the well will be hydraulically fractured, will it collapse before it reaches tensile failure?

Solution (Ref. Section 2-3)

At first, Mohr circles are drawn, and a typical failure envelope diagram as shown by Fig. 2-9 is constructed. Effective stresses are drawn, and therefore, whenever pore pressures are indicated in Table B-4, these values are subtracted from the confining and ultimate strength values for that test.

Figure B-4 is the graph for the failure envelope for this example. Seven Mohr circles describe a tangent curve, which is the failure envelope. Within this circle the formation is likely to be stable; outside it is unstable.

For this example, the state of stress of the well, a "dry hole," is described by the three circles in Fig. B-5 for each plane formed by the vertical and the two horizontal axes. The controlling plane of stress is the one formed by the minimum horizontal stress (the smallest of the three) and the vertical stress (the largest of the three). These two describe the controlling Mohr circle.

As can be easily concluded, the Mohr circle describing the well, being well within the failure envelope, implies a stable wellbore.

If the well is to be used as an injector, the increase in the pore pressure will result in a proportional decrease of the effective stresses. Since the stresses on the failure envelope are effective, the Mohr circle describing the well will move to the left. This shift, until the well Mohr circle touches the failure envelope, is the maximum tolerable value for the injection pressure to avoid wellbore collapse. The pressure shift (from Fig. B-5) is approximately 5200 psi, which is also the maximum allowable injection pressure.

If the well is to be hydraulically fractured, then from Eq. 2-50 (and assuming $p = 0$),

$$p_{breakdown} = 3(3800) - 7200 + 1600$$
$$= 5800 \text{ psi.} \qquad \text{(B-24)}$$

This value is larger than the one for shear failure. In reality, however, the pore pressure around the well will increase as a result of leakoff. It is a reasonable assumption that the breakdown pressure will be reduced by an amount equal to the increase in the pore pressure. This would imply that the breakdown pressure for this well will be one-half of the one calculated from Eq. B-24 and equal to 2900 psi.

A. Uniaxial tension test—sample broke down at 1600 psi			Circle 1
B. Uniaxial compression test—sample broke down at 18,000 psi			Circle 2
C. Triaxial tests			
Confining Pressure (psi)	**Pore Pressure (psi)**	**Ultimate Strength (psi)**	
5,000	0	32,000	Circle 3
8,000	5,000	34,000	Circle 4
12,000	0	46,000	Circle 5
20,000	5,000	56,000	Circle 6
20,000	0	61,000	Circle 7

Table B-4—Tests and data for Example B-7.

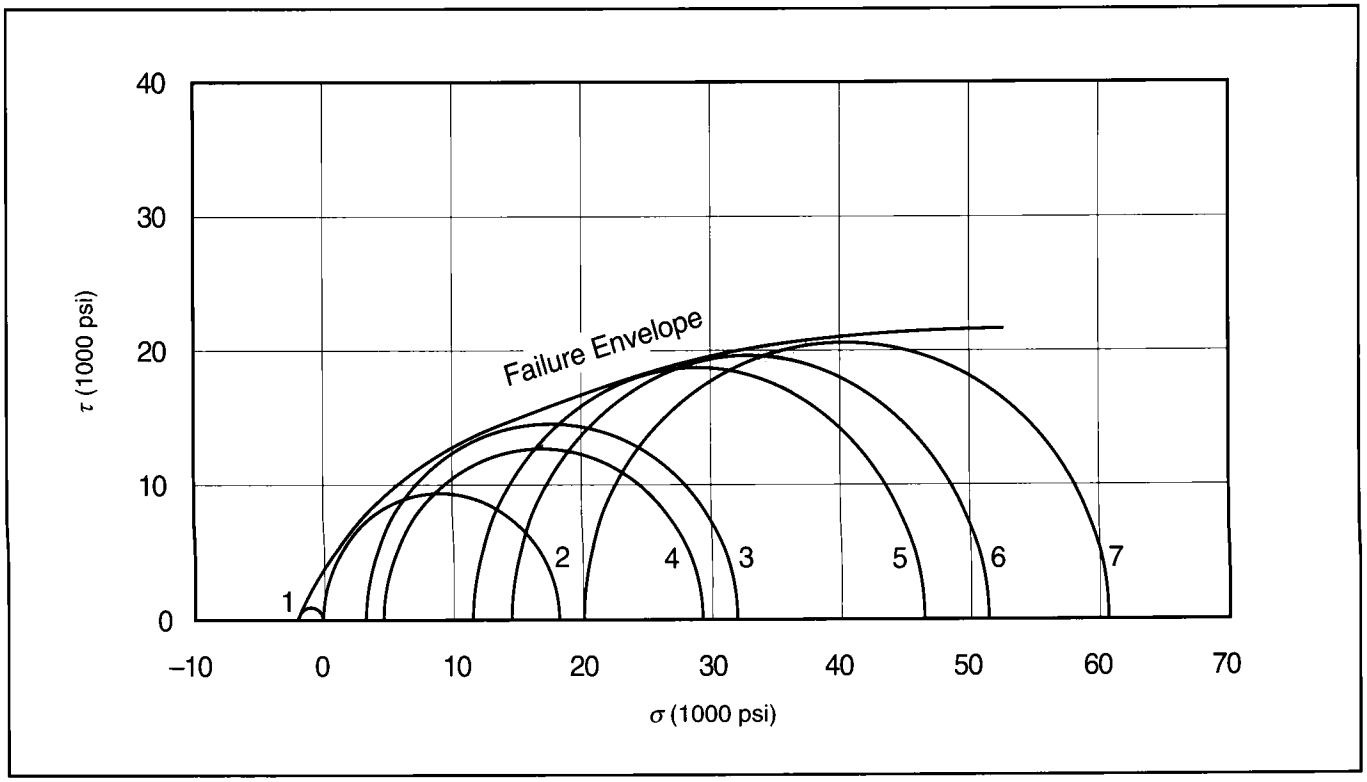

Figure B-4—Failure envelope and Mohr circles for tests for Example B-7.

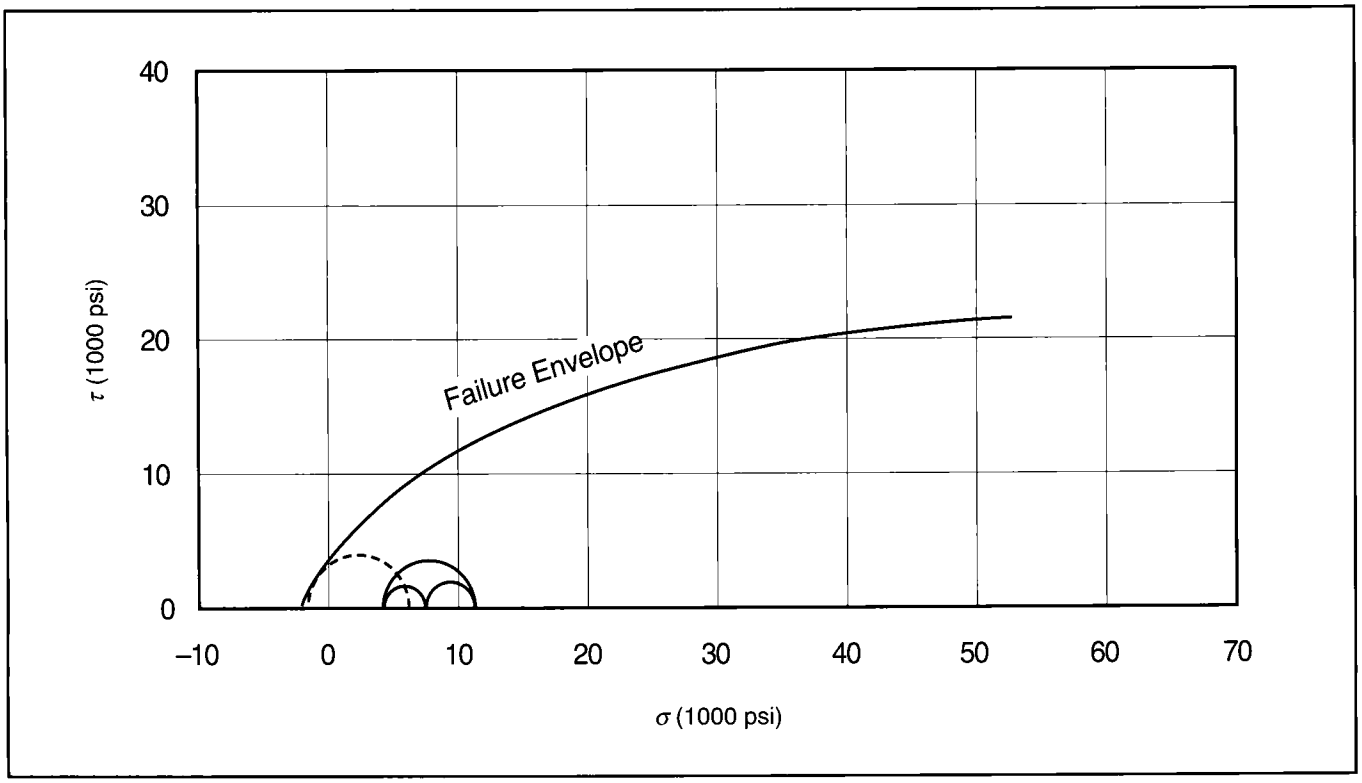

Figure B-5—Graphical solution to wellbore stability problem for Example B-5.

C. Fracturing Fluids and Proppants

EXAMPLE C-1

Determination of Rheological Properties of Power Law Fluids

A hydraulic fracturing fluid has exhibited the experimentally determined behavior shown in Fig. C-1. These data were measured in a concentric cylinder viscometer. Calculate the power law constants, determine the consistency for a pipe and a slot, and plot the apparent viscosity in a pipe for shear rates from 1 to 10^{-3} sec^{-1}. The ratio of the radius of the cup to that of the bob in the viscometer was equal to 2.

Solution (Ref. Sections 5-2.2 and 5-2.3)

From Fig. C-1, the slope is equal to 0.36, and thus $n = n' = 0.36$. The consistency index $K_v = 0.21$ lbf $sec^{n'}/ft^2$, which is obtained from the intercept at $\gamma = 1$. From the top equation in Table 5-1 (and noting that $\beta = 2$),

$$K = (0.21)\left[\frac{2^{2/0.36}(4-1)}{0.36\,(2^{2/0.36}-1)\,2}\right]^{-0.36} = 0.125. \quad \text{(C-1)}$$

Then, the power law for this fluid is from Eq. 5-4:

$$\tau_w = 0.125\dot{\gamma}^{0.36}. \quad \text{(C-2)}$$

From Table 5-1 the consistency index for pipe and slot can be calculated:

$$K_{pipe} = 0.125\left[\frac{3\,(0.36)+1}{4\,(0.36)}\right]^{0.36} = 0.143, \quad \text{(C-3)}$$

and

$$K'_{slot} = 0.125\left[\frac{2\,(0.36)+1}{3\,(0.36)}\right]^{0.36} = 0.148. \quad \text{(C-4)}$$

Finally, the apparent viscosity (again from Table 5-1) is given for a pipe by

$$\mu_a = \frac{47{,}880\,(0.143)}{\gamma^{1-0.36}} = \frac{6847}{\dot{\gamma}^{0.64}}. \quad \text{(C-5)}$$

A graph of the apparent viscosity vs. shear rate is shown in Fig. C-2.

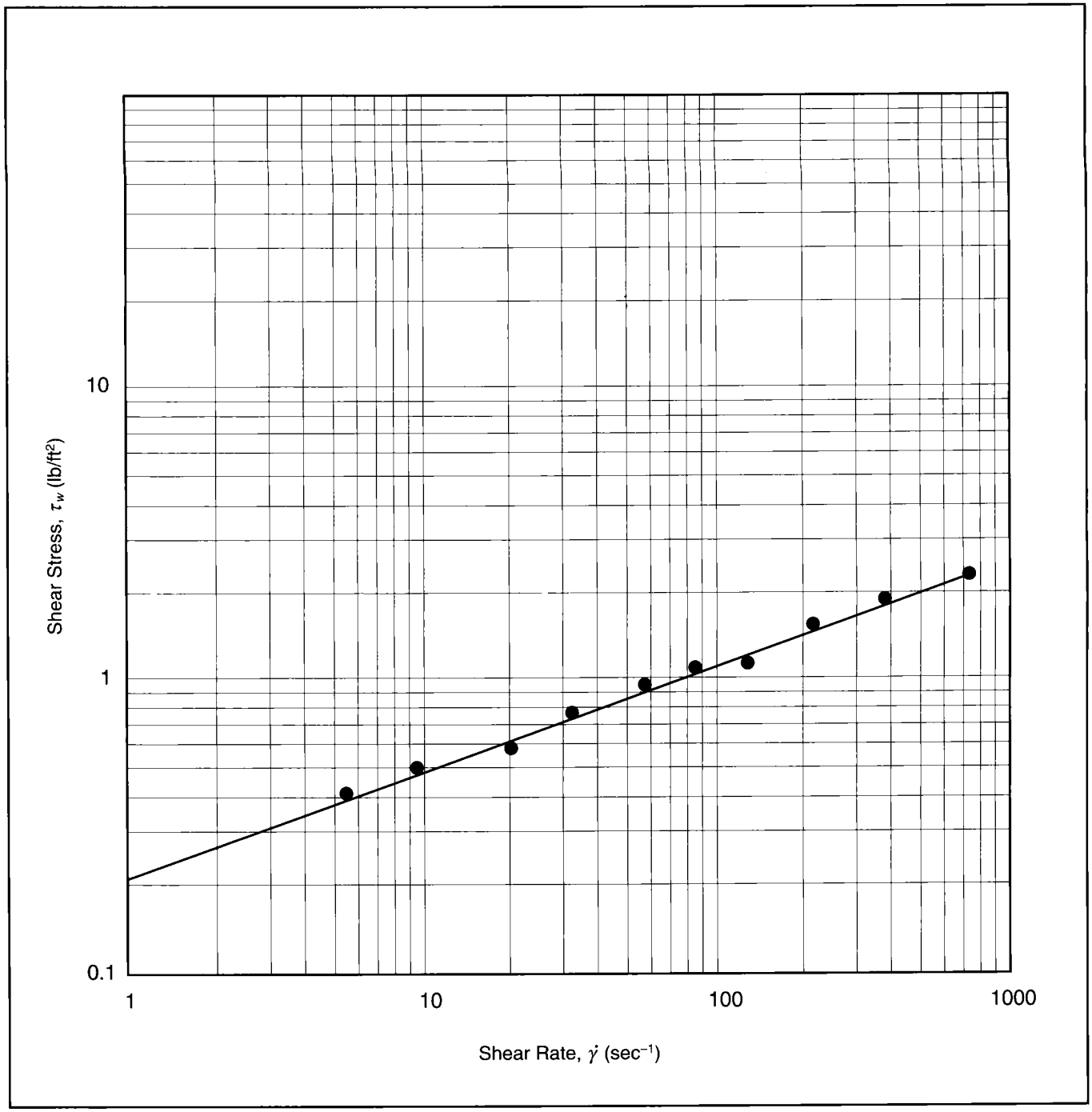

Figure C-1—Experimental data for Example C-1.

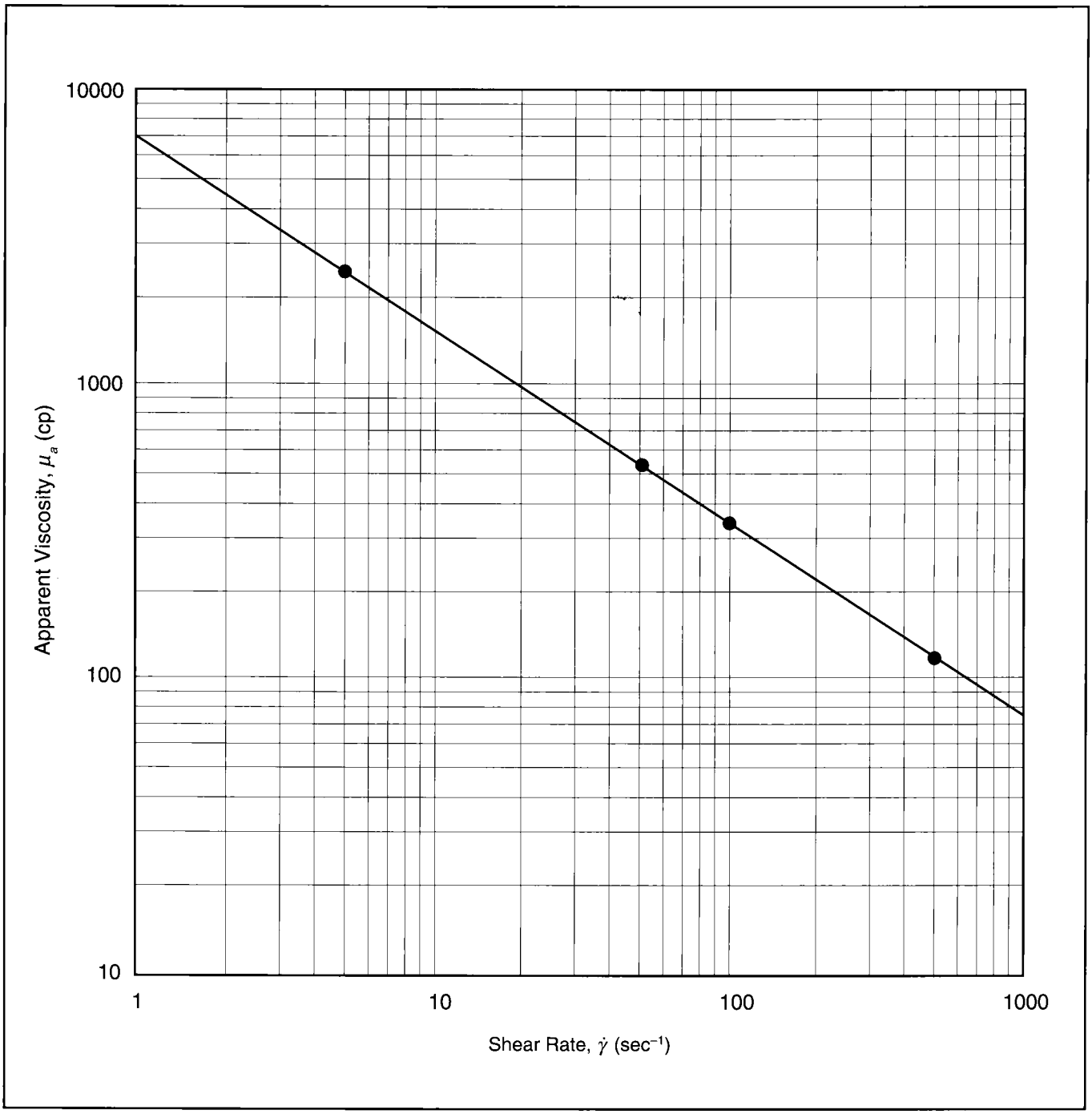

Figure C-2—Apparent viscosity in a pipe for the fluid in Example C-1.

EXAMPLE C-2

Calculation of Total Leakoff Coefficient

Assuming that the filter-cake leakoff coefficient is $C_w = 0.001$ ft/$\sqrt{\text{min}}$ and using the data in Table C-1, calculate the total leakoff coefficient for both the gas-well and the oilwell data.

Solution (Ref. Section 5-7)

From Eq. 5-16, the viscosity control coefficient can be calculated (this is the same for both the oil and the gas well):

$$C_v = 0.0469\sqrt{\frac{(0.001)\,(4000)\,(0.12)}{10}}$$

$$= 0.01 \text{ ft} / \sqrt{\text{min}}. \qquad \text{(C-6)}$$

From Eq. 5-17, the compressibility control coefficient can be calculated.

For the gas well,

$$C_c = (0.0374)\,(4000)\sqrt{\frac{(0.001)\,(0.12)\,(1.2 \times 10^{-4})}{0.025}} = 0.113. \qquad \text{(C-7)}$$

For the oil well,

$$C_c = (0.0374)\,(4000)\sqrt{\frac{(0.001)\,(0.12)\,(10^{-5})}{1}}$$

$$= 0.005. \qquad \text{(C-8)}$$

As can be seen, the compressibility coefficient for an oil well can be a very effective means of leakoff control; for a gas well it is not.

The total leakoff coefficient can be considered as a series of resistances, and thus

$$\frac{1}{C_L} = \frac{1}{0.001} + \frac{1}{0.01} + \frac{1}{0.113}, \qquad \text{(C-9)}$$

leading to $C_L = 9 \times 10^{-4}$ for the gas well. For the oil well a similar calculation leads to $C_L = 7.7 \times 10^{-4}$.

k	=	1 md
Δp	=	4000 psi
ϕ	=	0.12
c_t	=	1.2×10^{-4} psi (gas well)
c_t	=	10^{-5} psi (oil well)
μ	=	0.025 cp (gas well)
μ	=	1 cp (oil well)
μ_L	=	10 cp

Table C-1—Reservoir and fluid data for Example C-2.

EXAMPLE C-3

Leakoff Control Comparisons

Compare the total leakoff coefficient and control of it for Example C-2 assuming that the wall coefficient is halved (5×10^{-4}) or doubled (2×10^{-3}). Repeat the calculation by changing the leakoff viscosity from 10 cp to 1 cp and 100 cp. Use the data for the oil well only.

Solution (Ref. Section 5-7)

The total leakoff coefficient, using the results from Eqs. C-6 and C-8 and calculating it as in Eq. C-9, is equal to 4.7×10^{-4} (for $C_w = 5 \times 10^{-4}$) and 1.6×10^{-3} (for $C_w = 2 \times 10^{-3}$). This is a substantial change from the leakoff coefficient calculated in Example C-2. Essentially, the total leakoff coefficient is halved if C_w is halved and is doubled if C_w is doubled.

If the leakoff viscosity is 1 cp (0.1 of the value used in Example C-2), then the viscosity control coefficient is equal to 0.032 (as in Eq. C-6) and the total leakoff coefficient is equal to 9.6×10^{-4} (a 7% increase from the value in Example C-2).

If the leakoff viscosity is 100 cp (10 times the value in Example C-2), then the viscosity control coefficient is equal to 0.0032 and the total leakoff coefficient is equal to 7.6×10^{-4} (a 15% decrease from the value in Example C-2).

Thus, leakoff control is far more effective using a wall filter cake than by any other mechanism.

EXAMPLE C-4

Friction Pressure Drop Calculation

Calculate the pressure drop per 1000 ft of vertical tubing, with a 3.5-in. outside diameter, for a polymer solution at 100°F. The rheological properties, n' and K'_{pipe}, are 0.39 and 4.5×10^{-2} lbf-sec$^{n'}$/ft^2, respectively. Perform this calculation for a range of injection rates up to 100 BPM. The fluid density is 60 lb/ft^3. Plot the results on log-log paper.

Solution
(Ref. Section 5-2.3 and a fluid mechanics textbook)

To calculate the friction pressure drop for any type flow, the Reynold's numbers must first be calculated. For a power law fluid this is given by

$$N_{Re} = \frac{\rho v^{2-n'} d^{n'}}{K' 8^{n'-1} \left(\frac{3n'+1}{4n'}\right)^{n'}}. \tag{C-10}$$

While Eq. C-10 is for consistent units, for oilfield units it becomes

$$N_{Re} = \frac{0.249 \rho v^{2-n'} d^{n'}}{96^{n'} K' \left(\frac{3n'+1}{4n'}\right)^{n'}}, \tag{C-11}$$

where ρ is in lb/ft^3, v is in ft/sec, d is in in., and K' is in lbf-sec$^{n'}$/ft^2.

The velocity is given by the obvious:

$$v = \frac{q}{A} = \frac{4q}{\pi d^2}, \tag{C-12}$$

and in oilfield units,

$$v = 17.17 \frac{q}{d^2}, \tag{C-13}$$

where q is barrels per minute.

If the N_{Re} is less than 2100, laminar flow is in effect, and in such case the Fanning friction factor is

$$f_f = \frac{16}{N_{Re}}, \tag{C-14}$$

leading to the classic pressure drop resulting from friction

$$\Delta p_f = \frac{2 f_f \rho L v^2}{d}, \tag{C-15}$$

and in oilfield units,

$$\Delta p_f = \frac{5.2 \times 10^{-3} f_f \rho L v^2}{d}, \tag{C-16}$$

where the Δp_f is the pressure in pounds per square inch.

If N_{Re} is greater than 2100, the flow is turbulent and the Fanning friction factor is given by

$$f_f = \frac{c}{N_{Re}{}^b}, \tag{C-17}$$

where

$$c = \frac{\log n' + 2.5}{50}, \tag{C-18}$$

and

$$b = \frac{1.4 - \log n'}{7}. \tag{C-19}$$

The calculation of the pressure drop is then given by Eq. C-16.

A sample calculation is performed with $q = 20$ BPM.

From Eq. C-13 (and remembering that for OD = 3.5 in. the ID $\cong$ 3 in.), the velocity is

$$v = 17.17 \frac{20}{3^2} = 3.81 \text{ ft/sec.} \tag{C-20}$$

From Eq. C-11, the Reynold's number is then calculated:

$$N_{Re} = \frac{(0.249)\ (60)\ (38.1)^{1.61} (3^{0.39})}{(96^{0.39})\ (4.5 \times 10^{-2})\ (1.39)^{0.39}}$$

$$= 2.6 \times 10^4. \tag{C-21}$$

Therefore, the flow is turbulent.

From Eqs. C-17, C-18 and C-19, the friction factor is equal to 0.003, and from Eq. C-16,

$$\Delta p_f = \frac{(5.2 \times 10^{-3})\ (0.003)\ (60)\ (1000)\ (38.1)^2}{3}$$

$$= 453 \text{ psi.} \tag{C-22}$$

Figure C-3 is a plot of the expected pressure drops. Clearly, the laminar and turbulent flow regimes are indicated by the sharp bend in the results. These values are likely to be significantly lower in an actual operation because of the liberal use of friction reducing agents.

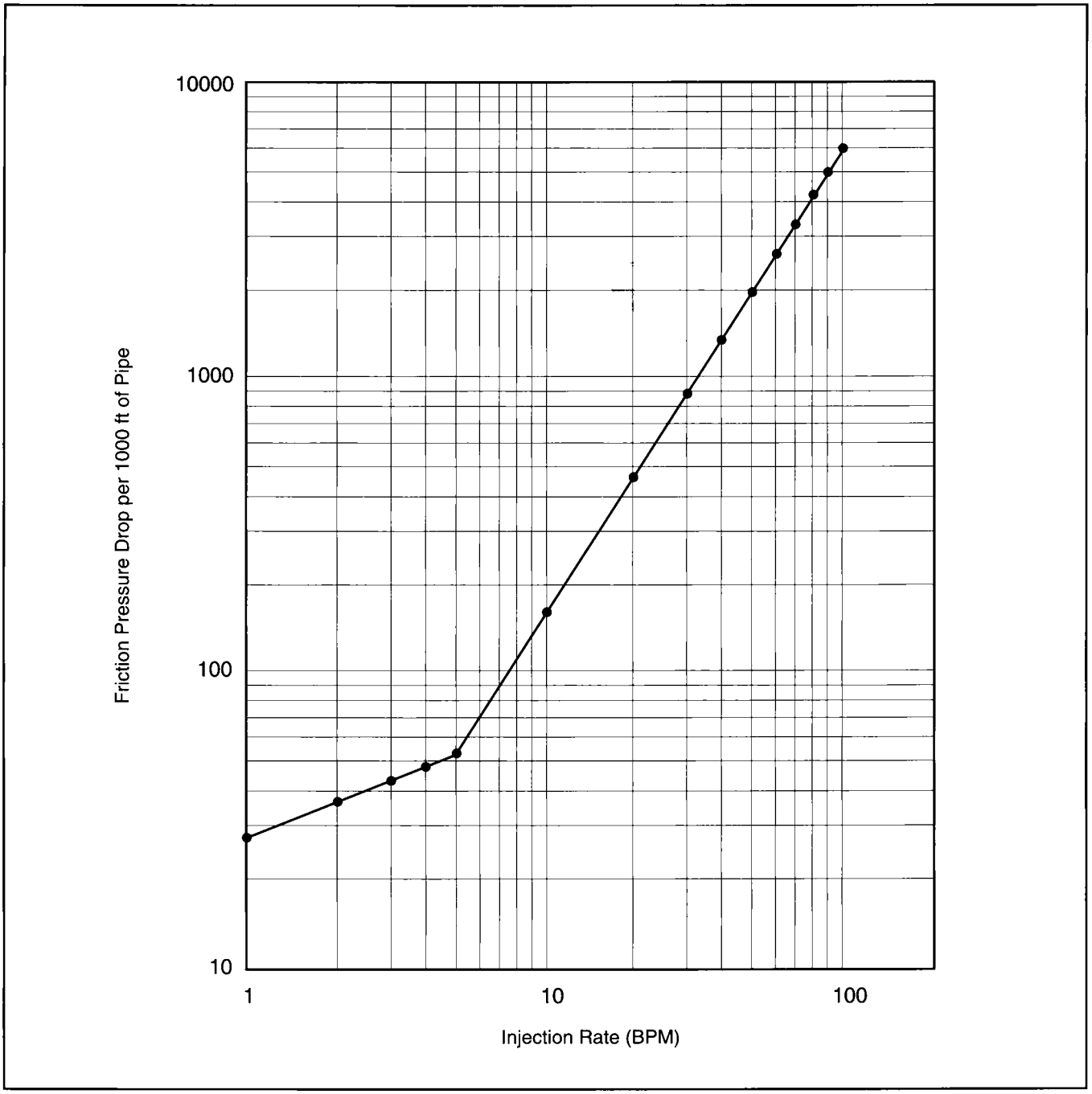

Figure C-3—Friction pressure drops for Example C-4.

EXAMPLE C-5

Shear and Temperature Effects on Apparent Viscosity During Fracturing

Given the rheological properties in Table C-2 and the simulated shear rate and temperature properties shown in Figs. 5-4 and 5-5, determine the apparent viscosities at 100 and 250 ft along the fracture after 25% and 75% of the fluid has been pumped.

Solution (Ref. Section 5-3)

A. 25% of fluid pumped

From Fig. 5-5 the temperature at 100 ft is 185°F and at 250 ft is 200°F (the maximum temperature). From Table C-2, the n' and K' are 0.392 and 0.258 (interpolation) and 0.4133 and 0.1169, respectively.

From Fig. 5-4, the shear rate is 130 sec^{-1} at 100 ft and 300 sec^{-1} at 250 ft.

The apparent viscosity is given by

$$\mu_a = 47{,}880\ K'\dot{\gamma}^{n'-1}, \qquad \text{(C-23)}$$

and thus at 100 ft,

$$\mu_a = (47{,}880)\ (0.258)\ (130^{-0.602}) = 660\ \text{cp}; \qquad \text{(C-24)}$$

whereas at 250 ft,

$$\mu_a = (47{,}880)\ (0.1169)\ (300^{-0.587}) = 197\ \text{cp}. \qquad \text{(C-25)}$$

This is a substantial reduction in the viscosity, and it has a major effect on the expected role of the pad fluid, which is to generate the desired fracture widths.

B. 75% of fluid pumped

Again, from Fig. 5-5 the temperatures are 155°F and 200°F, respectively, for the 100-ft and 250-ft locations. From Table C-2 the rheological properties for 155°F are 0.350 and 0.403, respectively.

From Fig. 5-4, the shear rate is 50 sec^{-1} at 100 ft and 60 sec^{-1} at 250 ft.

Thus,

$$\mu_a = (47{,}880)\ (0.350)\ (50^{-0.597}) = 1621\ \text{cp} \qquad \text{(C-26)}$$

at 100 ft, and

$$\mu_a = (47{,}880)\ (0.1169)\ (60^{-0.587}) = 506\ \text{cp} \qquad \text{(C-27)}$$

at 250 ft.

Temp (°F)	Time (hr)	n'	K'
125	0	0.4003	0.3735
	1	0.4120	0.3470
	2	0.4125	0.3449
	3	0.4145	0.3384
150	0	0.3437	0.4163
	1	0.3522	0.3839
	2	0.3579	0.3514
	3	0.3630	0.3231
	4	0.3994	0.2525
175	0	0.3770	0.3524
	1	0.3881	0.3082
	2	0.3942	0.2762
	3	0.3945	0.2575
200	0	0.4133	0.1169
	1	0.5686	0.0339
	2	0.6895	0.0139

Table C-2—Rheology of a borate crosslinked fluid containing 40-lb/1000 gal hydroxypropyl guar.

EXAMPLE C-6

Calculation of Settling Velocity

Using the data in Table C-3, calculate the settling velocity for a particle with a diameter equal to 2.5×10^{-4} m.

Solution (Ref. Section 5-6)

From Eq. 5-12, which is the modified Stokes law,

$$u_t = \frac{(9.78)\ (2650 - 1000)(2.5 \times 10^{-4})^2}{18\,(2)} + \frac{(9.78)\ (2650 - 1000)\ (2.5 \times 10^{-4})^2}{18\ (4)} \left(\frac{u_t}{2.5 \times 10^{-4}}\right)^{0.63}, \quad \text{(C-28)}$$

and

$$u_t = 2.8 \times 10^{-5} + 2.6 \times 10^{-3} u_t^{0.63}, \quad \text{(C-29)}$$

leading to $u_t = 3.18 \times 10^{-5}$ m/s.

ρ_{fluid}	=	1000 kg/m^3
$\rho_{proppant}$	=	2650 kg/m^3
n'	=	0.37
K'	=	4 Pa – $s^{n'}$
μ_o	=	2 Pa – s
d_p	=	2.5×10^{-4} m
g	=	9.78 m/sec^2

Table C-3—Data for Example C-6.

EXAMPLE C-7

Calculation of Stress-Induced Proppant-Pack Permeability Impairment: Long-Term Stresses

Use the data in Fig. 5-27 for 20/40 sand to calculate the stress-induced permeability reduction for 2000 and 4000 psi drawdown. Will the stress on the proppant pack increase or decrease with time? Assume that the reservoir is 10,000 ft deep with an average density equal to 165 lb/ft^3, the Poisson's ratio is 0.25, the initial reservoir pressure is 6500 psi, and the poroelastic constant is 0.7.

Solution (Ref. Section 5-9)

The effective minimum horizontal stress can be estimated from Eq. 2-41:

$$\sigma'_{H,min} = \frac{0.25}{0.75}\left[\frac{(165)\ (10{,}000)}{144} - (0.7)\ (6500)\right]$$

$$= 2303 \text{ psi.} \qquad \text{(C-30)}$$

This is the stress that the proppant will experience without drawdown. Thus, the proppant-pack permeability will be about 300,000 md (from Fig. 5-27).

With a 2000-psi drawdown (p_{wf} = 4500 psi) experienced near the wellbore, the instantaneous effective stress will increase by (0.7) (2000) = 1400 (σ' = 3700 psi); with a 4000-psi drawdown (p_{wf} = 2500 psi), the effective stress will increase by (0.7) (4000) = 2800 (σ' = 5100 psi) and result in permeability values equal to 200,000 and 150,000 md, respectively.

In the long term, the reservoir pressure will decline. As a result, the *absolute* minimum horizontal stress will decrease (e.g., for $\bar{p}$ = 5000 psi) as given by

$$\sigma_{H,min} = \frac{0.25}{0.75}\left[\frac{(165)\ (10{,}000)}{144} - (0.7)\ (5000)\right]$$

$$+ (0.7)\ (5000) = 6152 \text{ psi.} \qquad \text{(C-31)}$$

With the 4500-psi bottomhole pressure,

$$\sigma'_{H,min} = 6152 - (0.7)\ (4500) = 3000 \text{ psi;} \qquad \text{(C-32)}$$

and with the 2500-psi bottomhole pressure,

$$\sigma'_{H,min} = 6152 - (0.7)\ (2500) = 4400 \text{ psi.} \qquad \text{(C-33)}$$

Thus, the effective stress on the proppant decreases with time.

D. Fracture Calibration Treatments

EXAMPLE D-1

Calculation of the Fracture Length from Material Balance

Calculate the fracture half-length for the well, reservoir and treatment variables listed in Table D-1. What would be the impact of doubling the leakoff coefficient? What if it were an order of magnitude larger?

Solution (Ref. Section 7-2)

Since $h_p = 75$ ft and $h_f = 150$ ft, then $r_p = 0.5$.

From Eq. 7-7 (converting appropriate units) and using $2g_o \cong 3$,

$$x_f = \frac{(40)\,(5.615)\,(1)\,(60)}{(2)\,(150)\left[(0.2 / 12) + (3)\,(10^{-3})\,(0.5)\,(\sqrt{60})\right]}$$

$$= \frac{13{,}476}{300\,(0.0167 + 0.0116)} = 1587\,\text{ft}. \qquad \text{(D-1)}$$

The relative impact of the created fracture width (first term within the brackets in the denominator) and leakoff (the second term) can be compared readily.

Doubling the leakoff coefficient (or, conversely, halving it by its control) has a much more pervasive influence on the created length than the ability to increase the fracture width.

For this exercise, doubling the leakoff coefficient to 2×10^{-3} ft/$\sqrt{\text{min}}$ would result in a reduction in the fracture length to 1126 ft. If it were an order of magnitude larger, the fracture half-length would be 338 ft.

q_i	=	40 BPM
h_f	=	150 ft
w	=	0.2 in.
h_p	=	75 ft
t_p	=	1 hr
C_L	=	10^{-3} ft/$\sqrt{\text{min}}$

Table D-1—Well, reservoir and treatment variables for Example D-1.

A complete example for pressure decline is included in Reservoir Stimulation. *Only additional calculations are included in this volume.*

EXAMPLE D-2

Analysis of Pressure Profile During Pumping

Given the pressure data in Table D-2, conclude on the type of fracture generated and estimate the efficiency of the fracturing fluid. The power law exponent n' is 0.51.

Solution (Ref. Section 7-3)

Figure D-1 is a log-log plot of the bottomhole pressure increase vs. time. As can be seen readily, the increasing pressure trend suggests a normally propagating and contained PKN fracture. The slope, m, of the formed straight line is equal to 0.2.

From Eq. 7-46, if $\eta = 0$ the slope should be

$$m = \frac{1}{4\,(n' + 1)} = 0.166. \qquad \text{(D-2)}$$

Whereas if $\eta = 1$ from Eq. 7-47, the slope should be

$$m = \frac{1}{2n' + 3} = 0.249. \qquad \text{(D-3)}$$

By linear interpolation the efficiency is

$$\eta = \frac{0.2 - 0.166}{0.249 - 0.166} = 0.41. \qquad \text{(D-4)}$$

t (min)	Δp (psi)	t (min)	Δp (psi)
1	315	25	600
2	362	30	622
3	392	35	641
4	416	40	659
5	435	45	674
6	451	50	689
7	465	55	702
8	477	60	714
9	489	65	726
10	499	70	737
15	541	75	747
20	573		

Table D-2—Fracturing pressure data for Example D-2.

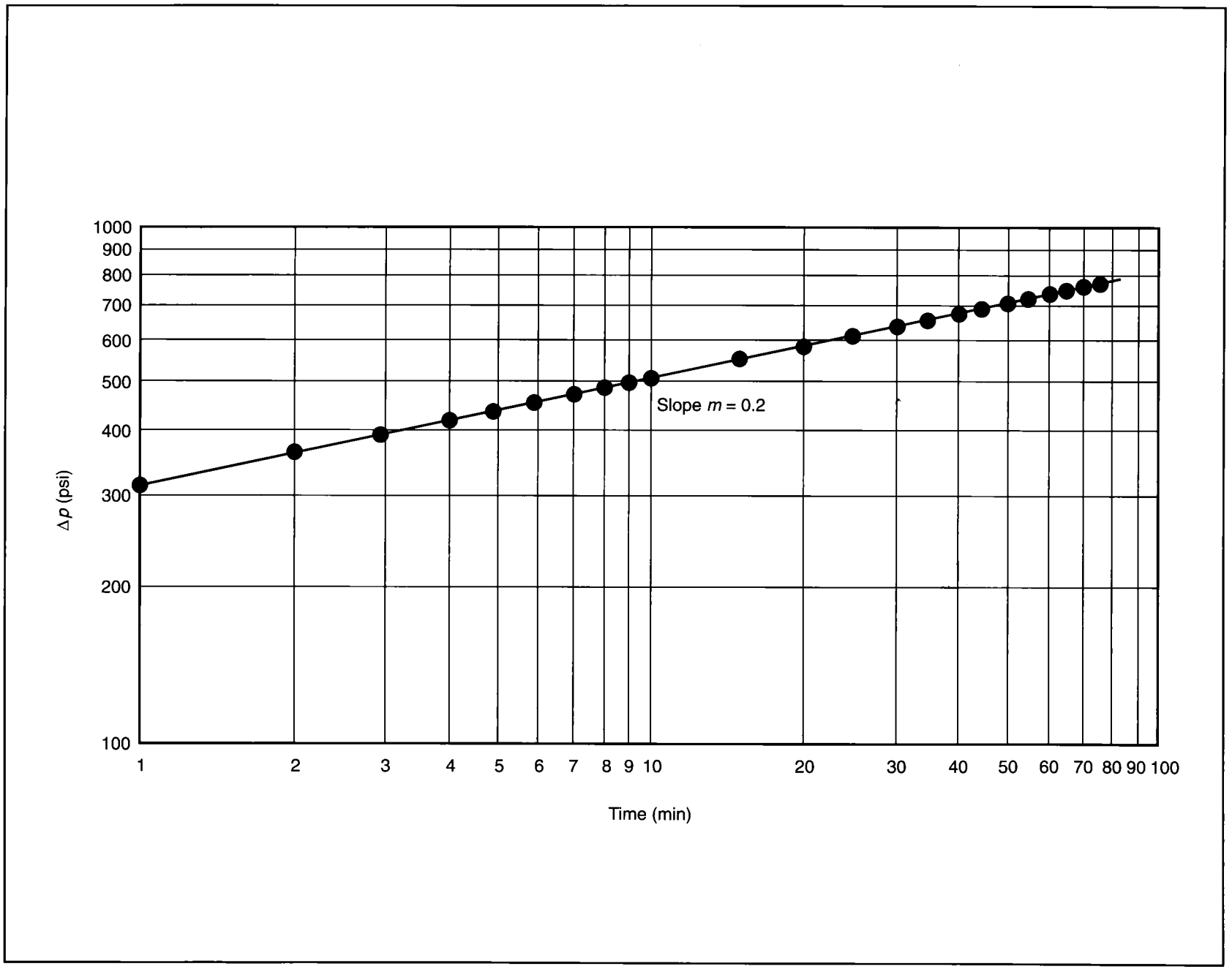

Figure D-1—Log-log plot of net pressure vs. time for Example D-2.

EXAMPLE D-3

Use of a Derivative Function in the Interpretation of Pressure During Pumping

Develop a pressure derivative function to interpret and confirm pressure patterns during pumping. Apply this to the PKN model for $\eta = 1$, $n' = 0.5$, and $\Delta p_f(1\text{min}) = 200$ psi.

Solution (Ref. Section 7-3)

All observed net pressures (irrespective of the model) are powers of t of the form

$$\Delta p_f = C_1 t^{C_2}, \tag{D-5}$$

where C_1 and C_2 are constants.

As given by Eqs. 7-46 to 7-51, log-log plots of Δp_f vs. t not only reveal the type of model in effect but also give a notion of the fluid efficiency (as shown in Example D-2).

These patterns can be identified and corroborated through the use of a derivative function as in pressure transient analysis given by Eq. 1-56.

Applying this function to Eq. D-5,

$$\frac{d\Delta p_f}{d\ln t} = t\frac{d\Delta p_f}{dt} \tag{D-6}$$

and

$$\frac{d\Delta p_f}{d\ln t} = tC_1C_2t^{C_2-1} = C_1C_2t^{C_2}. \tag{D-7}$$

Equation D-7 suggests that this derivative function would be parallel to the net pressure function, also forming the same log-log slope. The distance between the two lines would be log C_2. C_1 is the pressure value at $t = 1$, and C_2 is the slope of the net pressure curve. In fact, if and only if the two curves are parallel, the model (implied by Eqs. 7-46 to 7-51) is in effect.

In dealing with real data, the derivative function in Eq. D-6 is simply the slope of the net pressure data at any point multiplied by its corresponding value of time.

Applying this technique to the PKN model for $\eta = 1$ and $n' = 0.5$, then Eq. 7-47 becomes

$$\Delta p_f = 200t^{0.25}. \tag{D-8}$$

The derivative function would be

$$t\frac{d\Delta p_f}{dt} = 50t^{0.25}. \tag{D-9}$$

Figure D-2 is a plot of both net pressure and its derivative function. This type of analysis is helpful in dealing with real data, especially to detect deviations from the patterns predicted by the model. Derivatives respond faster for the visual inspection of data trends, as has been the case for pressure transient analysis.

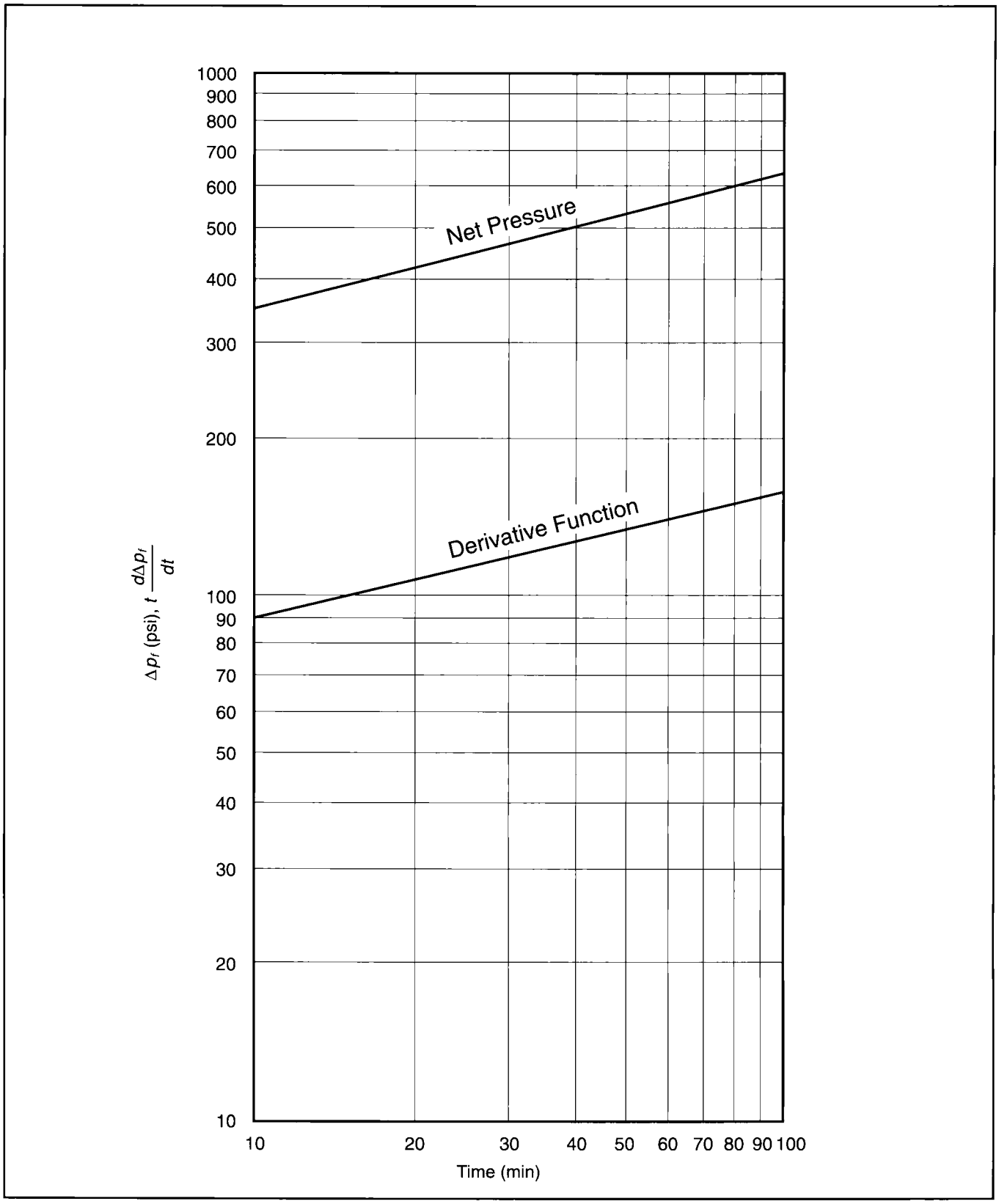

Figure D-2—Net pressure and pressure derivative for Example D-3.

EXAMPLE D-4

Calculation of Fracture Penetration and Net Pressure Increase vs. Time

Develop the relationships that would provide the fracture penetration and net pressure increase for the PKN model ($\eta = 1$). Apply this calculation to the reservoir with the variables in Table D-3.

Solution (Ref. Sections 3-3.43 and 7-3)

For $\eta \rightarrow 1$, from Eqs. 7-37 and 7-40 for the PKN model,

$$x_f = \frac{q_i t}{2h_f w}. \tag{D-10}$$

The average width, w, for a non-Newtonian fluid can be obtained from Eqs. 3-62 and 3-72 (and using a geometric factor to convert from maximum to average width). This results in

$$w = \left(\frac{\pi\gamma}{4}\right)\left[\left(\frac{128}{3\pi}\right)(n'+1)\left(\frac{2n'+1}{n'}\right)^{n'}\left(\frac{0.9775}{144}\right)\left(\frac{5.61}{60}\right)^{n'}\right]^{\frac{1}{2n'+2}}\left[\frac{q^{n'}K'x_f h_f^{1-n'}}{E}\right]^{\frac{1}{2n'+2}}. \tag{D-11}$$

Using all multipliers of $x_f^{1/(2n'+2)}$ as a constant, C_1, then from Eq. D-10,

$$x_f\left(C_1 x_f^{1/(2n'+2)}\right) = \frac{5.615 q_i t}{2h_f}, \tag{D-12}$$

and finally

$$x_f = \frac{1}{C_1}\left(\frac{5.615 q_i t}{2h_f}\right)^{(2n'+2)/(2n'+3)}. \tag{D-13}$$

From Eq. 7-13 for the PKN model,

$$\Delta p_f = \frac{w_{max} E}{2(1-\nu^2)h_f}, \tag{D-14}$$

and from Eqs. D-11 and D-12

$$\Delta p_f = \frac{C_1}{(\pi\gamma/4)} x_f^{1/(2n'+2)} \frac{E}{2(1-\nu^2)h_f}. \tag{D-15}$$

From Eq. D-11 and using the variables in Table D-3, the constant C_1 can be calculated:

$$C_1 = (0.589)(0.4395)(0.00753)$$

$$= 1.95 \times 10.^{-3} \tag{D-16}$$

From Eq. D-13,

$$x_f = 559.4 t^{0.75}, \tag{D-17}$$

where t is in minutes.

From Eq. D-15,

$$\Delta p_f = 53 x_f^{0.333}. \tag{D-18}$$

Table D-4 contains the results of this simulation for 10 min of pumping.

q_i	= 40 BPM
n'	= 0.5
t	= 10 min
K	= 0.02 lbf – sec$^{n'}$/ft^2
h_f	= 100 ft
E	= 3 × 10^6 psi
ν	= 0.25
γ	= 0.75

Table D-3—Well and reservoir variables for Example D-4.

t (min)	x_f (ft)	Δp_f (psi)
1	559	436
2	941	518
3	1275	573
4	1582	616
5	1870	651
6	2144	682
7	2407	708
8	2661	733
9	2907	754
10	3146	775

Table D-4—Fracture penetration and net pressure for Example D-4.

EXAMPLE D-5

Calculation of Distance to Restricted Fracture

Assume that after 30 min of pumping the pressure starts increasing at 200 psi/min. If $E' = 3 \times 10^6$ psi, $q_i = 40$ BPM and $h = 50$ ft, calculate the maximum distance to the point of restricted fracture.

Solution (Ref. Section 7-3.3)

Since $dp_w/dt = m = 200$ psi/min, then from Eq. 7-57,

$$x_f = \frac{2E'\eta q_i}{\pi h_f^2 m}. \qquad \text{(D-19)}$$

For the upper bound of the x_f value, $\eta = 1$, and therefore,

$$x_f = \frac{(2)\ (3 \times 10^6)\ (40 \times 5.615)}{(3.14)\ (50^2)\ (200)} = 860\,\text{ft}. \qquad \text{(D-20)}$$

EXAMPLE D-6

Comparison of Fluid Loss During Pumping and During Closure

If the pumping time and the closure time is the same (30 min), calculate the total fluid lost during pumping and closure. Use $C_L = 10^{-3}$ ft/min$^{1/2}$, $x_f = 1000$ ft, $h = 100$ ft and $h_f = 200$ ft. In both cases use an average between the upper and lower bounds.

Solution (Ref. Section 7-4.1)

From Eq. 7-66 and remembering that $A_p = 4x_f h_f$,

$$V_{Lp} = (2)\ (10^{-3})\ (4)\ (1000)\ (100)\ (30)^{1/2}$$

$$\frac{(4/3) + (\pi/2)}{2} = 6360\,\text{ft}^3 = 1133\,\text{bbl}. \qquad \text{(D-21)}$$

From Eq. 7-70 and since $\Delta t_D = 1$,

$$g(\Delta t_D) = \frac{2.44 + 2.57}{2} = 2.51. \qquad \text{(D-22)}$$

From Eq. 7-71,

$$g_o = \frac{1.33 + 1.57}{2} = 1.45. \qquad \text{(D-23)}$$

Then, finally, from Eq. 7-69 (and remembering that $r_p A_f = A_p$),

$$V_{Ls} = (2)\ (10^{-3})\ (4)\ (1000)\ (100)\ (30)^{1/2}$$

$$(2.51 - 1.45) = 4645\,\text{ft}^3 = 827\,\text{bbl}. \qquad \text{(D-24)}$$

Invariably, the rate of fluid loss during pumping is larger than during closure.

EXAMPLE D-7

Calculation of Fluid Efficiency from Closure Time

If the pumping time and the closure time of a calibration treatment are 30 and 15 min, respectively, what is the fluid efficiency? What would the closure time be for an efficiency equal to 0.75?

Solution (Ref. Section 7-4.1)

The dimensionless closure time Δt_D is given by

$$\Delta t_D = \frac{15}{30} = 0.5. \qquad \text{(D-25)}$$

Thus, from Fig. 7-18 (between the two bounds), $\eta \cong 0.3$.

If $\eta = 0.75$, then from Fig. 7-18, $\Delta t_D = 7$, and therefore $\Delta t = (7)\ (30) = 210$ min.

EXAMPLE D-8

Closure Time with Proppant

If 300,000 lb of proppant are pumped in a 500,000-gal total injection treatment, what should the closure time be? Use the treatment variables in Table D-5.

Solution (Ref. Section 7-4.1)

From Eq. 7-78,

$$v_{prop} = \frac{300{,}000}{(165)\ (1 - 0.37)\ (500{,}000 / 7.48)}$$

$$= 0.043. \qquad \text{(D-26)}$$

From Eq. 7-85,

$$\eta = 0.043\ (1 - 0.4) + 0.4 = 0.426. \qquad \text{(D-27)}$$

Since the injection rate is 30 BPM, then

$$t_p = \frac{500{,}000 / 42}{30} = 397 \text{ min.} \qquad \text{(D-28)}$$

With an efficiency equal to 0.426 from Fig. 7-18, $\Delta t_D \cong 1.2$, and therefore $\Delta t = (1.2)\ (397) \cong 476$ min (8 hr).

q_i	= 30 BPM
ρ_{prop}	= 165 lb/ft^3
η'	= 0.4 (from a calibration treatment)
ϕ_{prop}	= 0.38

Table D-5—Treatment variables for Example D-8.

EXAMPLE D-9

Impact of Fracture Height on Leakoff Coefficient and Fracture Length Calculation

Repeat the calculation in Section 7-4.5.1 but use $h_f = 140$ ft (instead of 70 ft). Use the same well and pressure data as in Tables 7-4 and 7-5.

Solution (Ref. Sections 7-4.5 and 7-4.5.1)

The fracture compliance can be calculated from Eq. 7-23a, and thus,

$$c_f = \frac{(3.14)\ (0.74)\ (140)}{(2)\ (4.3 \times 10^6)} = 3.8 \times 10^{-5}\ \text{ft/psi}. \quad \text{(D-29)}$$

This compares with 1.9×10^{-5} ft/psi for the example in Section 7-4.5.1.

The leakoff coefficient can then be found from Eq. 7-96:

$$C_L = \frac{(2)\ (465)\ (3.8 \times 10^{-5})}{(3.14)\ (50\ /\ 140)\ \sqrt{35}}$$

$$= 5.3 \times 10^{-3}\ \text{ft/min}^{1/2} \quad \text{(D-30)}$$

which is four times larger than the value in Section 7-4.5.1.

The fracture half-length can then be calculated from Eq. 7-87 using $\eta = 0.46$, $V_i = 2850\ \text{ft}^3$ and $g_o = 1.52$ (from Table 7-3, $\alpha = 0.6$). Thus,

$$x_f = \frac{(1 - 0.46)\ (2850)}{(2 \times 140)\ (2 \times 1.52)\ (5.3 \times 10^{-3})\ (50\ /\ 140)\ \sqrt{35}}$$

$$\cong 165\ \text{ft}, \quad \text{(D-31)}$$

which is one-fourth of the value calculated in Section 7-4.5.1.

This Page Intentionally Left Blank

E. Design and Modeling of Propped Fractures

EXAMPLE E-1

Calculation of Transient IPR Curves

Calculate transient inflow performance relationships (IPR) for 10 days, 30 days and 365 days using the data given in Table E-1. Use bottomhole pressures, above and below the bubblepoint pressure.

Solution (Ref. Section 8-2.1)

From Eq. 8-5,

$$F_{CD} = \frac{750}{(0.05)\ (1500)} = 10. \qquad \text{(E-1)}$$

Since A = 320 acres, the side of the square is 3734 ft, and the reservoir half-length is 1867 ft, which can contain the designed fracture half-length. Thus, Fig. 8-2 for F_{CD} = 10 can be used for the forecast.

For t = 10 days, the dimensionless time can be calculated from Eq. 8-3:

$$t_{Dxf} = \frac{(0.000264)\ (0.05)\ (10)\ (24)}{(0.11)\ (0.7)\ (10^{-5})\ (1500)^2}$$

$$= 1.83 \times 10^{-3}. \qquad \text{(E-2)}$$

From Fig. 8-2, p_D = 0.15, and from Eq. 8-6, the flow rate, if the flowing bottomhole pressure is the bubblepoint pressure, can be calculated:

$$q_b = \frac{(0.05)\ (50)\ (6300 - 4700)}{(141.2)\ (1.1)\ (0.7)\ (0.15)} = 245 \text{ STB/d}. \qquad \text{(E-3)}$$

From Eqs. 8-7 and 8-8,

$$q_{Vogel} = \frac{(245)\ (4700)}{(6300 - 4700)\ (1.8)} = 400 \text{ STB/d}, \qquad \text{(E-4)}$$

and finally, from Eq. 8-9,

$$q = 245 + 400\left[1 - 0.2\left(\frac{p_{wf}}{4700}\right) - 0.8\left(\frac{p_{wf}}{4700}\right)^2\right]. \qquad \text{(E-5)}$$

For t = 30 days, the $t_{Dxf} = 5.5 \times 10^{-3}$ and p_D (from Fig. 8-2) is 0.23. Then, from Eq. 8-6, q_b = 160 STB/d, and from Eqs. 8-7 and 8-8, q_{Vogel} = 261 STB/d. Finally, from Eq. 8-9,

$$q = 160 + 261\left[1 - 0.2\left(\frac{p_{wf}}{4700}\right) - 0.8\left(\frac{p_{wf}}{4700}\right)^2\right]. \qquad \text{(E-6)}$$

For t = 365 days, $t_{Dxf} = 6.7 \times 10^{-2}$ and p_D (from Fig. 8-2) is 0.6. Then, from Eq. 8-6, q_b = 61 STB/d, and from Eqs. 8-7 and 8-8, q_{Vogel} = 100 STB/d. From Eq. 8-9,

$$q = 61 + 100\left[1 - 0.2\left(\frac{p_{wf}}{4700}\right) - 0.8\left(\frac{p_{wf}}{4700}\right)^2\right]. \qquad \text{(E-7)}$$

Figure E-1 contains the standard q vs. p_{wf} plots for the three transient IPRs as calculated from Eqs. E-5, E-6 and E-7.

k	=	0.05 md
p_i	=	6300 psi
h	=	50 ft
p_b	=	4700 psi
ϕ	=	0.11
A	=	320 acres
c_t	=	10^{-5} psi^{-1}
x_f	=	1500 ft
B_o	=	1.1 res bbl/STB
$k_f w$	=	750 md-ft
μ_o	=	0.7 cp

Table E-1—Well and reservoir design data for Example E-1.

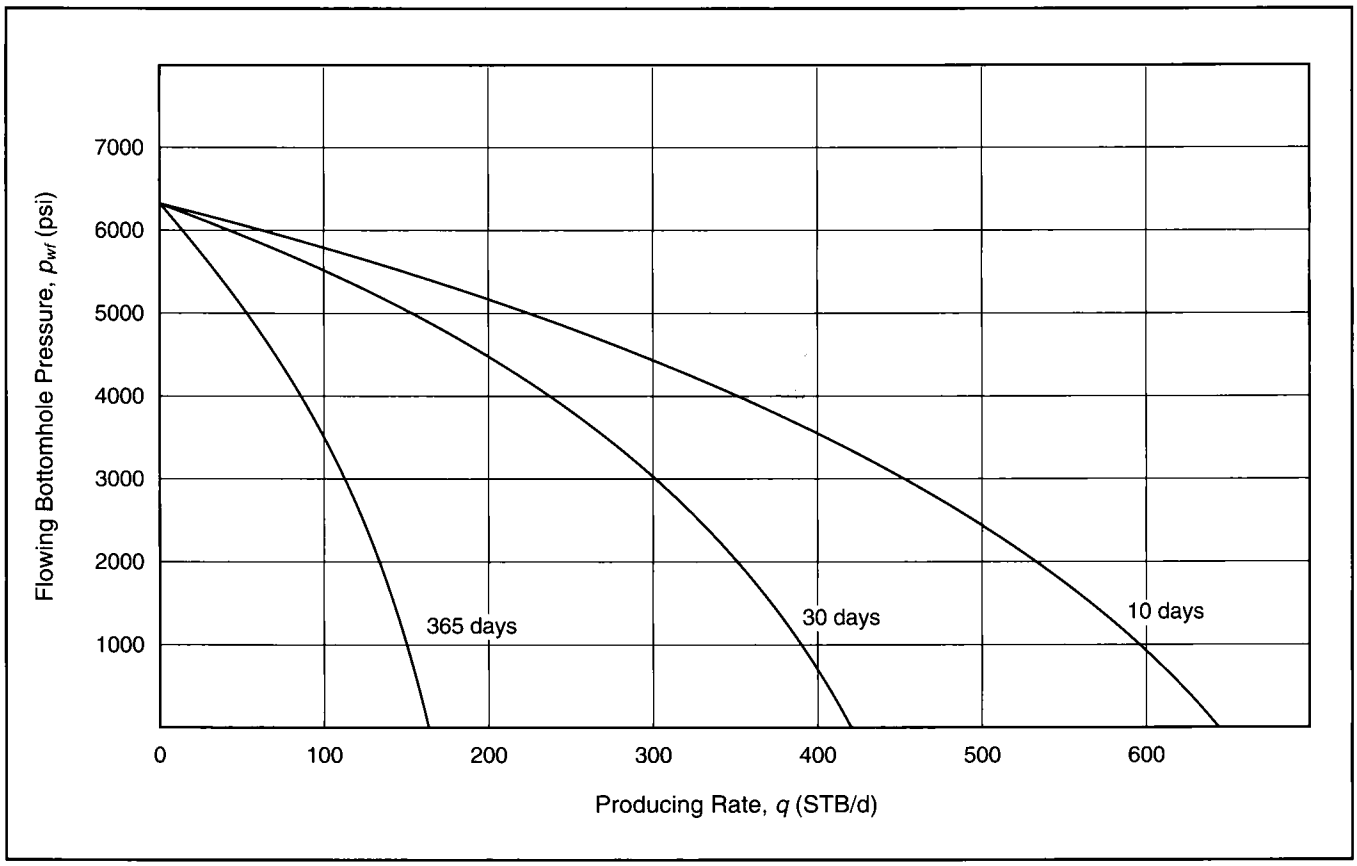

Figure E-1—Transient IPR curves for Example E-1.

EXAMPLE E-2

IPR Curves with x_f Variation

Construct transient IPR curves for the 1-yr time for fracture half-lengths equal to 500 and 1000 ft. Use all other variables as in Example E-1.

Solution (Ref. Section 8-2.1)

For this example the F_{CD} value is different for each fracture length. (It assumes that $k_f w$ is constant. In reality, this cannot be so because w is a function of x_f. However, for the purposes of this exercise, $k_f w$ = 750 md-ft.)

For x_f = 500 ft,

$$F_{CD} = \frac{750}{(0.05)\ (500)} = 30, \qquad \text{(E-8)}$$

and for x_f = 1000 ft,

$$F_{CD} = \frac{750}{(0.05)\ (1000)} = 15. \qquad \text{(E-9)}$$

From Eq. 8-3 and for t = 365 days, t_{Dxf} = 0.6 (for x_f = 500 ft), and t_{Dxf} = 0.15 (for x_f = 1000 ft). Then, from Fig. 8-2, p_D = 0.8 (for 500 ft), and p_D = 0.65 (for 1000 ft).

From Eq. 8-6, q_b is then 46 STB/d (for 500 ft) and 57 STB/d (for 1000 ft).

From Eqs. 8-6 and 8-8, q_{Vogel} is 75 STB/d and 93 STB/d, respectively. Finally, from Eq. 8-9,

$$q = 46 + 75\left[1 - 0.2\left(\frac{p_{wf}}{4700}\right) - 0.8\left(\frac{p_{wf}}{4700}\right)^2\right] \qquad \text{(E-10)}$$

for x_f = 500 ft, and

$$q = 57 + 93\left[1 - 0.2\left(\frac{p_{wf}}{4700}\right) - 0.8\left(\frac{p_{wf}}{4700}\right)^2\right] \qquad \text{(E-11)}$$

for x_f = 1000 ft.

Figure E-2 is the 1-yr transient IPR for three fracture half-lengths: x_f = 500 ft, x_f = 1000 ft, and x_f = 1500 ft (from Example E-1).

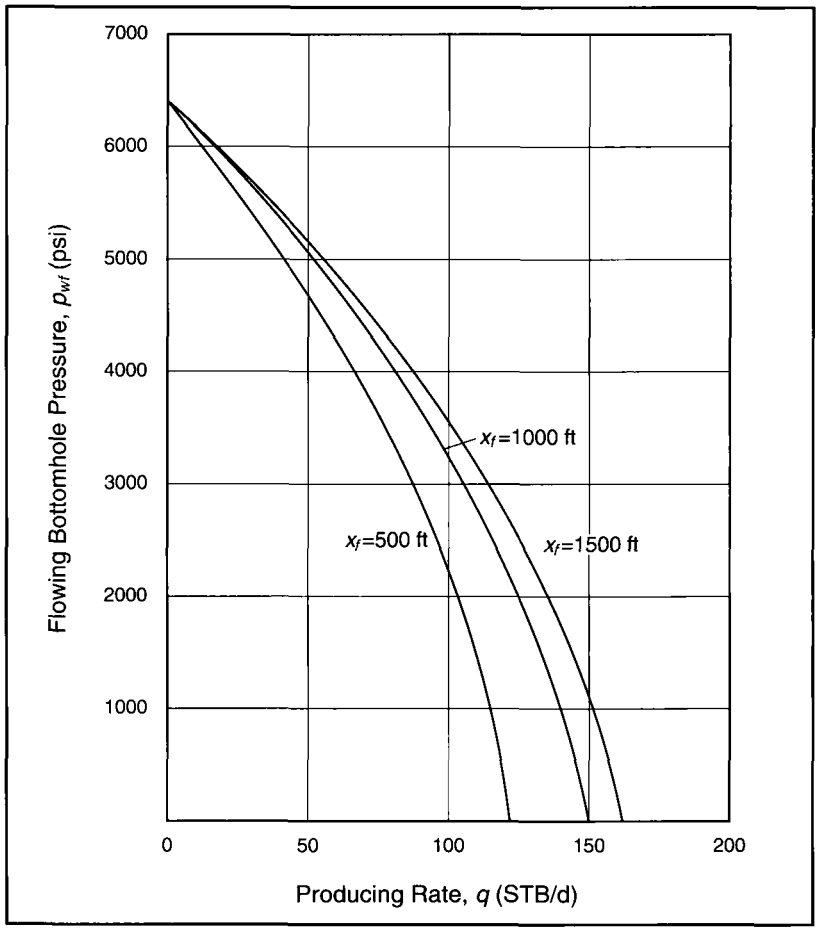

Figure E-2—Transient IPR curves for Example E-2.

EXAMPLE E-3

Combination of IPR and Vertical Lift Performance

Suppose that the well in Examples E-1 and E-2 is 8000 ft deep, with 2⅞-in. tubing. The GOR is 300 SCF/STB, and the wellhead pressure is 0 psi. What would be the producing rates after 1 yr for x_f = 500, 1000 and 1500 ft?

Solution (Ref. Section 8-2.2 and Brown et al.: *The Technology of Artificial Lift*, PennWell Books, 1980)

From Brown et al., and assuming that no water is produced (i.e., the fluid is 100% oil), for 2.441-in.-ID tubing, Table E-2 can be developed. A plot of the results in Fig. E-3 suggests that the 1-yr producing rates will be 108, 135 and 143 STB/d, respectively, for the three fracture half-lengths. These values are the intercepts between the transient IPR curves and the vertical lift performance (VLP) curve. Finally, Fig. E-4 is a plot of the results. Similar plots can be constructed for the cumula-tive production. As can be seen, increasing fracture length will result in increasing rates (increasing revenue). However, the benefits flatten out while costs increase rapidly. This will be demonstrated in later examples.

q (STB/d)	p_{wf} (psi)	Page in Brown et al. (1980)
50	1800	225
100	1600	228
200	1320	231

Table E-2—Vertical lift performance. Bottomhole pressures for various producing rates for Example E-3.

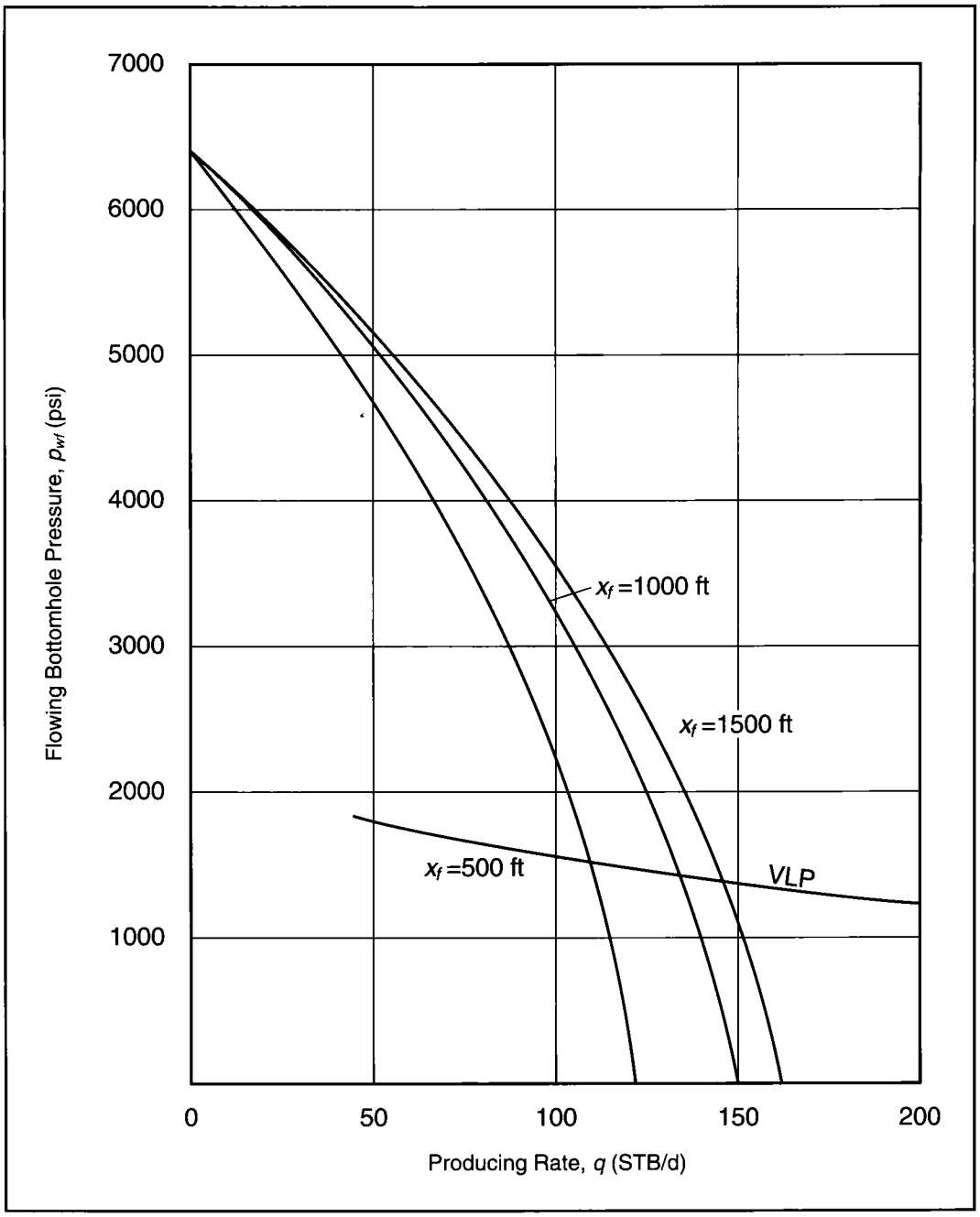

Figure E-3—Combination of IPR and VLP for Example E-3.

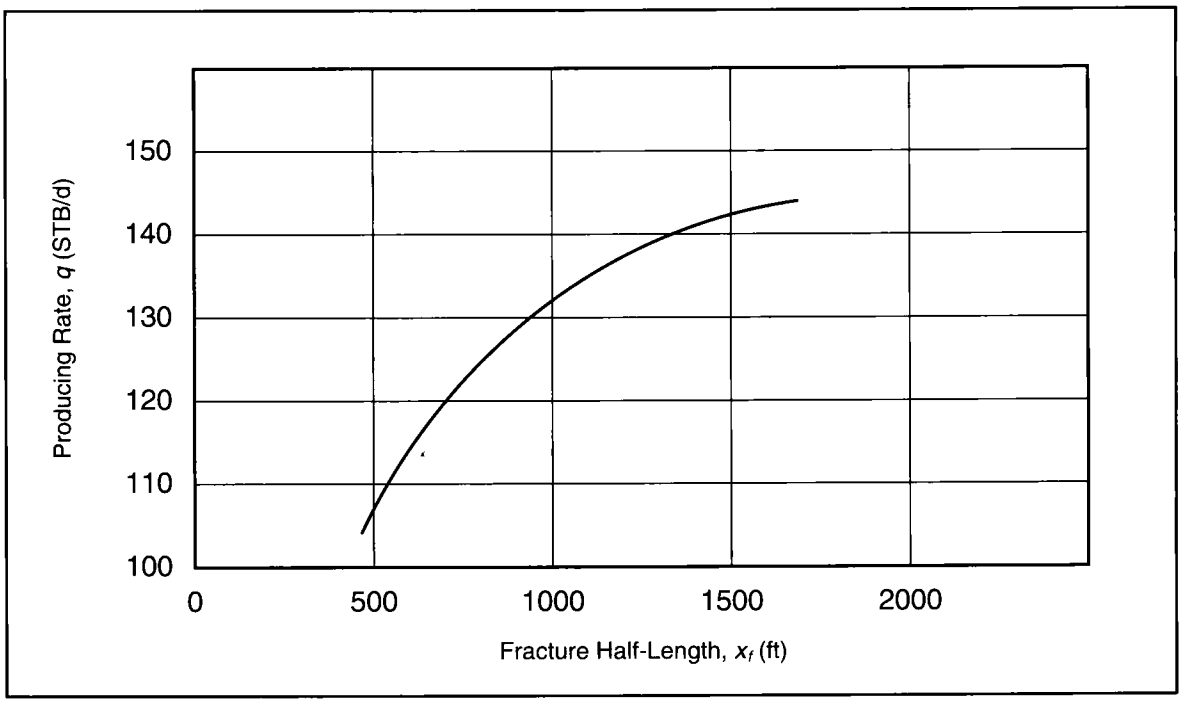

Figure E-4—One-year producing rate for various fracture lengths.

EXAMPLE E-4

Calculation of Fracture Width

Calculate the average fracture width of a 1000-ft fracture half-length for a Newtonian fluid. Repeat the calculation for a range of fractures from 100 ft to 500 ft for both the PKN and the KGD models. Use the data in Table E-3.

Solution (Ref. 8-2.4)

The width for the PKN model (which is the appropriate one for this problem since $x_f \gg h_f$) is given by Eq. 8-19 in coherent units. For the common units, listed in Table E-3, Eq. 8-19 becomes:

$$w = 0.3\left[\frac{q_i \mu (1 - \nu) x_f}{G}\right]^{\frac{1}{4}} \left(\frac{\pi}{4}\gamma\right), \qquad \text{(E-12)}$$

with the width, w, in inches.

The elastic shear modulus is given by

$$G = \frac{E}{2(1 + \nu)}, \qquad \text{(E-13)}$$

and therefore, for this problem,

$$G = \frac{3 \times 10^6}{2(1 + 0.25)} = 1.2 \times 10^6. \qquad \text{(E-14)}$$

From Eq. E-12,

$$w = 0.3\left[\frac{(40)(100)(0.75)(1000)}{1.2 \times 10^6}\right]^{\frac{1}{4}} \left(\frac{\pi}{4} 0.75\right)$$

$$= (0.38)(0.59) = 0.22 \text{ in.} \qquad \text{(E-15)}$$

In the right side of Eq. E-15, the two parentheses denote the maximum width (at the wellbore) and the PKN geometric factor. The product of the two is the average fracture width.

In order to calculate the width with the KGD model, Eq. 8-21 with coherent units is transformed into

$$w = 0.29\left[\frac{q_i \mu (1 - \nu) x_f^2}{G h_f}\right]^{\frac{1}{4}} \left(\frac{\pi}{4}\right) \qquad \text{(E-16)}$$

for the common units in Table E-3. Figure E-5 is a graph of the average width for the two models for a range of fracture half-lengths from 100 to 500 ft.

As can be seen easily from Eqs. E-12 and E-16, control of the fracture width during execution is not accomplished easily. To double the width for a given reservoir (i.e., given ν, E and h_f) at a desired fracture length would require an increase of the product $q_i\mu$ by a factor of 16. Because the viscosity is associated with undesirable side effects such as residual proppant-pack damage, increasing the rate is the remaining means of width control. For this problem, doubling the rate to 80 BPM (this would have an impact on treating pressure and fracture height migration) would increase the average width by a factor of $2^{0.25}$, or 1.2 (i.e., by 20%).

q_i	=	40 BPM
h_f	=	100 ft
E	=	3×10^6 psi
ν	=	0.25
$\bar{\mu}$	=	100 cp
γ	=	0.75

Table E-3—Variables to calculate fracture width for Example E-4.

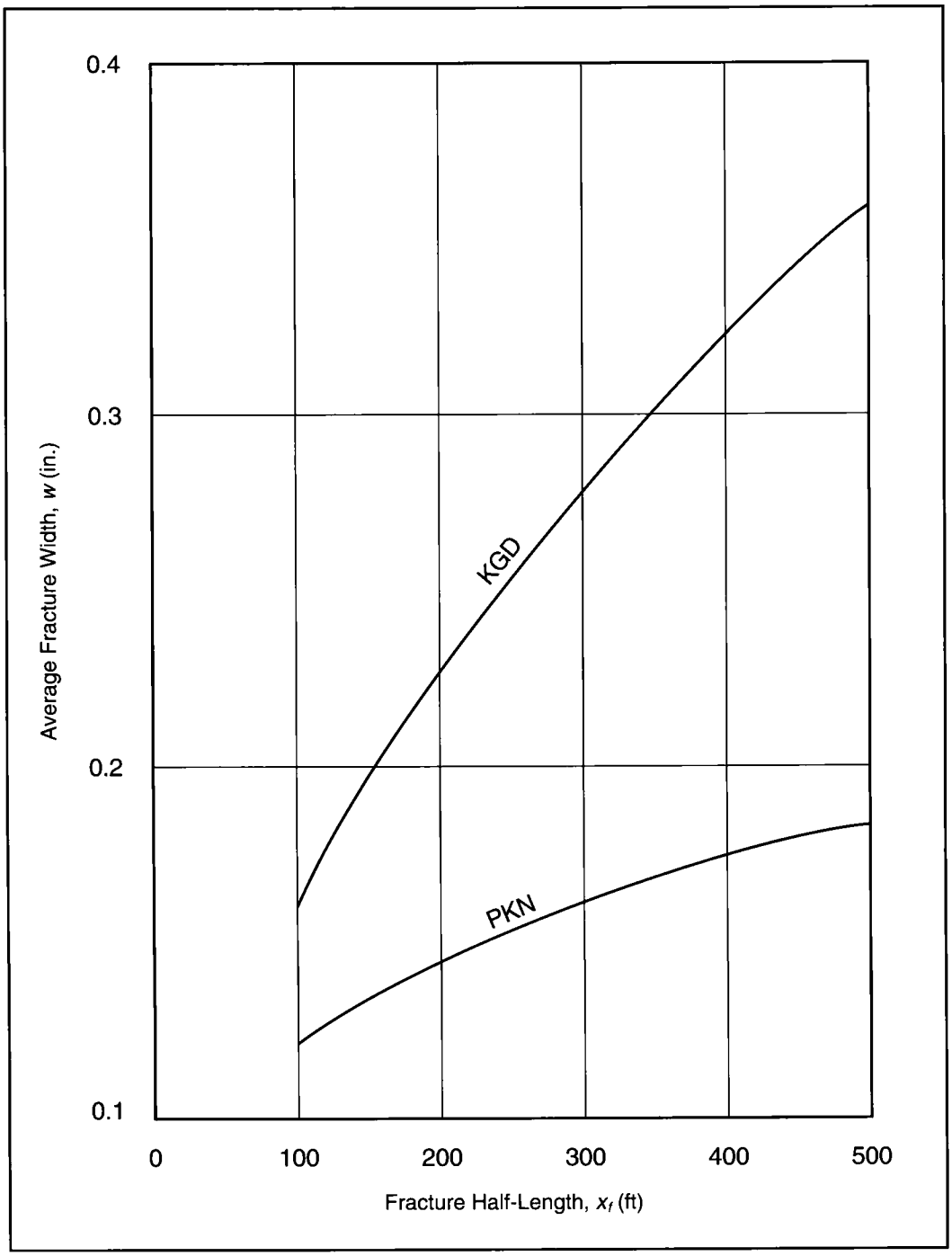

Figure E-5—Average width for a range of fracture lengths using the KGD and PKN models.

EXAMPLE E-5

Calculation of Width Using a Non-Newtonian Fluid

Calculate the width of a hydraulic fracture using the reservoir variables in Table E-3 but with a fracturing fluid with $K'=6\times10^{-3}$ lbf sec$^{n'}$/ft^2 and $n'=0.75$.

Solution (Ref. Section 3-3.4.3)

The maximum fracture width calculated for a non-Newtonian fluid is given by Eqs. 3-72 and 3-62. In the units given in Table E-3, Eqs. 3-72 and 3-62 yield

$$w_{max} = 12\left[\left(\frac{128}{3\pi}\right)(n'+1)\left(\frac{2n'+1}{n'}\right)^{n'}\left(\frac{0.9775}{144}\right)\left(\frac{5.61}{60}\right)^{n'}\right]^{\frac{1}{2n'+2}}\left[\frac{q^n K' x_f h_f^{1-n'}}{E}\right]^{\frac{1}{2n'+2}}, \quad \text{(E-17)}$$

where the width is in inches.

Substituting the given variables in Table E-3, Eq. E-17 results in

$$w_{max} = 12\left[(13.59)\,(1.75)\,(3.33)^{0.75}\,(0.0068)\,(0.0935)^{0.75}\right]^{0.286}\left[\frac{40^{0.75}(6\times10^{-3})\,(1000)\,100^{0.25}}{3\times10^6}\right]^{0.286}$$

$$= 0.4 \text{ in.} \quad \text{(E-18)}$$

The average width would be multiplied by 0.59, as in Example E-4; i.e., $w = 0.24$ in.

EXAMPLE E-6

Calculation of Total Fluid Volume Requirements and Pad Portion

Assuming that the average fracture width is 0.24 in. (from Example E-5) and using the variables in Table E-4, calculate the total fluid volume requirements and the pad portion. Repeat the calculation for a very low (0.15) and a very high (0.75) efficiency.

Solution (Ref. Sections 8-2.4 and 8-2.6)

The first variable to calculate is the multiplier to the fluid loss coefficient, effective during pumping. This is given by Eq. 8-20.

$$K_L = \frac{8}{3}(0.35) + 3.14(1 - 0.35) = 2.97. \quad \text{(E-19)}$$

The leakoff area, A_f, is then

$$A_f = 4(100)(1000) = 4 \times 10^5 \text{ft}^2. \quad \text{(E-20)}$$

Then, from Eq. 8-18 (in the textbook, the leakoff term must be divided by 2),

$$40t = \left(\frac{4 \times 10^5}{2}\right)\left(\frac{1}{5.615}\right)\left(\frac{0.24}{12} + (2.97)(5 \times 10^{-3})(0.75)\sqrt{t}\right). \quad \text{(E-21)}$$

Equation E-21 reduces to

$$t - 9.9\sqrt{t} - 17.8 = 0, \quad \text{(E-22)}$$

which is a quadratic equation, and its real solution yields $t = 131$ min (2 hr and 11 min).

This result is an inverse calculation. It calculates the time required to generate a fracture volume while the penalty of leakoff is in effect.

The total volume required to generate the fracture is then

$$V_i = (40)(42)(131) = 2.2 \times 10^5 \text{ gal}. \quad \text{(E-23)}$$

From Eq. 8-32 the pad volume may then be calculated:

$$V_{pad} = (2.2 \times 10^5)\left(\frac{1 - 0.35}{1 + 0.35}\right)$$

$$= 1.06 \times 10^5 \text{ gal}, \quad \text{(E-24)}$$

representing 48% of the total volume. At 40 BPM it would require 63 min of pumping.

If the efficiency were 0.15, then

$$K_L = \frac{8}{3}(0.15) + 3.14(1 - 0.15) = 3.07, \quad \text{(E-25)}$$

and the quadratic equation becomes

$$t - 10.3\sqrt{t} - 17.8 = 0, \quad \text{(E-26)}$$

resulting in a total pumping time equal to 139 min.

The total volume required is then

$$V_i = (40)(42)(139) = 2.34 \times 10^5 \text{ gal}. \quad \text{(E-27)}$$

The pad volume would be significantly different.

$$V_{pad} = 2.34 \times 10^5 \left(\frac{1 - 0.15}{1 + 0.15}\right)$$

$$= 1.73 \times 10^5 \text{ gal}, \quad \text{(E-28)}$$

representing 74% of the total volume and requiring 103 min of pumping.

If the efficiency were 0.75, then

$$K_L = \frac{8}{3}(0.75) + 3.14(1 - 0.75) = 2.79, \quad \text{(E-29)}$$

and the quadratic equation becomes

$$t - 9.3\sqrt{t} - 17.8 = 0. \quad \text{(E-30)}$$

The required time is then 119 min, and the total fluid volume is

$$V_i = (119)(40)(42) = 2.0 \times 10^5 \text{ gal}. \quad \text{(E-31)}$$

The pad volume is

$$V_{pad} = 2.0 \times 10^5 \left(\frac{1 - 0.75}{1 + 0.75}\right) = 2.8 \times 10^4 \text{ gal}, \quad \text{(E-32)}$$

requiring only 17 min of pumping and representing 14% of total fluid demand.

q_i	=	40 BPM
η	=	0.35
w	=	0.24 in.
C_L	=	5×10^{-3} ft/min$^{0.5}$
x_f	=	1000 ft
r_p	=	$0.7 = (h_p/h_f)$
h_f	=	100 ft

Table E-4—Variables for total fluid volume calculation for Example E-6.

EXAMPLE E-7

Calculation of the Ramped Proppant Schedule and Total Proppant Injected

Assuming that t_i (total injection time) is 7 hr, the t_{pad} is 3.5 hr, and the efficiency is 0.35, calculate the ramped proppant schedule for three end-of-job slurry concentrations, c_f (6, 10 and 16 ppg). Calculate the total mass of proppant if the injection rate is 40 BPM.

Solution (Ref. Section 8-2.6)

As shown in Example E-6, the pad volume can be readily calculated if the efficiency is known. The *end* of the pad injection marks the beginning of the ramped proppant schedule.

The slurry concentration, $c_p(t)$ in pounds per gallon (ppg), is given by Eqs. 8-45 and 8-46. For example, if c_f= 6 ppg, then from Eq. 8-45,

$$\varepsilon = \frac{1 - 0.35}{1 + 0.35} = 0.48, \tag{E-33}$$

and from Eq. 8-46,

$$c_p(t) = 6\left(\frac{t - 3.5}{7 - 3.5}\right)^{0.48}. \tag{E-34}$$

At $t = 3.5$ hr, of course, $c_p(t) = 0$. At $t = 4$ hr, then $c_p(t) = 2.4$ ppg.

Figure E-6 is a graph of the slurry concentration vs. time for the three end-of-job concentrations.

Integration of Eq. 8-46 from $t = t_{pad}$ to $t = t_i$ results in

$$\bar{c}_p = \int_{t_{pad}}^{t_i} c_f \left(\frac{t - t_{pad}}{t_i - t_{pad}}\right)^{\varepsilon} dt$$

$$= \frac{c_f}{\varepsilon + 1}(1 - 0) = \frac{c_f}{\varepsilon + 1}. \tag{E-35}$$

Thus, the "average" slurry concentrations would be 4.05, 6.76 and 10.8 ppg, respectively.

For 1 gal of slurry there are c_p lb of proppant. If this quantity is divided by the density of the proppant (e.g., 165 lb/ft^3) and converted into gallons, then this would be the volumetric fraction of proppant:

$$v_p = \frac{7.48}{165} c_p. \tag{E-36}$$

Thus, for the three cases at hand, the "average" volumetric fractions of proppant are 0.18, 0.31 and 0.49, respectively. During the 3.5 hr of pumping proppant, a total of (3.5)(60)(40)(42) = 352,800 gal were injected, and the masses of proppant would be

$$M_p = c_p V_i. \tag{E-37}$$

Therefore, the masses of proppant are 1.43×10^6 lb, 2.38×10^6 lb and 3.81×10^6 lb, respectively.

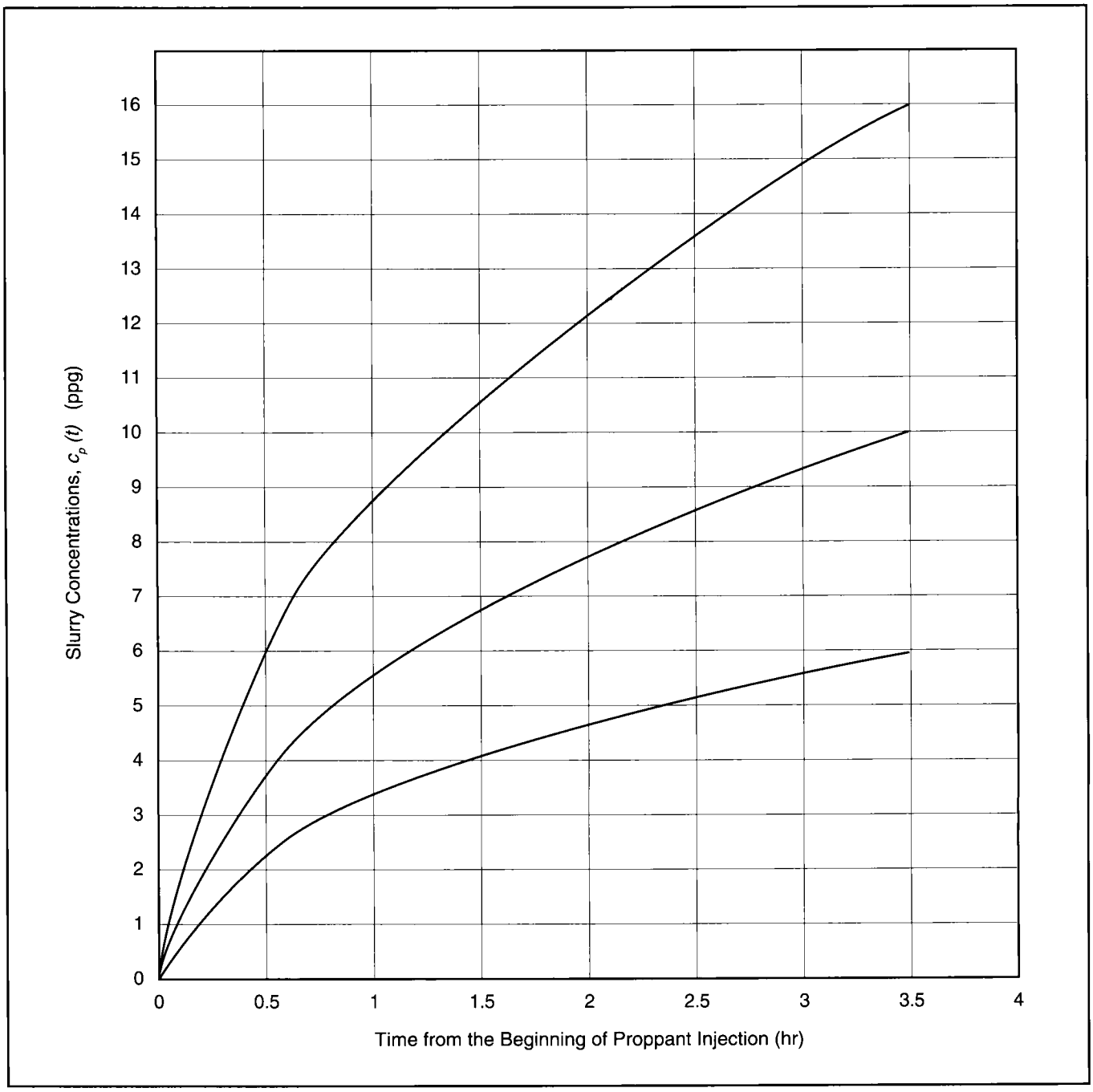

Figure E-6—Slurry concentration for ramped proppant schedule (Example E-7).

EXAMPLE E-8

Calculation of the Propped Fracture Width

Using the results of Example E-7 ($c_f = 10$ ppg) and assuming that the total fracture generated has $x_f = 2500$ ft and $h_f = 200$ ft, calculate the propped width. Assume that $\phi_p = 0.33$ and $\rho_p = 165$ lb/ft^3.

Solution (Ref. Section 8-2.6)

Equation 8-48 provides the propped fracture width. The areal concentration of proppant inside the fracture C_p is simply

$$C_p = \frac{M_p}{2x_f h_f} = \frac{2.38 \times 10^6 \text{ lb}}{2 \times 2500 \times 200} = 2.38 \text{ lb/ft}^2. \quad \text{(E-38)}$$

Then, from Eq. 8-46,

$$w_p = \frac{(12)\ (2.38)}{(1 - 0.33)\ (165)} = 0.26 \text{ in.} \quad \text{(E-39)}$$

EXAMPLE E-9

Net Pressure Determination

Using the data in Table E-5, calculate the net pressure in the fracture for the PKN model when the fracture half-length is 1000 ft. Plot the treating pressure for both the PKN and the KGD models for fracture half-lengths up to 2000 ft.

Solution (Ref. Sections 8-2.7 and 7-2.3.1)

Equation 8-51 relates the net pressure at the wellbore for the PKN model while Eq. 8-52 describes the net pressure for the KGD model. These relationships are not exact.

To reach an exact relationship, Eq. 7-13 is adjusted in terms of G (and remembering that $d = h_f$ for PKN); i.e.,

$$w_{max} = \frac{\Delta p_f h_f (1 - \nu)}{G}, \tag{E-40}$$

and then after combination with Eq. 8-19, the net pressure Δp_f can be obtained:

$$\Delta p_f = 2.31 \left[\frac{G^3 q_i \mu x_f}{(1 - \nu)^3 h_f^4} \right]^{\frac{1}{4}}. \tag{E-41}$$

For the units in Table E-5, Eq. E-41 becomes

$$\Delta p_f \text{ (psi)} = 0.0254 \left[\frac{G^3 q_i \mu x_f}{(1 - \nu)^3 h_f^4} \right]^{\frac{1}{4}}. \tag{E-42}$$

For the KGD model, the equation is

$$\Delta p_f \text{ (psi)} = 0.050 \left[\frac{G^3 q_i \mu}{(1 - \nu)^3 h_f x_f^2} \right]^{\frac{1}{4}}. \tag{E-43}$$

Thus, at $x_f = 1000$ ft,

$$\Delta p_f \text{ (psi)} = 0.0254 \left[\frac{(2.5 \times 10^6)^3 (40) (100) (1000)}{(1 - 0.25)^3 90^4} \right]^{\frac{1}{4}}$$

$$= 990 \text{ psi}. \tag{E-44}$$

For the PKN model, the net pressure (for any x_f) is

$$\Delta p_f = 175 x_f^{\frac{1}{4}}; \tag{E-45}$$

whereas for the KGD model, the relationship is

$$\Delta p_f = 9809 x_f^{-\frac{1}{2}}. \tag{E-46}$$

Figure E-7 is a graph of the treating pressure for the two models, remembering that the treating pressure is

$$p_f = \Delta p_f + 6000. \tag{E-47}$$

(Note that it is unlikely that the KGD model would be applicable for such long fracture lengths, hence the dashed line.)

G	=	2.5×10^6 psi
ν	=	0.25
q_i	=	40 BPM
h_f	=	90 ft
μ	=	100 cp
$\sigma_{H,min}$	=	6000 psi

Table E-5—Variables for net pressure determination in Example E-9.

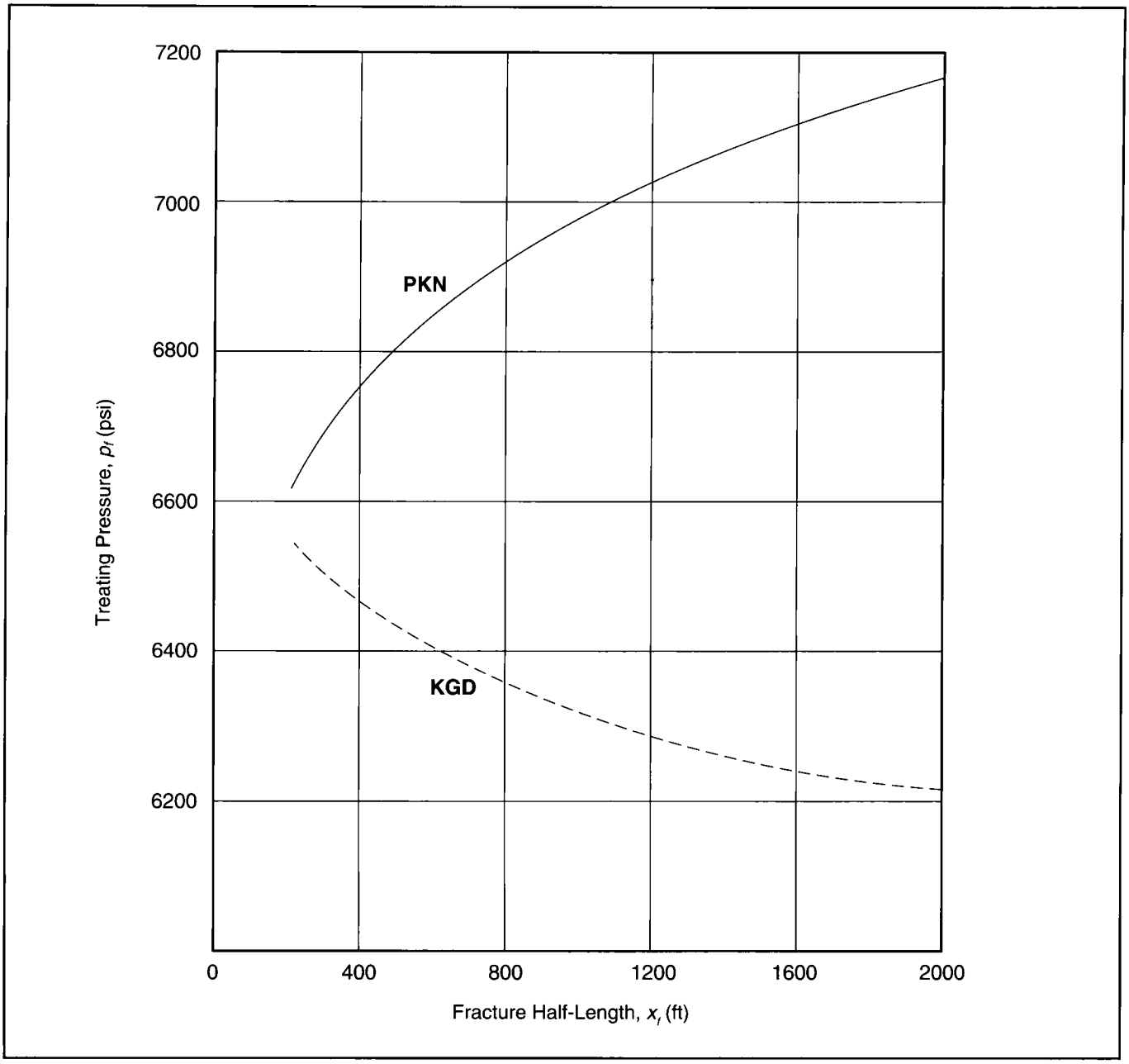

Figure E-7—Treating pressures by the PKN and KGD models for Example E-9.

EXAMPLE E-10

Net Pressure Control

Assuming that the net pressure during the fracture propagation described in Example E-9 must be maintained below 800 psi to control fracture height migration, what should the injection rate be at the 1500-ft fracture half-length point?

Solution (Ref. Section 8-2.7)

Equation E-42 can be rearranged:

$$q_i = \frac{2.4 \times 10^6 \Delta p_f^4 (1 - \nu)^3 h_f^4}{G^3 \mu x_f}, \qquad \text{(E-48)}$$

and thus

$$q_i = \frac{(2.4 \times 10^6)(800^4)(0.75^3)(90^4)}{(2.5 \times 10^6)^3 (100)(1500)} \approx 12 \text{ BPM}. \qquad \text{(E-49)}$$

EXAMPLE E-11

Net Present Revenue

Forecast of performance of a hydraulically fractured well suggests the following incremental cumulative production over what the unstimulated well would deliver:

Year 1: 40,000 STB
Year 2: 30,000 STB
Year 3: 18,000 STB
Year 4: 6,000 STB
Year 5: 2,000 STB.

Calculate the net present value (NPV) of the incremental production. Assume $20/STB as the price of oil. Use 20% and 100% discount rates.

Solution (Ref. Section 8-2.8)

The NPV of the incremental (net) revenue is given by Eq. 8-57.

Thus, for this problem, the revenue NPV for the 20% discount rate is

$$\begin{aligned} \text{NPV} &= \frac{(40{,}000)\,(20)}{1+0.2} + \frac{(30{,}000)\,(20)}{(1+0.2)^2} \\ &\quad + \frac{(18{,}000)\,(20)}{(1+0.2)^3} + \frac{(6000)\,(20)}{(1+0.2)^4} \\ &\quad + \frac{(2000)\,(20)}{(1+0.2)^5} \\ &= 6.67 \times 10^5 + 4.17 \times 10^5 + 2.08 \times 10^5 \\ &\quad + 0.58 \times 10^5 + 0.16 \times 10^5 \\ &= \$1.366 \times 10^6. \end{aligned} \tag{E-50}$$

Ignoring the last two years would mean only 5% difference in the NPV.

For the 100% discount rate (applicable in locations with hyperinflation), then

$$\begin{aligned} \text{NPV} &= \frac{(40{,}000)\,(20)}{1+1} + \frac{(30{,}000)\,(20)}{2^2} \\ &\quad + \frac{(18{,}000)\,(20)}{2^3} + \frac{(6000)\,(20)}{2^4} \\ &\quad + \frac{(2000)\,(20)}{2^5} \\ &= 4 \times 10^5 + 1.5 \times 10^5 + 0.45 \times 10^5 \\ &\quad + 0.075 \times 10^5 + 0.013 \times 10^5 \\ &= \$6.038 \times 10^5. \end{aligned} \tag{E-51}$$

Ignoring the last two years would mean only 1.5% difference in the NPV.

Finally, the 5-yr NPV ratio between the value at a 20% discount rate and that at a 100% discount rate is 2.3.

EXAMPLE E-12

Permeability and Optimum Fracture Half-Length

Using the data in Table E-6 for an oil well, graph the optimum fracture half-length vs. reservoir permeability. The permeability values are $k = 0.01$, 0.1 and 1 md. What are the F_{CD}, 1-yr NPV and production rate (for a year) at the optimum lengths?

Solution (Ref. Sections 8-3 and 8-4)

A parametric study was done using the NPV concept for fracture design. This is an interesting study because it touches on routine issues affecting fracture treatments. Important operational variables here are the injection rate (20 BPM) and the retained proppant-pack permeability (30% after stress effects are accounted for; damage is caused by polymer residue). Figure E-8 is a graph of the optimum fracture half-length vs. reservoir permeability. If the reservoir permeability is 0.01 md, then the optimum fracture half-length is 1400 ft. If the permeability is larger, 0.1 and 1 md, then the optimum fracture half-length decreases to 1300 ft and 900 ft, respectively.

This is well known in hydraulic fracture design; the tighter the reservoir, the longer the fracture should be.

There are additional findings that are significant. Fig. E-9 is a graph of the dimensionless fracture conductivity vs. permeability at the optimum fracture half-length. The dimensionless conductivity ranges from 14 for the 0.01-md permeability to 1.5 for the 0.1-md permeability and 0.2 for the 1-md permeability. This is a major conclusion. While a conductivity equal to 14 is quite good (and its increase may not result in appreciable well performance improvement), a conductivity equal to 0.2 could be improved considerably. Thus, while in very tight reservoirs the proppant type and especially the residual damage of the fracturing fluid should receive cursory attention; in the case of higher permeability reservoirs, they become *critical*. It is very important to use higher permeability proppants and to employ the best, least damaging fracturing fluids in high-permeability reservoirs.

Often, fracture treatment evaluation is based on the well posttreatment performance. However, the production rate must be compared with what an optimum treatment should deliver for that particular reservoir. Thus, "folds" of increase is not a meaningful comparison for similar treatments but for similar treatments in reservoirs of equal permeability.

Figures E-10 and E-11 are intended to drive the point home. The first is a graph of the 1-yr NPV for the optimum fracture half-lengths for the three permeabilities. The 1-yr NPVs are $210,000, $520,000 and $850,000, respectively. These figures would favor further the higher permeability reservoirs if better proppants and fluids were used. Thus, it should be remembered always that while hydraulic fracturing *can* improve well performance significantly, it cannot supplant nature. Reservoir permeability remains a significant variable for well production.

This is illustrated further in Fig. E-11. Here, the production rate for the three permeabilities is plotted vs. time for the first year. As can be seen easily, the 1-md permeability reservoir consistently outperforms the lower permeability reservoirs in spite of the fact that the latter would require significantly larger treatments. Furthermore, this plot illustrates the error in using the posttreatment rate as the sole measure of success for the fracture treatment (often without the knowledge of the reservoir permeability).

The expected performance of a 100-ft fracture half-length in the 1-md reservoir is plotted as a dashed line. It is obvious again that a far less than optimum treatment in a higher permeability reservoir can easily outperform an optimum job in a lower permeability reservoir. This should be expected. However, it should be noted that in one year, an optimum job in the 1-md reservoir would produce more than 100,000 STB, whereas the smaller job would produce only 80,000 STB. Thus, this last comparison shows the necessity to optimize the treatments. Furthermore, intelligent posttreatment evaluation requires the knowledge of an important reservoir variable such as the permeability.

Reservoir Data	Formation thickness, h	40 ft
	Reservoir porosity, ϕ	0.077
	Reservoir temperature, T	215° F
	Initial reservoir pressure, p_i	4000 psi
	Oil API gravity	42
	Gas specific gravity	0.662
	Reservoir oil saturation	0.55
	Drainage area	160 acres
Plumbing and Well Producing Data	Well: pumping	
	Producing gas-oil ratio	600 SCF/STB
	Flowing bottomhole pressure, p_{wf}	500 psi
	Tubing inside diameter	2.441 in.
	Tubing outside diameter	2.875 in.
	Tubing length (measured depth)	7383 ft
Fracture Mechanics Data	Fracture geometry model	PKN
	Minimum horizontal stress	5571 psi
	Young's modulus, E	4.5×10^6 psi
	Poisson's ratio, v	0.2
	Leakoff height, h_p	38 ft
	Fracture gross height, h_f	140 ft
	Leakoff coefficient, C_L	3×10^{-3} ft/$\sqrt{\text{min}}$
	Spurt loss coefficient, S_p	1 gal/100 ft^2
Proppant Data	Proppant type	20/40 sand
	Proppant specific gravity	2.65
	Proppant diameter	0.0248 in.
	Retained permeability factor	0.3
Fracturing Fluid Data	Fluid	Crosslinked borate
	K'	4.5×10^{-2} lbf sec$^{n'}$/ft^2
	n'	0.6
	Viscosity at 170^{-1} sec	276 cp
Operational Constraints	Maximum net pressure	1500 psi
	Maximum pump rate	20 BPM
	Maximum slurry concentration	8 ppga
Economic Data	Proppant cost	$0.09/lb
	Fluid cost	$0.43/gal
	Horsepower cost	$4/hp-hr
	Miscellaneous costs	$20,000
	Discount rate	12%
	Oil unit revenue	$20/STB

Table E-6—Data for fracture design parametric studies in Examples E-12 to E-16.

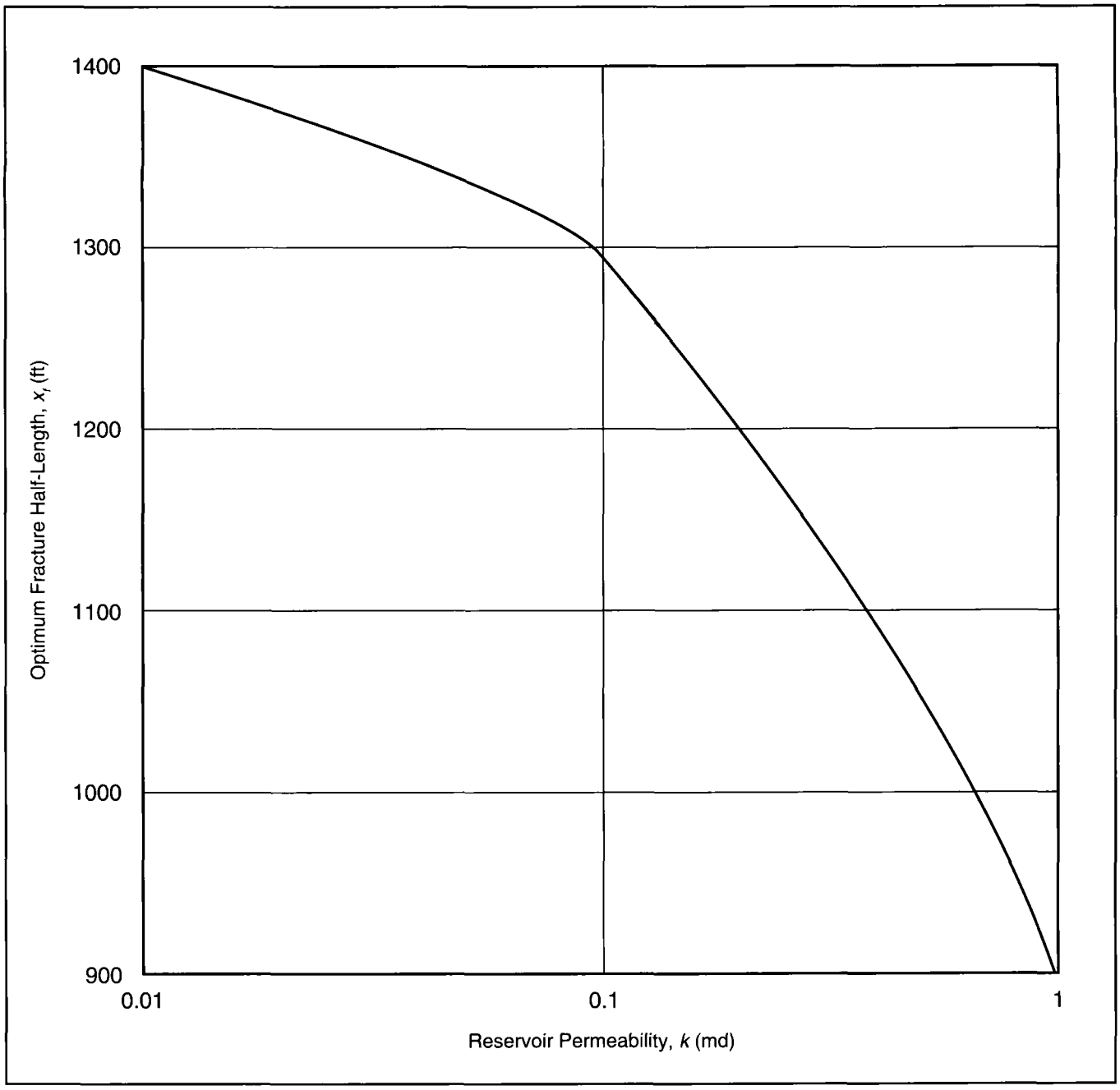

Figure E-8—Optimum fracture half-length vs. reservoir permeability.

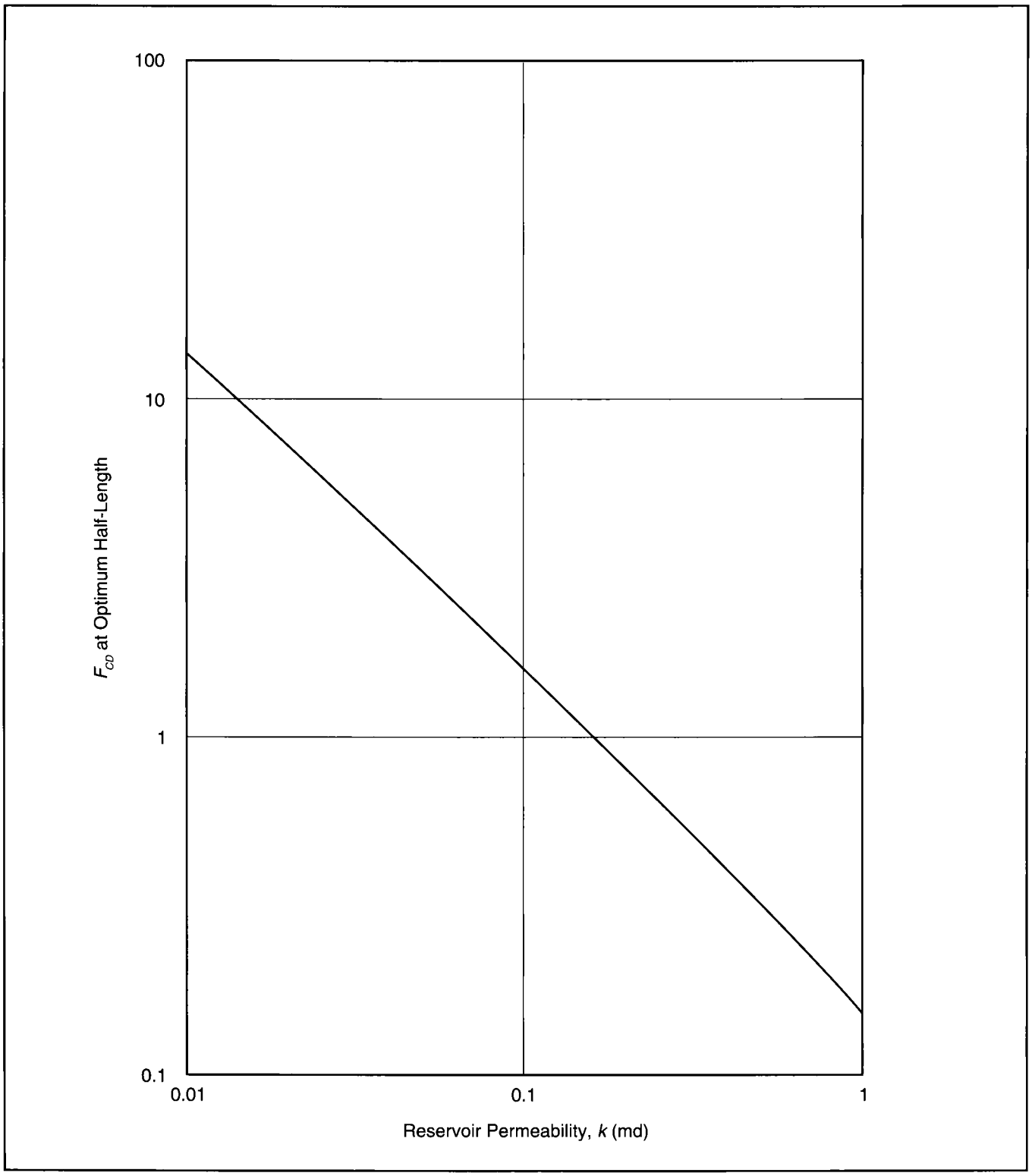

Figure E-9—Dimensionless conductivity at optimum fracture half-length.

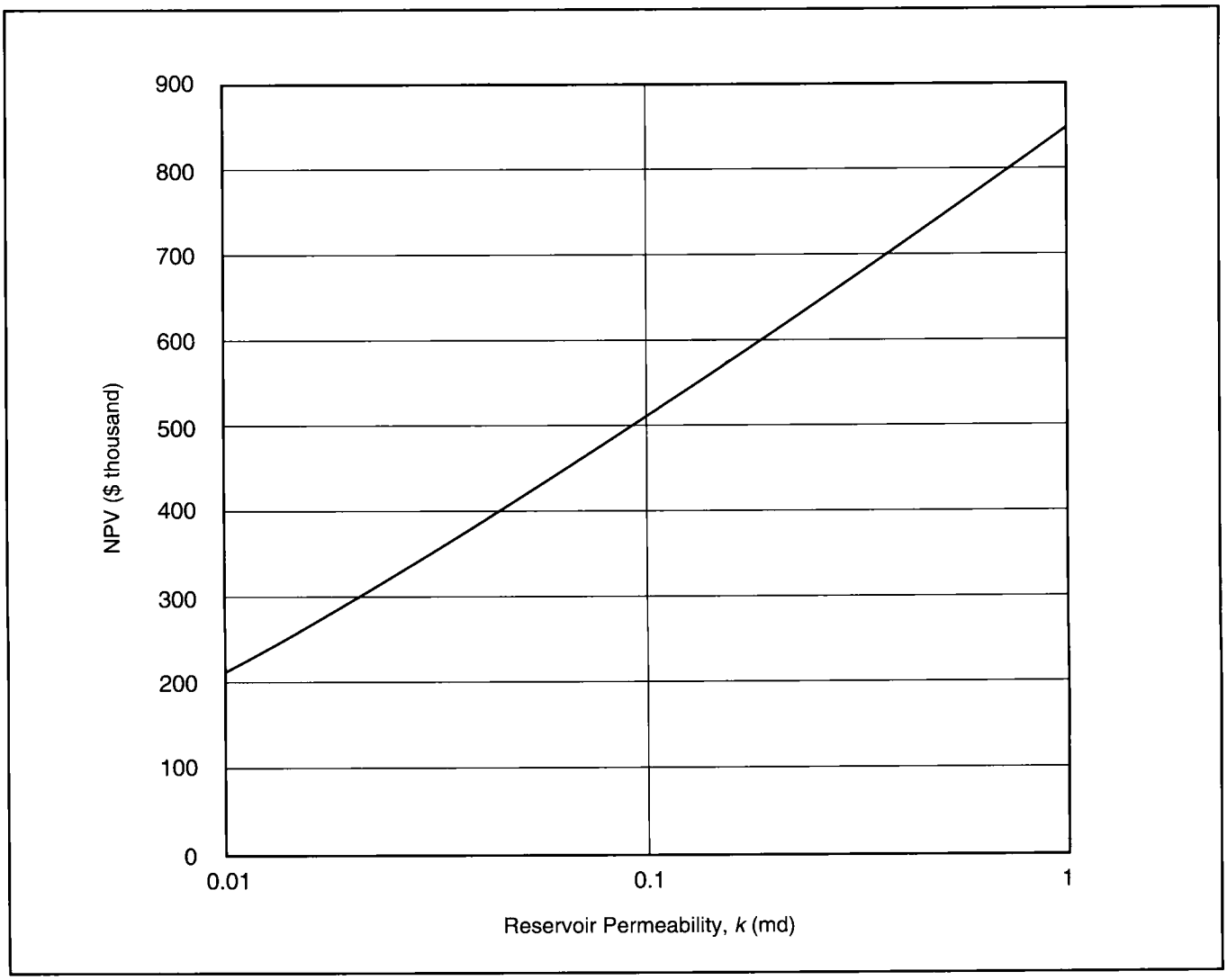

Figure E-10—One-year NPV at optimum fracture half-length.

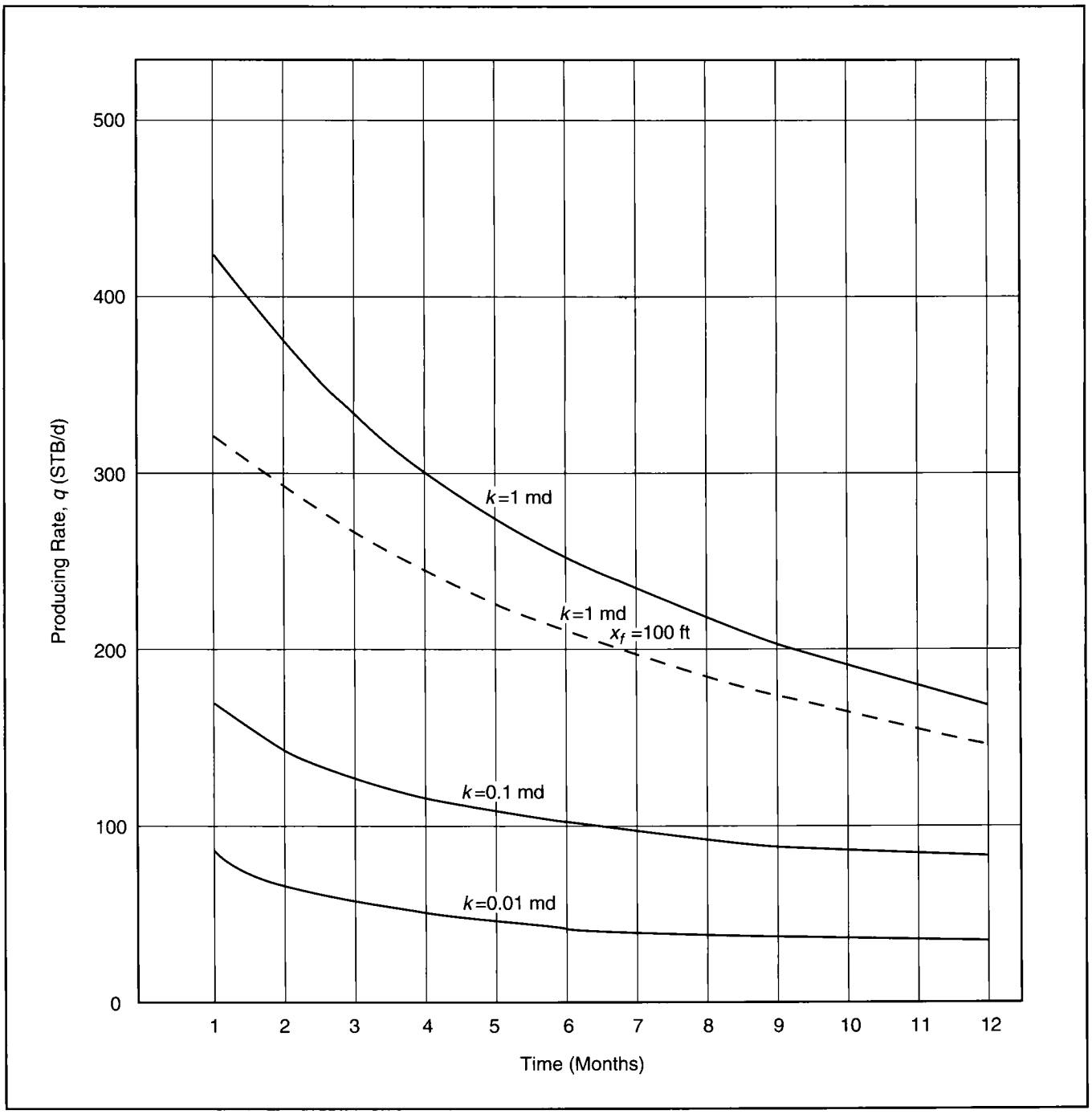

Figure E-11—Production rate with optimum fracture half-lengths.

EXAMPLE E-13

Closure Stress and Proppant Selection

With the data in Table E-6 (use k = 1 md), show the impact of the closure stress on proppant selection and the resulting 1-yr NPV.

Solution (Ref. Sections 8-3 and 8-4)

Three proppants have been selected: 20/40 sand, 20/40 ISP and 20/40 bauxite. Furthermore, three closure stresses were used: 4457 psi, 5571 psi and 6685 psi. In all three cases, after stress effects were accounted for, the polymer-induced damage was taken as 70% (i.e., 30% retained permeability).

Table E-7 contains the results of these simulations. While the cost of the proppants is disproportionate ($0.09/lb for sand, $0.67/lb for ISP and $0.75/lb for bauxite), it can be seen clearly that proppants that sustain their permeability at higher stresses result in higher NPVs. For this example, ISP is better for the two lower stress values, but bauxite overtakes ISP at the higher stress. If an even lower stress reservoir were to be fractured, then sand may appear more attractive. The NPV is affected both by the cost of the proppant and, more importantly, by the resulting fracture permeability and thus fracture conductivity.

Stress (psi)	Proppant	Optimum Fracture Half-Length, ft	1-Yr NPV ($000)
4457	Sand	2000	1500
	ISP	1600	2575
	Bauxite	700	985
5571	Sand	1900	1210
	ISP	1400	2250
	Bauxite	1300	2005
6685	Sand	1100	600
	ISP	1300	1900
	Bauxite	1300	1960

Table E-7—Stress, proppant type and NPV.

EXAMPLE E-14

Leakoff Coefficient and Injection Rate

For the 1-md reservoir, calculate the impact of the injection rate on the 1-yr NPV for two leakoff coefficients equal to 5×10^{-3} ft/$\sqrt{\text{min}}$ and 9×10^{-4} ft/$\sqrt{\text{min}}$, respectively.

Solution (Ref. Sections 8-3 and 8-4)

Five injection rates were used (10, 20, 40, 60 and 80 BPM), and all other variables were held constant as given in Table E-6. (This is not entirely realistic since the fracture height would be different for these injection rates. However, for the purpose of this comparison, the fracture height is held constant.) The two leakoff coefficients would depend on the success or failure of the deposited filter cake or the intensity of thief zones. Such a disparity can be observed in actual treatments within the same reservoir.

Figure E-12 is a graph of the optimum 1-yr NPV for the range of injection rates and the two leakoff coefficients.

Three conclusions can be drawn:

1. The lower leakoff coefficient would result in consistently higher NPV.
2. The problem can be remedied by using a larger injection rate. For example, the same NPV for $C_L = 9 \times 10^{-4}$ ft/$\sqrt{\text{min}}$ and 10 BPM can be realized for $C_L = 5 \times 10^{-3}$ ft/$\sqrt{\text{min}}$ and 20 BPM ($2.19 million).
3. The impact of increasing the injection rate is far more pronounced in the higher leakoff coefficient. This is shown by the steeper slope in the curve for $C_L = 5 \times 10^{-3}$ ft/$\sqrt{\text{min}}$.

(Note that the optimum fracture half-lengths were 1500 ft for all injection rates for $C_L = 9 \times 10^{-4}$ ft/$\sqrt{\text{min}}$. For $C_L = 5 \times 10^{-3}$ ft/$\sqrt{\text{min}}$, they were 1300 ft for 10 and 20 BPM and 1400 ft for the other three injection rates.)

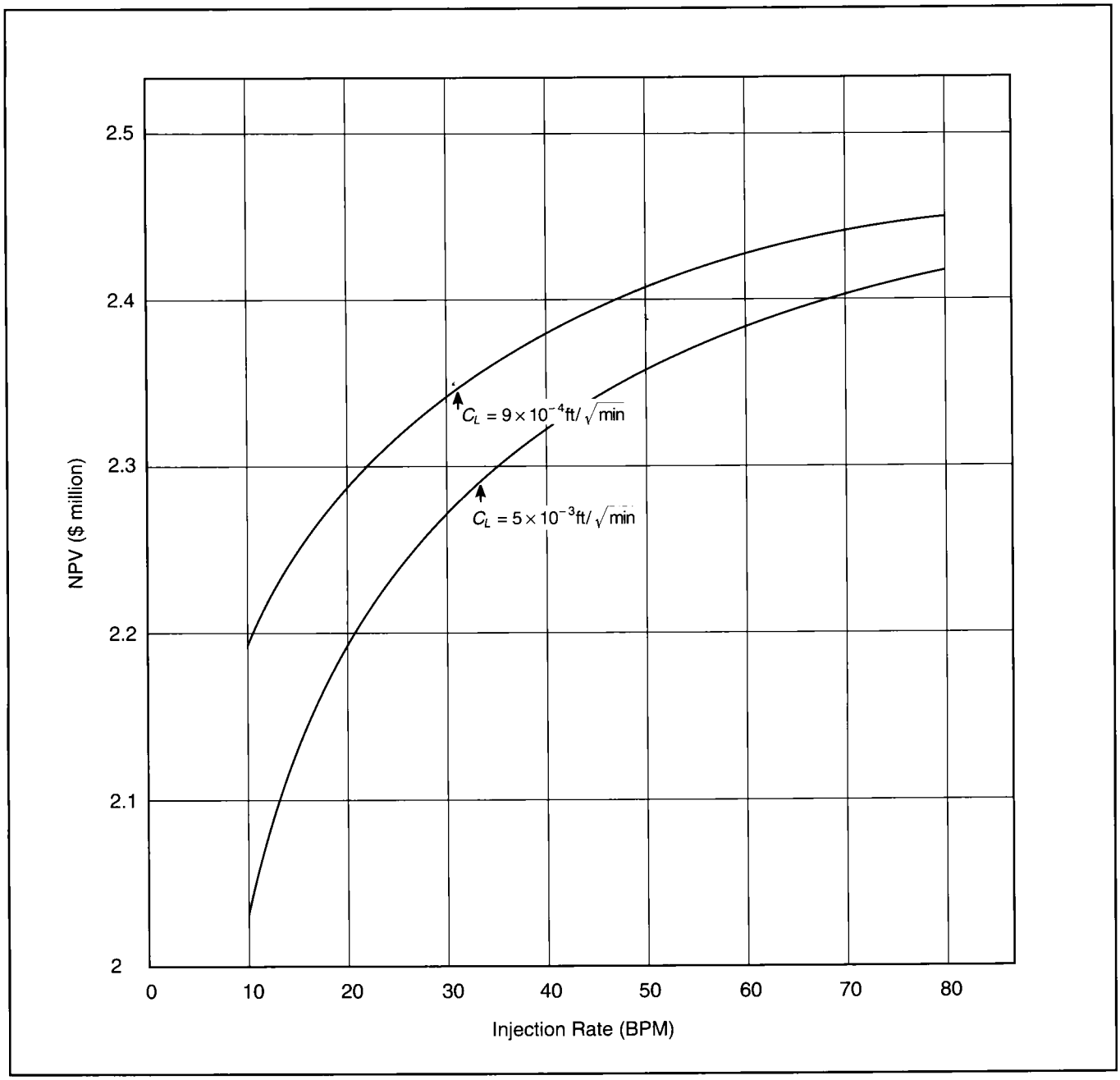

Figure E-12—One-year NPV (at optimum lengths) for two leakoff coefficients and a range of injection rates.

EXAMPLE E-15

Reservoir Permeability and Proppant-Pack Permeability Damage

Using the data in Table E-6 and for the three permeabilities ($k = 0.01$, 0.1 and 1 md), determine the effect on the 1-yr optimum NPV for proppant-pack permeability damage equal to 50%, 70% and 90% (i.e., 50%, 30% and 10% retained).

Solution (Ref. Sections 8-3 and 8-4)

Two proppants were used: 20/40 sand and 20/40 ISP. Figure E-13 contains the result of the simulation. The first conclusion is that the relative impact of the proppant-pack damage is far more severe in higher permeability reservoirs. This is reflected by the much steeper curve for the 1-md case compared to the curve for the 0.01-md case. Using ISP instead of sand helps. For the 1-md reservoir, the same optimum NPV can be obtained if sand is used with 50% damage or if ISP is used with 90% damage.

However, if the reservoir permeability is too small (0.01 md) and thus a higher fracture conductivity is relatively ineffective, the incremental benefits may not justify the significantly additional costs of using ISP over sand; hence, the "flip-flop" between the sand and ISP curves for the 0.01-md case.

EXAMPLE E-16

Discount Rate Impact on NPV

Calculate the effect of three discount rates (15%, 50% and 100%) on the optimum fracture half-length.

Solution (Ref. Sections 8-3 and 8-4)

Figure E-14 is a graph of the 1-yr NPV vs. fracture half-length for the three discount rates. As should be expected, a higher discount rate results in a lower optimum half-length. For the three discount rates the optimum half-lengths are 1600 ft, 1400 ft and 800 ft, respectively.

Additionally, the larger discount rates result in a more bell-like shape of the NPV curve. There is frequent confusion associated with a flatter curve. For example, in Fig. E-14 the incremental NPV (for the 15% rate) from a fracture half-length equal to 800 ft to the optimum ($x_f = 1600$ ft) is only $45,000, while the treatment costs are doubled (from $85,000 to $167,000). However, it should be remembered always that the NPV already incorporates costs, plus it assesses the required 15% discount rate. In other words, if the latter is the acceptable rate then all the incremental NPV constitutes an appropriate return on the original investment.

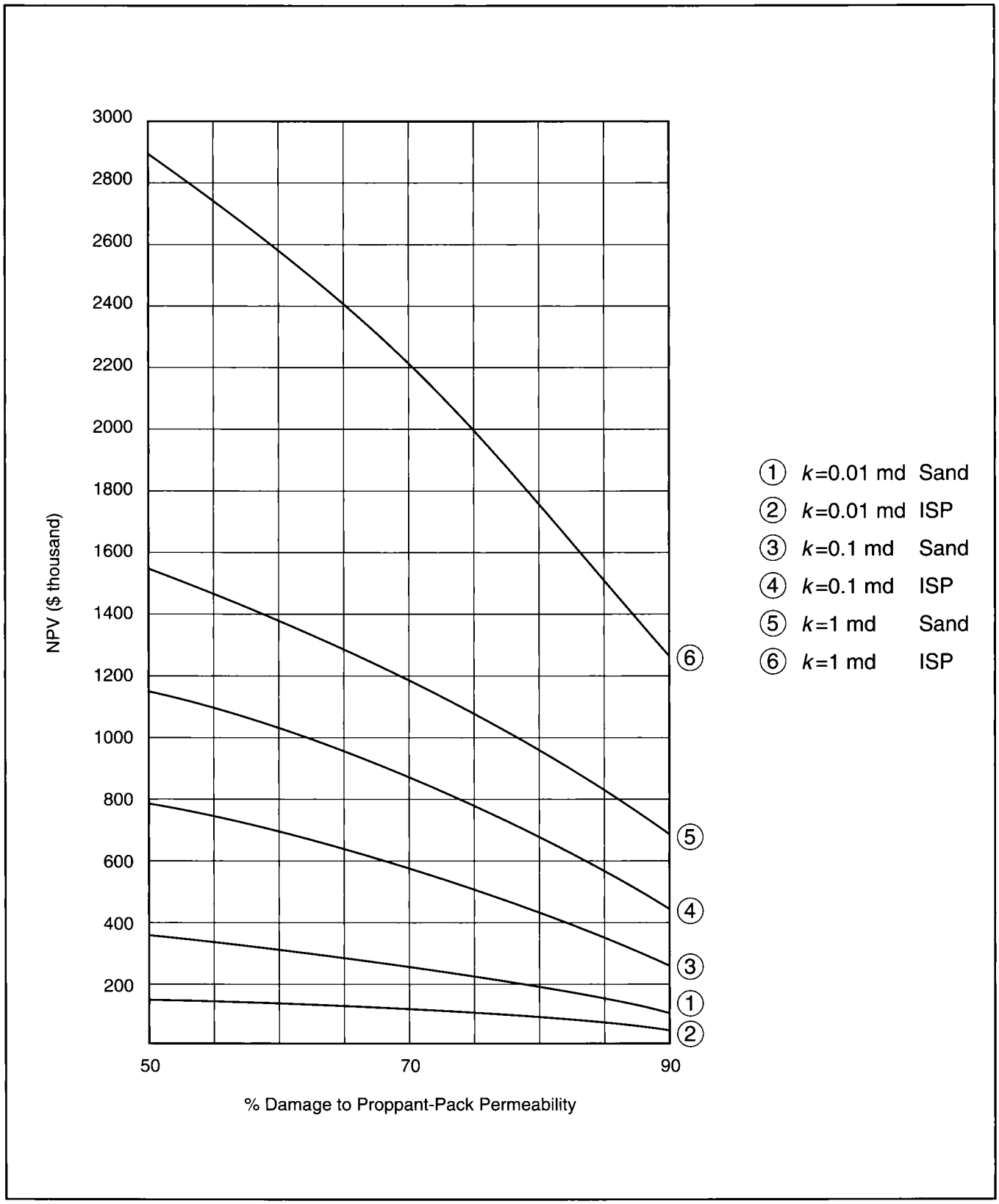

Figure E-13—One-year optimum NPV: reservoir permeability and proppant-pack damage.

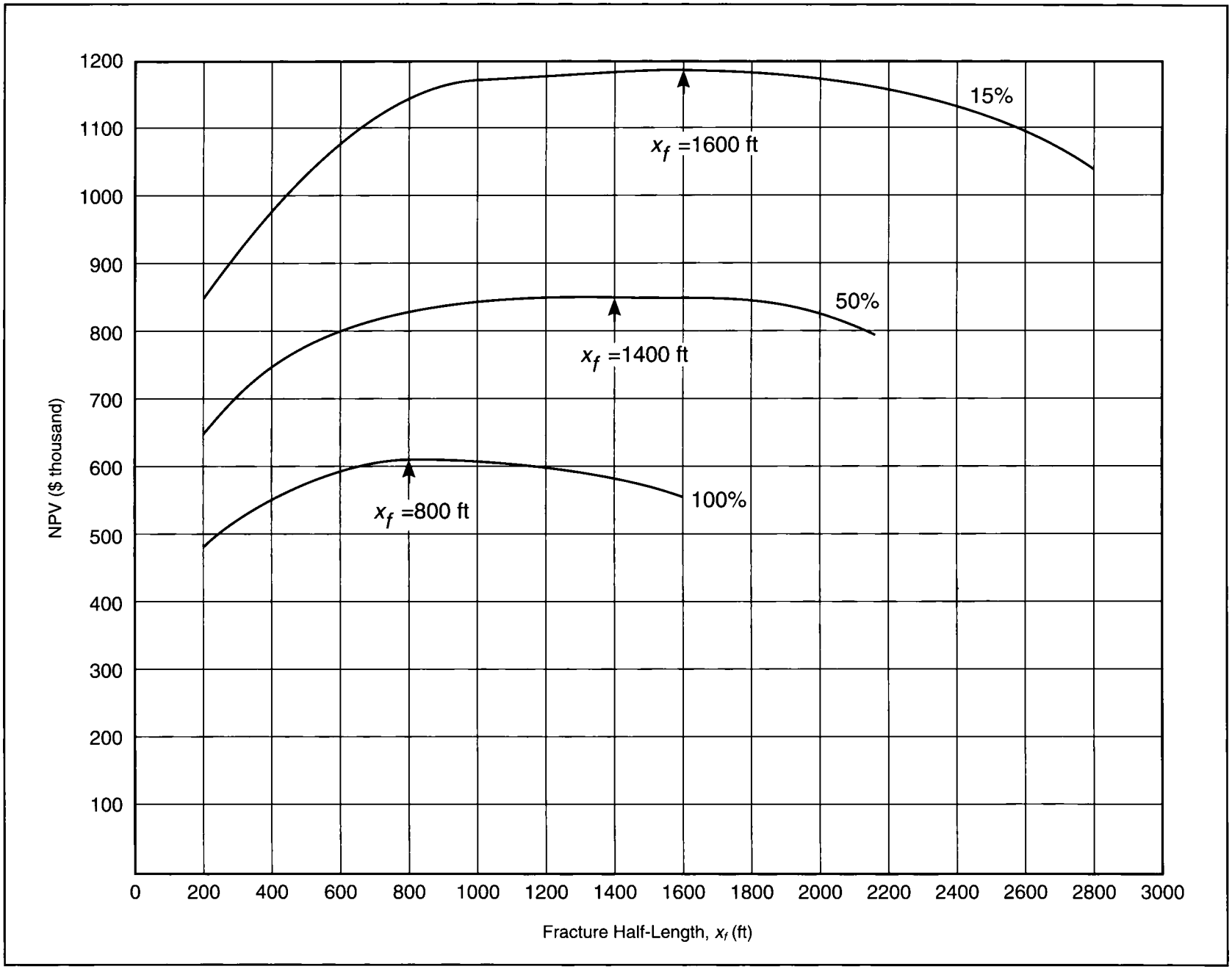

Figure E-14—One-year optimum NPV for various discount rates.

This Page Intentionally Left Blank

F. Evaluation of Treatments and Postfracture Performance

EXAMPLE F-1

Calculation of Folds of Productivity Index Increase from a Fractured Well

Assume a well with the variables shown in Table F-1. Calculate the folds of productivity index increase for three fracture lengths: 500, 1000 and 1500 ft.

Solution (Ref. Section 11-2)

From the McGuire and Sikora solution (Fig. 11-1), the group of variables in the abscissa must be calculated. Note that w must be in inches and A in acres. Thus,

$$\frac{wk_f}{k}\sqrt{\frac{40}{A}} = \frac{(0.2)(180{,}000)}{0.1}\sqrt{\frac{40}{160}}$$

$$= 1.8\times 10^5. \qquad \text{(F-1)}$$

Since A = 160 acres, then

$$r_e = \left[\frac{(160)(43{,}560)}{3.14}\right]^{\frac{1}{2}} = 1490\,\text{ft}. \qquad \text{(F-2)}$$

For the three fracture lengths, the penetration ratios L/r_e are equal to 0.33, 0.67 and 1, respectively. Therefore, the ordinate values are 6, 10 and 12, respectively.

The folds of increase J/J_o can then be obtained (for example, for the 500-ft fracture) from

$$\frac{J}{J_o} = 6\Big/\left(\frac{7.13}{\ln 0.472\, r_e/r_w}\right) = 6.5. \qquad \text{(F-3)}$$

For the 1000-ft and 1500-ft lengths, the folds of increase are then 10.8 and 13, respectively.

w	=	0.2 in.
A	=	160 acres
k_f	=	180,000 md
r_w	=	0.328 ft
k	=	0.1 md

Table F-1—Well and reservoir variables for Example F-1.

EXAMPLE F-2

Calculation of Effective Wellbore Radius and Fracture (Equivalent) Skin Effect

Assuming that a 1000-ft-long fracture in a reservoir with 1 md permeability has a dimensioned conductivity, $k_f w$, equal to 2000 md-ft, calculate the effective wellbore radius and the skin effect. The actual wellbore radius is 0.328 ft.

Solution (Ref. Section 11-2)

The relative capacity parameter, a, can be calculated from Eq. 11-1:

$$a = \frac{(3.14)(1)(1000)}{(2)(2000)} = 0.785. \qquad \text{(F-4)}$$

Then, from Fig. 11-4, the dimensionless effective wellbore radius is 0.3.

From Eq. 11-3,

$$r'_w = (0.3)(1000) = 300. \qquad \text{(F-5)}$$

Since $r'_w = r_w e^{-s}$, then

$$s = \ln\frac{r_w}{r'_w} = \ln\frac{0.328}{300} = -6.8. \qquad \text{(F-6)}$$

This skin effect is the equivalent skin effect as a result of the presence of the fracture of the given length and conductivity. Essentially, at pseudoradial flow, this is the skin effect (and effective wellbore radius) that the reservoir will "see."

EXAMPLE F-3

Relative Importance of Increasing Fracture Length or Conductivity

Assume that two reservoirs have permeabilities equal to 0.05 and 5 md, respectively. Investigate the relative importance of creating fractures of 500- and 1500-ft half-lengths with $k_f w$ products of 500 and 1500 md-ft.

Solution (Ref. Section 11-2)

The relative capacity parameter, a, as given by Eq. 11-1 can be calculated. For the 0.05-md reservoir and for $x_f = 500$ ft and $k_f w = 500$ md-ft,

$$a = \frac{(3.14)(0.05)(500)}{2(500)} = 0.08. \qquad \text{(F-7)}$$

If the $k_f w$ product is 1500 md-ft, then $a = 0.026$ (i.e., an even more conductive fracture). In both cases, the dimensionless effective wellbore radius is equal to 0.5. Thus, in a low-permeability reservoir, even a low $k_f w$ product (lackluster fracture) can result in a major increase in production. If, on the other hand, x_f increases to 1500 md-ft with $k_f w = 1500$ md-ft, then while $r'_{wD} = 0.5$ from Eq. 11-3, r'_w increases threefold. Since $r'_w = r_w e^{-s_f}$, where s_f is the fracture skin effect, increasing the fracture half-length would result in a major increase in production. Thus, the conclusion for a very low permeability reservoir is that a longer fracture length is extremely important, whereas $k_f w$ is relatively less important.

For the 5-md reservoir, $x_f = 500$ ft and $k_f w = 500$ md-ft.

$$a = \frac{(3.14)(5)(500)}{2(500)} = 8, \qquad \text{(F-8)}$$

and thus as shown by Eq. 11-6, the effective wellbore radius is not affected by increasing the fracture length. Thus, a longer fracture would not result in any appreciable benefit. However, doubling the $k_f w$ product would result in the doubling of r'_w. The conclusion for high-permeability reservoirs, resulting in low-conductivity fractures, is that the $k_f w$ product and its maximization are crucial. Using a high-permeability proppant—one that can sustain its integrity under stress for a long period of time—and especially low-damage fracturing fluids is essential to the success of hydraulic fracture treatments in high-permeability reservoirs. Fracture length in this case is relatively less important.

EXAMPLE F-4

Prediction of the Beginning and End of Bilinear Flow

Given the well, reservoir and fracture variables in Table F-2, calculate the real time of the beginning and end of bilinear flow. What would be the flow rates at these instances in time if the reservoir pressure were 5300 psi and the flowing bottomhole pressure 2300 psi? What would be the flow rate after a month?

Solution (Ref. Sections 11-3 and 11-5)

From the variables in Table F-2 and Eq. 11-11, the dimensionless fracture conductivity, F_{CD}, is calculated first.

$$F_{CD} = \frac{1000}{(1)(1000)} = 1. \tag{F-9}$$

Thus, from Fig. 11-23 at this value of F_{CD}, the beginning of the bilinear flow is at a dimensionless time $t_{Dxf} = 4.5 \times 10^{-5}$, corresponding to a dimensionless pressure $p_D = 0.2$. The end of the bilinear flow period is at $t_{Dxf} = 1.5 \times 10^{-3}$ with a dimensionless pressure $p_D = 0.45$.

Equation 11-10 can be rearranged to provide the real time, t.

$$t = \frac{t_{Dxf}\,\phi\mu c_t\,x_f^2}{0.000264k}, \tag{F-10}$$

and for $t_{Dxf} = 4.5 \times 10^{-5}$,

$$t = \frac{(4.5 \times 10^{-5})(0.1)(1)(10^{-5})(1000^2)}{(0.000264)(1)}$$

$$= 0.17 \text{ hr}, \tag{F-11}$$

which can be masked easily by wellbore storage effects.

From Eq. 11-8, which defines the dimensionless pressure, the flow rate can be obtained. (This is only approximately correct. For constant pressure production, the *transient rate* can be calculated from an appropriate solution. The solution presented in Section 11-5 is for pressure transients. However, comparisons presented in the literature have shown little difference in the calculations of the rate from the method outlined here and the formal solution.)

Thus,

$$q = \frac{kh\Delta p}{141.2 p_D B\mu}, \tag{F-12}$$

and since $\Delta p = 5300 - 2300 = 3000$ psi, then

$$q = \frac{(1)(100)(3000)}{(141.2)(0.2)(1.1)(1)} = 9660 \text{ STB/d}. \tag{F-13}$$

The end of bilinear flow is at $t_{Dxf} = 1.5 \times 10^{-3}$, and therefore

$$t = \frac{(1.5 \times 10^{-3})(0.1)(1)(10^{-5})(1000^2)}{(0.000264)(1)}$$

$$= 5.7 \text{ hr}. \tag{F-14}$$

Similarly,

$$q = \frac{(1)(1000)(3000)}{(141.2)(0.45)(1.1)(1)} = 4290 \text{ STB/d}. \tag{F-15}$$

It should be noted that such short periods can be masked by wellbore storage; i.e., it is possible that no bilinear flow is detected if the wellbore storage period is lengthy.

Finally, after a month, from Eq. 11-10,

$$t_{Dxf} = \frac{(0.000264)(1)(30 \times 24)}{(0.1)(1)(10^{-5})(1000^2)} = 0.19. \tag{F-16}$$

Then, from Fig. 11-23, $p_D = 1.5$.

From Eq. F-12,

$$q = \frac{(1)(100)(3000)}{(141.2)(1.5)(1.1)(1)} = 1290 \text{ STB/d}. \tag{F-17}$$

This flow rate represents a marked decrease from the very large value at 5.7 hr (4290 STB/d). The nature of fractured wells is such that they experience a much steeper production rate decline than nonfractured wells.

k	=	1 md
μ	=	1 cp
$k_f w$	=	1000 md-ft
c_t	=	10^{-5} psi^{-1}
x_f	=	1000 ft
B_o	=	1.1 resbbl/STB
ϕ	=	0.1
h	=	100 ft

Table F-2—Well and reservoir variables for Example F-4.

EXAMPLE F-5

Fracture Face Damage

Clay swelling from a water-base fracturing fluid resulted in a permeability impairment of 95% ($k/k_s = 20$). If the fracture half-length is 500 ft and the penetration of damage, b_s, is 2 in., estimate the impact of this damage on production.

Solution (Ref. Section 11-4)

From Eq. 11-20,

$$s_{fs} = \frac{(3.14)(2/12)(19)}{(2)(500)} = 9.9 \times 10^{-3}, \qquad \text{(F-18)}$$

and the reciprocal $s_{fs}^{-1} = 100$.

From Fig. 11-21 it can be determined that $r'_w/x_f = 0.5$; i.e., there is no impact on the well performance as a result of this damage.

EXAMPLE F-6

Apparent Fracture Face Damage

Long-term production from a very tight, heavy gas-condensate well ($r_w = 0.328$ ft) results in a skin effect during pseudoradial flow equal to –6.4. If the liquid gas condensate extends 20 ft into the reservoir (normal to the fracture), calculate the apparent reservoir permeability-to-gas reduction. The fracture half-length, measured early in the life of the well, is 1000 ft.

Solution (Ref. Section 1-4)

The variables on the ordinate of Fig. 11-21 can be calculated:

$$\frac{r'_w}{x_f} = \frac{r_w e^{-s}}{x_f} = \frac{(0.328)e^{+6.4}}{1000} = 0.2. \qquad \text{(F-19)}$$

Therefore, from Fig. 11-21, $s_{fs}^{-1} = 1.2$, and thus, $s_{fs} = 0.83$.

Using Eq. 11-20 and rearranging,

$$\frac{k}{k_s} = \frac{(2)(1000)(0.83)}{(3.14)(20)} + 1 = 27.4. \qquad \text{(F-20)}$$

Therefore, the apparent permeability impairment is

$$\left(1 - \frac{1}{27.4}\right) = 0.96, \qquad \text{(F-21)}$$

or 96% reduction.

EXAMPLE F-7

Posttreatment Pressure Transient Test Design

A fracture treatment was successful in an oil reservoir having 1 md permeability. The fracture design was intended to create a 1000-ft half-length with a $k_f w = 1000$ md-ft. Using the data in Table F-3, predict the length of time that the well should be definitely within the bilinear flow. What would be the pressure drop at that time if the test flow rate is 500 STB/d?

Solution (Ref. Section 11-6)

This exercise is to give a rough estimate of the required test duration to provide meaningful and interpretable data. Often, it is necessary to assume plausible values of the variables to be calculated in order to design a test of appropriate duration. The foldout curves at the end of Chapter 11 can be used for this calculation.

At first, the dimensionless fracture wellbore storage coefficient must be estimated. This is given by Eq. 11-22.

The dimensioned wellbore storage coefficient C is simply the well volume multiplied by the fluid compressibility within the tubing string. Assuming that only oil is produced, the oil compressibility can be used. If gas is liberated in the tubing, which is often the case, then its impact must be taken into account. For the purpose of this exercise, the oil is assumed to have a very low bubblepoint pressure. Thus,

$$C = V_w c_o$$

$$= \frac{\pi(2.441)^2}{(4)(144)(5.615)}(12{,}000)(6\times 10^{-6})$$

$$= 4.17\times 10^{-4}\ \text{bbl/psi}. \qquad \text{(F-22)}$$

From Eq. 11-22,

$$C_{Df} = \frac{(5.615)(4.17\times 10^{-4})}{(2)(3.14)(0.1)(10^{-5})(37)(1000^2)}$$

$$= 1\times 10^{-5}. \qquad \text{(F-23)}$$

Since a 1000-ft half-length fracture with $k_f w = 1000$ md-ft was intended, then

$$F_{CD} = \frac{1000}{(1000)(1)} = 1, \qquad \text{(F-24)}$$

and therefore the first foldout type curve can be used for the calculation.

At $C_{Df} = 10^{-5}$, to be well within the bilinear flow regime, the ratio t_{Dxf}/C_{Df} must be equal to 100 (from the type curve). Thus,

$$t_{Dxf} = (100)(1\times 10^{-5}) = 10^{-3}. \qquad \text{(F-25)}$$

From the definition of the dimensionless time (Eq. 11-10) and rearrangement,

$$t = \frac{(10^{-3})(0.1)(2)(10^{-5})(1000^2)}{(0.000264)(1)} = 7.5\ \text{hr}. \qquad \text{(F-26)}$$

The dimensionless pressure at that time is 0.43 (from the type curve). Thus, from Eq. 11-8 and rearrangement,

$$\Delta p = \frac{(0.43)(141.2)(500)(1.1)(2)}{(1)(37)}$$

$$= 1805\ \text{psi}. \qquad \text{(F-27)}$$

k	=	1 md
μ	=	2 cp
ϕ	=	0.1
B_o	=	1.1 resbbl/STB
H	=	12,000 ft
c_o	=	6×10^{-6} psi^{-1}
d_{tbg}	=	2.441 in.
c_t	=	1×10^{-5} psi^{-1}
h	=	37 ft

Table F-3—Posttreatment test data for Example F-7.

EXAMPLE F-8

Moderate-Permeability Oil Well—Interpretation of Posttreatment Tests

A moderate-permeability oil well (k ≅ 2 md) flowed for 30 days at an average rate of 375 STB/d. This was followed by a 10-day pressure buildup test. Figure F-1 is a summary of the measured rate and pressures for this test. Table F-4 contains the relevant well and reservoir data. Interpret this test and calculate fracture geometry and/or conductivity variables.

Solution (Ref. Section 11-6)

As with all pressure transient tests, the first step is flow regime identification through a pressure and pressure derivative log-log diagnostic plot. This is shown in Fig. F-2. As should be expected, for such a moderate-permeability (high by fracture candidate standards) reservoir, the fracture conductivity should be low ($F_{CD} \cong 1$), and thus only bilinear flow should be evident. This is clear on Fig. F-2. After the end of wellbore storage effects, denoted by the early-time 45° straight line, a lengthy quarter-slope straight line appears. This is marked on the figure. No linear flow is evident, and therefore the calculation of fracture half-length is not possible for the duration of this test. (Long-term flow data may allow the calculation of the fracture length if pseudoradial flow appears. This method is outlined in Section 11-8.)

The analysis shown in Fig. F-2 leads to the specialized plot shown in Fig. F-3, where the quarter-root of time is plotted against the pressure on Cartesian coordinates. This should form a straight line through the points identified on the log-log plot forming a quarter slope.

The slope of the straight line on Fig. F-3 is equal to 249 psi/hr$^{0.25}$. Using Eq. 11-12 the $k_f w$ product can be calculated.

$$k_f w = \left[\frac{(44.1)(375)(1.1)(1.2)}{(53)(249)}\right] \left[\frac{1}{(0.12)(1.2)(9\times 10^{-6})(2)}\right]^{0.5}$$

$$= 1030 \text{ md-ft}. \qquad \text{(F-28)}$$

Since the fracture was *designed* for $x_f = 700$ ft, then the F_{CD} can be approximated:

$$F_{CD} = \frac{1030}{(2)(700)} = 0.7. \qquad \text{(F-29)}$$

The latter is only an estimate since the actual fracture length cannot be determined from the test.

k	=	2 md
t_p	=	1 month
ϕ	=	0.12
q	=	375 STB/d
h	=	53 ft
p_{wf}	=	2125 psi (at $\Delta t = 0$)
c_t	=	9×10^{-6} psi^{-1}
r_w	=	0.328 ft
B_o	=	1.1 resbbl/STB

Table F-4—Well and reservoir data for Example F-8.

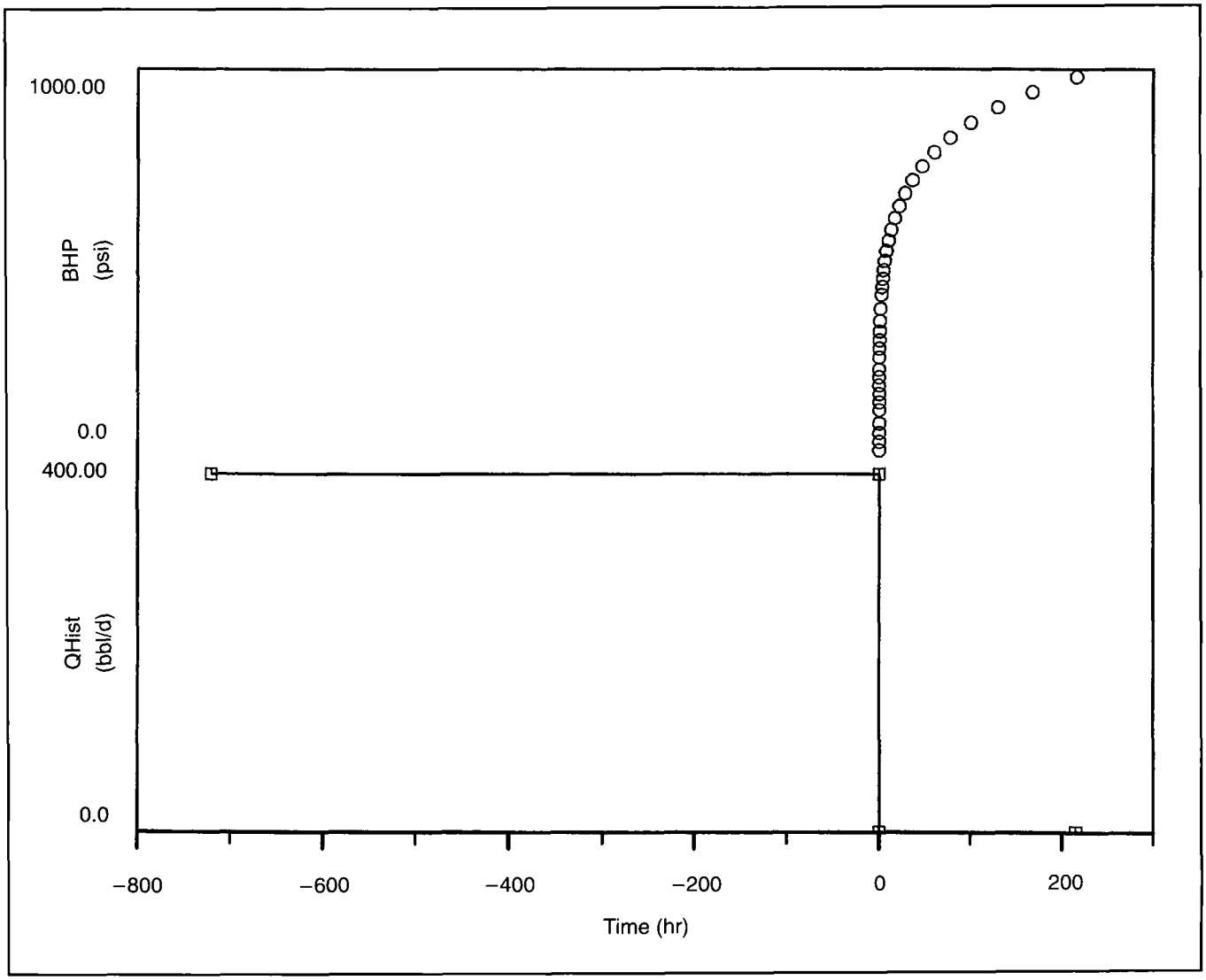

Figure F-1—Summary of rate and pressure transients for Example F-8.

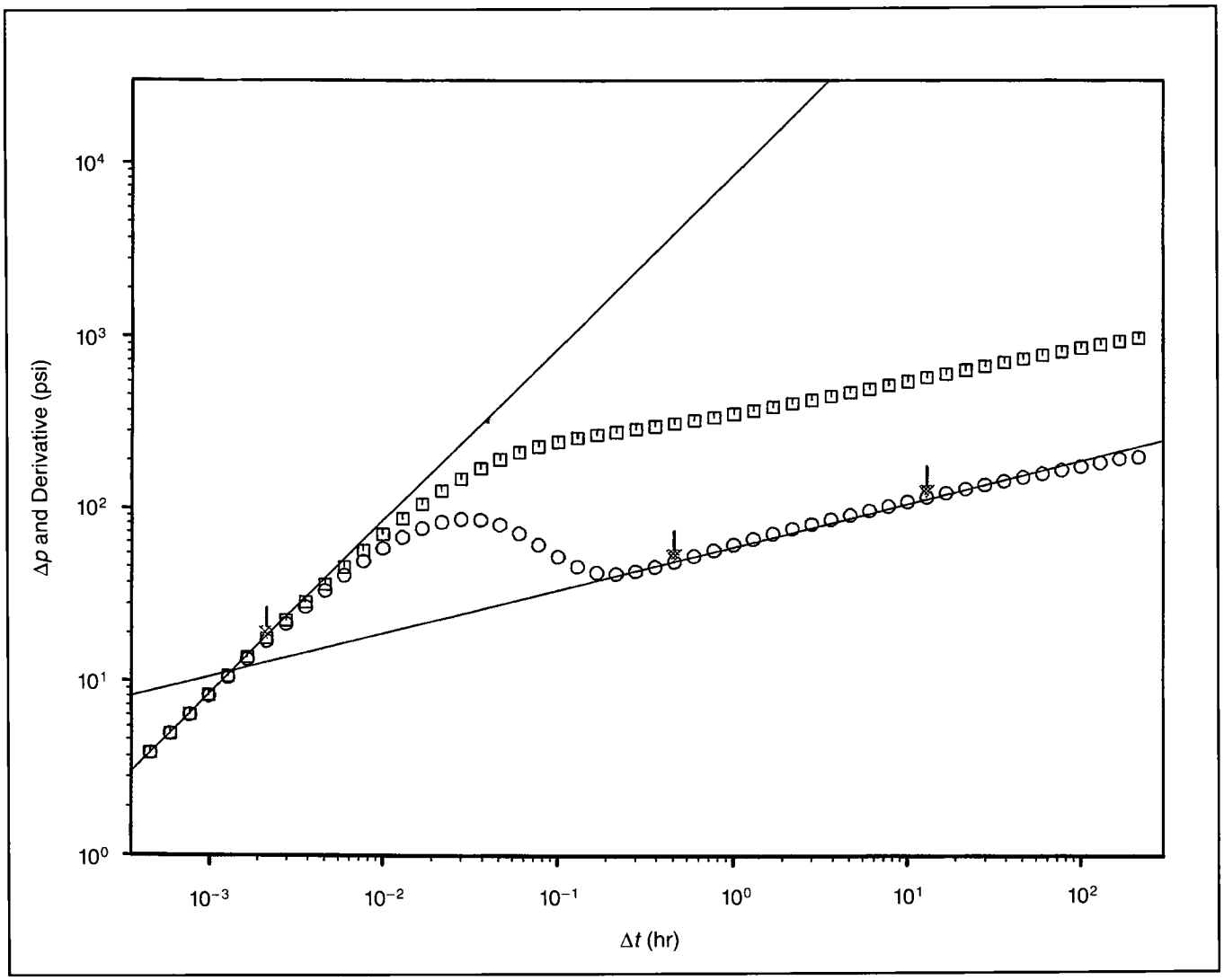

Figure F-2—Flow regime identification for Example F-8.

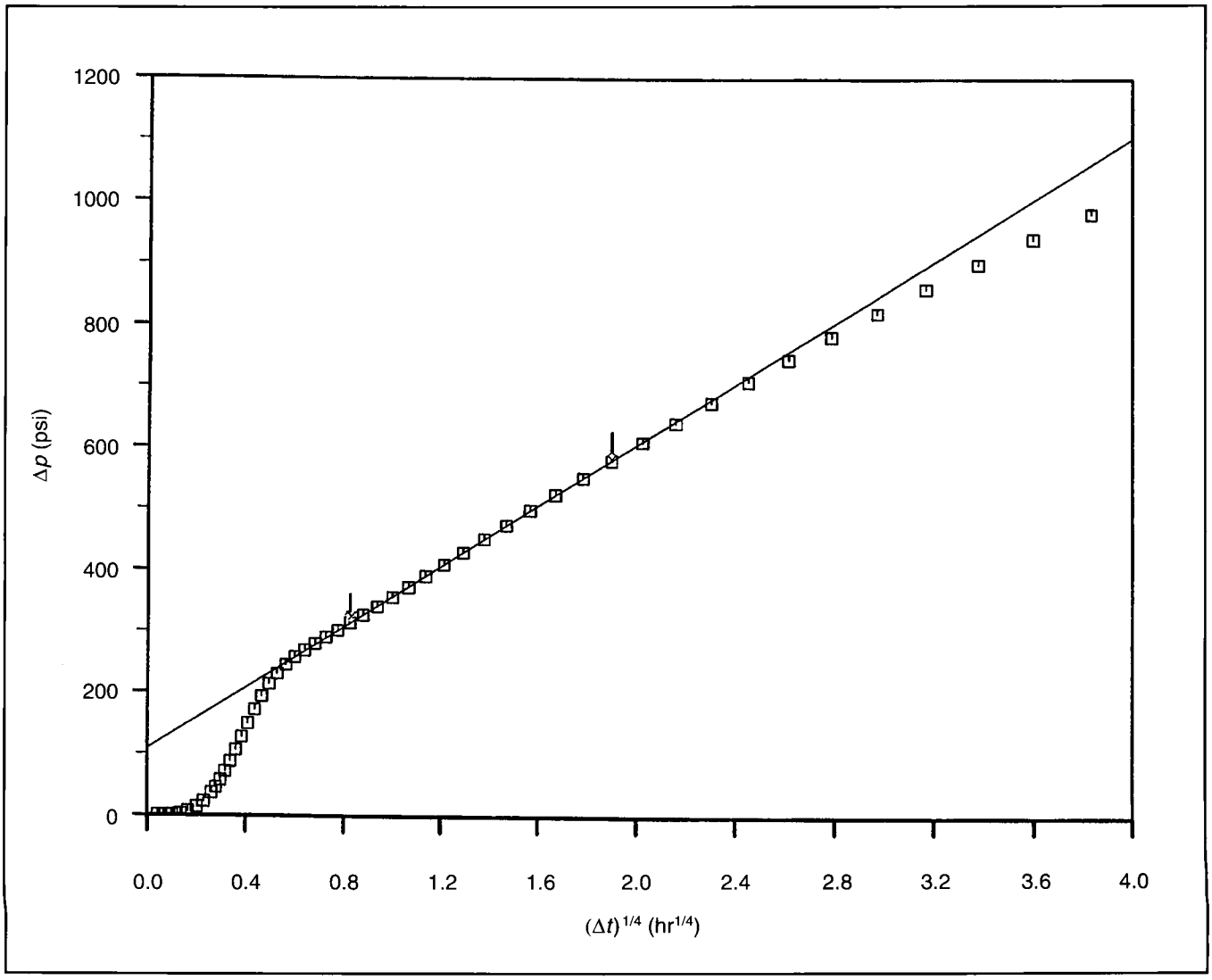

Figure F-3—Specialized quarter-root of time plot for Example F-8.

EXAMPLE F-9

Very Tight Oil Well— Interpretation of Posttreatment Test

A very tight oil well was flowed above the bubblepoint for 60 days and then was shut in for 50 days. The flow rate was 195 STB/d. A summary of the test is shown in Fig. F-4. The permeability, obtained from a pretreatment test, was 0.003 md. Calculate the fracture geometry and conductivity. Table F-5 contains the relevant well and reservoir data.

Solution (Ref. Section 11-6)

Figure F-5 is the log-log diagnostic plot for this test. Since the permeability is very low, it should be expected that the fracture conductivity should be very high ($F_{CD} > 100$), and thus no bilinear flow should be evident. Instead, linear flow, represented by the half-slope straight line on Fig. F-5, should denote the large conductivity fracture. (In this test, the larger than 0.5 slope at later time is attributed to superposition effects. If the buildup time is of the same order of duration as the flow time, e.g., 50 days, then distortion of the data can occur. Further explanation of this trend is outside the scope of this example.)

The linear flow trends lead to the specialized plot in Fig. F-6 where the square root of time vs. pressure is plotted on Cartesian coordinates. The slope is equal to 47.4 psi/hr$^{0.5}$.

Thus, from Eq. 11-14 the fracture half-length may be calculated.

$$x_f = \frac{(4.064)(195)(1.3)}{(135)(47.4)} \left(\frac{0.3}{(0.003)(0.09)(1.5 \times 10^{-5})} \right)^{0.5} = 1380\,\text{ft}. \quad \text{(F-30)}$$

Since this fracture was *designed* for a $k_f w$ product equal to 1300 md-ft, then

$$F_{CD} = \frac{1300}{(0.003)(1380)} = 314, \quad \text{(F-31)}$$

which readily justifies the appearance of linear flow and the lack of bilinear flow.

k	=	0.003 md
t_p	=	60 days
ϕ	=	0.09
q	=	195 STB/d
h	=	135 ft
p_{wf}	=	3300 psi
c_t	=	1.5×10^{-5} psi^{-1}
r_w	=	0.328 ft
B_o	=	1.3 resbbl/STB

Table F-5—Well and reservoir data for Example F-9.

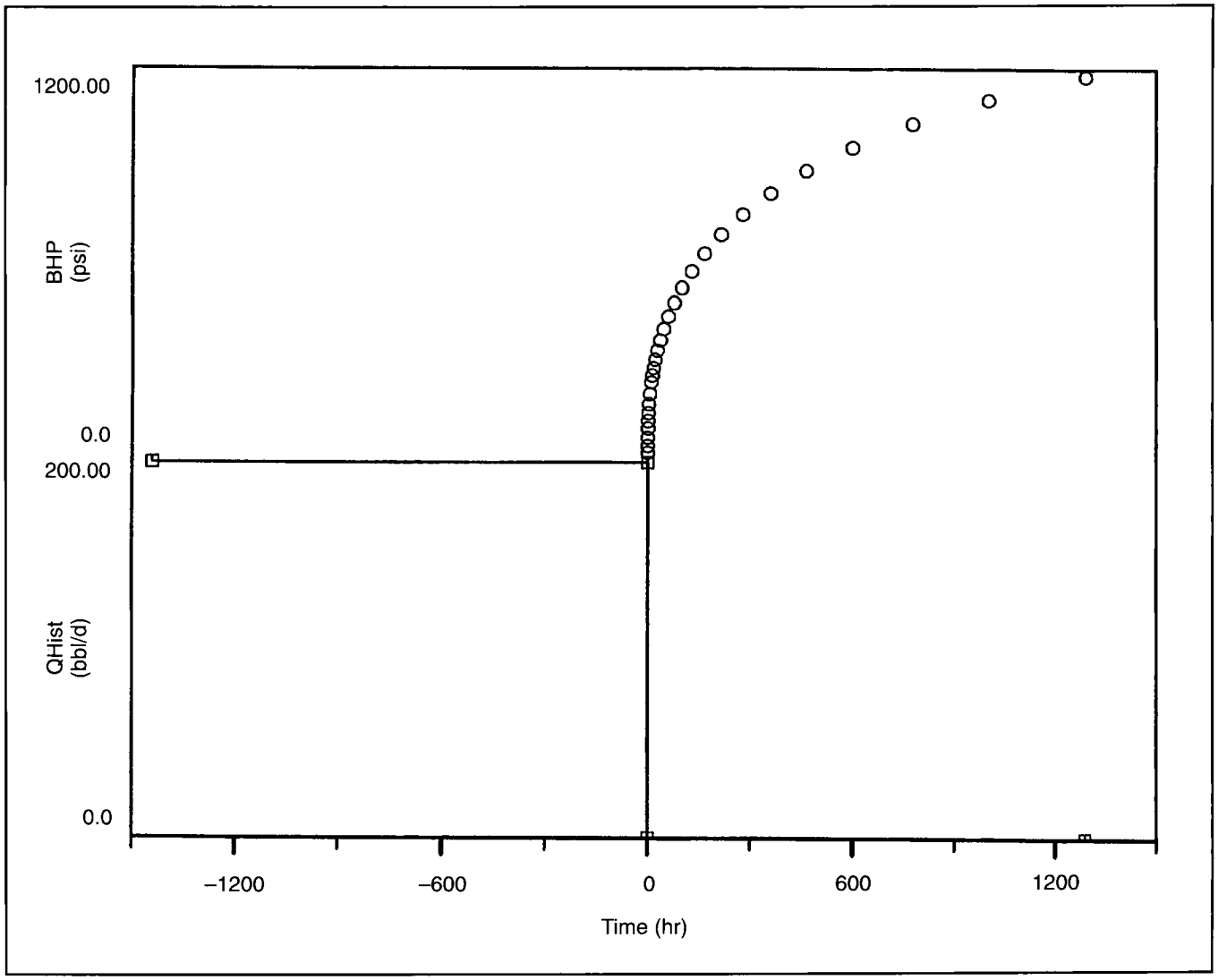

Figure F-4—Summary of rate and pressure transients for Example F-9.

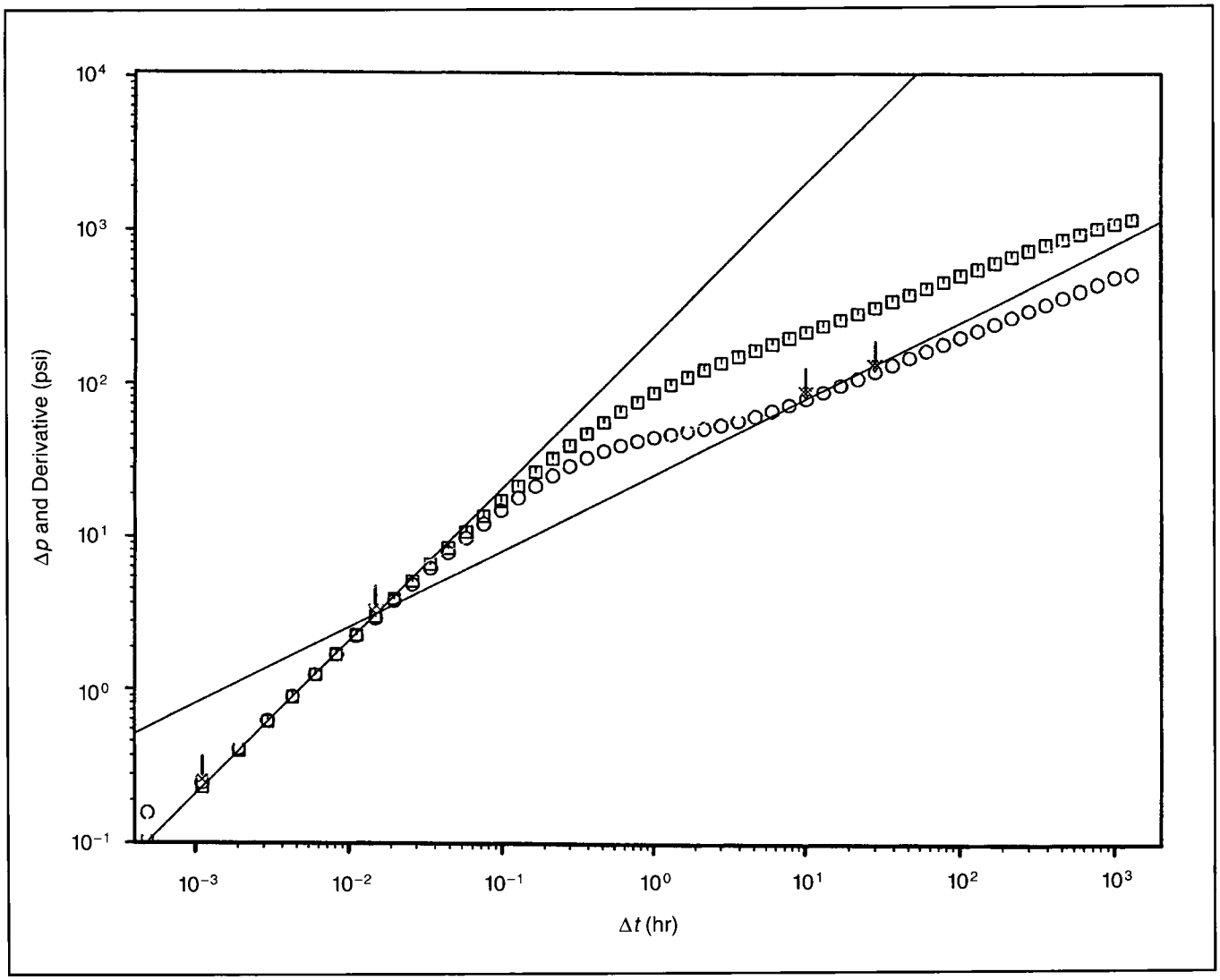

Figure F-5—Flow regime identification for Example F-9.

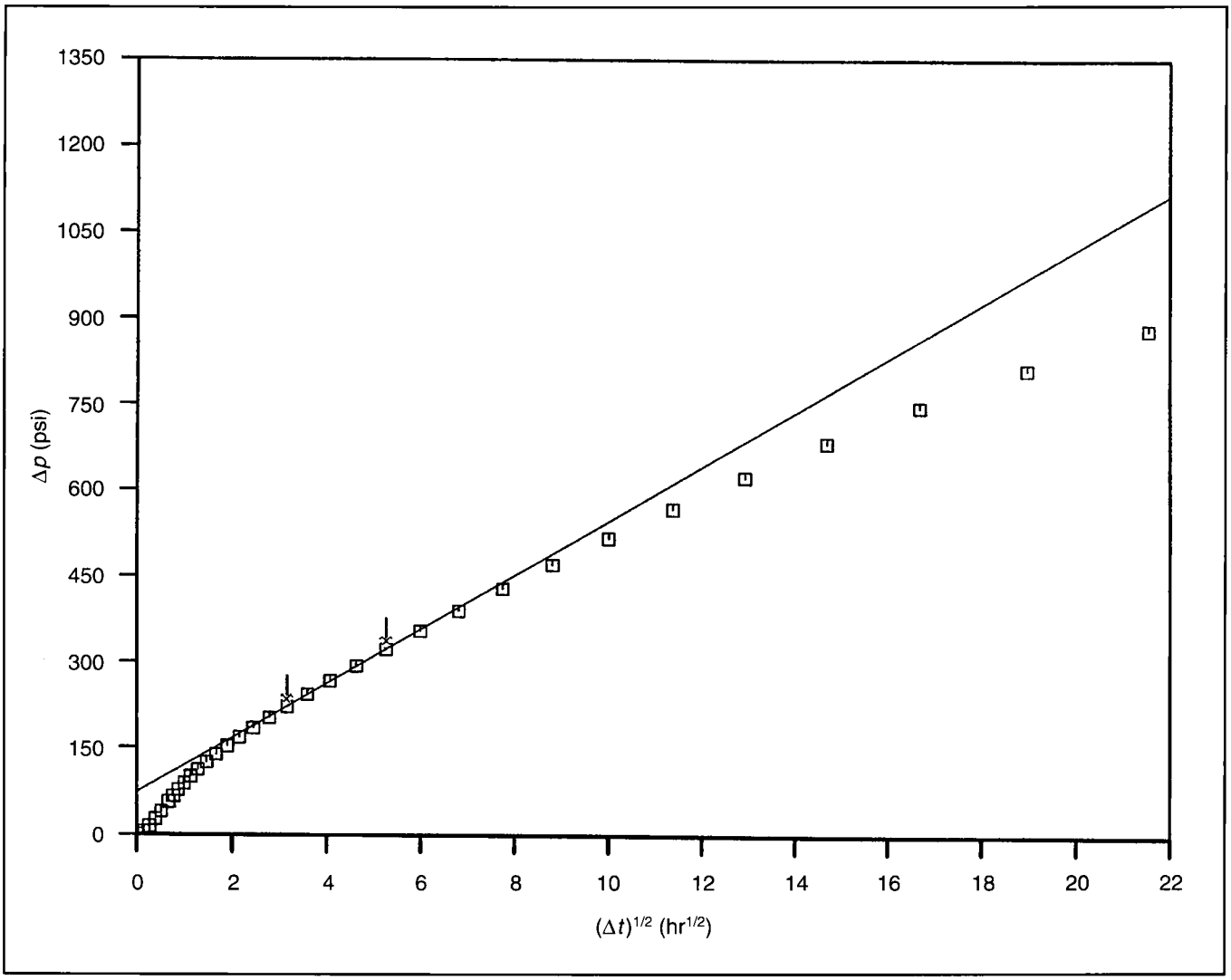

Figure F-6—Specialized square root of time plot for Example F-9.

EXAMPLE F-10

Interpretation of a Long-Flowing, Hydraulically Fractured Well

Over three years, a fractured gas well exhibited the pressure and rate history as shown in Fig. F-7. The relevant and known well and reservoir variables appear in Table F-6. Interpret the well behavior and obtain any reservoir and fracture characteristics that are possible.

Solution (Ref. Section 11-8)

Figure F-8 contains a log-log diagnostic plot of the influence function, its derivative and the convolution derivative for this well. The real-gas pseudopressure function is used.

Clearly, the flat derivative and convolution derivative on the right side of the data denote pseudoradial, infinite acting behavior. The noise in the data is typical in interpreting wellhead data. However, even with the noise, these data allow a very definitive interpretation for this well. In addition, the earlier half-slope in Fig. F-8 indicates a very high conductivity fracture.

Figure F-9 is a specialized plot for the infinite acting behavior. A rate-convolved time function is used. (This is the current state of the art and is outside the scope of this exercise. A semilogarithmic plot of $\Delta m(p)/q$ vs. log t as outlined in Chapter 11 would suffice.)

From Fig. F-9, the permeability is equal to 0.45, and the skin effect is equal to –6.3. From the definition of the effective wellbore radius for a high-conductivity fracture ($r'_w = r_w e^{-s} = x_f/2$), the fracture half-length is equal to 360 ft. This is an effective length and could be quite different from the real length because of damage (and reduction of the conductivity) to the proppant pack, reservoir permeability, anisotropy, etc.

ϕ	=	0.18
T	=	268°F
h	=	55 ft
γ_g	=	0.65
S_g	=	0.65
r_w	=	0.328 ft

Table F-6—Well and reservoir variables for Example F-10.

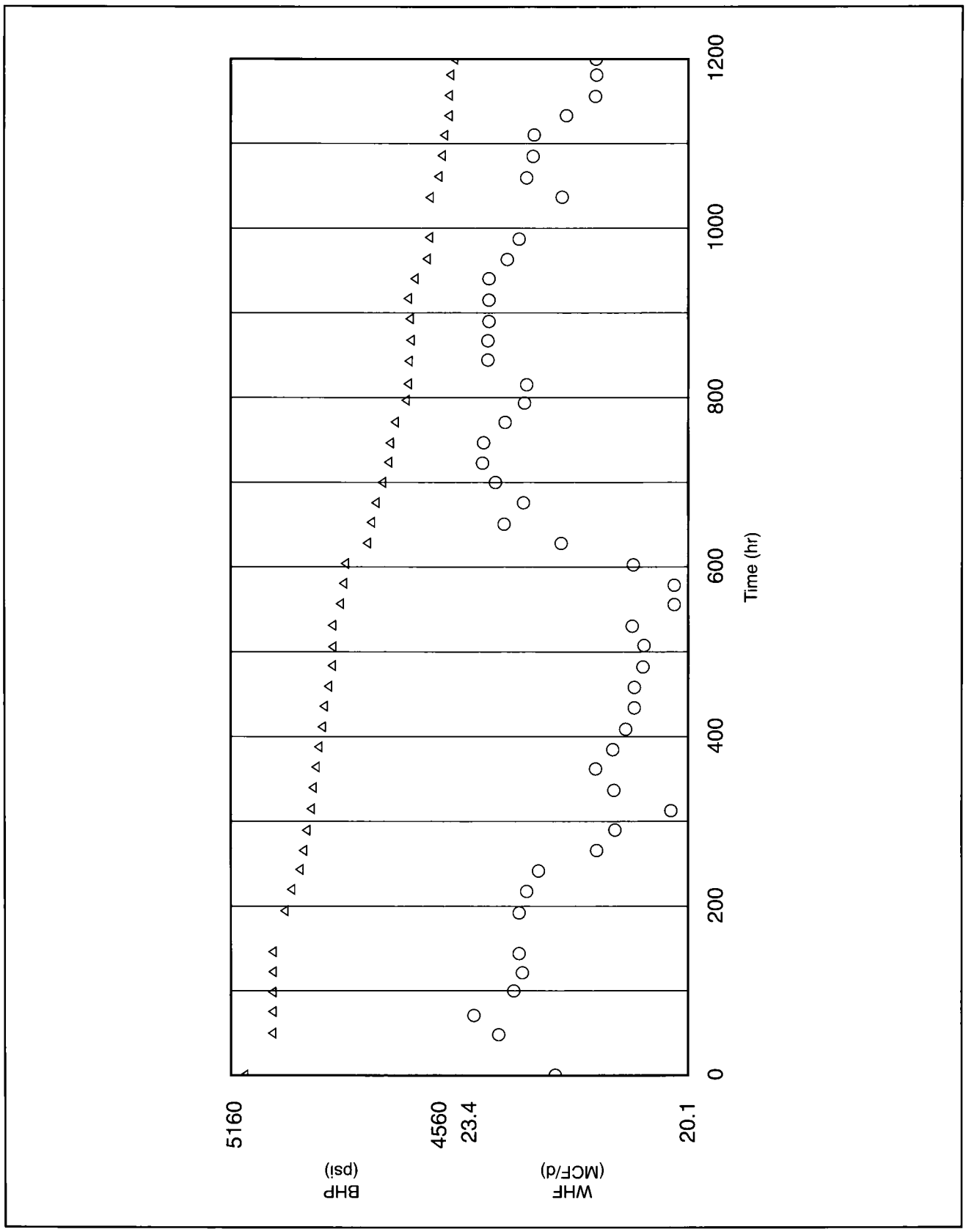

Figure F-7—Pressure and rate history for the well in Example F-10.

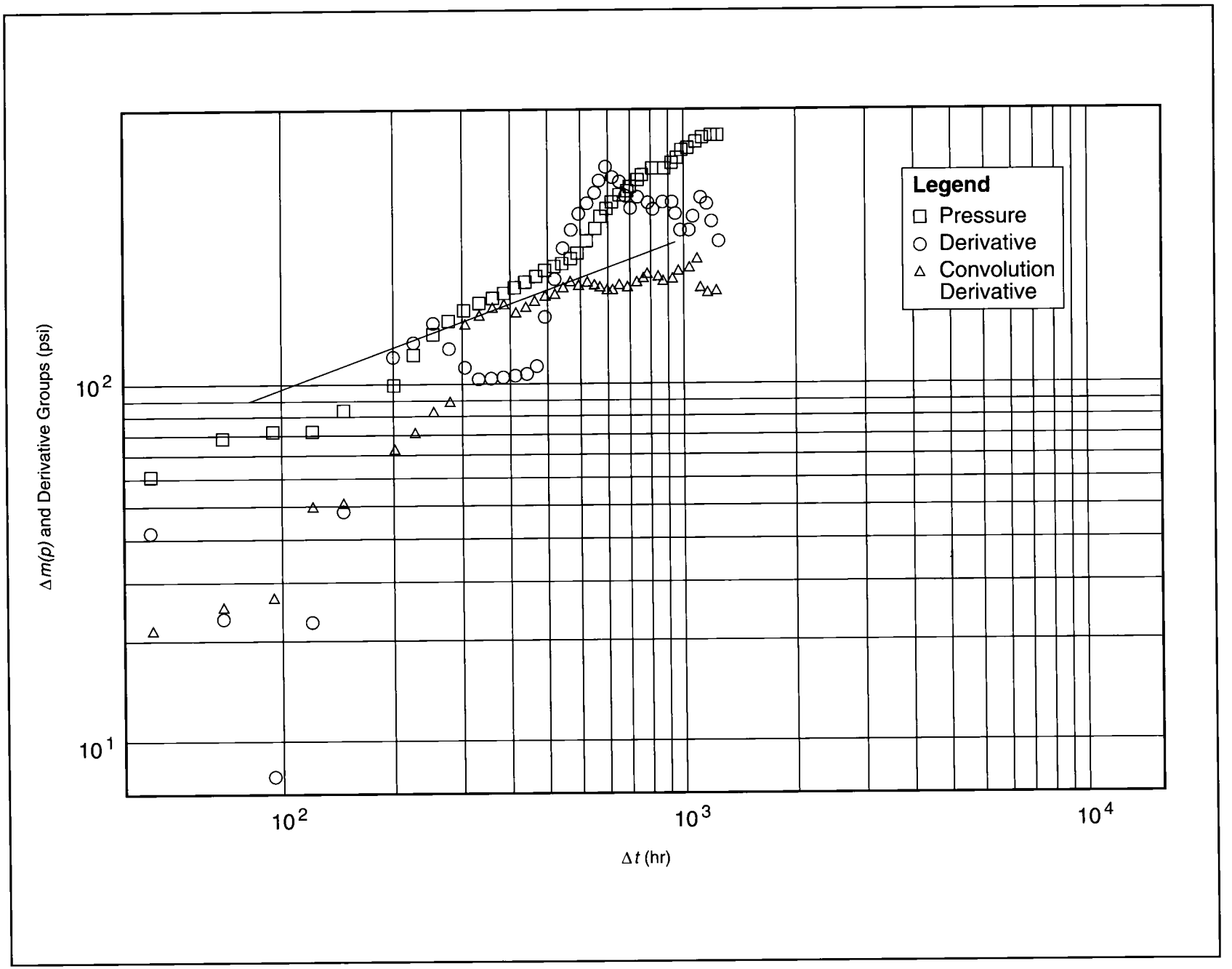

Figure F-8—Log-log diagnostic plot of influence function, its derivative and convolution derivative for Example F-10.

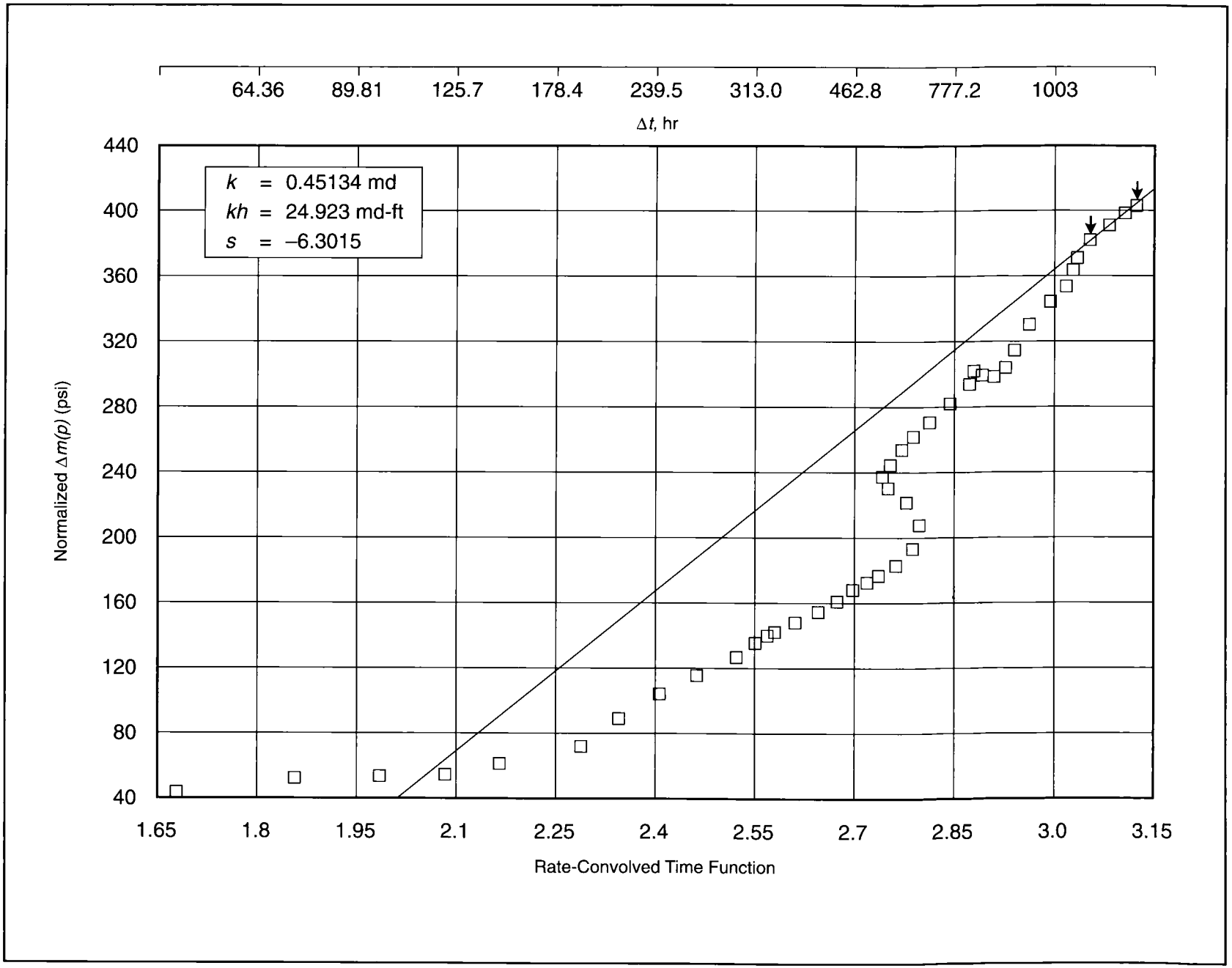

Figure F-9—Rate-convolved time vs. influence function for Example F-10.

This Page Intentionally Left Blank

G. Design of Matrix Treatments

EXAMPLE G-1

Treatment Selection for Damage Removal

What treatment would you recommend for the following types of damage?

a) Water block in an oil well with a temperature equal to 300°F

b) $CaSO_4$ scale

c) FeS scale

d) Organic deposits

Solution (Ref. Section 12-5)

From Fig. 12-8, the following treatments are recommended.

a) Nonaqueous acetic acid

b) EDTA

c) HCl plus a reducing agent and a sequestering agent

d) Aromatic solvents

EXAMPLE G-2

Calculation of Skin-Effect Reduction in a Dolomite Reservoir

Calculate the skin-effect reduction in a dolomite reservoir where the dolomite concentration is 60%. Acid, consisting of 15% HCl, is to be used. The well, reservoir and treatment variables are presented in Table G-1.

Solution (Ref. Sections 13-3 and 14-5)

The stoichiometric constant of the reaction between dolomite $CaMg(CO_3)_2$ and HCl is 4.

First, the acid capacity number, Ac, is calculated from Eq. 13-8. The acid concentration is 15% by weight. Thus, in 1 liter of solution (assuming $\rho \cong 1$ g/cm^3),

$$C = \frac{(150/36.5)}{1 \text{ liter}} = 4.1 \text{ moles/liter}, \qquad \text{(G-1)}$$

where 36.5 is the HCl molecular weight. The dolomite concentration, since it is 60% by weight, can be calculated as follows.

In 1 liter of rock, the total weight is 2650 g, of which $(2650 \times 0.6) = 1590$ g is dolomite. Since the molecular weight of dolomite is equal to 184, its concentration is 1590/184 = 8.64 moles/liter. Thus, from Eq. 13-8, the acid capacity number is

$$Ac = \frac{(0.15)(4.1)}{(4)(8.64)} = 0.018. \qquad \text{(G-2)}$$

The Peclet number for radial geometry is given by

$$N_{Pe} = \frac{q}{Dh}, \qquad \text{(G-3)}$$

and thus

$$N_{Pe} = \frac{(1 \text{ BPM})(2.648 \times 10^3 \text{ cm}^3\text{/s/BPM})}{(10^{-5} \text{ cm}^2\text{/s})(100 \text{ ft} \times 30.48 \text{ cm/ft})}$$

$$= 8.69 \times 10^4. \qquad \text{(G-4)}$$

Finally, from Eq. 13-13 and remembering that $d = 2$ for surface reaction limited kinetics (for dolomites),

$$\Delta s = -\frac{1}{2} \ln \left[1 + (0.018)(8.69 \times 10^4)^{-0.333} \frac{(1.7 \times 10^4)(56.8)}{(3.14)(30.48)(0.15)(0.1)^2} \right]$$

$$= -4. \qquad \text{(G-5)}$$

q_i	=	1 BPM
h	=	100 ft
D	=	10^{-5} cm^2/s
r_w	=	0.328 ft = 0.1m
ϕ	=	0.15
ρ_{rock}	=	2.65 g/cm^3
V_i	=	15,000 gal (56.8 m^3)

Table G-1—Well, reservoir and treatment variables for Example G-2.

EXAMPLE G-3

Calculation of Skin-Effect Reduction in a Limestone Reservoir

What would be the skin-effect reduction if the reservoir in Example G-2 were 100% limestone and the acid formulation a 28% by weight HCl solution? Keep all other variables the same.

Solution (Ref. Section 13-3)

A 28% by weight solution of HCl has a density approximately equal to 1 g/cm^3, and thus the acid concentration is

$$C = \frac{280/36.5}{1 \text{ liter}} = 7.67 \text{ moles/liter}, \qquad \text{(G-6)}$$

where 36.5 is the molecular weight of HCl.

The weight of 1 liter of rock is 2650 g, and since all of it is $CaCO_3$ (MW = 100), its concentration is 26.50 moles/liter. The stoichiometric constant of HCl reacting with $CaCO_3$ is 2. Thus, the acid capacity number can be calculated from Eq. 13-8.

$$Ac = \frac{(0.15)(7.67)}{(2)(26.5)} = 0.0217. \qquad \text{(G-7)}$$

The Peclet number is the same. However, the fractal dimension for mass transfer limited kinetics is equal to 1.6. Therefore, from Eq. 13-13,

$$\Delta s = -\frac{1}{1.6} \ln \left[1 + (0.0217)(8.69 \times 10^4)^{-0.333} \frac{(1.7 \times 10^4)(56.8)}{(3.14)(30.48)(0.15)(0.1)^{1.6}} \right]$$

$$= -4.5. \qquad \text{(G-8)}$$

EXAMPLE G-4

Impact of Injection Rate and Acid Volume on Skin-Effect Reduction

Using the variables in Example G-3, demonstrate the effect of injection rate and volume of acid injected on the skin-effect reduction. Use a range of injection rates from 0.25 to 5 BPM. Use a range of injection volumes from 25 gal/ft to 300 gal/ft.

Solution (Ref. Section 13-3)

From Eq. 13-13, replacing the Peclet number by its expression and grouping variables after substitution,

$$\Delta s = -\frac{1}{1.6} \ln \left[1 + 5.81 \times 10^4 \left(\frac{q_i}{0.03048} \right)^{-0.333} \right], \qquad \text{(G-9)}$$

where q_i is in cm^3/s (1 BPM = 2.648×10^3 cm^3/s). Equation G-9 is for 150 gal/ft (i.e., a total of 15,000 gal).

Figure G-1 is a plot of the skin effect decrease vs. injection rate showing a mild reduction in the skin-effect decline with increasing injection rate.

Assuming a commonly used injection rate of 1 BPM, then from Eq. 13-13 after grouping variables,

$$\Delta s = -\frac{1}{1.6} \ln [1 + 23.2V], \qquad \text{(G-10)}$$

where V is the injected acid volume in m^3. (Note: 1 m^3 = 264 gal.)

Figure G-2 is a plot of the skin-effect decrease vs. acid volume injected, showing a significant impact at small incremental volumes and then flattening out by virtue of the logarithmic relationship.

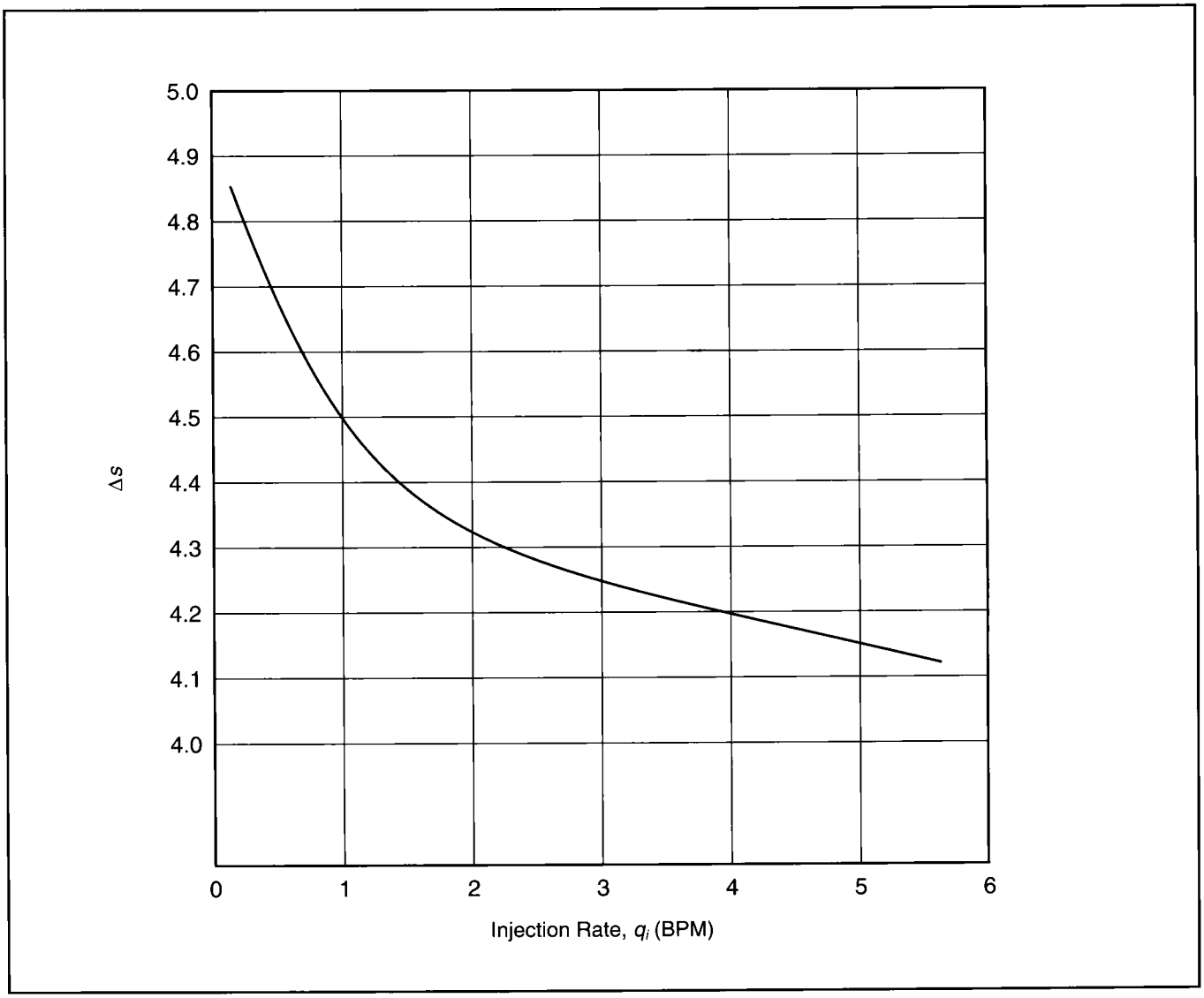

Figure G-1—Skin-effect reduction for a range of injection rates.

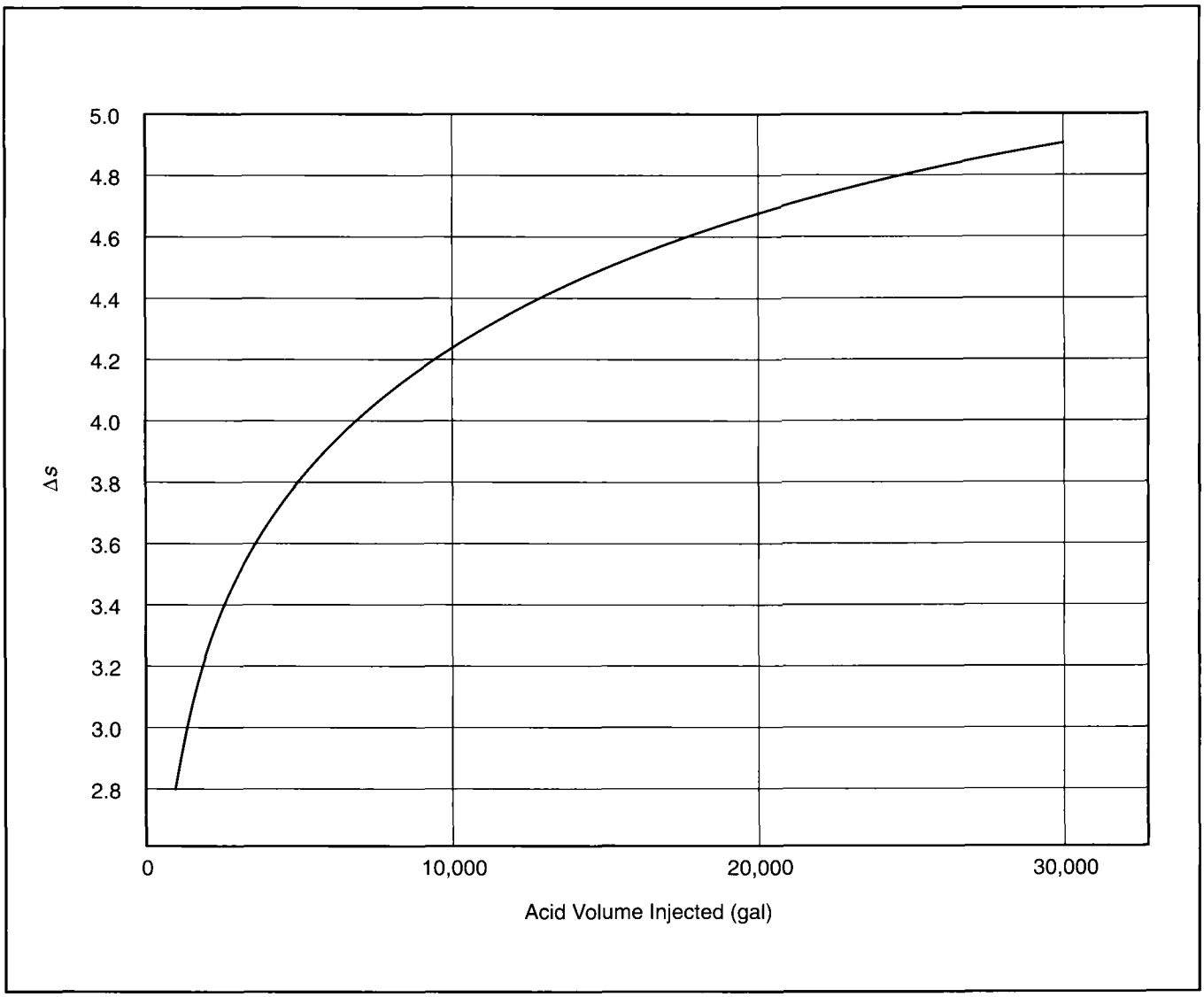

Figure G-2—Skin-effect reduction for a range of injection volumes (h = 100 ft; therefore, divide by 100 to obtain gal/ft).

EXAMPLE G-5

Well Production Rate Improvement vs. Size of Stimulation Treatment

Using the well and reservoir data in Table G-2, calculate the steady-state production rate and graph as a function of volumes of acid injected. Assume that the original skin effect was 10.

Solution (Ref. Section 13-3)

The steady-state equation as applied to this well would result in a production rate, q (STB/d), given by:

$$q = \frac{(50)(100)(5000-3000)}{(141.2)(1)(1.1)\left[\ln(1053/0.328)+s\right]}$$

$$= \frac{6.44\times 10^4}{8+s} \qquad \text{(G-11)}$$

Figure G-3 is a plot of volumes of acid injected (taken from Fig. G-2) vs. well production rate (subtracting the skin-effect reduction from the original value of 10 and substituting in Eq. G-11). As can be seen, production rate improvement levels off after a very substantial relative increase at small injection volumes. However, optimum injection volumes must be determined on the basis of incremental rates. The concept of the net present value (NPV) should be applied for a properly optimized treatment.

k	=	50 md
B	=	1.1 resbbl/STB
h	=	100 ft
μ	=	1 cp
p_i	=	5000 psi
r_e	=	1053 ft (80 acre)
p_{wf}	=	3000 psi
r_w	=	0.328 ft

Table G-2—Well and reservoir variables for Example G-5.

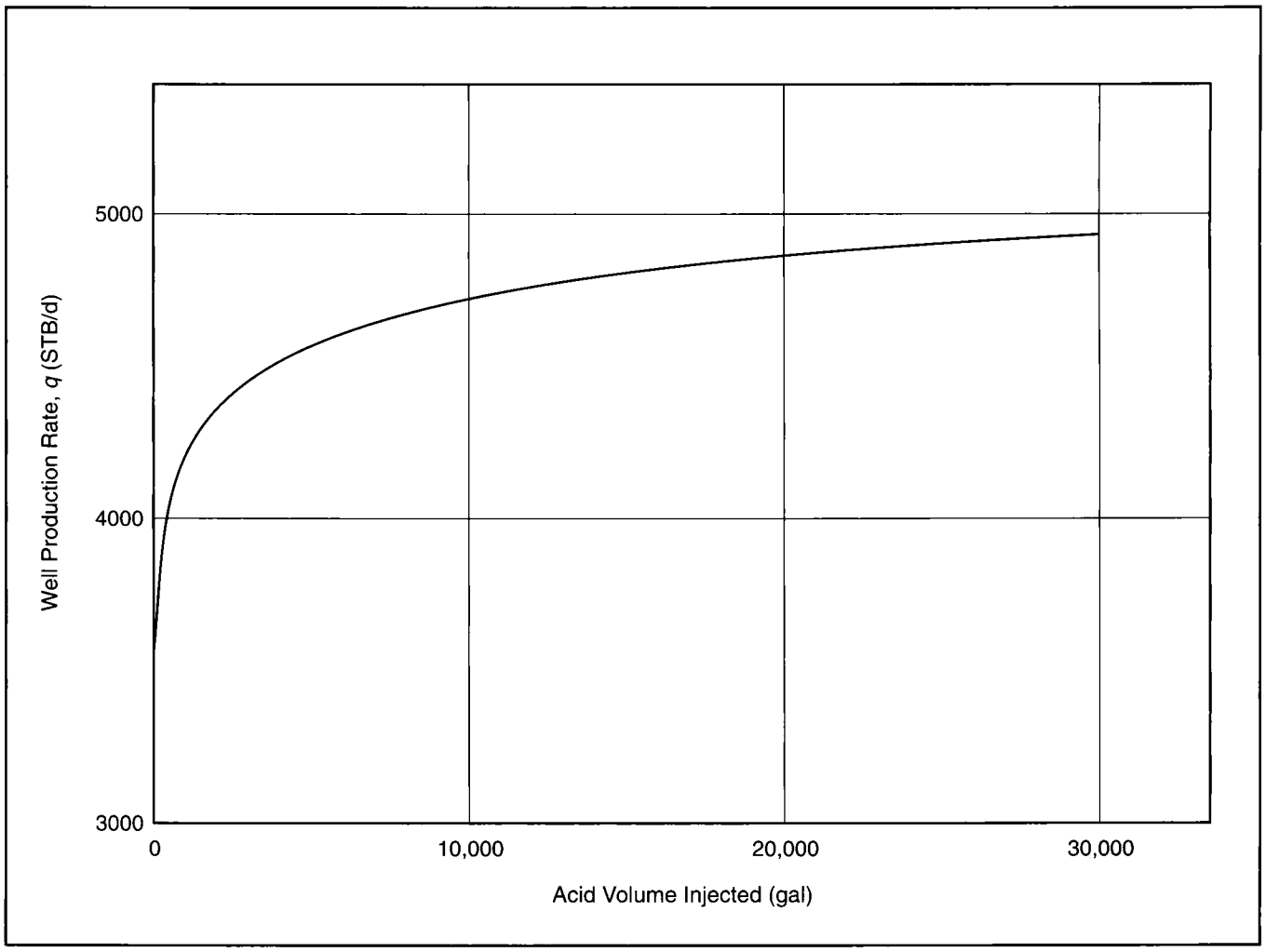

Figure G-3—Stimulation and resulting production rate improvement for well in Example G-5.

EXAMPLE G-6

Calculation of Acid Dissolving Power

Estimate the acid dissolving power in gallons of rock per gallons of acid for a limestone. Use density of limestone as 2.7 g/cm^3. The acid is 28% by weight.

Solution (Ref. Section 14-7)

The stoichiometric relationship of the reaction between HCl and limestone ($CaCO_3$) is:

$$\underset{100}{CaCO_3} + \underset{73}{2HCl} \rightarrow \underset{111}{CaCl_2} + \underset{18}{H_2O} + \underset{44}{CO_2}.$$

Thus, for 100 g of $CaCO_3$, there is a need for 73 g of HCl.

One gallon of 28% HCl has a volume of 3785 cm^3 and weighs approximately 3785 g. Therefore, it contains 1060 g of HCl, which can dissolve (1060) (100/73) = 1452 g of $CaCO_3$. Since the density is 2.7 g/cm^3, the volume of limestone that can be dissolved is 538 cm^3, or 0.142 gal. Thus, the dissolving power of acid is 0.142 gal of rock/gal of acid.

EXAMPLE G-7

Fluid Volume Requirements

Calculate the fluid volume requirements for the acidizing of a sandstone assuming that kaolinite clay is to be removed with mud acid. The weight fraction of the kaolinite is 5%. The dissolving power of acid is 0.05 gal of rock/gal of acid. The porosity is 0.25, and the well radius is 0.328 ft. Do this for depths of damage from 1 to 5 ft.

Solution (Ref. Section 14-7)

From Eq. 14-8, the volume of acid required per foot of formation thickness can be calculated.

$$V_{acid} = 7.48\,\frac{(3.14)(1-0.25)(0.05)(r_s^2 - 0.328^2)}{(0.05)}$$

$$= 17.6\,(r_s^2 - 0.328^2). \qquad \text{(G-12)}$$

Figure G-4 is a plot of the volume of acid required to remove the range of damage.

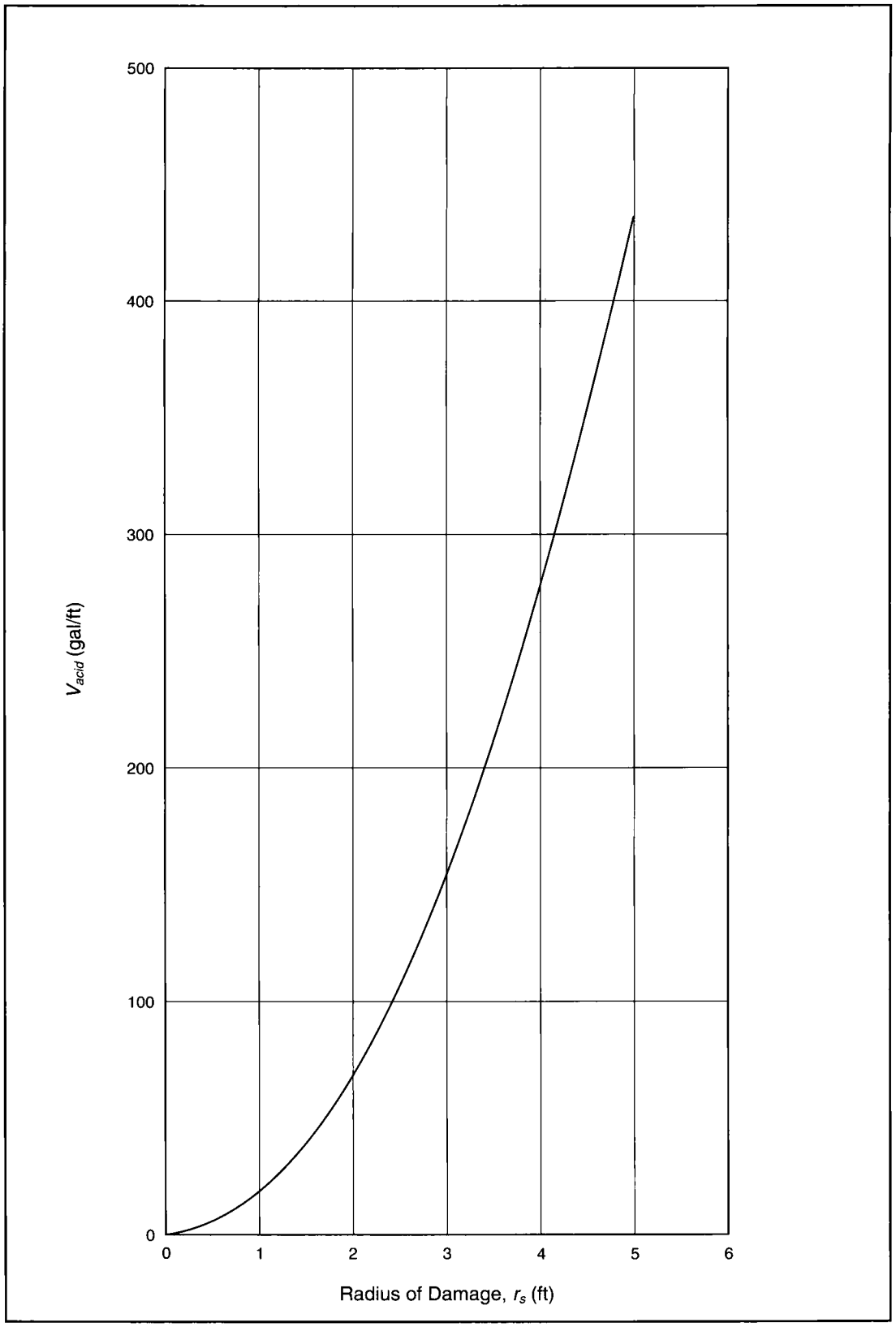

Figure G-4—Volume of acid required (gal/ft) to remove damage.

EXAMPLE G-8

Maximum Injection Rate

Calculate the maximum injection rate for matrix stimulation (to avoid fracturing) for the well described in Table G-3. What would be the effect if the permeability were 1 md?

Solution (Ref. Section 14-7)

From Eq. 14-6,

$$q_{imax}\,(\text{BPM}) = \frac{(4.917\times 10^{-6})(100)(50)\left[(0.7)(10{,}000)-200-5000\right]}{(0.7)(1)\left[\ln(1053/0.328)+20\right]}$$

$$= 2.25\ \text{BPM}. \qquad \text{(G-13)}$$

If the permeability were 1 md, then this rate (to avoid fracturing) should be 0.0225 BPM, which is outside the possibility of today's pumping equipment. Thus, a low-permeability reservoir not only will not benefit from a matrix stimulation treatment but also, because of its permeability, may not lend itself to such a treatment.

k	=	100 md
Δp_{safe}	=	200 psi
h	=	50 ft
p	=	5000 psi
g_f	=	0.7 psi/ft
μ	=	0.7 cp
H	=	10,000 ft
B	=	1 resbbl/STB
r_e	=	1053 ft (80-acre)
s	=	20
r_w	=	0.328 ft

Table G-3—Well and reservoir variables for Example G-8.

EXAMPLE G-9

Increase of Injection Rate During Treatment

As acid reacts with the damage, the skin effect is reduced. Using the data in Table G-3, show the allowable increase in injection rate as the skin effect is reduced from 20 to 0.

Solution (Ref. Section 14-7)

Equation 14-6, after substitution of variables, becomes

$$q_{imax} = \frac{63.2}{8.07+s}. \qquad \text{(G-14)}$$

Therefore, if s = 20, q_{imax} = 2.25 BPM; if s = 10, q_{imax} = 3.5 BPM; and when s = 0, q_{imax} = 7.8 BPM.

H. Diversion and Treatment Evaluation

EXAMPLE H-1

Need for Diversion

Assume that a reservoir consists of three layers:

Layer	k	h	s
1	10 md	20 ft	2
2	400 md	10 ft	8
3	50 md	30 ft	17

Calculate the distribution of acid to be injected. Use $\ln(r_e/r_w) = 8$.

Solution (Ref. Section 15-1)

The initial flow rate injected in each layer (it will change as acid reacts and reduces the skin effect) is given by Eq. 14-6. Assuming that the pressure gradient is the same in each layer ($g_f H - \Delta p_{safe} - p$ = constant) and B and μ are the same, then

$$q_i \propto \frac{kh}{\left[\ln(r_e/r_w) + s\right]}. \qquad \text{(H-1)}$$

Thus, using the given layer variable,

q_1 = constant × 20
q_2 = constant × 250
q_3 = constant × 60,

and the distribution would be

Layer 1: 6%
Layer 2: 76%
Layer 3: 18%.

Layer 2, which is only 17% of the total formation, initially takes more than 76% of all acid injected. This will deteriorate during injection, as the skin effect in Layer 2 is reduced. On the other hand, Layer 3, consisting of 50% of the formation, takes less than 20% of the initial acid; hence, the need for diversion.

EXAMPLE H-2

Diverter Pseudoskin

Calculate the required pseudoskin to be supplied by a diverter to distribute the injection of acid based on the layer thicknesses in Example H-1.

Solution (Ref. Section 15-5)

To distribute the injected acid based on the thickness of each layer, then

$$\frac{h_1}{h_2} = \frac{q_1}{q_2} = \frac{\left[kh/(\ln(r_e/r_w) + s + s_{cake})\right]_1}{\left[kh/(\ln(r_e/r_w) + s + s_{cake})\right]_2}. \qquad \text{(H-2)}$$

A similar expression can be written between Layers 1 and 3.

Assuming that s_{cake} for the zone that takes the least acid (Layer 1) is zero, then after simplification and substitution,

$$1 = \frac{\left[10/(8+2)\right]}{\left[400/(8+8+s_{cake})\right]}, \qquad \text{(H-3)}$$

resulting in $s_{cake} = 384$. Similarly, between Layers 1 and 3,

$$1 = \frac{\left[10/(8+2)\right]}{\left[50/(8+17+s_{cake})\right]}, \qquad \text{(H-4)}$$

resulting in $s_{cake} = 25$.

EXAMPLE H-3

Diverter Cake Resistance

Calculate the required cake resistance to provide a diverter pseudoskin equal to 50. Assume that there are 50 perforations, with $r_{perf} = 0.333$ in. [8.46×10^{-3} m] and $L_{perf} = 12$ in. [0.3048 m]. The formation thickness is 20 m, and the permeability is 50 md [4.93×10^{-14} m^2].

Solution (Ref. Section 15-5)

From Eq. 15-3 and rearrangement,

$$R_{cake} = \frac{A s_{cake}}{2\pi k h}. \tag{H-5}$$

The area A is

$$A = N_{perf} \times 2\pi r_{perf} L_{perf}, \tag{H-6}$$

and therefore,

$$A = (50)\,(2)\,(3.14)\,(8.46 \times 10^{-3})\,(0.3048)$$

$$= 0.81 \text{ m}^2. \tag{H-7}$$

Finally,

$$R_{cake} = \frac{(0.81)\,(50)}{(2)\,(3.14)\,(4.93 \times 10^{-14})\,(20)}$$

$$= 6.54 \times 10^{12} \text{ m}^{-1}. \tag{H-8}$$

EXAMPLE H-4

Diverter Pseudoskin Factor and Diverter Quantity

Assuming that there is a linear relationship between cake resistance and the diverter pseudoskin factor and that there is a linear relationship between resistance and mass of diverter per unit area, develop a relationship between injection rate per layer and this pseudoskin factor as a function of time.

Solution (Ref. Section 15-5)

(With special thanks to Dr. L. Prouvost)

The injection rate in each layer is given by Eq. 15-5, and the relationship for the s_{cake} is given by Eq. 15-3. From Eq. 15-4, the injection rate can be given in terms of mass of diverter cake deposited per unit area and the diverter concentration in the acid:

$$q_i = \frac{A}{C_{div}} \frac{d\rho_A}{dt}. \tag{H-9}$$

If a linear relationship is assumed between R, the cake resistance, and the ρ_A, the mass of diverter, then from Eq. 15-3,

$$s_{cake} = \frac{2\pi kh}{A}(K_1 \rho_A), \tag{H-10}$$

where K_1 is a constant.

Then Eq. 15-5 becomes

$$q_i = \frac{2\pi kh}{\mu\left[\ln(r_e/r_w) + s + \frac{2\pi kh}{A}(K_1\rho_A)\right]}, \tag{H-11}$$

which then is equated with Eq. H-9. Thus,

$$\frac{A}{C_{div}} \frac{d\rho_A}{dt} = \frac{2\pi kh}{\mu\left[\ln(r_e/r_w) + s + \frac{2\pi kh}{A}(K_1\rho_A)\right]}, \tag{H-12}$$

which defines an ordinary differential equation.

Simple solution results in

$$q_i = \frac{2\pi kh\Delta p}{\mu\left[\ln(r_e/r_w) + s\right]} \frac{1}{\sqrt{1 + K_2 t}}, \tag{H-13}$$

where

$$K_2 = \frac{8\pi^2 (kh)^2 K_1 \Delta p C_{div}}{A^2 \mu\left[\ln(r_e/r_w) + s\right]^2}. \tag{H-14}$$

K_1 is the experimentally determined slope between mass of diverter per unit area and the resistance of the diverter cake.

EXAMPLE H-5

Development of Injection Rate Profile

Assuming that a layer exhibits the characteristics in Table H-1 and assuming that the diverter constant K_1 is equal to 6.15×10^{16} and if $C_{div} = 0.1\%$, calculate the injection rate evolution.

Solution (Ref. Section 15-5)

From Eq. H-14,

$$K_2 = \left[\frac{8\,(3.14)^2\,(4.93 \times 10^{-14})^2\,(15.24)^2}{(0.8)\,(10^{-3})} \right.$$

$$\left. \frac{(6.15 \times 10^{16})\,(3.45 \times 10^{6})\,(0.001)}{(8+15)^2} \right]$$

$$= 2.2 \times 10^{-2}\ s^{-1}, \qquad \text{(H-15)}$$

leading to (from Eq. H-13)

$$q_i = \frac{(2)\,(3.14)\,(4.93 \times 10^{-14})\,(15.24)\,(3.45 \times 10^{6})}{(10^{-3})\,(8+15)\sqrt{1 + 2.2 \times 10^{-2}\,t}}$$

$$= \frac{7 \times 10^{-4}}{\sqrt{1 + 2.2 \times 10^{-2}\,t}} \left(\frac{m^3}{s} \right), \qquad \text{(H-16)}$$

where t must be in seconds.

Figure H-1 is a plot of the injection rate evolution for this layer vs. time. (Units have been converted to BPM and minutes.)

k	=	50 md [4.93×10^{-14} m^2]
ln (r_e/r_w)	=	8
h	=	50 ft [15.24 m]
s	=	15
Δp	=	500 psi [3.45×10^6 Pa]
A	=	0.8 m^2
μ	=	1 cp [10^{-3} Pa-s]

Table H-1—Well and layer variables for Example H-5.

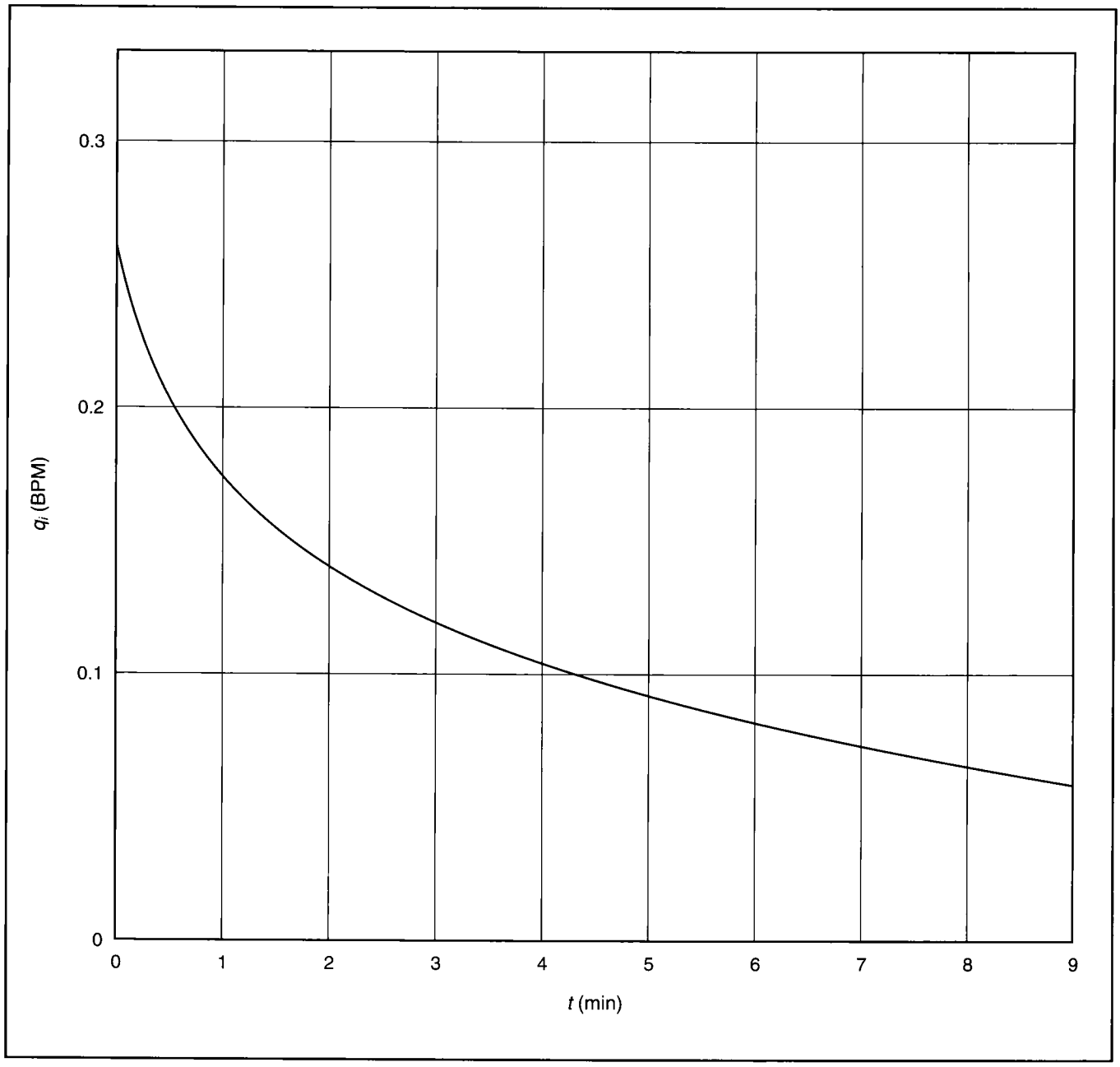

Figure H-1—Injection rate evolution in layer of Example H-5.

EXAMPLE H-6

Design of a Matrix Treatment

Table H-2 contains the variables for a carbonate formation to be acidized. Calculate the maximum allowable injection rate and the volume of acid required to remove all of the skin effect. Do the above assuming a single layer.

If the formation is considered a two-layer system, with one permeability twice as large as the other (assume equal heights), calculate the concentration of diverter required in the high-permeability layer to accept 40% of the total (maximum) injection rate within 3 min of pumping. The acid is 28% HCl.

Solution (Ref. Sections 13-3, 14-6 and 15-5)

A. Maximum injection rate

From Eq. 14-6,

$$q_{imax}\,(\text{BPM}) = \frac{(4.917\times 10^{-6})\,(10)\,(75)\,[(0.7)\,(8200) - 200 - 4300]}{(0.7)\,(1)\,(8+4)}$$

$$= 0.55\ \text{BPM}. \qquad \text{(H-17)}$$

B. Volume of acid

The acid capacity number for such a treatment has been calculated by Eq. G-7 (in Example G-3) and is equal to 0.0217.

The Peclet number can be calculated from Eq. G-3 with appropriate unit conversions using the maximum injection rate calculated from Eq. H-17.

$$N_{Pe} = \frac{(0.55)\,(2.648\times 10^{3}\ \text{cm}^3/\text{s/BPM})\,(\text{BPM})}{(10^{-5}\ \text{cm}^2/\text{s})\,(75)\,(30.48\ \text{cm/ft})\ \text{ft}}$$

$$= 6.4\times 10^{4}. \qquad \text{(H-18)}$$

From Eq. 13-13 and rearrangement, we can solve for the volume of acid required to result in $\Delta s = 4$. Thus,

$$V = \frac{\pi h \phi r_w^d}{A c N_{Pe}^{-1/3} b}\,(e^{d\Delta s} - 1), \qquad \text{(H-19)}$$

and after substitution (remembering that $d = 2$),

$$V = \frac{(3.14)\,(22.86)\,(0.2)\,(0.1)^2}{(0.0217)\,(6.4\times 10^4)^{-1/3}\,(1.7\times 10^4)}$$

$$(e^{(2)(4)} - 1) = 46.2\ \text{m}^3, \qquad \text{(H-20)}$$

or 12,200 gal, or approximately 160 gal/ft.

C. Concentration of diverter

Since the permeability of the high-permeability zone is twice the permeability of the other zone (since $h_1 = h_2$),

$$h_1 k_1 + 2 k_1 h_1 = \bar{k} h, \qquad \text{(H-21)}$$

where $h_1 = h_2 = 75/2$.

Therefore,

$$3k_1 = 2\bar{k} = 20, \qquad \text{(H-22)}$$

leading to $k_1 = 6.7$ md, and thus $k_2 = 13.4$ md.

From Eq. H-13,

$$tK_2 = \left[\frac{2\pi k h \Delta p}{q_i \mu \left[\ln (r_e/r_w) + s\right]}\right]^2 - 1, \qquad \text{(H-23)}$$

and therefore (by appropriate unit conversions),

$$(3)\,(60)\,K_2 = \left[\frac{(2)\,(3.14)\,(13.4)\,(9.86\times 10^{-16})\,(37.5)}{(0.4)\,(0.47)\,(2.65\times 10^{-3})}\right.$$

$$\left.\frac{(0.3048)\,(1240)\,(6.9\times 10^3)}{(0.7)\,(10^{-3})\,(8+4)}\right]^2 - 1, \qquad \text{(H-24)}$$

leading to $K_2 = 1.5\times 10^{-2}\,\text{s}^{-1}$.

From Eq. H-14,

$$C_{div} = \frac{K_2 A^2 \mu \left[\ln (r_e/r_w) + s\right]^2}{8\pi^2 (kh)^2 K_1 \Delta p}, \qquad \text{(H-25)}$$

and therefore,

$$C_{div} = \left[\frac{(1.5\times 10^{-2})\,(0.8)^2}{(8)\,(3.14)^2\,(13.4)^2\,(9.86\times 10^{-16})^2\,(37.5)^2}\right.$$

$$\left.\frac{(0.7)\,(10^{-3})\,(8+4)^2}{(0.3048)^2\,(6.15\times 10^{16})\,(1240)\,(6.9\times 10^3)}\right]$$

$$= 0.001, \qquad \text{(H-26)}$$

or 0.1% by weight.

k	=	10 md
μ	=	0.7 cp
h	=	75 ft [22.86 m]
$\ln (r_e/r_w)$	=	8
f_g	=	0.7
s	=	+4
H	=	8200 ft
r_w	=	0.328 ft [0.1 m]
Δp_{safe}	=	200 psi
D	=	10^{-5} cm^2/s
$\bar{p}$	=	4300 psi
ϕ	=	0.2
B	=	1 resbbl/STB
K_1	=	6.15 × 10^{16} (in Eq. H-14)
A	=	0.7 m^2

Table H-2—Carbonate formation variables for Example H-6.

EXAMPLE H-7

Calculation of Bottomhole Injection Pressure from Wellhead Values

Calculate the bottomhole injection pressure if the wellhead pressure is 50 psi and the injection rate is 1 BPM. Table H-3 contains all other pertinent variables.

Solution (Ref. Section 16-2)

The velocity is given by

$$u = \frac{q}{A} = \frac{1 \text{ BPM } (0.0936 \text{ ft}^3/\text{s/BPM})}{(3.14)\,(0.203)^2/4} = 2.89 \text{ ft/s.} \quad \text{(H-27)}$$

The Reynolds number can be calculated from Eq. 16-4:

$$N_{Re} = \frac{(60 \text{ lb/ft}^3)(2.89 \text{ ft/s})(0.203 \text{ ft})}{1 \text{ cp } (6.719 \times 10^{-4} \text{ lb/ft - s})}$$

$$= 5.2 \times 10^4. \quad \text{(H-28)}$$

Thus, since this is highly turbulent flow, the Fanning friction factor can be obtained from Eq. 16-6. This can be done through trial and error, resulting in $f = 0.01$.

The friction pressure drop is given (in oilfield units) by Eq. 16-8:

$$\Delta p_{friction} = \frac{(1.525)\,(60)\,(1^2)\,(0.01)\,(10{,}000)}{(2.441)^5}$$

$$= 106 \text{ psi.} \quad \text{(H-29)}$$

Finally, the bottomhole injection pressure can be calculated from Eq. 16-1 (with appropriate substitution for the hydrostatic pressure):

$$p_{iw} = 500 + \frac{(60)\,(10{,}000)}{144} - 106 = 4561 \text{ psi.} \quad \text{(H-30)}$$

ρ	=	60 lb/ft^3
L	=	10,000 ft
d_{tbg}	=	2.441 in. [0.203 ft]
H	=	10,000 ft
μ	=	1 cp

Table H-3—Well and treatment variables for Example H-7.

EXAMPLE H-8

Prediction of Pressure Response at Zero Skin Effect

Both the Paccaloni technique and the Prouvost and Economides technique use a comparison between the measured bottomhole injection pressure and the simulated injection pressure to calculate the evolving skin effect. With the data appearing in Table H-4, develop and plot the pressure response vs. time. What would happen if, after 20 min of injection, the injection rate dropped from 1 BPM to 0.333 BPM?

Solution (Ref. Sections 1-2.2, 16-3 and 16-4)

The equation to calculate the pressure response (assuming that wellbore storage effects are eliminated quickly, which would be the case in a high-permeability reservoir) is a modification of Eq. 1-13:

$$p_{wi} = p_i + \frac{162.6qB\mu}{kh}\left(\log t + \log\frac{k}{\phi\mu c_t r_w^2} - 3.23\right), \quad \text{(H-31)}$$

where q is in STB/d and t is in hours. Equation H-31 can be modified to account for q_i in BPM and t in minutes.

$$p_{wi} = p_i + \frac{2.34\times10^5 q_i B\mu}{kh}\left(\log t + \log\frac{k}{\phi\mu c_t r_w^2} - 5.0\right). \quad \text{(H-32)}$$

The steady-state relationship would be

$$p_{wi} = p_i + \frac{2.34\times10^5 q_i B\mu \ln(r_b/r_w)}{kh}, \quad \text{(H-33)}$$

and is independent of time. The variable r_b is the acid bank as described by Paccaloni. Figure H-2 is a graph of the expected injection pressure response with zero skin effect, and for the first 20 min, there is a "smooth" evolution of the injection pressure difference. If no changes in injection rate are observed, then ultimately the transient injection pressure would evolve into a roughly constant departure from the one calculated from the steady-state relationship.

After the change of the injection rate to 0.333 BPM, the steady-state pressure response will experience the step drop shown in Fig. H-2 after 20 min. The transient response, though, would obey a superposition relationship (where Δt is from the time of the change in the injection rate).

$$\Delta p = \Delta p\,(t + \Delta t) + \Delta p\,(\Delta t), \quad \text{(H-34)}$$

where the first pressure drop is at a rate of 1 BPM and the second pressure drop at a rate equal to $0.333 - t = -0.667$ BPM (see Eq. 1-21). Thus, the injection pressure would be:

$$p_{wi} = p_i + \frac{2.34\times10^5 q_i B\mu}{kh}\left[\log(t+\Delta t) + \log\frac{k}{\phi\mu c_t r_w^2} - 5.0\right] + \frac{2.34\times10^5 (q_{2i} - q_i) B\mu}{kh}\left[\log\Delta t + \log\frac{k}{\phi\mu c_t r_w^2} - 5.0\right]. \quad \text{(H-35)}$$

p_i	=	4000 psi
k	=	100 md
q_i	=	1 BPM
h	=	50 ft
B	=	1 resbbl/STB
ϕ	=	0.20
μ	=	1 cp
c_t	=	6×10^{-6} psi^{-1}
r_b	=	3 ft
r_w	=	0.328 ft

Table H-4—Well and treatment variables for Example H-8.

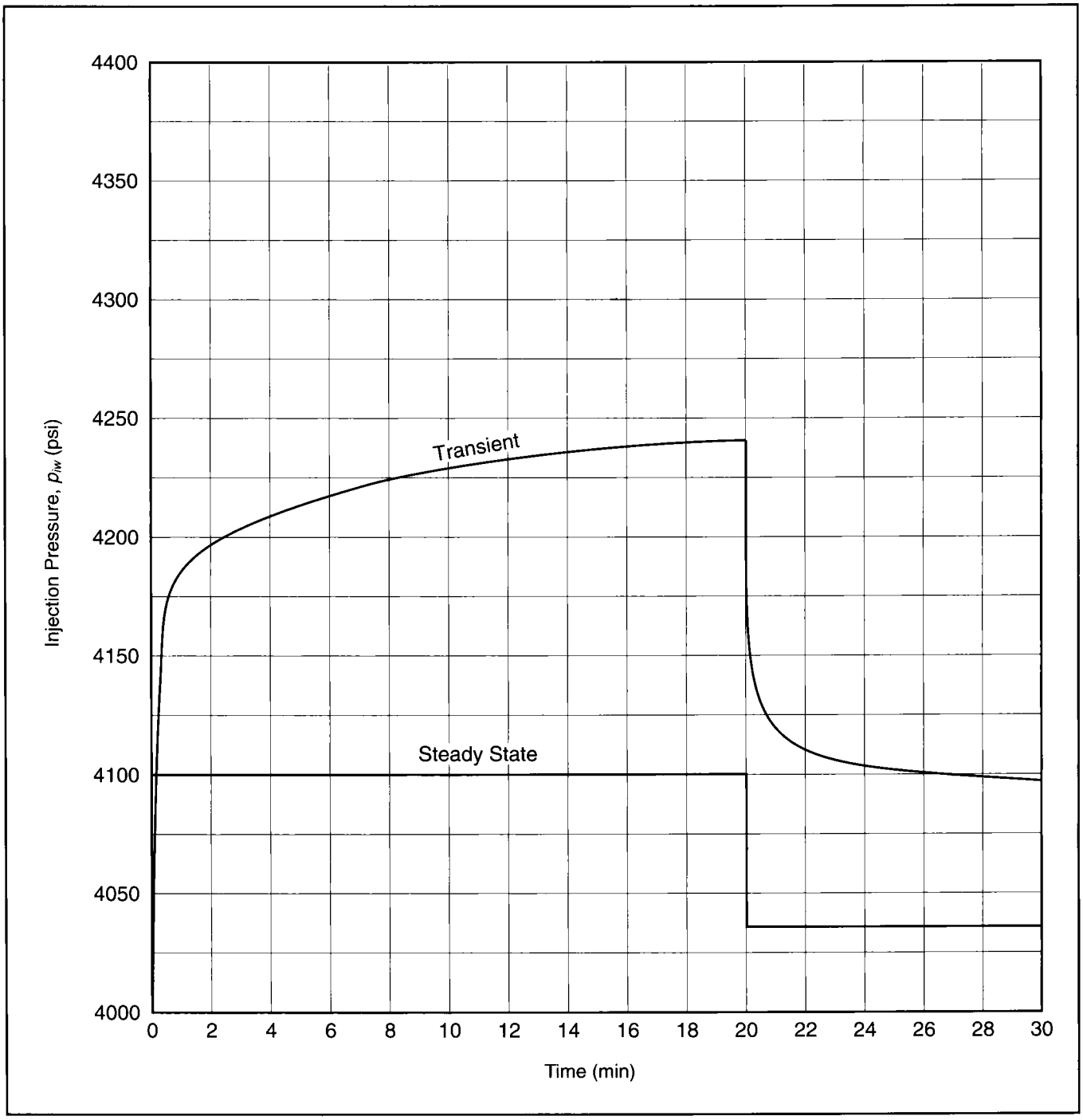

Figure H-2—Transient and steady-state pressure response for Example H-8.

EXAMPLE H-9

Calculation of the Skin-Effect Evolution

Using the "observed" injection pressure history shown in Fig. H-3, plot the evolution of the skin effect using the transient and steady-state simulated injection pressures at zero skin effect. Use the results in Example H-8.

Solution (Ref. Sections 16-3, 16-4 and 16-6)

Equation 16-15 can be used to calculate the evolution of the skin effect using the two techniques. Table H-5 contains the pressure departure $[p_{meas}(t) - p_{sim}(t)]$ for the two models.

The skin effect as a function of time would then be ($s_o = 0$)

$$s_{(t)} = \frac{0.021\,\Delta p_{departure}}{q_{(t)}}, \qquad \text{(H-36)}$$

where $q_{(t)}$ is the injection rate and $\Delta p_{departure}$ is the pressure difference between measured and simulated as shown in Table H-5.

Figure H-4 is a plot of the skin-effect evolution vs. time for the two evaluation models.

As can be easily surmised, if the injection rate is constant, the two models follow each other reasonably well with the pressure departure as indicated in Fig. H-2. However, if the injection rate changes, then while the transient model is immune to this change, the steady-state assumption of an acid bank of finite radius cannot handle the change. To accommodate the reduced rate, an *increase* in the calculated skin effect will result.

Time (min)	$\Delta p_{transient}$ (psi)	$\Delta p_{steady\text{-}state}$ (psi)
1	420	500
2	398	491
4	350	457
6	317	432
8	290	412
12	234	364
20	188	302
21	58	139
22	52	126
26	39	94
30	27	86

Table H-5—Pressure departure for transient and steady-state simulations for Example H-9.

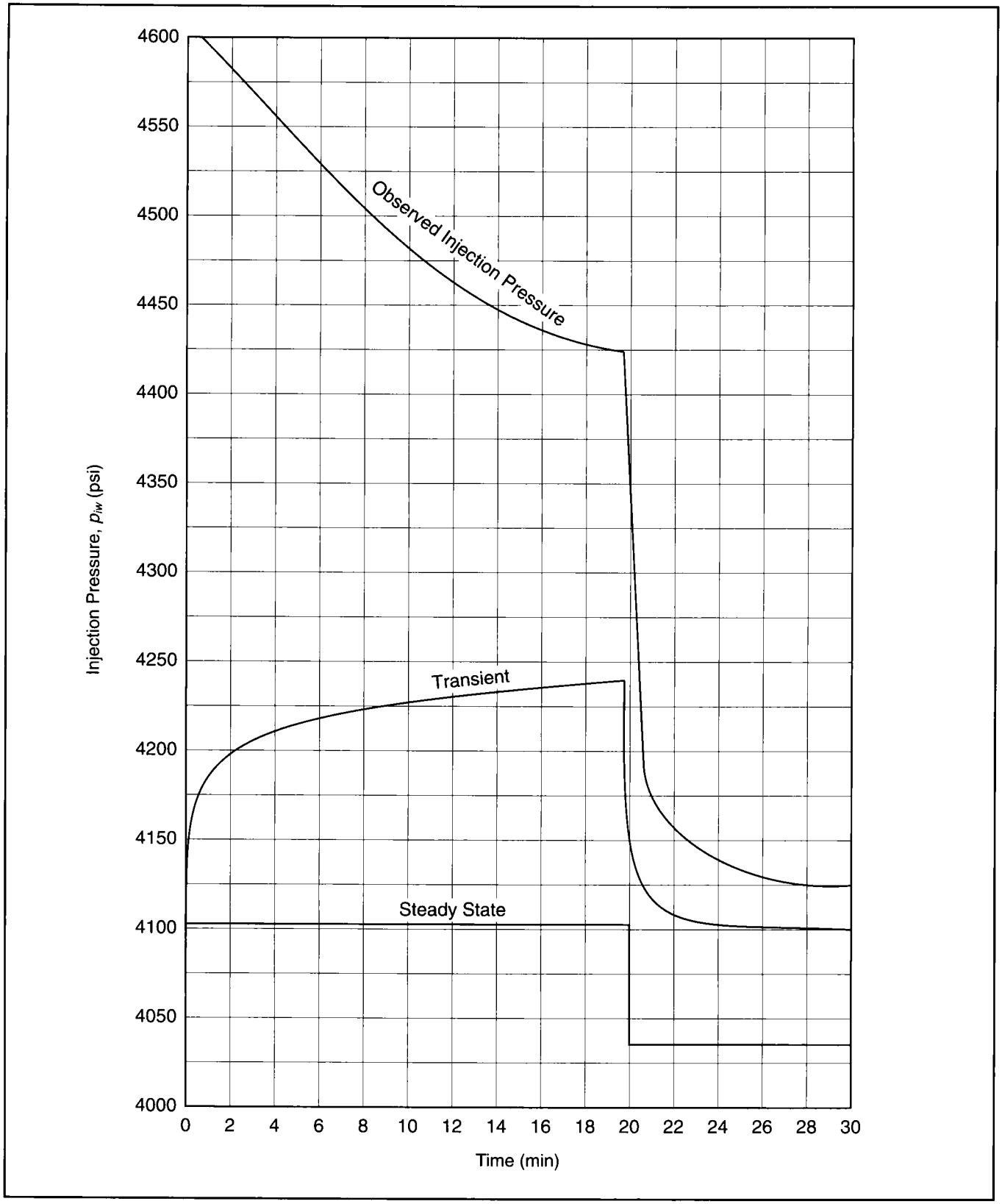

Figure H-3—Observed and simulated injection pressures for Example H-9.

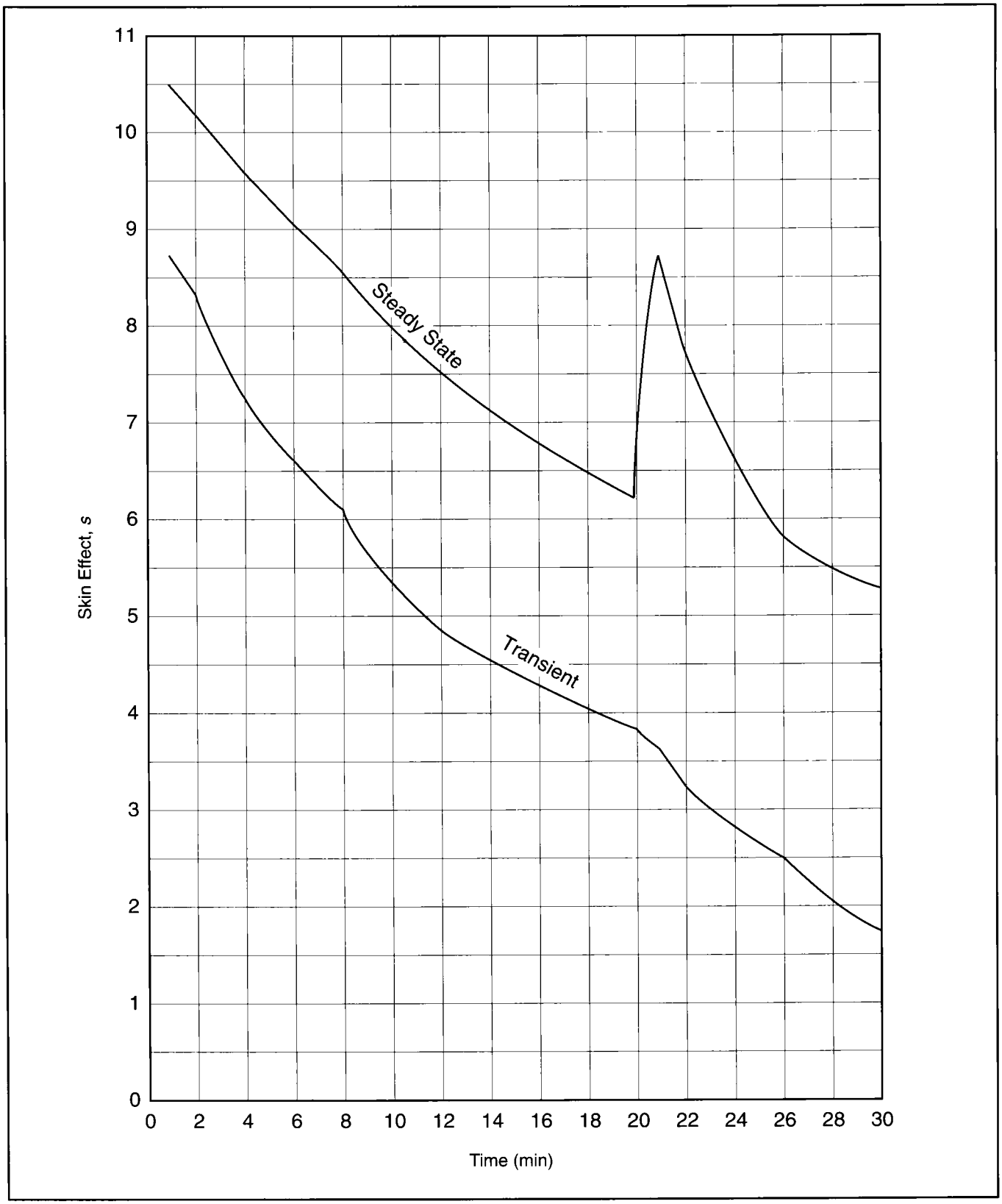

Figure H-4—Skin-effect evolution using transient and steady-state models.

I. Design and Performance of Acid Fractures

EXAMPLE I-1

Acid-Fracture Penetration

Assuming that the velocity along an acid fracture, u_x, is given by

$$u_x = \frac{q_i}{2\Gamma wh}, \tag{I-1}$$

where q_i is the injection rate, and Γ is equal to 1 for the KGD model and $\pi/4$ for the PKN model, show a relationship between acid fracture penetration, x_{fa}, and treatment variables. Using the data in Table I-1, calculate the acid penetration. The width of the fracture is already generated through the injection of a polymer pad.

Solution (Ref. Section 18-2.1)

The acid penetration is given by Eq. 18-17, and combination with Eq. I-1 results in

$$x_{fa} = \frac{q_i}{h}\frac{w}{8\Gamma D_{eff}}. \tag{I-2}$$

From Table I-1 and by converting units into a consistent set,

$$x_{fa} = \left[\frac{(20)\,(2.648\times 10^3\ \text{cm}^3/\text{s/BPM})}{(70)\,(30.48\ \text{cm/ft})}\right.$$

$$\left.\frac{(0.20)\,(2.54\ \text{cm/in.})}{(8)\,(1)\,(4\times 10^{-4})}\right] = 4.27\times 10^3\ \text{cm}, \tag{I-3}$$

or 140 ft.

Obviously, the two controlling variables are the injection rate (usually q_i/h = 0.2 to 0.4 BPM/ft) and the effective diffusion coefficient, D_{eff}. High-efficiency acids with low D_{eff} would result in long acid-fracture penetrations.

q_i	=	20 BPM
w	=	0.20 in.
h	=	70 ft
D_{eff}	=	4×10^{-4} cm²/s
Γ	=	1 (KGD model)

Table I-1—Treatment variables for Example I-1.

EXAMPLE I-2

Calculation of Effective Acid-Fracture Conductivity

Estimate the effective conductivity of an acid fracture if the closure pressure is 7000 psi, the rock embedment strength is 60,000 psi and the fracture width is 0.1 in. Repeat this calculation for two bottomhole pressures, 1000 psi and 4000 psi, respectively.

Solution (Ref. Section 18-4)

Case 1 (p_{wf} = 1000 psi)

The effective stress, σ', is approximately 6000 psi (7000 – 1000, using Biot's constant equal to 1).

Therefore, from Eqs. 18-19, 3-158 and 3-155,

$$c_1 = 1.77\times 10^8\,(0.1)^{2.47} = 6\times 10^5, \tag{I-4}$$

$$c_2 = (3.8 - 0.28\ln 60{,}000)\times 10^{-3}$$

$$= 7.19\times 10^{-4}, \tag{I-5}$$

and

$$wk_f = 6\times 10^5 e^{-(7.19\times 10^{-4})(6000)}$$

$$= 8027\ \text{md-in.}, \tag{I-6}$$

or 670 md-ft.

If p_{wf} = 4000 psi, then Eq. I-6 changes to

$$wk_f = 6\times 10^5 e^{-(7.19\times 10^{-4})(3000)}$$

$$= 6.94\times 10^4\ \text{md-in.}, \tag{I-7}$$

or 5800 md-ft, denoting the significance of the drawdown pressure and the resulting effective stress on the conductivity of an acid fracture.

EXAMPLE I-3

Calculation of Effective Fracture Length and Dimensionless Fracture Conductivity

A fracture with an actual length of 150 ft is in a highly anisotropic medium where $k_y/k_x = 0.05$. Calculate the effective fracture length and the dimensionless fracture conductivity using the results of Example I-2 and a reservoir permeability equal to 0.2 md.

Solution (Ref. Section 18-1)

The effective fracture half-length can be estimated from Eq. 18-4:

$$\bar{x}_f = 150\,(0.05)^{1/4} = 71\text{ ft}, \tag{I-8}$$

whereas the dimensionless fracture conductivity is

$$F_{CD} = \frac{670}{(0.2)\,(150)} = 22\,(\text{for } p_{wf} = 1000\text{ psi}) \tag{I-9}$$

and

$$F_{CD} = \frac{5800}{(0.2)\,(150)} = 190\,(\text{for } p_{wf} = 3000\text{ psi}). \tag{I-10}$$

It is evident that acid fractures should be used in higher permeability reservoirs where length is less important than fracture conductivity. In low-permeability carbonate reservoirs, propped fractures, with their much longer lengths, are indicated in spite of the solubility of the rock. This will be demonstrated in later examples.

EXAMPLE I-4

Performance of an Acid Fracture

Calculate the oil and gas cumulative production after 10 days for the two fractures described in Table I-2. In both cases, the effective stress is 3000 psi and the formation strength is 60,000 psi.

Solution (Ref. Section 18-5)

A. Oil well

The dimensionless time at 10 days is

$$t_{Dxf} = \frac{(0.000264)\,(1)\,(10\times 24)}{(0.21)\,(1)\,(9\times 10^{-6})\,(100^2)} = 3.35, \qquad \text{(I-11)}$$

leading to $Q_D \approx 2.5$ from Fig. 18-13.

Then, from Eq. 18-22 and rearrangement,

$$N_p = \frac{(2.5)\,(0.21)\,(28)\,(9\times 10^{-6})\,(100^2)\,(2000)}{(3.73\times 10^{-2})\,(1.15)}$$

$$= 62{,}000 \text{ STB.} \qquad \text{(I-12)}$$

B. Gas well

The dimensionless time at 10 days is

$$t_{Dxf} = \frac{(0.000264)\,(0.2)\,(10\times 24)}{(0.16)\,(0.025)\,(1.2\times 10^{-4})\,(100^2)}$$

$$= 2.64, \qquad \text{(I-13)}$$

and from Fig. 18-13, $Q_D = 2$.

Then, from Eq. 18-23 and rearrangement,

$$G_p = \frac{(2)\,(0.16)\,(50)\,(1.2\times 10^{-4})\,(100^2)\,(1.6\times 10^{7})}{(0.376)\,(0.95)\,(640)}$$

$$= 1.3\times 10^{6} \text{ MSCF.} \qquad \text{(I-14)}$$

Oil Well		Gas Well	
k	= 1 md	k	= 0.2 md
h	= 28 ft	h	= 50 ft
ϕ	= 0.21	ϕ	= 0.16
μ	= 1 cp	μ	= 0.025 cp
c_t	= 9×10^{-6} psi^{-1}	Z	= 0.95
x_f	= 100 ft	T	= 640°R
B	= 1.15 resbbl/STB	c_t	= 1.2×10^{-4} psi^{-1}
$p_i - p_{wf}$	= 2000 psi	$p_i^2 - p_{wf}^2$	= 1.6×10^{7} psi^2
		x_f	= 100 ft

Table I-2—Well and reservoir data for Example I-4.

EXAMPLE I-5

Comparison of Propped and Acid Fracture Performance

Using Fig. 18-19 and the definitions of dimensionless time and cumulative production, show that a 45° straight line drawn through any point on the curves in Fig. 18-19 will intersect all others at points representing equal real time and equal real cumulative production.

Solution (Ref. Section 18-6)

The slope on the log-log plot of Fig. 18-19 between any two points is

$$\log Q_{D1} - \log Q_{D2} = m(\log t_{Dxf1} - \log t_{Dxf2}). \quad \text{(I-15)}$$

Setting $m = 1$ (45°) and removing the log signs,

$$\frac{Q_{D1}}{Q_{D2}} = \frac{t_{Dxf1}}{t_{Dxf2}}. \quad \text{(I-16)}$$

After substitution of the definitions, the fracture lengths cancel out for a given reservoir,

$$\frac{(N_{p1})}{(N_{p2})} = \frac{(t_1)}{(t_2)}, \quad \text{(I-17)}$$

and if $t_1 = t_2$, then $N_{p1} = N_{p2}$.

The implications of the above are that a 45° line through any curve describing the performance of an acid fracture will intercept a number of curves of various F_{CD} values. Points above this 45° line would mean higher N_p (for the same time), whereas points below would mean lower N_p.

For example, suppose that $t_{Dxf} = 0.1$ and $\sigma' = 7000$ psi. Then $Q_D = 0.12$. If $F_{CD} = 5$, the corresponding $t_{Dxf} = 0.15$ and $Q_D = 0.22$. If $x_{fa} = 100$ ft, then

$$x_{fp} = \sqrt{\frac{(0.1)\,(100)^2}{0.15}} = 82\text{ ft} \quad \text{(I-18)}$$

would be the required propped length to produce the same cumulative production (if $F_{CD} = 5$ were possible).

If $F_{CD} = 1$, then the 45° line would intersect that curve at $t_{Dxf} = 0.02$, and therefore,

$$x_{fp} = \sqrt{\frac{0.1}{0.02}(100)^2} = 224\text{ ft}. \quad \text{(I-19)}$$

In both cases, if a more conductive fracture (for a given x_f) or a longer fracture (for a given F_{CD}) can be generated, then a propped fracture would be more attractive than the acid fracture. (In Fig. 18-19, the points would be above the 45° line.) For example, if $F_{CD} = 1$ and $x_f = 1000$, then

$$(t_{Dxf})_2 = (t_{Dxf})_1\left(\frac{224}{1000}\right)^2 = 1 \times 10^{-3}. \quad \text{(I-20)}$$

From Fig. 18-19, $Q_D = 3 \times 10^{-3}$.

Therefore, when comparing this with the acid fracture and remembering that

$$Q_D \sim \frac{N_p}{x_f^2}, \quad \text{(I-21)}$$

then

$$\frac{N_{p2}}{N_{p1}} = \frac{(Q_D)_2(x_f^2)_2}{(Q_D)_1(x_f^2)_1} = \frac{(3 \times 10^{-3})\,(1000^2)}{(0.12)\,(100^2)} = 2.5, \quad \text{(I-22)}$$

meaning that this propped fracture would produce 2.5 times the cumulative recovery of the acid fracture within the same time.

J. Stimulation of Horizontal Wells

EXAMPLE J-1

Deliverability of a Damaged Horizontal Gas Well

Estimate the steady-state flow rate for a horizontal gas well using lengths of 1000 ft and 1500 ft, respectively, and for a range of skin effects. Table J-1 contains the relevant well and reservoir data.

Solution (Ref. Section 19-2)

Equation 19-3 is for an oil well. (While Eq. 19-3 in the textbook is as published by Joshi (SPE 15375, 1986; *JPT*, June 1988), it has been shown by Economides et al. (SPE 20717, 1990) that it must be augmented. The term $2r_w$ must be replaced by $(\beta + 1)r_w$. All calculations in this volume use this correction.) It can be readily modified for a gas well, and using oilfield units, it becomes

$$q = \frac{k_H h (\bar{p}^2 - p_{wf}^2)}{1424 \mu Z T \left(\ln \frac{a + \sqrt{a^2 - (L/2)^2}}{L/2} + \frac{\beta h}{L} \ln \frac{\beta h}{(\beta + 1) r_w} + s \right)}, \quad \text{(J-1)}$$

where a can be obtained from Eq. 19-2. The skin effect has been added to the denominator in the usual manner.

If $L = 1000$ ft and since $r_{eH} = 2107$ ft, then from Eq. 19-2, $a = 2137$ ft. Substituting all known variables from Table J-1 into Eq. J-1 results in

$$q = \frac{2591}{2.46 + s}. \quad \text{(J-2)}$$

The calculation, repeated for $L = 1500$ ft, leads to $a = 2175$ ft, and from Eq. J-1,

$$q = \frac{2591}{1.95 + s}. \quad \text{(J-3)}$$

Figure J-1 contains the expected flow rates for the two well lengths for a range of skin effects (damaged horizontal well). If the skin effect is equal to zero (no damage), then the well production rate (for $L = 1000$ ft) will be approximately 1 MMSCF/d. For a well with moderate damage ($s = 5$), the rate will be approximately 350 MSCF/d.

As can be seen for a 1500-ft well, the nondamage production rate is 1300 MSCF/d (a gain of 300 MSCF/d over the 1000-ft well). The damaged well would not gain appreciably over the 1000-ft well. This is important because lack of stimulation may reduce significantly the expected benefits from a longer well.

k_H	=	0.1 md
μ	=	0.0219 cp
h	=	25 ft
Z	=	0.925
$\bar{p}$	=	5068 psi
T	=	650°R [190°F]
p_{wf}	=	2000 psi
β	=	3 [$k_H = 10\ k_v$]
r_w	=	0.229 ft
A	=	320 acres [$r_{eH} = 2107$ ft]

Table J-1—Well and reservoir data for Example J-1.

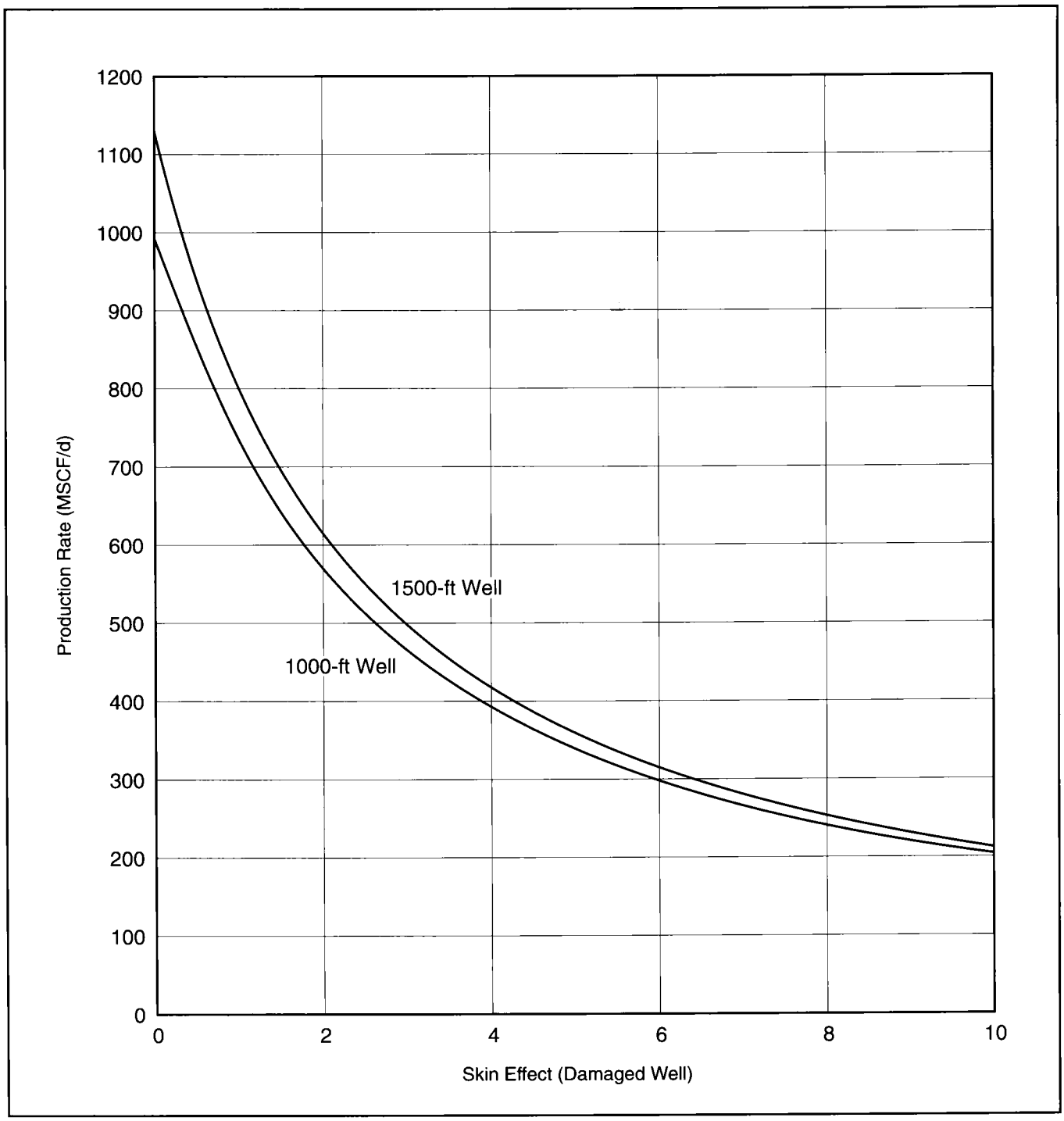

Figure J-1—Deliverability of the horizontal well in Example J-1.

EXAMPLE J-2

Material Balance Calculation for a Reservoir with a Horizontal Well

Suppose that a 500-ft horizontal well is drilled in a reservoir with the variables shown in Table J-2. Forecast the performance for a closed reservoir configuration.

Solution (Ref. Section 19-2)

At first, an estimation of minimum reserves should be calculated assuming h = 15 ft and A = 320 acres:

$$G_i = \frac{Ah\phi S_g}{B_g} = \frac{(320)\,(43,560)\,(15)\,(0.1)\,(0.6)}{(0.00347)}$$

$$= 3.6 \times 10^9 \text{ SCF.} \qquad \text{(J-4)}$$

The value of B_g in resft^3/SCF is calculated by

$$B_g = \frac{T(°R)\,p_{sc}}{p_{res}\,T_{sc}} = \frac{(650)\,(14.7)}{(5300)\,(520)} = 0.00347. \qquad \text{(J-5)}$$

Then, a forecast of performance at stabilized pseudosteady-state conditions can be calculated. This is shown in Fig. J-2 for various values of the skin effect using Eq. J-1. The impact of damage is shown, and the necessity for *good* stimulation is apparent. If the skin is equal to +5, then the flow rate is only 1.7 MMSCF/d; whereas if the skin effect is eliminated by aggressive stimulation, the flow rate will be 4.3 MMSCF/d.

A long-term forecast of performance was then calculated, incorporating gas material balance and the horizontal well deliverability. Since the initial pressure is taken as 5300 psi and since the Z is equal to 1.03, then $\bar{p}/Z = 5146$. The material balance equation ($\bar{p}/Z$ vs. cumulative production) is then

$$G_p = 3.6 \times 10^9 - 7 \times 10^5 \left(\frac{\bar{p}}{Z}\right). \qquad \text{(J-6)}$$

Table J-3 contains a schedule of production for a declining average reservoir pressure.

Combination of well deliverability (rate) with the cumulative production results in rate vs. time (Fig. J-3) and cumulative production vs. time (Fig. J-4) relationships. These graphs are plotted for skins equal to 0 and 2, which indicate very moderate damage. After a year (from the emergence of boundaries), the cumulative production will be 8×10^8 SCF for $s = 0$ and 5.5×10^8 SCF for $s = 2$. This is a substantial difference, again indicating the need for careful stimulation.

k	=	1 md
γ_g	=	0.633
A	=	320 acres
T	=	190°F = 650°R
L	=	500 ft
$\bar{p}$	=	5300 psi
h	=	15 ft
p_{wf}	=	2500 psi
r_w	=	0.271 ft
β	=	3

Table J-2—Well and reservoir data for Example J-2.

$\bar{p}$ (psi)	Z	$\bar{p}/Z$ (psi)	G_p (10^8 SCF)	ΔG_p (10^8 SCF)
5300	1.030	5146		
4900	0.992	4940	1.42	1.42
4500	0.966	4658	3.39	1.97
4100	0.940	4361	5.47	2.08
3700	0.921	4022	7.85	2.38
3300	0.905	3646	10.50	2.63
2900	0.887	3270	13.10	2.61

Table J-3—Pressure decline and cumulative production for well in Example J-2.

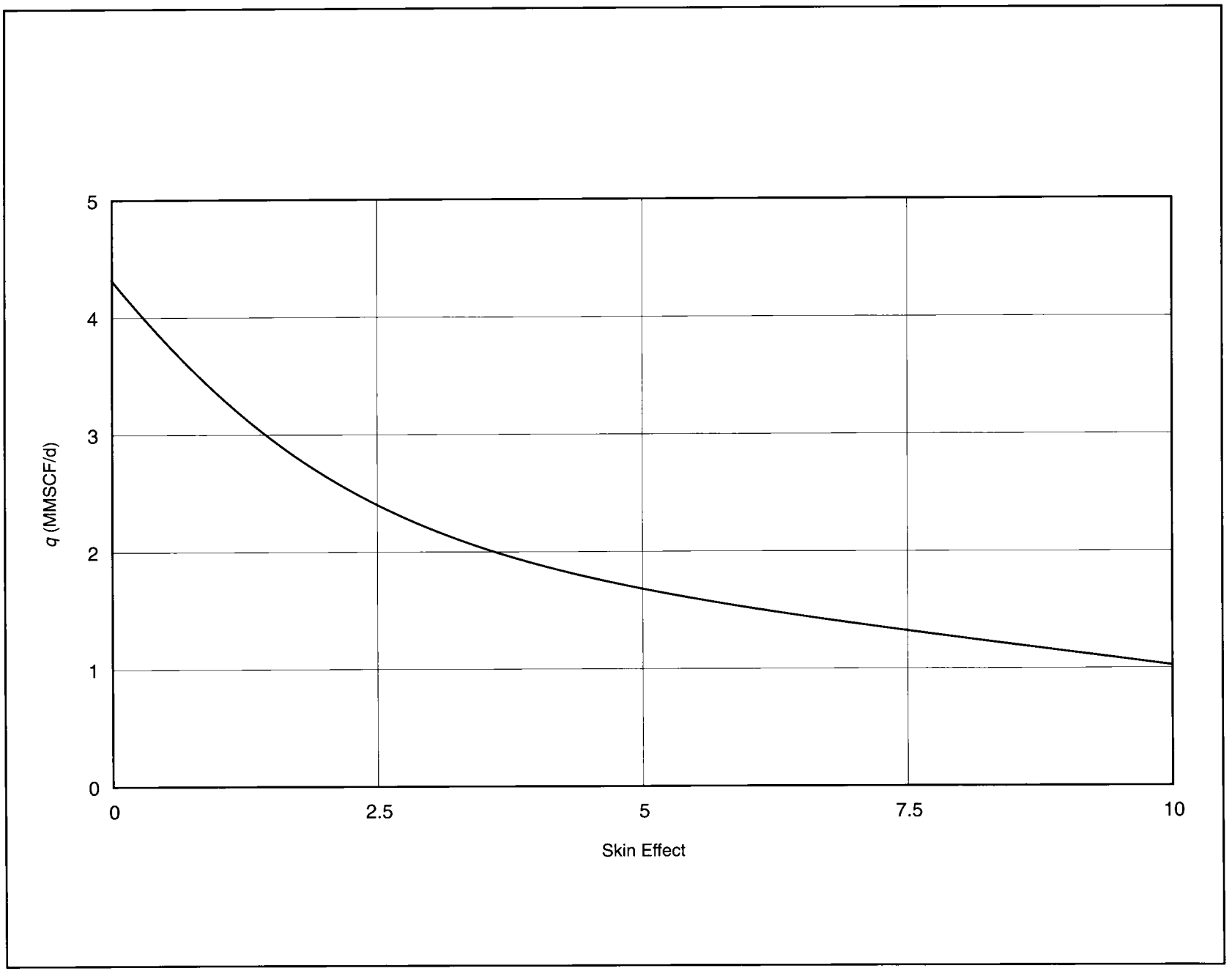

Figure J-2—Production at pseudosteady-state conditions from damaged 500-ft horizontal well in Example J-2.

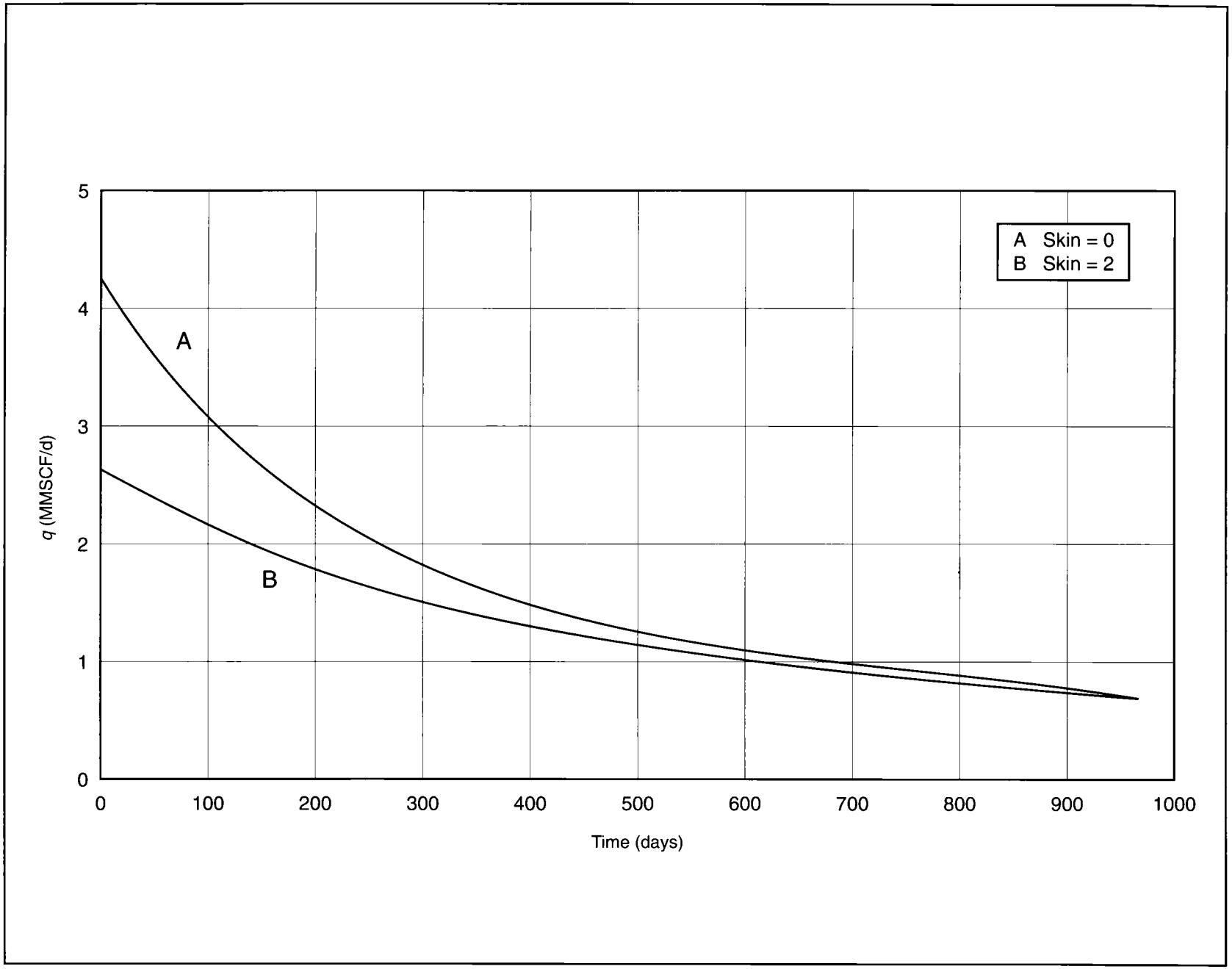

Figure J-3—Production rate decline for horizontal well in Example J-2.

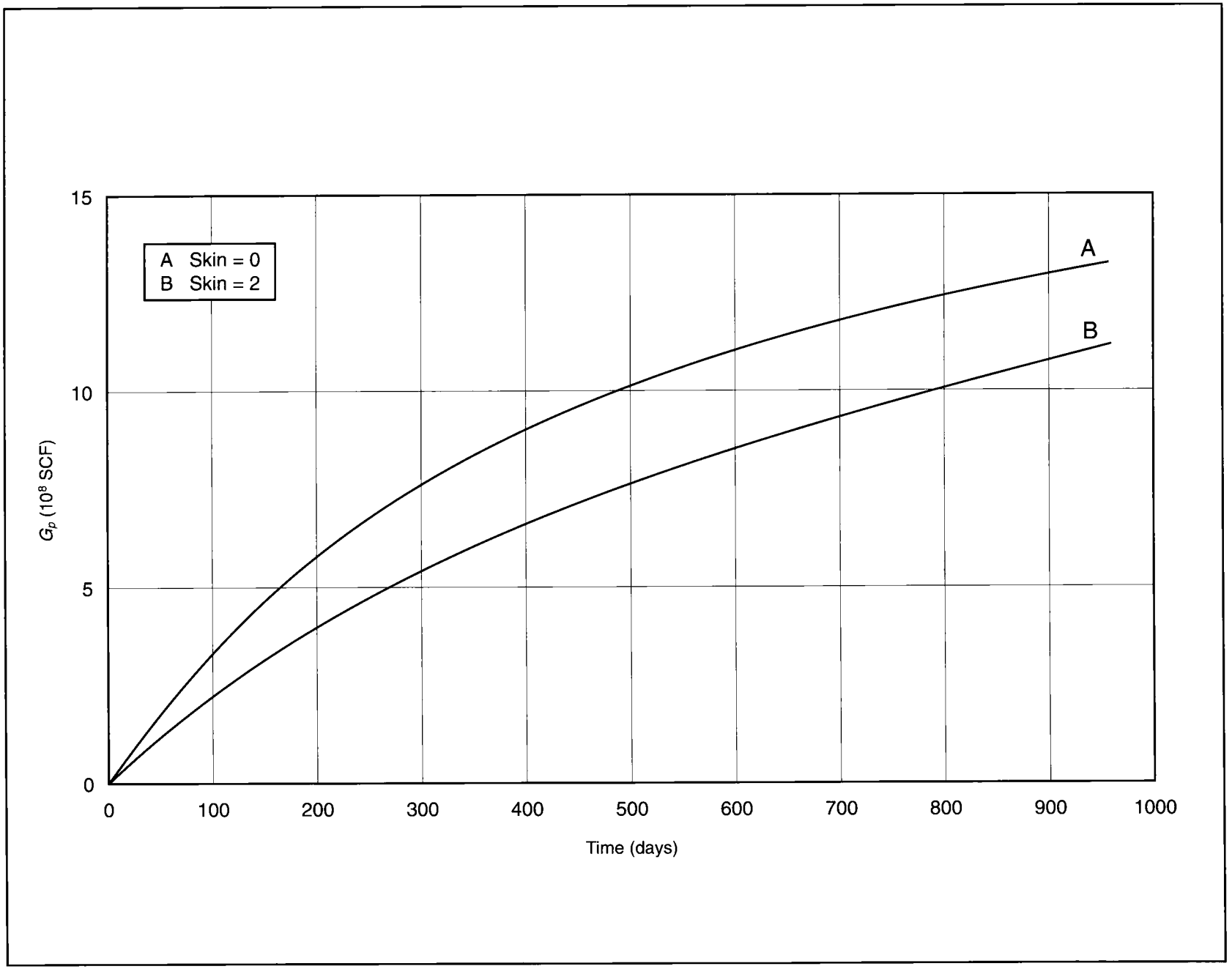

Figure J-4—Cumulative production forecast for the horizontal well in Example J-2.

EXAMPLE J-3

Horizontal Well Inflow Performance with Pressure-Sensitive Skin Effect

A vertical well exhibited a very rapid increase in the calculated skin effect in two successive pressure buildup tests only a month apart. While the calculated apparent permeability remained largely constant (as it should), the skin effect increased from a near zero value to a very large +18. The drawdown before the second test was 1300 psi. Further analysis has shown that phase changes in the reservoir and the resulting relative-permeability-to-oil reduction *could not* account for the increase in the skin effect.

A stimulated horizontal well (0 skin effect) could produce as much as 2500 STB/d from a 500-ft length, as can be readily calculated from Eq. 19-3.

Table J-4 contains pertinent well and reservoir variables for this example.

A significant possibility is to look at a pressure-sensitive skin effect (i.e., drawdown-dependent phenomena). This concept implies that fines migration and other causes, which are highly dependent on the drawdown pressure, can result in a high skin effect. Therefore, make an attempt toward optimization to show the composite impact of drawdown and skin effect.

Solution (Ref. Section 19-2)

A simple linear relationship between drawdown and skin effect can be presumed from the two pressure-buildup tests analyzed in the vertical well. Since the skin effect was found to be approximately equal to 0 at the initial reservoir stage and then degenerated to +18 after 1 month at $\Delta p = 1300$ psi, a simple equation for the skin effect can be written (remembering that $s = 0$ at $\Delta p = 0$):

$$s = \frac{18}{1300}\Delta p = 0.0138\,\Delta p. \qquad \text{(J-7)}$$

This relationship is not unlike the type of equation used to evaluate the skin effect caused by turbulence in a gas well.

Consequently, the inflow performance relationship for a horizontal well (Eq. 19-3) can be written as

$$q = \frac{6.62\,\Delta p}{\left[\ln \frac{a+\sqrt{a^2-(L/2)^2}}{L/2} + \frac{70}{L} + 0.0138\,\Delta p\right]}, \qquad \text{(J-8)}$$

where a is given by Eq. 19-2.

Table J-4 contains the variables used in Eq. 19-3 to develop Eq. J-8. From Eq. J-8, the inflow performance of various length horizontal wells can be calculated with a drawdown-dependent skin effect.

Thus, the following relationships can be written for a 500-ft, 1000-ft and 1500-ft horizontal well, respectively:

$$q = \frac{6.62\,\Delta p}{2.65 + 0.0138\,\Delta p} \text{ for } L = 500\text{ ft}, \qquad \text{(J-9)}$$

$$q = \frac{6.62\,\Delta p}{1.87 + 0.0138\,\Delta p} \text{ for } L = 1000\text{ ft}, \qquad \text{(J-10)}$$

and

$$q = \frac{6.62\,\Delta p}{1.44 + 0.0138\,\Delta p} \text{ for } L = 1500\text{ ft}. \qquad \text{(J-11)}$$

Equations J-9 through J-11 imply continuously increasing q with Δp, although the slope of the curve will decrease at large Δp. However, no *optimum* pressure drop can be obtained. (Taking the derivate of q with respect to Δp and setting it equal to 0 would show a point where a maximum or minimum q would be encountered. However, no such point of inflection can be detected from a relationship of the form of Eqs. J-9 through J-11.)

Figure J-5 is a graph of expected flow rates for the three horizontal well lengths for a range of pressure drawdowns (selected so that p_{wf} is larger than the bubblepoint pressure). These flow rates (with the pressure-dependent skin effect assumption) are significantly smaller than the expected flow rates with 0 skin effect for these well lengths.

Figure J-6 shows the productivity index ratios of 1000-ft and 1500-ft wells compared to the 500-ft well. As can be seen, these PI ratios decline significantly at large pressure drawdowns. For example, the PI increase at 1500 psi drawdown between a 1500-ft well and a 500-ft well is only 5%. Figure J-6 should be used for an economic evaluation of the desirability of a longer well. Thus, the issue is whether the incremental costs of drilling a 1500-ft well over a 500-ft well can be justified on the basis of the incremental rate. For this particular case, the daily incremental rate at steady state is 448 – 425 = 23 STB/d. The annual incremental production is 8400 STB if the two wells were producing constantly. This must be balanced against incremental drilling costs. Depending on the investment constraints (expected ROR, etc.), Fig. J-6 can be valuable in this decision-making process.

k_H	=	50 md
μ	=	0.18 cp
h	=	8 ft
β	=	3
B	=	2.38 resbbl/STB
r_w	=	0.328 ft
A	=	160 acres [r_e = 1490 ft]

Table J-4—Well and reservoir variables for Example J-3.

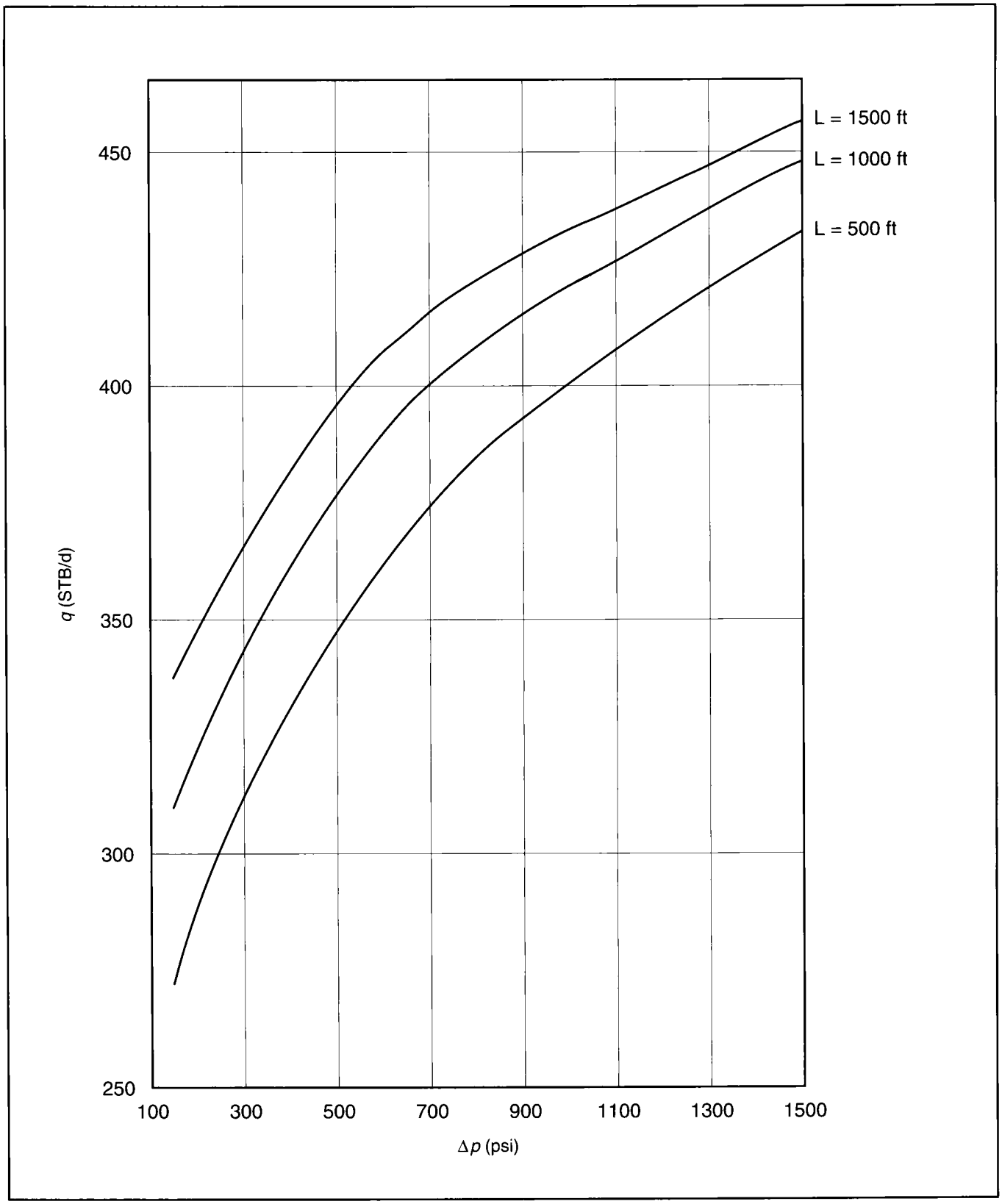

Figure J-5—Expected flow rates for various length horizontal wells with a pressure-sensitive skin effect for Example J-3.

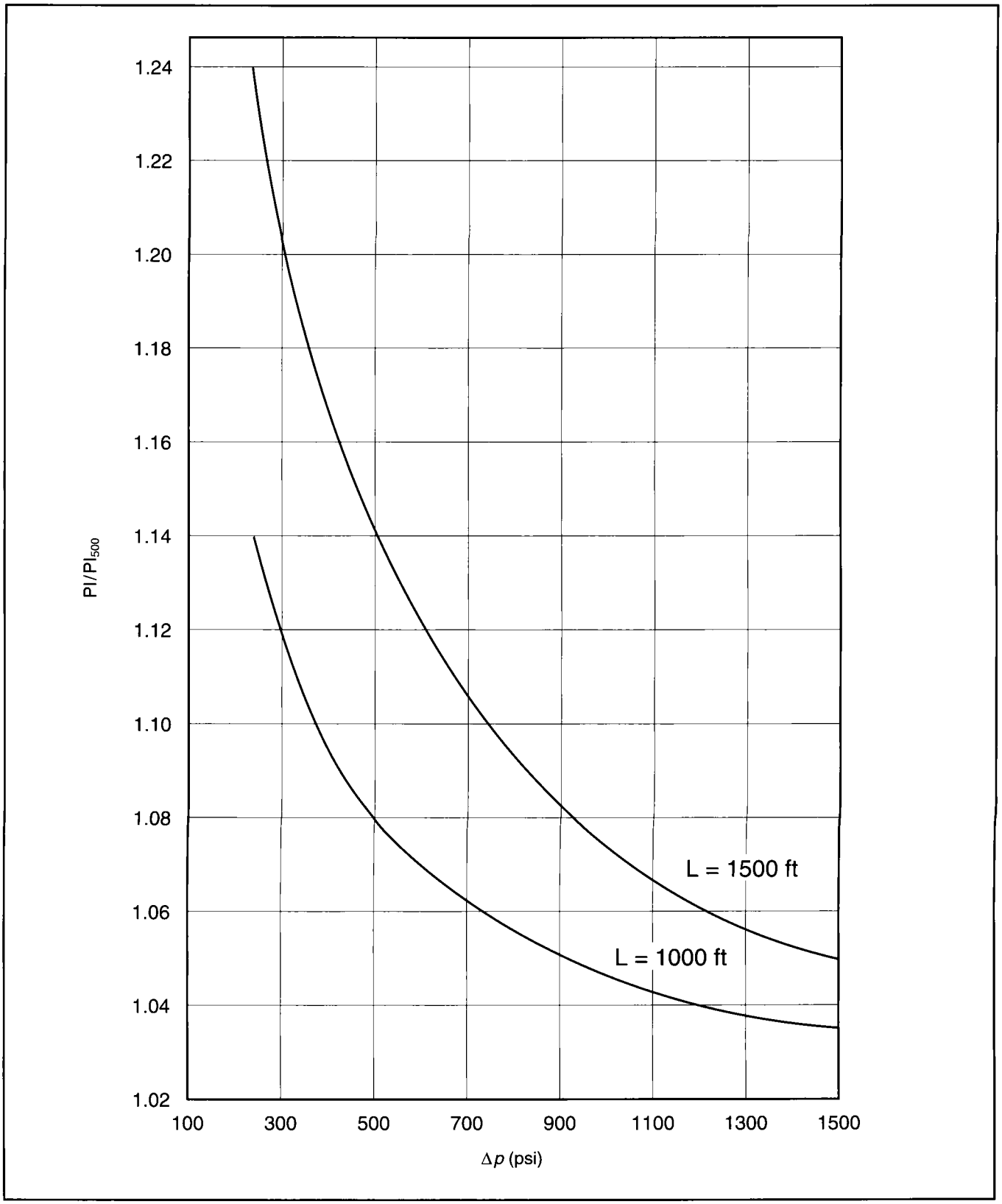

Figure J-6—Productivity index increases over a 500-ft well with a pressure-sensitive skin effect for Example J-3.

EXAMPLE J-4

Optimum Horizontal Well Length

For the well in Example J-3, it is shown that in spite of the pressure-dependent skin effect no optimum bottomhole flowing pressure can be identified. This is because any horizontal well length with that type of inflow performance relationship does not have an inflection point leading to a maximum flow rate. However, it is evident that while flow rates are monotonically increasing, the values for different well lengths are getting nearer at higher pressures. This means that an optimization, based on incremental revenue and incremental costs, is necessary to identify the appropriate well length. This can be done for any bottomhole pressure, although the results presented in Example J-3 would suggest the lower possible bottomhole pressure (i.e., largest Δp) that would still avoid two-phase or other operational problems.

Δp (psi)	L (ft)	q	Δq	ΔN_P	$\Delta\$$ (1000)	NPV (1000)
300	500	266				
	750	283	17	6205	255	145
	1000	296	30	10950	450	230
	1250	307	41	14965	615	285
	1500	317	51	18615	764	324
600	500	342				
	750	356	14	5110	210	100
	1000	366	24	8760	360	140
	1250	374	32	11680	480	150
	1500	382	40	14600	600	160
900	500	378				
	750	389	11	4015	166	56
	1000	397	19	6935	284	64
	1250	404	26	9490	389	59
	1500	409	31	11315	465	25
1200	500	399				
	750	408	9	3285	135	25
	1000	415	16	5840	239	19
	1250	421	22	8030	330	0
	1500	425	26	9490	389	−51
1500	500	413				
	750	421	8	2920	120	10
	1000	427	14	5110	210	−10
	1250	431	18	6570	270	−60
	1500	435	22	8030	330	−110

Table J-5—Incremental NPV for various pressure drops and well lengths for Example J-4.

Solution (Ref. Sections 8-2.8 and 19-2)

The economic analysis presented here uses the Net Present Value (NPV) concept. In terms of incrementals, it can be written as

$$\text{NPV} = \sum_{n=1}^{n} \frac{(\Delta\$)_n}{(1+i)^n} - \Delta Cost, \tag{J-12}$$

where $(\Delta\$)_n$ is the incremental revenue in year n, i is the time value of money (at least inflation rate, preferably the rate of return) and $\Delta Cost$ is the incremental cost associated with the investment.

The basis for the analysis is a 500-ft horizontal well, and the incremental costs are \$440/ft. Table J-5 contains the incremental NPV for various pressure drops and well lengths. The price of oil was taken as \$18/STB, and the time value of money as 15%. An example calculation for the results in Table J-5 is shown below. ($\Delta p = 600$ psi, and a comparison between a 500-ft well and a 1000-ft well is done.)

First, from Eq. J-9, $q_{500} = 342$ STB/d, and from Eq. J-10, $q_{1000} = 366$ STB/d. Thus, Δq (the daily rate difference) = 24 STB/d, which can be roughly translated to ΔN_P (incremental annual production) = 8760 STB. (Even if it is not entirely steady-state flow for both wells, this difference is a reasonable approximation without respect to the type of flow.)

Using \$18/STB and $i = 0.15$, the incremental net revenue discounted to time 0 (for 3 yr) is then

$$\sum_{n=1}^{3} \frac{(\Delta\$)_n}{(1+i)^n} = \frac{(8760)(18)}{1.15} + \frac{(8760)(18)}{(1.15)^2} + \frac{(8760)(18)}{(1.15)^2} = \$360 \times 10^3. \tag{J-13}$$

However,

$$\Delta Cost = (1000 - 500)\text{ ft } (\$440/\text{ft}) = \$220 \times 10^3, \tag{J-14}$$

resulting in

$$\text{NPV} = 360 \times 10^3 - 220 \times 10^3 = \$140 \times 10^3. \tag{J-15}$$

Figure J-7 is a plot of the incremental NPV vs. horizontal well length for a number of pressure drops. Since $\Delta p = 1500$ psi is more desirable than any other Δp (see Fig. J-5), then it is obvious that the intended length of 500 ft is very near the best. At 750 ft, the incremental NPV is only \$10,000, and it becomes negative for wells of greater length. Thus, a decision to drill a short, 500-ft well is justified by this economic analysis.

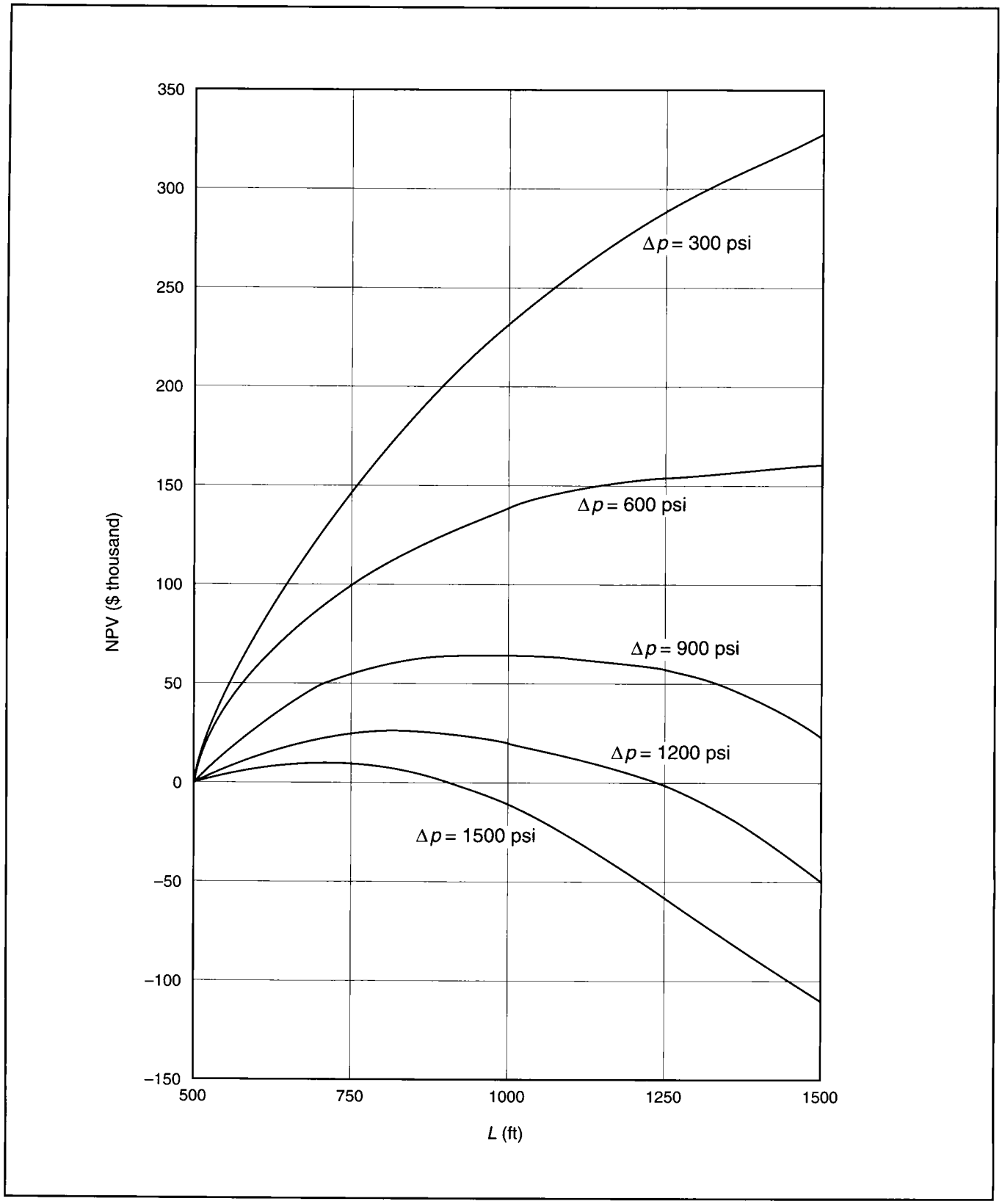

Figure J-7—Incremental NPV for various length horizontal wells for Example J-4.

EXAMPLE J-5

Vertical Fractured Wells vs. Openhole Horizontal Wells

Assume that vertical wells in a reservoir with the characteristics in Table J-6 are routinely fractured hydraulically. If one contemplates a 1500-ft horizontal well, what fracture length would be necessary in a vertical well to produce comparably? Assume a very large conductivity fracture. What should the fracture length be if $\beta = 0.25$?

Solution (Ref. Section 19-3)

From Eq. 19-2, $a = 3028$ ft. Then from Eq. 19-7 (also corrected by substituting $2r_w$ with $(\beta + 1)\, r_w$),

$$r'_{wD}\, x_f = \frac{(2980)\,(750)}{\left[\left(3028 + \sqrt{3028^2 - 750^2}\right)\left(\frac{(3)(100)}{(4)(0.328)}\right)^{(3)(100)/1500}\right]}$$

$$= 114 \text{ ft.} \qquad \text{(J-16)}$$

Since this is a large conductivity fracture, $r'_{wD} = 0.5$ (see Fig. 11-4), and therefore, $x_f = 228$ ft. Thus, a fractured well would be far more attractive than a horizontal well since $x_f = 228$ ft can be achieved readily and much more economically.

If $\beta = 0.25$, then the right-hand side of Eq. 19-7 is equal to 375 ft, and therefore, $x_f = 750$ ft. The latter is much more difficult to accomplish in practice because reservoirs with $\beta = 0.25$ are highly naturally fractured, and therefore, neither $F_{CD} \rightarrow \infty$ nor $x_f \approx 800$ ft is likely to be created.

This example demonstrates that an unfractured horizontal well is not a likely substitute for fractured vertical wells in almost all reservoirs that traditionally have undergone this type of stimulation. However, in highly fissured reservoirs that also experience routine screenouts and where it is not possible to propagate long fractures, a horizontal well could be a viable alternative.

k	=	0.5 md
β	=	3
r_{eH}	=	r_{eV} = 2980 ft
h	=	100 ft
r_w	=	0.328 ft

Table J-6—Well and reservoir data for Example J-5.

EXAMPLE J-6

Performance of a Single Hydraulic Fracture Connected Transversely to a Horizontal Well

Calculate the production rate of a hydraulic fracture intercepting transversely a horizontal well. Compare with the performance of the same fracture intercepted by a vertical well. Table J-7 contains the relevant well data.

Solution (Ref. Section 19-6)

First, the dimensionless fracture conductivity is calculated (Eq. 11-11):

$$F_{CD} = \frac{1200}{(1)\,(1200)} = 1. \qquad \text{(J-17)}$$

The dimensionless time, given by Eq. 11-10, can be calculated for this problem as a function of real time:

$$t_{Dxf} = \frac{(0.000264)\,(1)\,(24)\,t}{(0.15)\,(0.7)\,(10^{-5})\,(1200^2)} = 4.2 \times 10^{-3} t, \qquad \text{(J-18)}$$

where t must be in *days*.

Using the large foldout type curve for $F_{CD} = 1$ at the end of Chapter 11, the production rate for a fractured vertical well can be readily calculated.

For example, if $t = 30$ days, then from Eq. J-18, $t_{Dxf} = 0.126$, and the ratio $t_{Dxf}/c_{Df} = 1.26 \times 10^3$. From the type

k	=	1 md
r_w	=	0.328 ft
h	=	75 ft
ϕ	=	0.15
$k_f w$	=	1200 md-ft
B	=	1.1 resbbl/STB
μ	=	0.7 cp
x_f	=	1200 ft
c_t	=	10^{-5} psi^{-1}
C_{Df}	=	10^{-4}
$p_i - p_{wf}$	=	1500 psi

Table J-7—Well and reservoir data for Example J-6.

curve, $p_D = 1.4$. Then, using Eq. 11-8 for the definition of the dimensionless pressure and rearrangement,

$$q = \frac{(1)\,(75)\,(1500)}{(1.4)\,(141.2)\,(1.1)\,(0.7)} = 740 \text{ STB/d}. \quad \text{(J-19)}$$

For the same fracture intercepted by a horizontal well, the skin effect due to the choke from the contact must be calculated. From Eq. 19-40,

$$(s_{ch})_c = \frac{(1)\,(75)}{1200}\left[\ln\frac{75}{(2)\,(0.328)} - \frac{3.14}{2}\right] = 0.2. \quad \text{(J-20)}$$

Then, from Eq. 19-41,

$$(p_D)_{total} = p_D + (s_{ch})_c = 1.4 + 0.2 = 1.6, \quad \text{(J-21)}$$

and from a simple ratio,

$$q = \frac{(740)\,(1.4)}{1.6} = 648 \text{ STB/d}. \quad \text{(J-22)}$$

Figure J-8 is a graph of the production history of the fractured vertical well and the (orthogonally) fractured horizontal well.

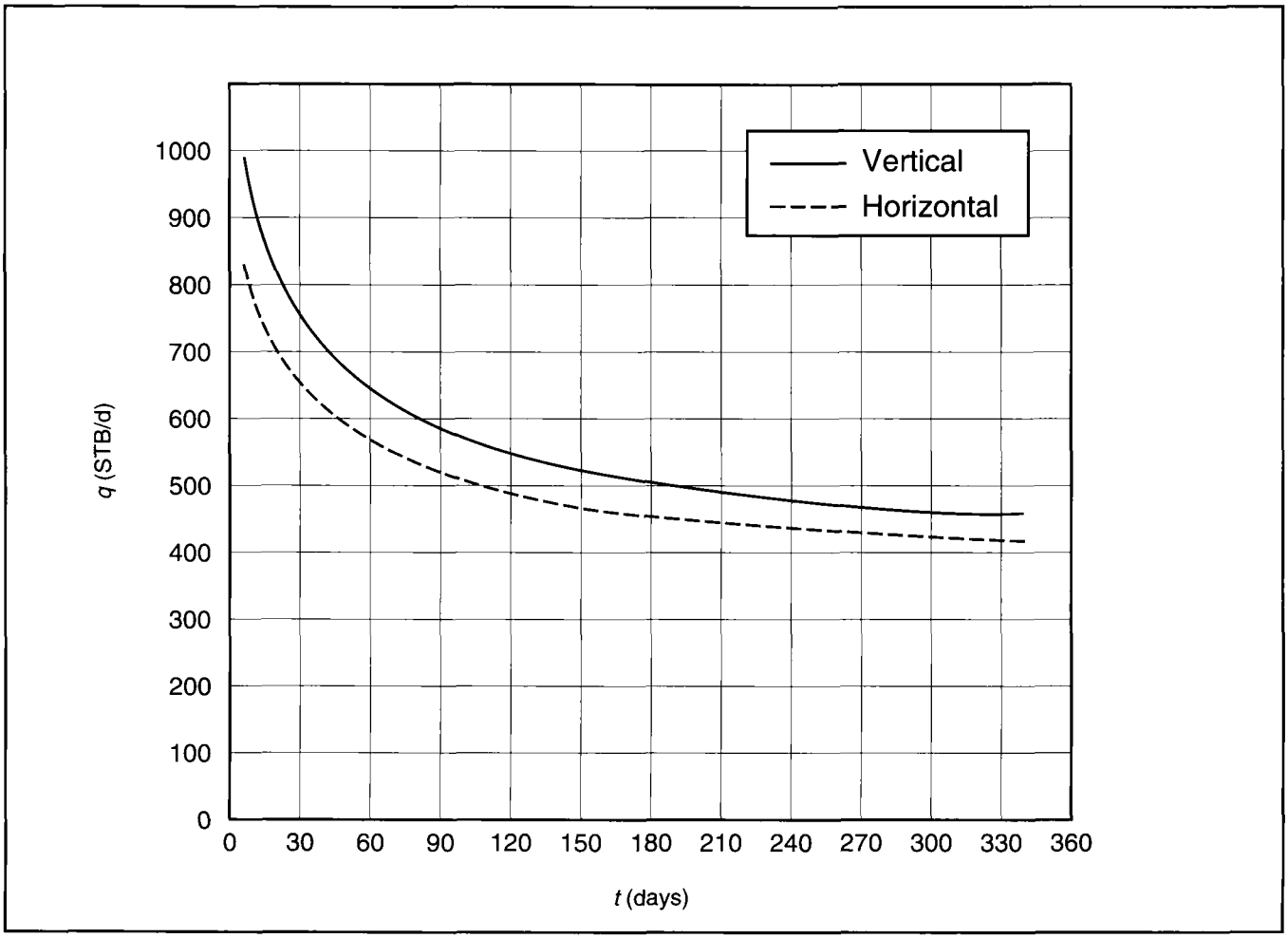

Figure J-8—Comparison of performance of fractured vertical well with transversely fractured horizontal well for Example J-6.

EXAMPLE J-7

Reduction of the Skin Effect of a Transversely Fractured Horizontal Well

Assuming that $k = 1$ md, $h = 100$ ft and $r_w = 0.328$ ft, outline a technique to reduce the choke skin effect.

Solution (Ref. Section 19-6)

From Eq. 19-40,

$$(s_{ch})_c = \frac{(1)\,(100)}{k_f w}\left[\ln\frac{100}{(2)\,(0.328)} - 1.57\right]$$

$$= \frac{345}{k_f w}. \qquad \text{(J-23)}$$

It is then obvious that if $k_f w$ is large, $(s_{ch})_c$ is small. A way to accomplish this is to make the near wellbore $k_f w$ as large as possible. Thus, tailing in with high-strength proppants or resin-coated proppants is indicated.

EXAMPLE J-8

Interference Among Multiple Parallel Fractures

What would be the increase in the excess pressure during fracturing and the decrease in the fracture width if a second fracture is completed 100 ft or 500 ft away from an existing 500-ft half-length fracture.

Solution (Ref. Section 19-5.2.3)

Figure 19-21 shows a correlation for the solution to this problem. The ratio y/x_f is equal to $(100/2)/500 = 0.1$ if the distance is 100 ft, and equal to 0.5 if the distance is 500 ft. Thus, the width ratio and the pressure ratio for the 100-ft distance are 0.85 and 1.64, respectively. For the 500-ft distance, they are 0.96 and 1.1, respectively. This denotes the very significant impact of fracture spacing on their interference. In general, if $y/x_f \cong 1$, there is virtually no interference.

EXAMPLE J-9

Performance of a Longitudinally Fractured Horizontal Well

Using the data in Table J-8, calculate the expected productivity index increase (from that of a fractured vertical well) if a horizontal well of length equal to $2x_f$ is longitudinally fractured.

Solution (Ref. Section 19-6.2)

Figure 19-23 can provide the solution to this problem. For the first case (k = 1 md),

$$F_{CD} = \frac{1000}{(1)\,(1000)} = 1. \qquad \text{(J-24)}$$

Since L = 2000 ft ($2x_f$), then L/h = 40. From Fig. 19-23, $(PI)_H/(PI)_v = 4.6$.

For the second case (k = 10 md), F_{CD} = 10, and from Fig. 19-23, $(PI)_H/(PI)_v = 1.9$.

k_fw	=	1000 md-ft
k	=	1 md or 10 md
h	=	50 ft
x_f	=	1000 ft

Table J-8—Reservoir and fracture data for Example J-9.

EXAMPLE J-10

Twisting Longitudinal to Transverse Fracture

Suppose that a horizontal well is to be hydraulically fractured. As Section 19-5.2.1 suggests, all fractures initiated from long intervals will likely be first longitudinal, twisting later into transverse direction (if the well is drilled along the minimum horizontal stress direction). Calculate the impact of the twisting action and devise a criterion to reduce the effect.

Solution (Ref. Sections 19-5.2.1 and 19-6)

If a fracture initiates as perfectly orthogonal (i.e., if the entry point has a width equal to the fracture width), then the area of contact between the well and the fracture is

$$A_t = \pi d_w w_t, \qquad \text{(J-25)}$$

where d_w is the well diameter and w_t the width of the transverse fracture.

A longitudinal fracture with two wings has an area of contact

$$A_l = 2Lw_l, \qquad \text{(J-26)}$$

where L is the length of the perforated interval and w_l the width of the longitudinal fracture.

To develop the criterion, the two areas are set equal, and after rearrangement,

$$\frac{w_l}{w_t} = \frac{\pi d_w}{2L} \approx 1.5\frac{d_w}{L}, \qquad \text{(J-27)}$$

which suggests that if the perforated interval is larger than one and one-half times the well diameter, the width of the twisting fracture will be reduced substantially. For example, if $L = 10\ d_w$, then $w_l = 0.15\ w_t$. In such a case, the choke skin effect will increase accordingly. In example J-6, the $(s_{ch})_c$ would be equal to (0.2/0.15) = 1.3, and the resulting flow rate (at 30 days) would be equal to 384 STB/d, which is a significant reduction.

Thus, if multiple transverse fractures are indicated, their connection with the well must be minimized. Cutting the casing with an abrasive jet may be the most appropriate means for fracture initiation.

This Page Intentionally Left Blank

P. Practical Considerations for Fracture Treatment Design

J. Ernest Brown, Dowell Schlumberger
Michael J. Economides, Mining University Leoben

P-1

Introduction

It should be obvious to the reader that hydraulic fracturing, as applied to petroleum engineering, is a particularly complicated enterprise. Understanding the fracturing process, the interactions of fluid pressure, viscosity and leakoff characteristics with the elastic properties and leakoff characteristics of the rock has been the subject of *Reservoir Stimulation* and the preceding chapters of this volume. The purpose of hydraulic fracturing is, of course, the placement of an optimum fracture of certain geometry and conductivity to allow maximum incremental production (over that of the unstimulated well) at the lowest cost.

Accomplishing this, while taking into account all the presented technology, requires significant attention to the treatment execution. This involves the appropriate selection of fluids and proppants, control and monitoring of rate, pressure and viscosity, and identification of those additives that would affect the desired fluid properties.

This chapter includes sections on proppant and fluid selection (Sections P-2 and P-3). Data on proppant and proppant conductivity and rheological data of all common fluids and their friction pressure drops are presented extensively. A fracturing fluid selection guide, encompassing a body of experience in almost all types of reservoirs, is also offered. The topic of conductivity damage from fracturing fluids and the extremely important subject of breakers are treated in two subsections.

Treatment sizing (volumes, pressures, blending and mixing) is covered in Section P-4, whereas the role of perforations, their number and their breakdown are discussed in Section P-5.

The issue of zonal isolation, the means of its accomplishment and the risks associated with its negligence are the subject of Section P-6. Limited entry, a widely used technique in multizonal fracturing, is critiqued.

Finally, actual location execution considerations are covered in Sections P-7 (equipment hookup) and P-8 (location quality assurance). Both of these sections offer guidelines essential for the successful execution of any fracturing treatment.

P-2

Proppant Selection

To select a proppant with a desired fracture conductivity for a specific treatment, both the reservoir producing capacity and the proppant permeability must be considered. The size and type of the proppant must then be considered when designing an appropriate fracturing treatment.

P-2.1: Types of Proppants

Table P-1 contains the size, specific gravity and porosity of the most common proppants. These data, using Eq. 8-48, allow the calculation of the propped fracture width (Table P-2) if the total mass of proppant injected and the generated fracture area are known. The ratio of these two variables is often referred to as the proppant concentration within the fracture. In addition, Table P-2 contains the average number of particle diameters for each proppant width. Finally, the actual propped width will be somewhat reduced as a result of particle embedment, a serious problem in very soft formations.

Of the several types of proppants available for hydraulic fracturing, sand is the most common. Today, fracturing quality sand is available from several sources. In the United States, premium sands come from Illinois, Minnesota and Wisconsin. They are mined from the Jordan Sandstone and the St. Peter Sandstone. These sands are often referred to as "northern white sand," "northern sand," "white sand," "Ottawa sand," "Jordan sand," "St. Peter's sand" and "Wonewoc sand." Even though these sands may come from different sources and may even have different appearances, they perform similarly during conductivity testing. While the two premium sands may be easily distinguished by color, their performance during conductivity testing shows they are very similar.

Standard grade sands come from the Hickory Sandstone near Brady, Texas. These sands have a darker color than many of the northern sands. Some of the common names are "Texas brown sand," "brown sand," "Brady sand" and "hickory sand." Although not considered premium sands, at lower closure stresses the brown sands have a higher proppant-pack permeability than their northern counterparts.

The conductivity of sand can be improved by applying a thin coating of resin to the sand grains. The resin coating helps increase the strength of the sand, reduces the amount of fines created as the proppant undergoes fatigue and spreads

Type	Mesh Size	Particle Size (in.)	Specific Gravity	Porosity
Northern White Sand	12/20	0.0496	2.65	0.38
	16/30	0.035	2.65	0.39
	20/40	0.0248	2.65	0.40
Texas Brown Sand	12/20	0.0496	2.65	0.39
	16/30	0.035	2.65	0.40
	20/40	0.0248	2.65	0.42
Curable Resin-Coated Sand	12/20	0.0496	2.56	0.43
	16/30	0.035	2.56	0.43
	20/40	0.0248	2.55	0.41
Precured Resin-Coated Sand	12/20	0.0496	2.55	0.38
	16/30	0.035	2.56	0.37
	20/40	0.0248	2.55	0.37
ISP	12/20	0.0496	3.18	0.42
	20/40	0.0248	3.23	0.42
ISP-Lightweight Sintered Bauxite	20/40	0.0248	2.72	0.40
	16/20	0.04	3.7	0.43
	20/40	0.0248	3.7	0.42
	40/70	0.0124	3.7	0.42
Zirconium Oxide	20/40	0.0248	3.15	0.42

Table P-1—Typical proppants and their characteristics. (Note that porosity decreases under closure stress.)

the loading force over a larger area. There are several varieties of resin-coated sand. The resin can be precured or hardened during the manufacturing process or cured in the formation. Curable resins are often used strictly for controlling proppant flowback after treatments. In recent years, dual-coated resins have become increasingly popular. These proppants have the increased strength of a hardened inside coating and reduced point loading from a curable outside coating.

Fractures exposed to even higher stresses need specialized man-made proppants. These proppants include intermediate strength ceramics, zirconia and bauxite. Bauxite is an aluminum oxide material and is perhaps the best proppant available today for resisting crushing. Zirconia proppant is made from zirconium oxide, and the ISP proppants are blends of aluminum oxide and silicone oxide.

P-2.2: Stress and Time Effects

In general, as many attempts for design optimization demonstrate, treatments must incorporate more proppant at higher slurry concentrations. Furthermore, using proppants with higher permeabilities maximizes potential production, a fact substantiated by the proppant permeability values now reported throughout the industry. Originally, proppant permeability charts were derived by performing short-term laboratory tests on proppants at varying closure pressures. Recent developments have shown that this type of test procedure greatly overpredicts the ultimate permeability of a given proppant. Leaving the proppant exposed to a high closure pressure over a longer period of time substantially reduces its effective permeability. Recent work shows that proppants should be exposed to closure pressures for several days before permeability measurements are made.

In the past, the standard proppant permeability and conductivity tests were performed in a test cell where the proppant was contained between two parallel steel plates. Pressure could be applied directly, and downhole temperatures could be readily simulated by heating the cell. The permeability was measured by flowing 2% KCl water through the pack and then applying Darcy's law. Thus, the permeability of a proppant pack (related to the propped width as shown earlier by the proppant concentration) can be measured at various

Type	Mesh Size	Propped Width (1 lb/ft^2)	Number of Particle Diameters	Propped Width (2 lb/ft^2)	Number of Particle Diameters
Northern White Sand	12/20	0.12	2.4	0.24	4.8
	16/30	0.12	3.4	0.24	6.8
	20/40	0.12	4.8	0.24	9.6
Texas Brown Sand	12/20	0.12	2.4	0.24	4.8
	16/30	0.12	3.4	0.24	6.8
	20/40	0.13	5.2	0.26	10.4
Curable Resin-Coated Sand	12/20	0.13	2.6	0.26	5.2
	16/30	0.13	3.7	0.26	7.4
	20/40	0.12	4.8	0.24	9.6
Precured Resin-Coated Sand	12/20	0.12	2.4	0.24	4.8
	16/30	0.11	3.1	0.22	6.2
	20/40	0.11	4.4	0.22	8.8
ISP	12/20	0.10	2.0	0.20	4.0
	20/40	0.10	4.0	0.20	8.0
ISP-Lightweight	20/40	0.12	4.8	0.24	9.6
Sintered Bauxite	16/20	0.09	2.3	0.18	4.6
	20/40	9.09	3.6	0.18	7.2
	40/70	0.09	7.3	0.18	14.6
Zirconium Oxide	20/40	0.10	4.0	0.20	8.0

Table P-2—Propped fracture width for various proppants and proppant concentrations. (Proppant concentration here refers to the total mass of proppant injected divided by the generated fracture area.)

expected stresses and can be readily converted to conductivity. The latter is simply the product of the proppant-pack permeability and propped width.

Permeability reduction at higher stresses is attributed to the dislodging of fragments from particles (thus reducing their sphericity), the crushing of other particles and the partial plugging of the flow path by the created fines.

Short-time measurements fail to account for long-term effects resulting from exposure to given stresses. Fatigue of the particles can be quantified through an extended time test where proppant is kept at the expected stress value for up to 200 hr. Figure P-1 is a representative test showing on the left the closure stress impact on proppant-pack permeability and fracture conductivity (2 lb/ft^2). For example, at 2000 psi the permeability is 600,000 md and the conductivity is 2500 md-ft; at 5000 psi these values are 180,000 md and 1000 md-ft, respectively. However, as can be seen on the right, from the continuation of the figure at an extended time exposure (at 5000 psi), the values level off after 50 hr and are substantially lower than the short-time measurements. The permeability is 73,000 md, and the conductivity is 430 md-ft. This major reduction would have a significant effect on the forecast of fractured well performance.

In addition, proppant embedment results in width reduction and thus fracture conductivity reduction. The previously described apparatus is used, but instead of steel plates, the *proppant is enclosed by reservoir rock material of medium* hardness. A common rock used for this purpose is Ohio Sandstone with a Young's modulus equal to 6×10^6 psi. For example, while long-term fracture conductivity of 20/40 ISP at 5000 psi between steel plates is 6200 md-ft, it becomes 5700 md-ft between the rock plates, an 8% reduction. Needless to say, this effect will be far more severe in soft rock such as a chalk or at higher closure stresses. Table P-3 contains fracture conductivity values at 1 lb/ft^2 concentration for various proppants and closure stresses, including embedment. Table P-4 contains the same information for 2 lb/ft^2 concentrations.

P-2.3: Proppant Size and Conductivity

At lower closure stresses, higher fracture conductivities can be obtained by simply increasing the mesh size of the proppant. This larger flow capacity is a result of the corresponding larger pore sizes between the grains. However, as the closure stress increases, the larger mesh sizes begin to lose their advantage. The rate of permeability reduction is always higher in larger mesh sizes because larger sizes have lower strength and their resistance to higher stresses is impaired. This causes a more pronounced loss in sphericity and increased fines generation. As a result, the permeability of the larger proppants is reduced to a much greater degree. It is conceivable that above a certain stress level a larger mesh size may, in fact, exhibit a lower permeability than a similar proppant of smaller size. The permeability curves in Fig. P-2 show the stress-sensitive values of three different sizes of proppants and the crossover of their permeability at a high stress.

P-2.4: Proppant Slurry

The easiest way to improve fracture conductivity is to increase the slurry concentration. Higher concentrations result in wider propped fractures and therefore in improved conductivity. Slurry concentrations should be designed to prevent the proppant concentration in the fracture from falling below 0.5 lb/ft^2 and should be above 1 lb/ft^2 whenever possible. To obtain a 1 lb/ft^2 concentration throughout the fracture, slurry concentrations need to approach or even exceed 10 ppga. Slurry concentrations of this magnitude often lead to fears of screenouts. However, as Fig. 9-16 shows, there is no more risk of bridging with a slurry concentration of 20 ppga than there is with one of 5 ppga.

There are two disadvantages in the placement of large-mesh proppants. First, there is an increased risk of premature screenout because of the larger grain size. Hydraulic fracture widths must be three to four times wider than the diameter of the proppant to prevent bridging. Based on the average diameter of sizes listed in Table P-1, a 12-20 mesh proppant requires twice the hydraulic fracture width of a 20-40 mesh proppant. The other problem with larger mesh sizes is that their settling rate is greater. Therefore, deep-penetrating fractures will be more difficult to obtain when using these proppants.

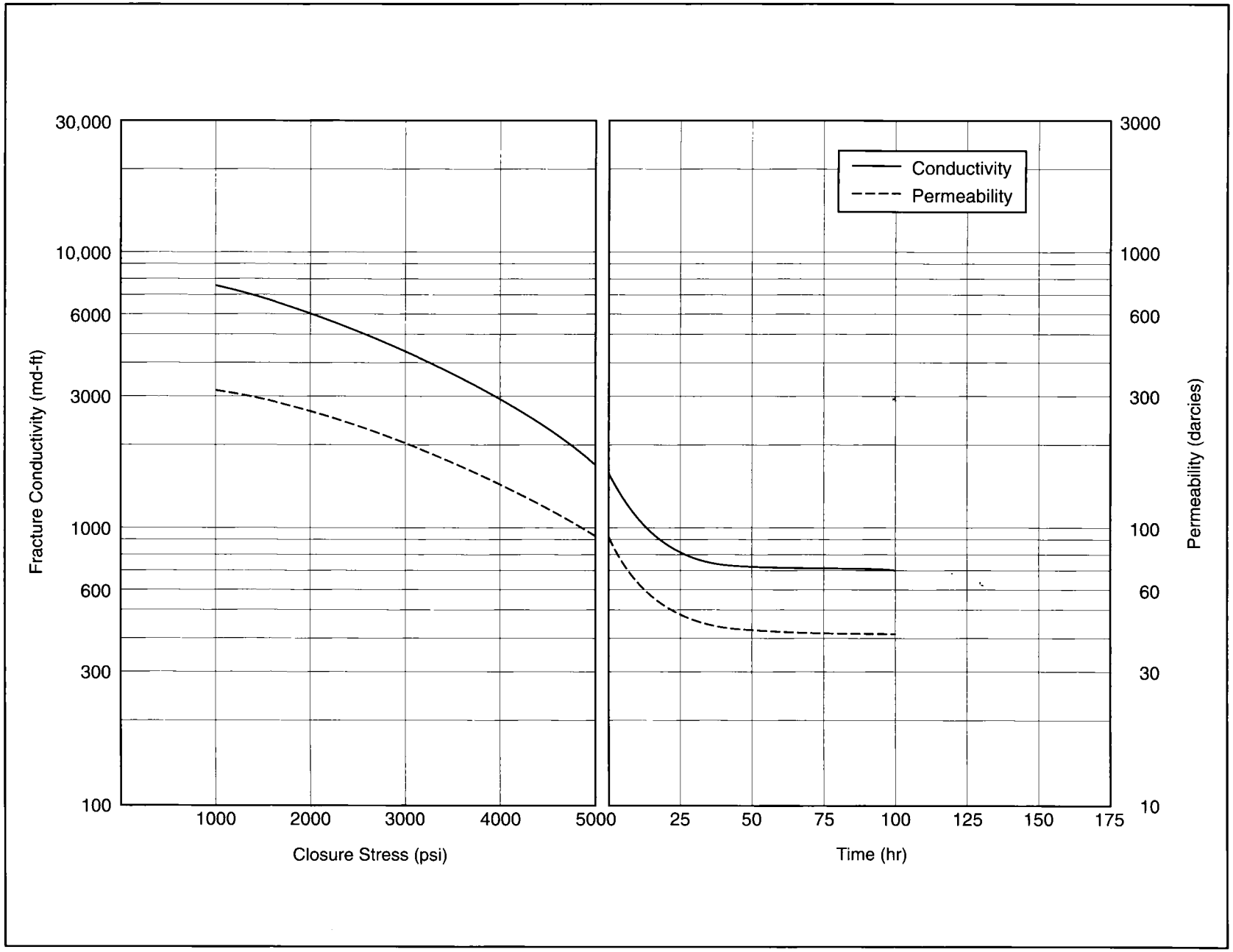

Figure P-1—Fracture conductivity and proppant-pack permeability of 20/40 brown sand at 2 lb/ft^2, 225°F. Time effects at 5000 psi closure stress (from STIMLAB, 1986).

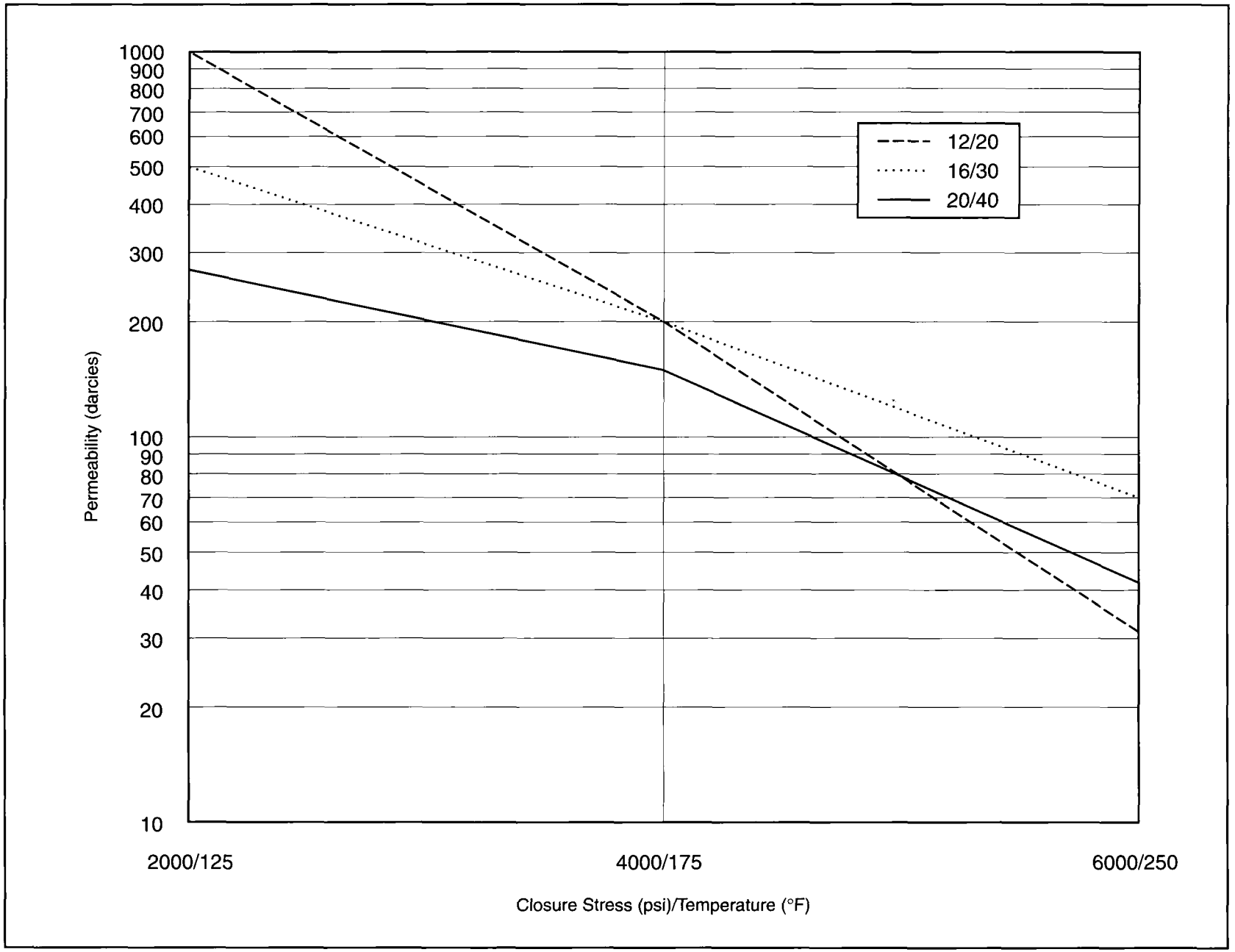

Figure P-2—Long-term conductivity and permeability of three different mesh sizes at 1 lb/ft^2. Hickory sand between Ohio Sandstone with 2% KCl (from STIMLAB, 1988).

Type	Fracture Conductivity (md-ft)				
	2000 psi	**4000 psi**	**6000 psi**	**8000 psi**	**10,000 psi**
20/40 Northern Sand	1970	1210	380	—	—
20/40 ISP-Lightweight	3770	2580	1330	660	310

Table P-3—Long-term fracture conductivity for various proppants at 1 lb/ft^2 and 200°F (from STIMLAB, 1988).

Type		Fracture Conductivity (md-ft)			
	2000 psi	**4000 psi**	**6000 psi**	**8000 psi**	**10,000 psi**
20/40 Northern Sand	4330	2470	730	250	140
20/40 Brown Sand	3590	1670	560	150	—
20/40 Precured Resin-Coated Sand	4090	3690	2390	1300	510
20/40 ISP	8420	7090	4940	3330	2100
20/40 ISP-Lightweight	8570	7160	5000	2940	1330

Table P-4—Long-term fracture conductivity for various proppants at 2 lb/ft^2 (from STIMLAB, 1988).

P-3

Fracturing Fluid Selection

While historically there have been several hundred fracturing fluids used by the industry, three considerations must govern their selection. In order of importance these are:

1. Ability to create a fracture with large conductivity (i.e., transport high proppant-slurry concentrations).
2. Result in as little polymer-induced proppant-pack damage as possible.
3. Require lower pumping and treatment pressure capacity by reducing the friction pressure drop.

All these considerations are affected by the polymer load that controls both the fluid viscosity and the resulting friction pressure drop. Thus, it is important that the amount of polymer is engineered appropriately so that it is adequate but not excessive.

There are other less important considerations in fluid selection. While these should be taken into account, they should not govern the fluid selection to the detriment of the previously mentioned important concerns. These include minimization of fracture face damage, which would be the result of unavoidable leakoff and compatibility problems between the fracturing fluid and reservoir fluids and rock. In addition, there has been much concern in the industry about posttreatment cleanup. This concern led to the use of energized and foamed fluids. Although they have a decided edge on cleanup, these fluids become impractical when high slurry concentrations are necessary because proppant is added exclusively to the liquid portion of the foam. Thus, superhigh proppant concentrations may be needed to exceed the proppant handling capabilities of today's pumping equipment. Foams may then be more appropriate in very tight formations where the fracture conductivity is less important.

P-3.1: Fracturing Fluid Selection Guide

Figure P-3 represents a compendium of current and evolving industry practices. While this selection guide should be considered as general recommendations, the actual use (or even appropriate use) of fluids may be lopsided toward certain types of fluids. Furthermore, this chart should always be used with a degree of caution, bearing in mind the considerations outlined in the previous subsection. Thus, fracturing fluid must be engineered with the particular reservoir in mind and with consideration for the desired performance of the fracturing treatment.

The first and obvious division is whether the well is oil or gas. In the case of a gas well (the left branch in Fig. P-3), the reservoir temperature provides the first decision. If the temperature is less than 225°F, then all fracturing fluids can be used with the obvious considerations of diminishing permanent fracture damage. The temperature limitation is that below which borate-crosslinked fluids can be used. This is an important limit in all fracturing treatments because (as will be shown later) these fluids have demonstrated several favorable properties.

Figure P-3 allows the division for below –225°F gas wells to offer the flexibility of using linear gels or foams, but with the strong recommendation to always consider borate-crosslinked fluids first.

If the gas well temperature is more than 225°F, then organometallic-crosslinked polymer fluids are indicated. While these are far more damaging than borate-crosslinked fluids, they are necessary at these high temperatures. At ultrahigh temperatures (>300°F), titanate or zirconate-crosslinked hydroxypropyl guar (HPG) must be used. If the reservoir is underpressured, these fluids can be energized with the addition of nitrogen or carbon dioxide.

In an oil well, the water sensitivity of the reservoir rock has traditionally prompted a division between water-base fluids and oil-base fluids. However, this consideration is often the cause of inappropriate fluid selection and less-than-optimum fracturing treatments. Essentially, if the reservoir is mildly or moderately water sensitive, the selection process outlined for a gas well should be followed.

While the use of oil-base fluids in oil wells is often suggested, these fracturing fluids deserve certain additional considerations. The cost of pumping is much greater than for water-base pumping fluids because of the cost of the oil itself. Excessive hydraulic horsepower may be needed to place fracture treatments using oil-base fluids because of their inordinately high friction pressure losses.

Finally, safety considerations must be addressed because of the flammability of the base fluid. Any problem leading to fluid leakage has the potential for posing an extreme fire hazard.

The perceived advantage of oil-base fluids is that the reservoir is exposed only to a fluid that is related to the reservoir fluids. However, several studies have shown that fluid leakoff and relative permeability-induced damage are not usually severe problems. Figure P-4 shows that a damaged zone of 5 in. (much deeper than most fluids will reach during leakoff) has a minimal effect on production as long as the fracture itself has adequate conductivity. With this in mind, water-base fluids can be used in most all reservoirs without creating significant damage. Figure P-4 suggests that a tenfold decrease in the reservoir permeability (or even a hundredfold decrease) has very limited impact on the productivity index ratio between the fractured and the unfractured well. Thus, fracture face damage should never be a criterion for the fracturing fluid selection to the detriment of fracture conductivity. This issue is discussed extensively in Chapter 11 of *Reservoir Stimulation.*

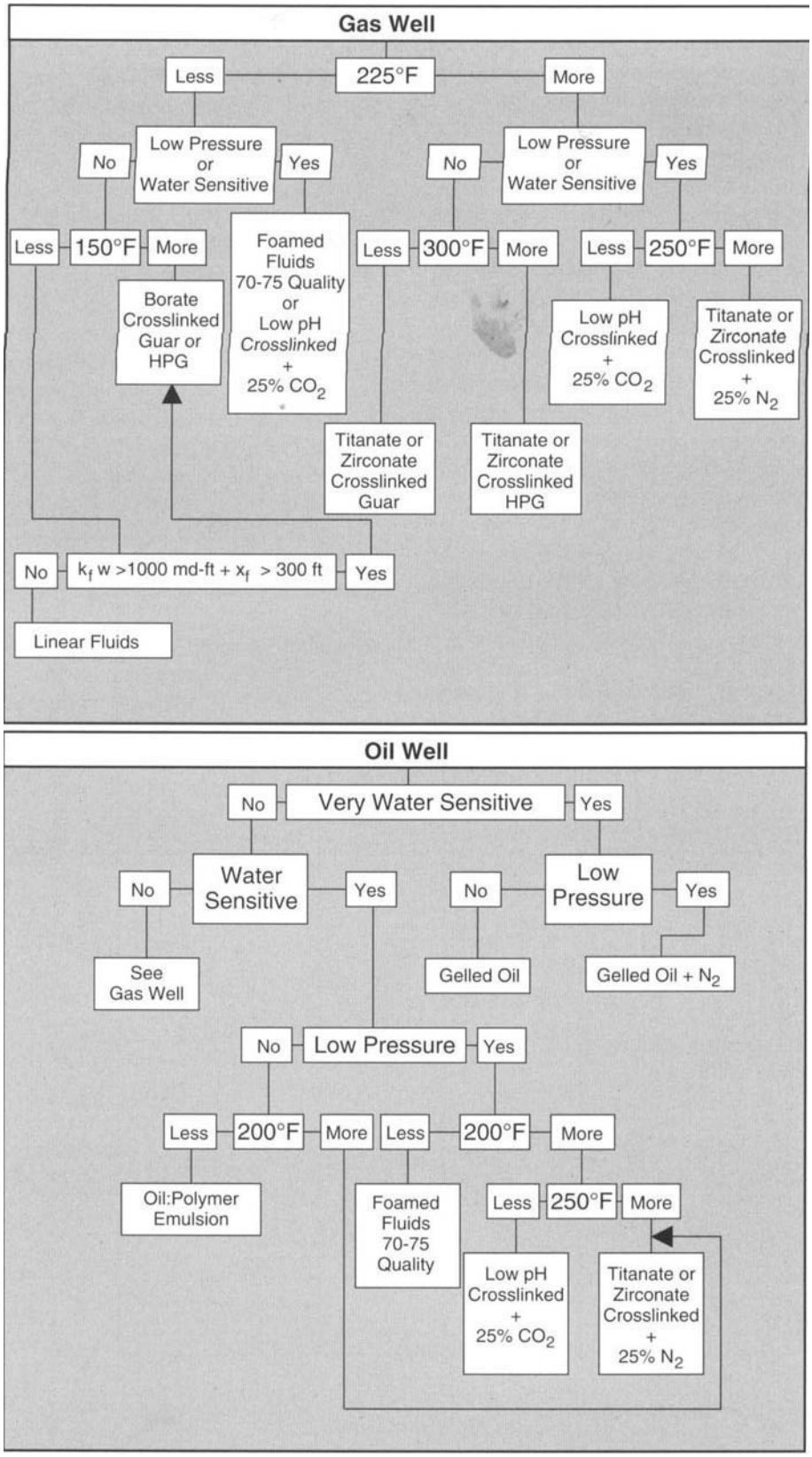

Figure P-3—Fracturing fluid selection guide.

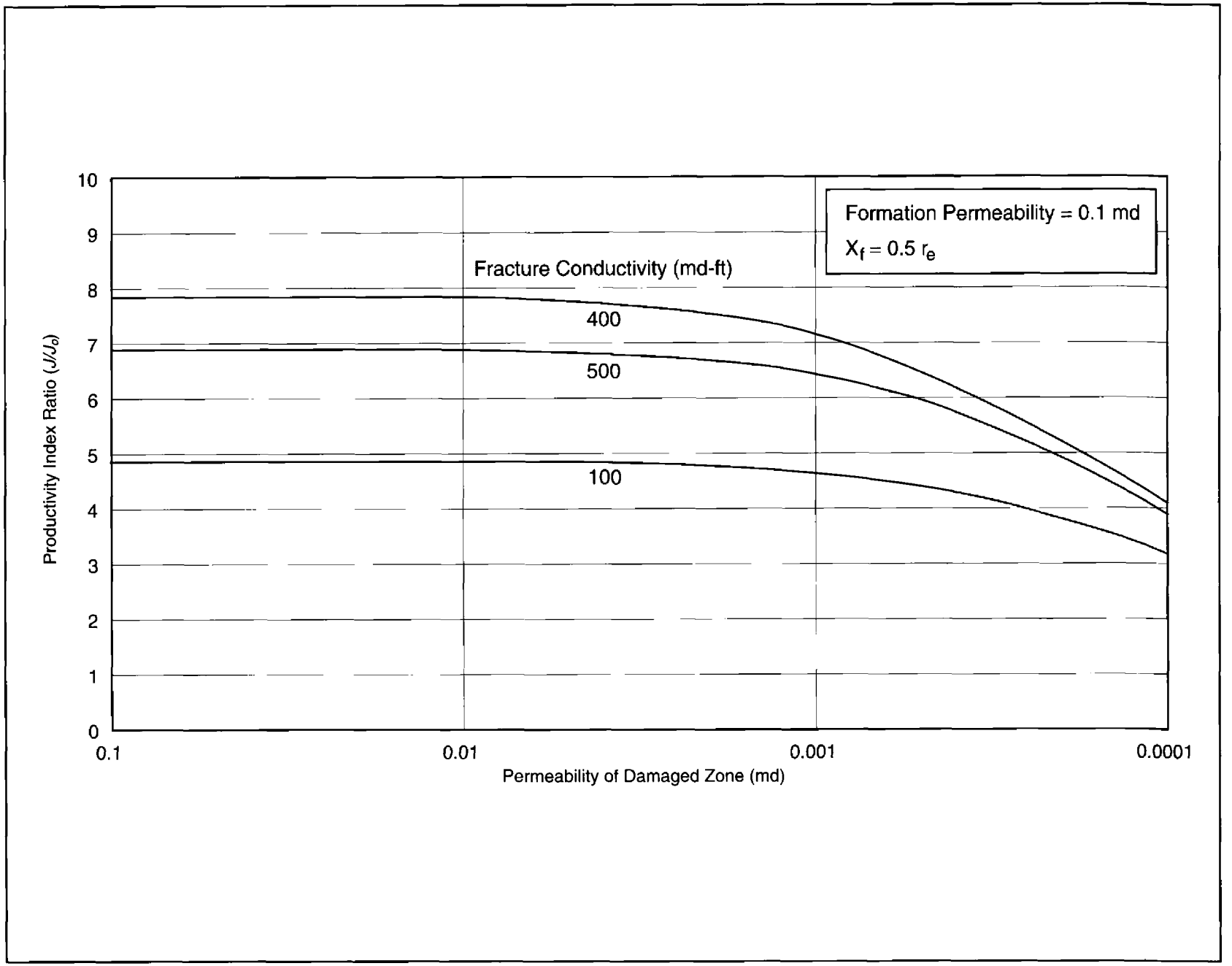

Figure P-4—Effect on productivity index ratio (J_o, unfractured) of 5-in. damage around fracture (from Holditch, 1978).

P.3.2: Rheological Properties and Viscosity Requirements

Experience has shown that the viscosity of fracturing fluids must nearly always be above 100 cp at 170 sec^{-1} to successfully transport proppant throughout the fracture. When designing a fluid to meet this requirement, the reservoir static temperature must be taken into account. As shown in Fig. 5-5, the temperature of the fracturing fluid approaches this maximum temperature in the first 25 to 30% of the fracture. The viscosity of a fracturing fluid will decrease as a function of both increasing temperature and increasing exposure time at this temperature.

Wells with temperatures above 300°F require fracturing fluids with polymer loads of 50 to 60 lb/1000 gal for the pad fluid and for the early proppant stages. As treatment progresses, polymer loading may be reduced because this portion of the treatment will not be exposed to reservoir temperature for an extended period of time. The final stages can be as low as 30 lb/1000 gal and may incorporate a less damaging crosslinker (i.e., borate instead of an organometallic material). Currently, major advances in continuous fluid mixing allow the engineering and tailoring of fracture fluids and additives to affect optimum properties.

The data that follow cover common fracturing fluids and include the power law rheological properties n' and K' and a calculated apparent viscosity at 170 sec^{-1}. The latter can be readily obtained using the method outlined in Table 5-1. Example calculations are shown in Chapter C of this volume.

Figures P-5 through P-7 include the n', K' and apparent viscosity, respectively, of 30 lb/1000 gal borate-crosslinked gel; Figs. P-8 through P-10 contain the same variables for 40 lb/1000 gal fluids. The time dependency occurs because of the delayed crosslink nature of these fluids. These are some of the most common fracturing fluids and the ones recommended for the majority of fracturing treatments.

Figures P-11 through P-13 include the n', K' and apparent viscosity for 40 lb/1000 gal zirconate-crosslinked fluid; Figs. P-14 through P-16 are for 50 lb/1000 gal fluid; and Figs. P-17 through P-19 are for 60 lb/1000 gal fluid. The latter has been used in reservoirs with static temperatures up to 400°F.

Figures P-20 and P-21 contain the rheological properties of three different quality foams (55Q, 65Q and 75Q) with 30 lb of polymer/1000 gal of liquid. Figure P-22 shows the apparent viscosity of these fluids and their substantially lower values when compared to the crosslinked liquid fluids. These viscosities would have a highly detrimental effect on the created fracture width, and in moderate-permeability reservoirs ($k > 0.5$ md), such a fracture would exhibit lower posttreatment production.

However, if foams are made with crosslinked polymer fluids, they exhibit much higher viscosities. Figures P-23 through P-25 contain the rheological properties and apparent viscosities of foams made with 40-lb crosslinked polymer at 150°F, whereas Figs. P-26 through P-28 contain the same information at 200°F. In both cases, three quality foams are used: 25Q, 50Q and 65Q.

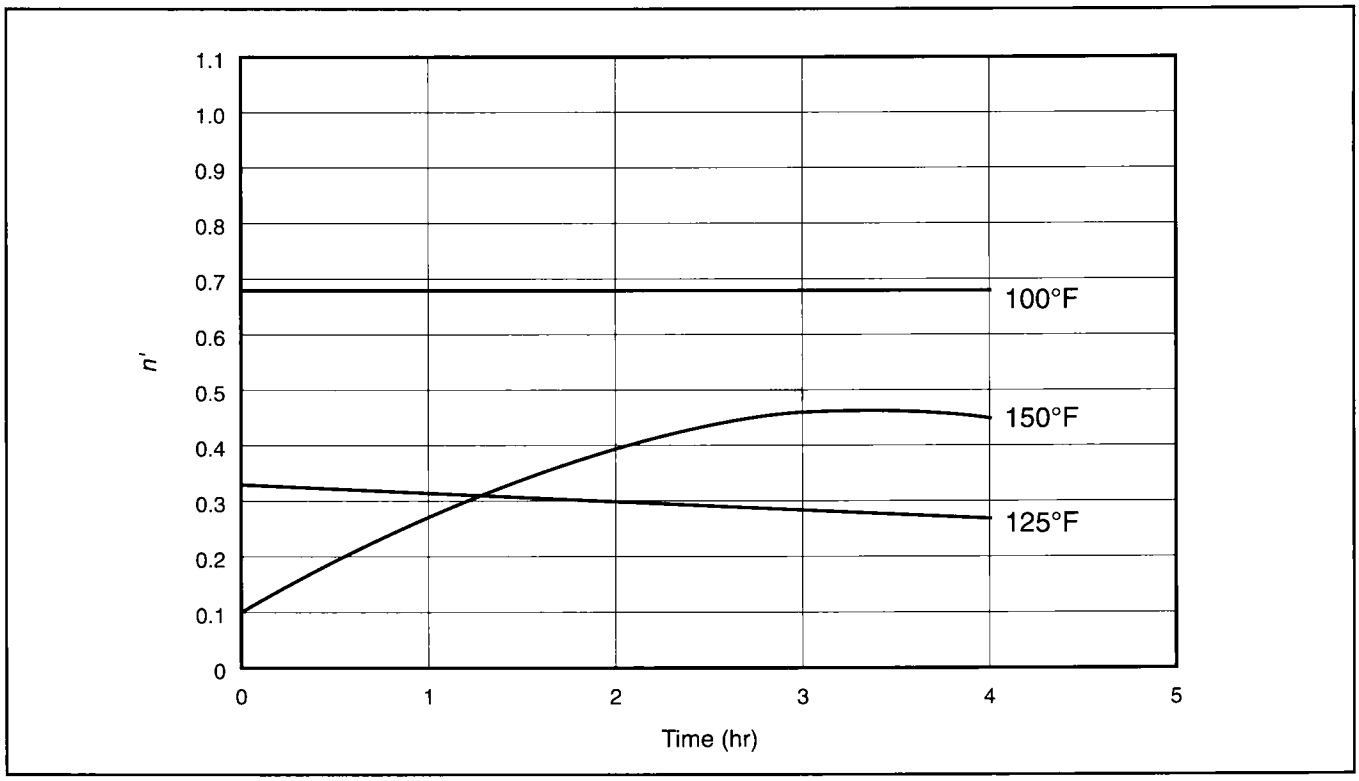

Figure P-5—*n'* for 30 lb/1000 gal borate-crosslinked fluid.

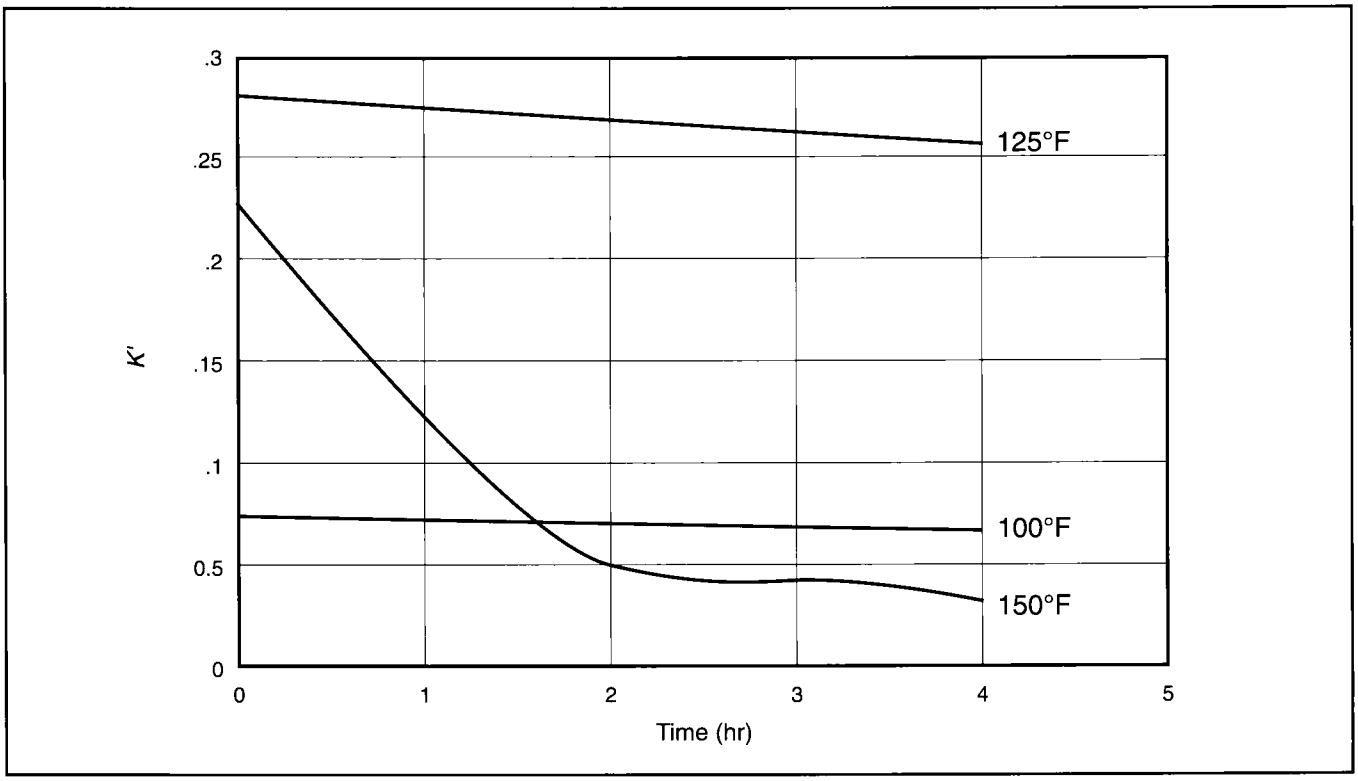

Figure P-6—*K'* for 30 lb/1000 gal borate-crosslinked fluid.

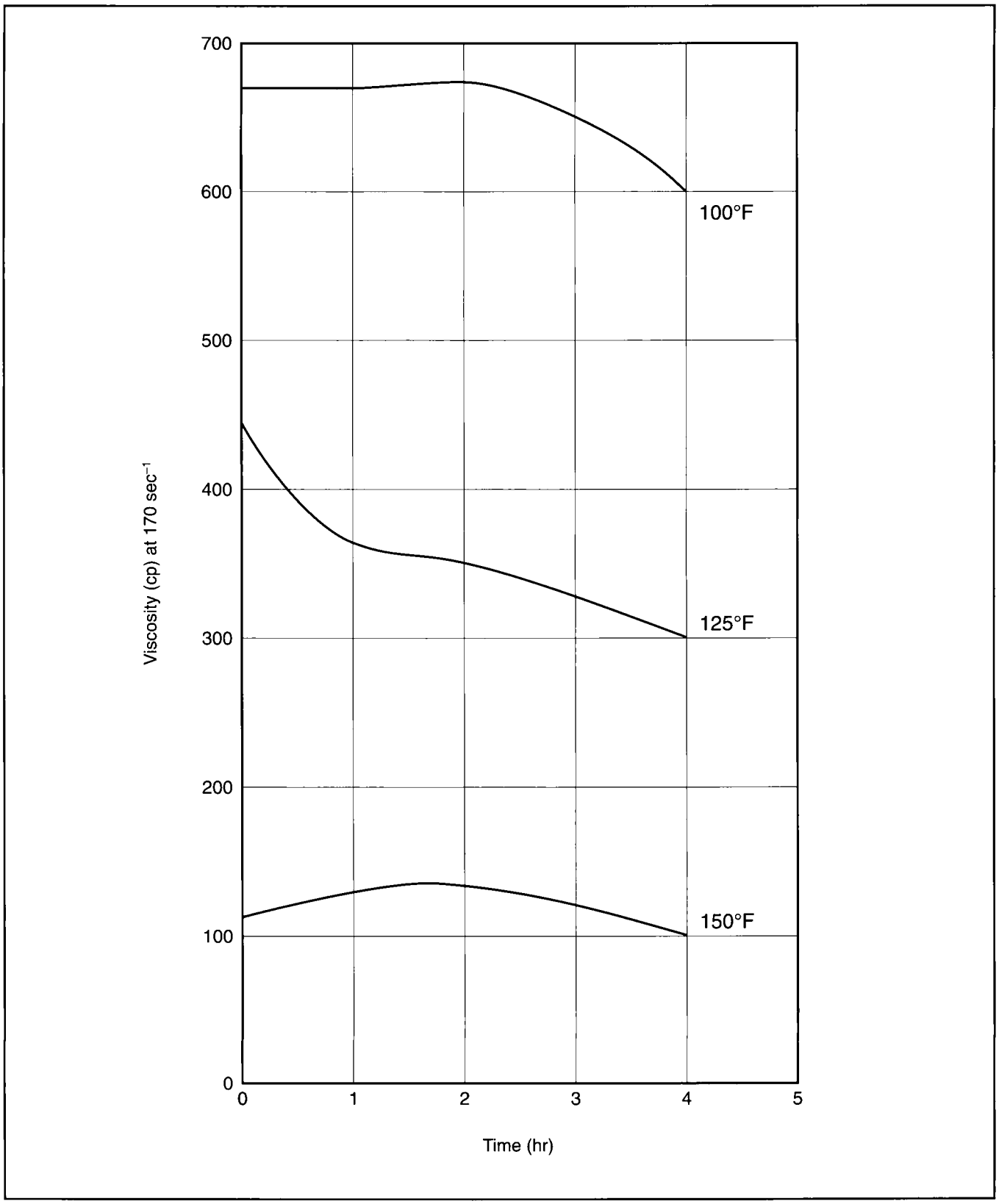

Figure P-7—Apparent viscosity at 170 sec^{-1} for 30 lb/1000 gal borate-crosslinked fluid.

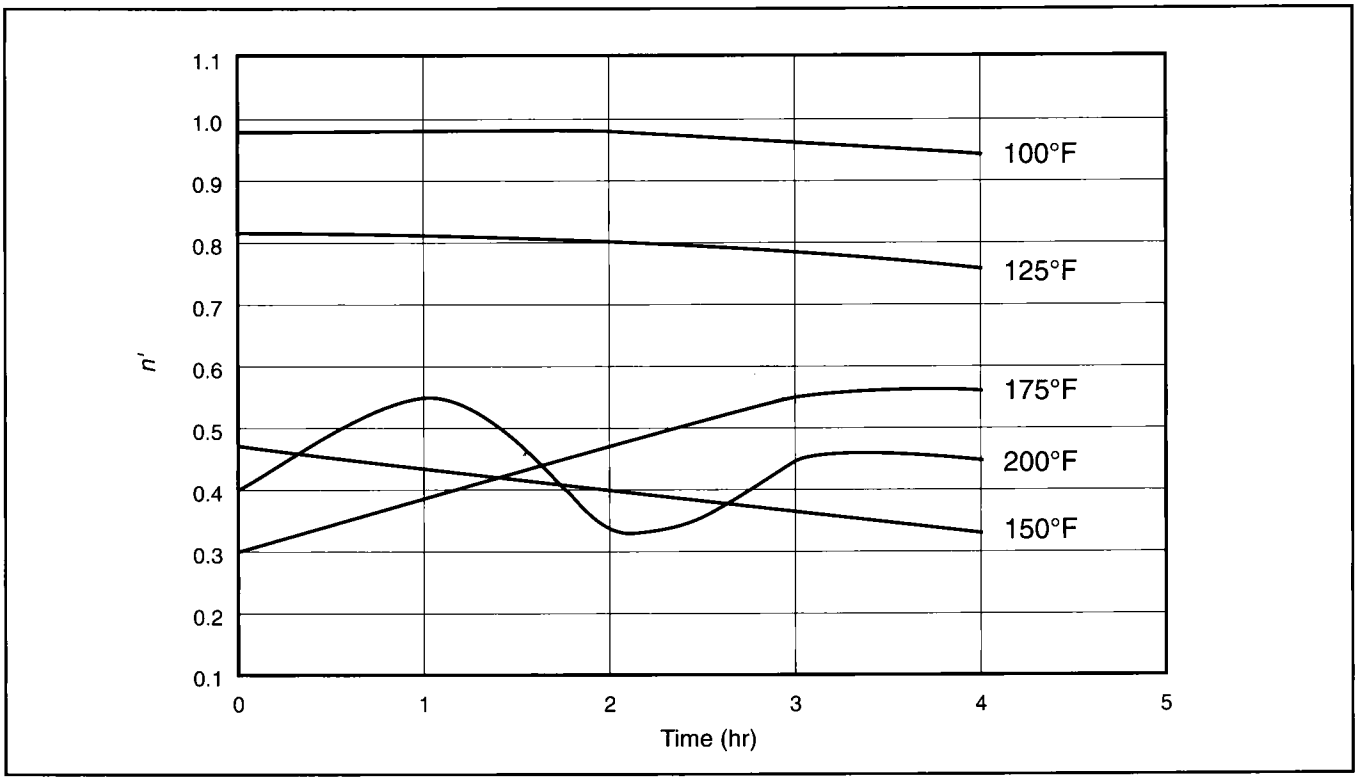

Figure P-8—*n'* for 40 lb/1000 gal borate-crosslinked fluid.

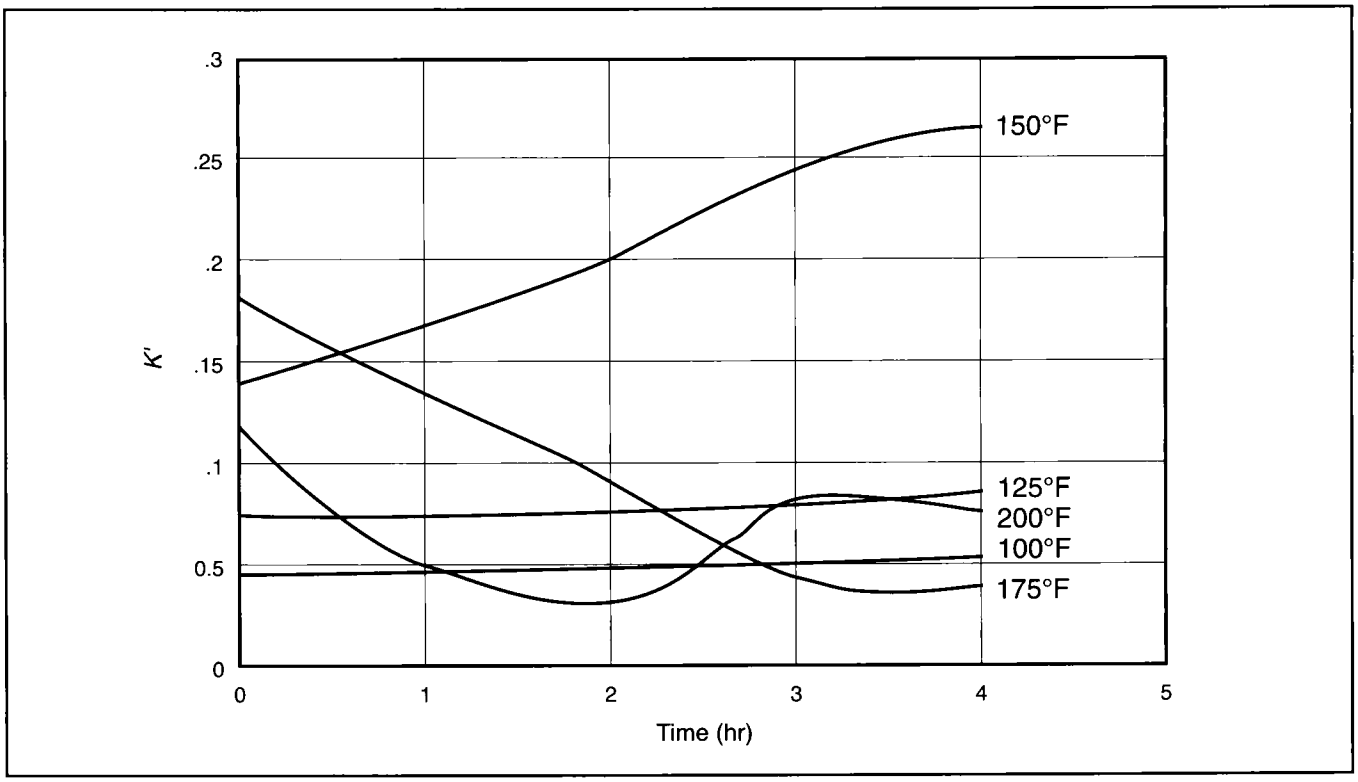

Figure P-9—*K'* for 40 lb/1000 gal borate-crosslinked fluid.

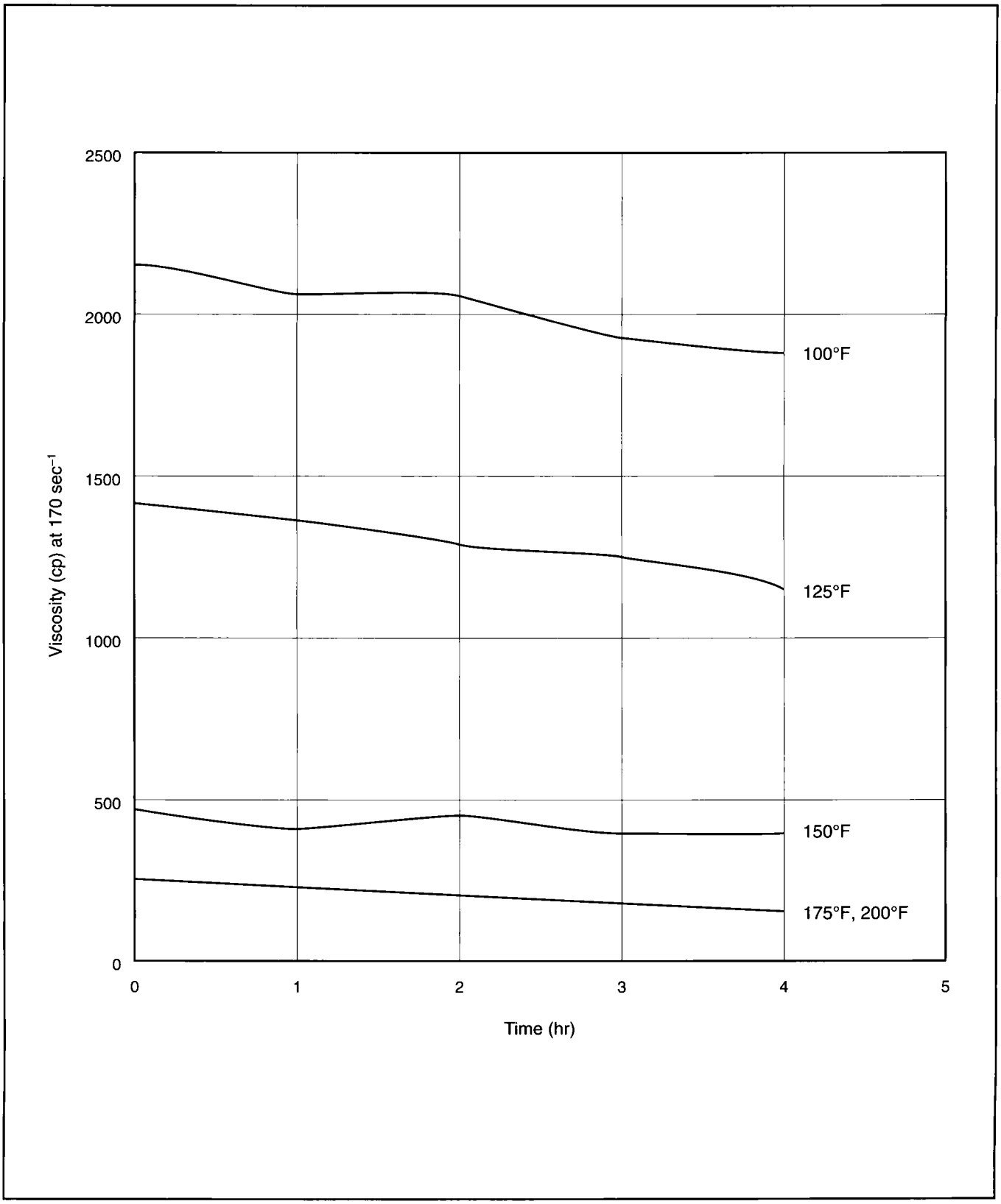

Figure P-10—Apparent viscosity at 170 sec^{-1} for 40 lb/1000 gal borate-crosslinked fluid.

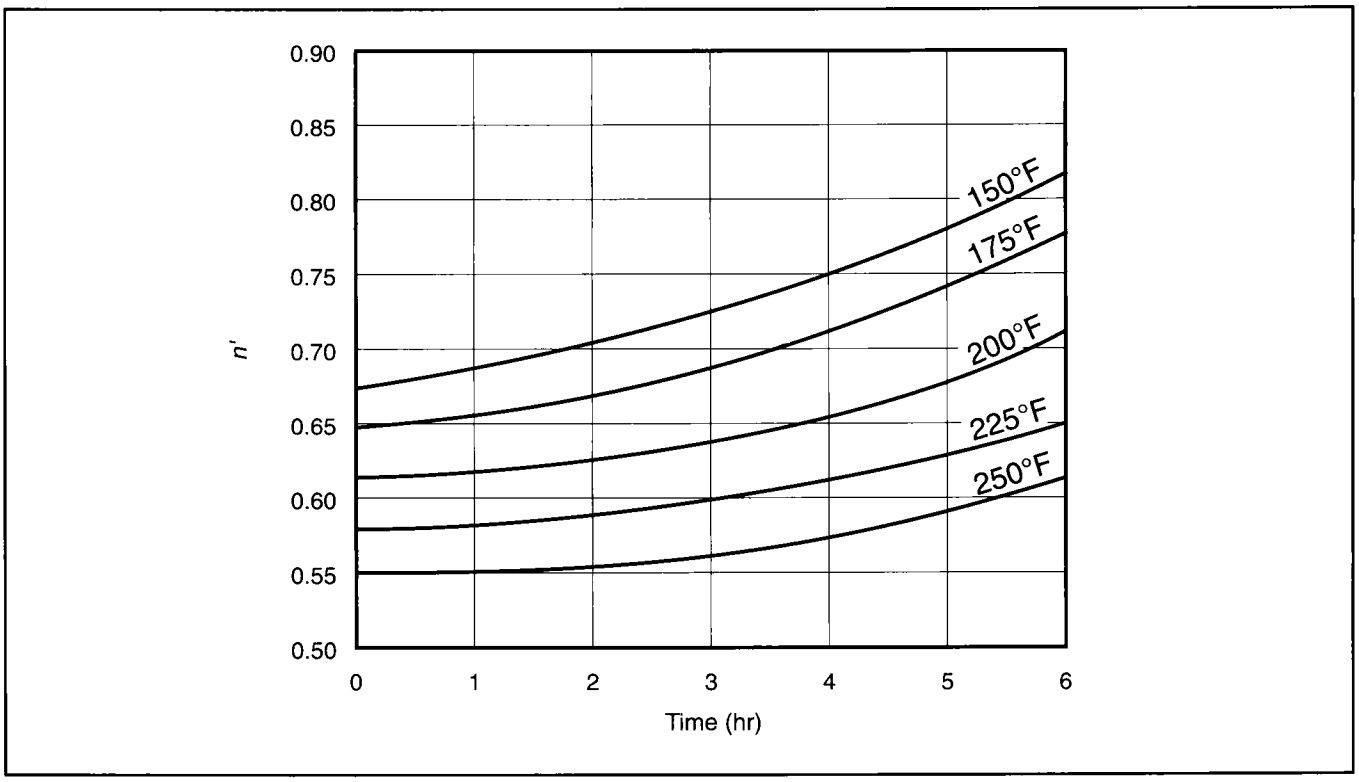

Figure P-11—*n'* for 40 lb/1000 gal zirconate-crosslinked fluid.

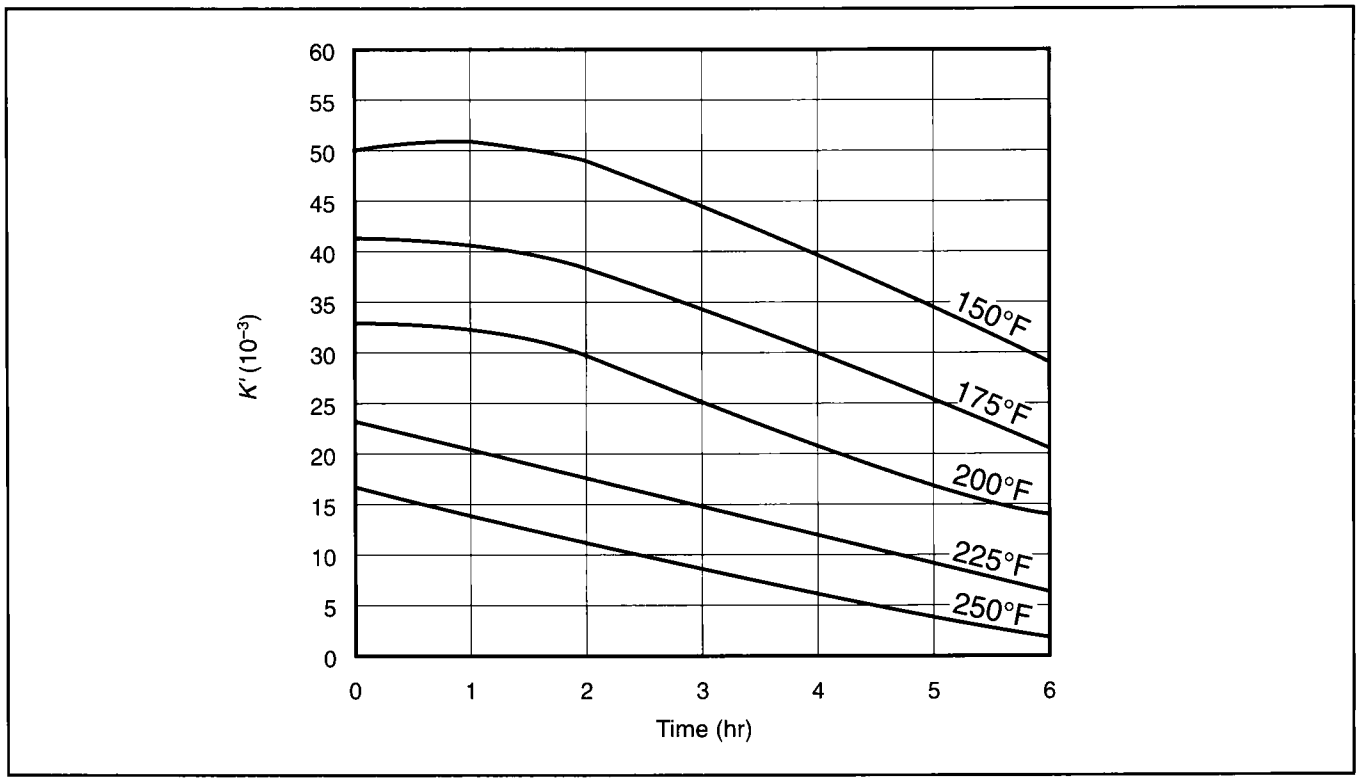

Figure P-12—*K'* for 40 lb/1000 gal zirconate-crosslinked fluid.

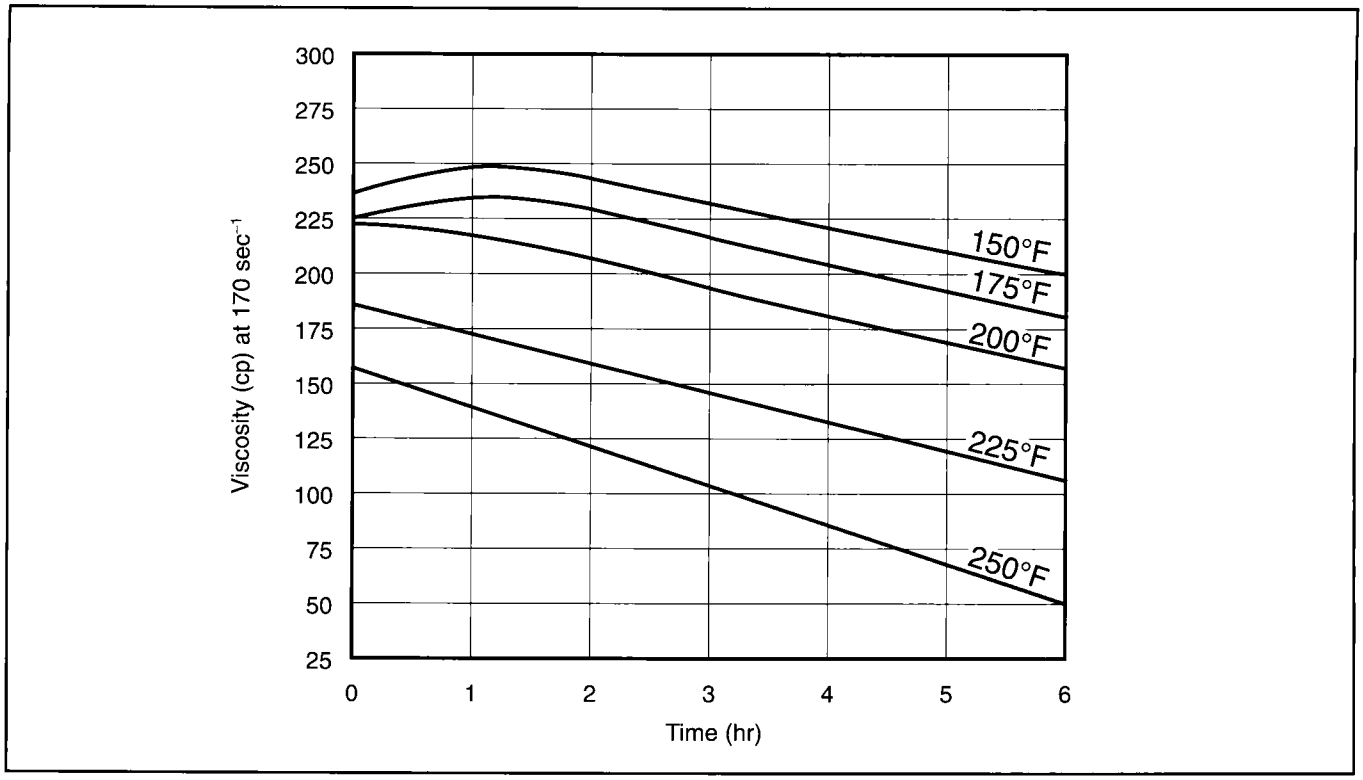

Figure P-13—Apparent viscosity at 170 sec^{-1} for 40 lb/1000 gal zirconate-crosslinked fluid.

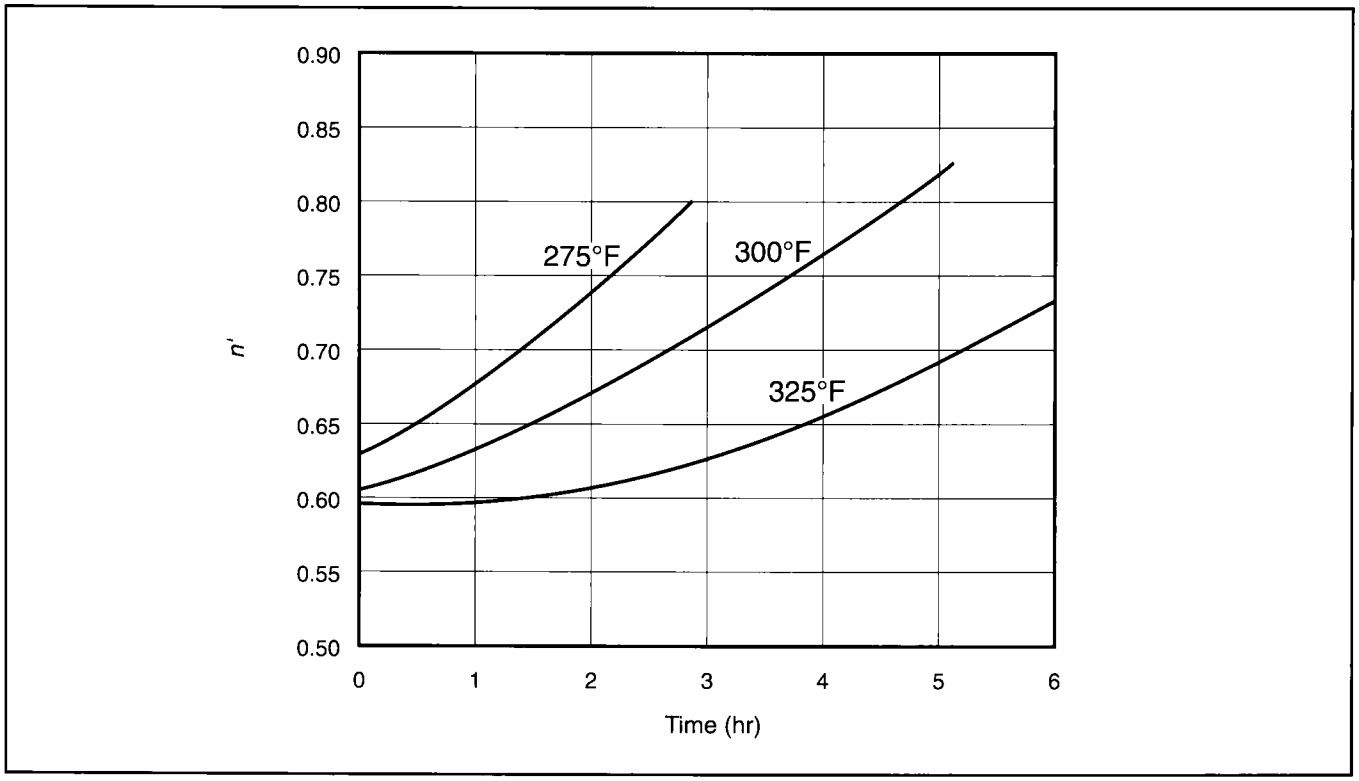

Figure P-14—*n'* for 50 lb/1000 gal zirconate-crosslinked fluid.

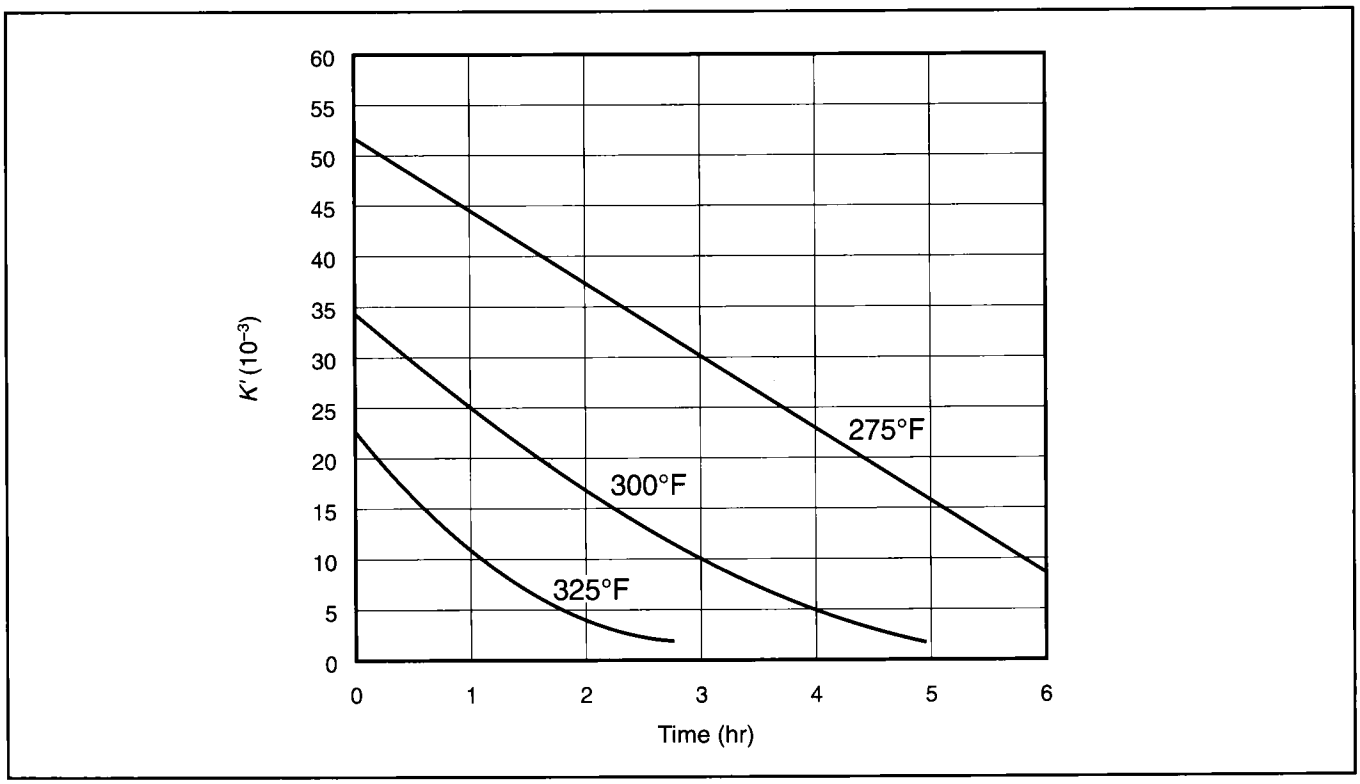

Figure P-15—*K'* for 50 lb/1000 gal zirconate-crosslinked fluid.

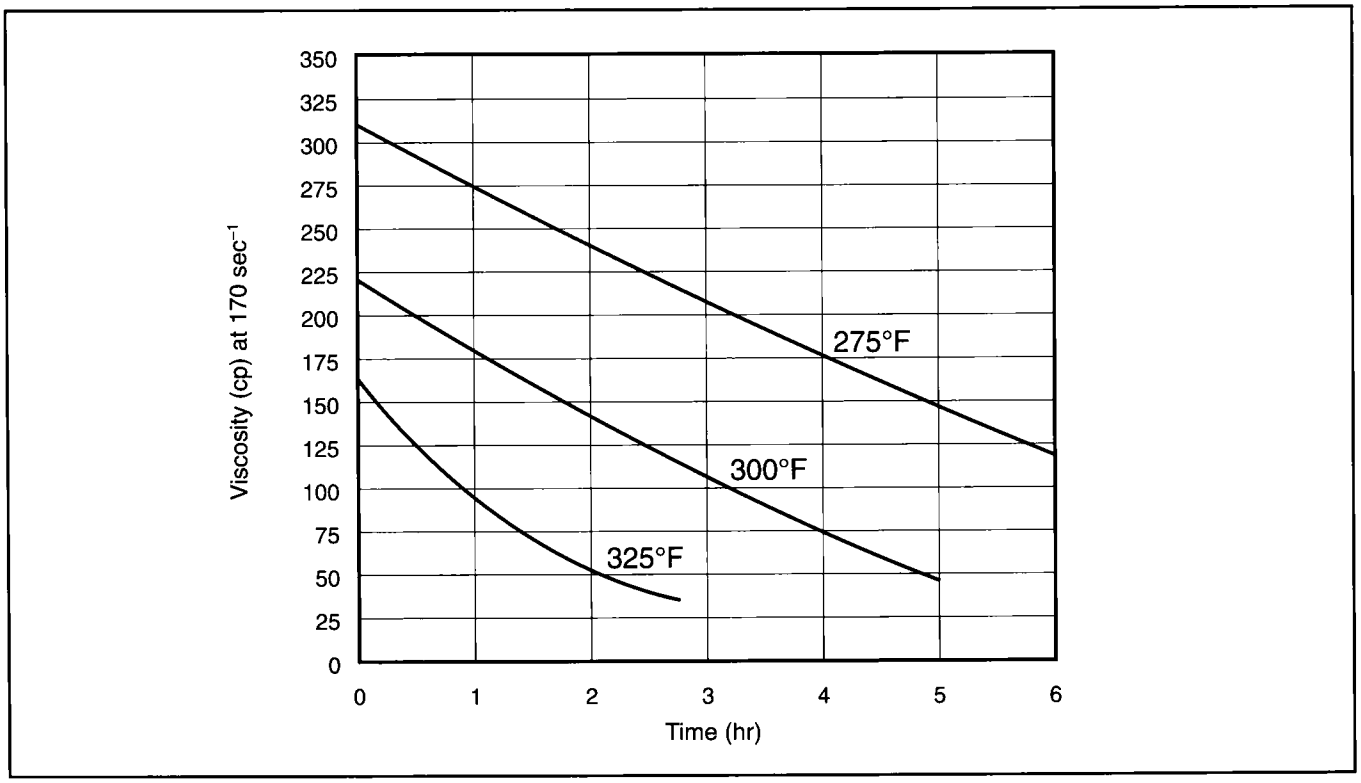

Figure P-16—Apparent viscosity at 170 sec^{-1} for 50 lb/1000 gal zirconate-crosslinked fluid.

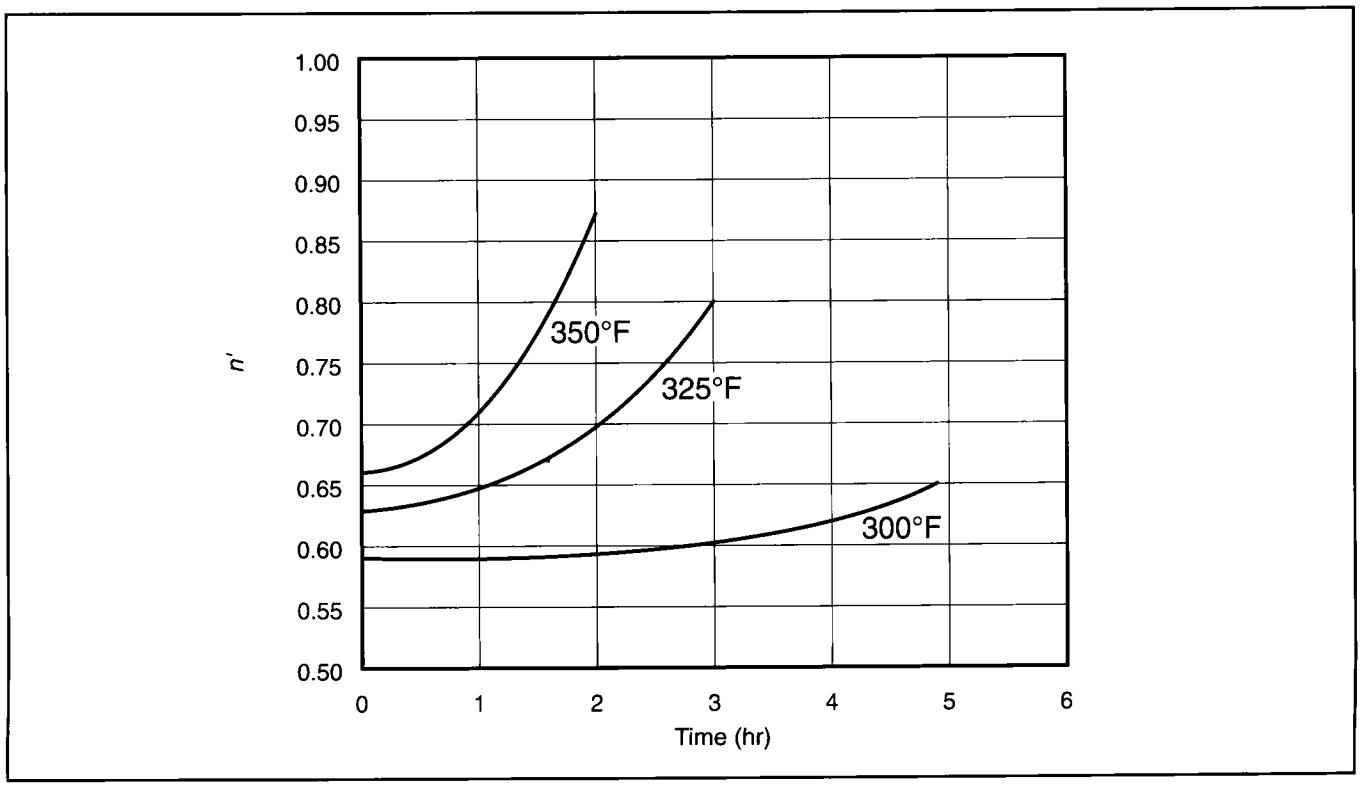

Figure P-17—*n'* for 60 lb/1000 gal zirconate-crosslinked fluid.

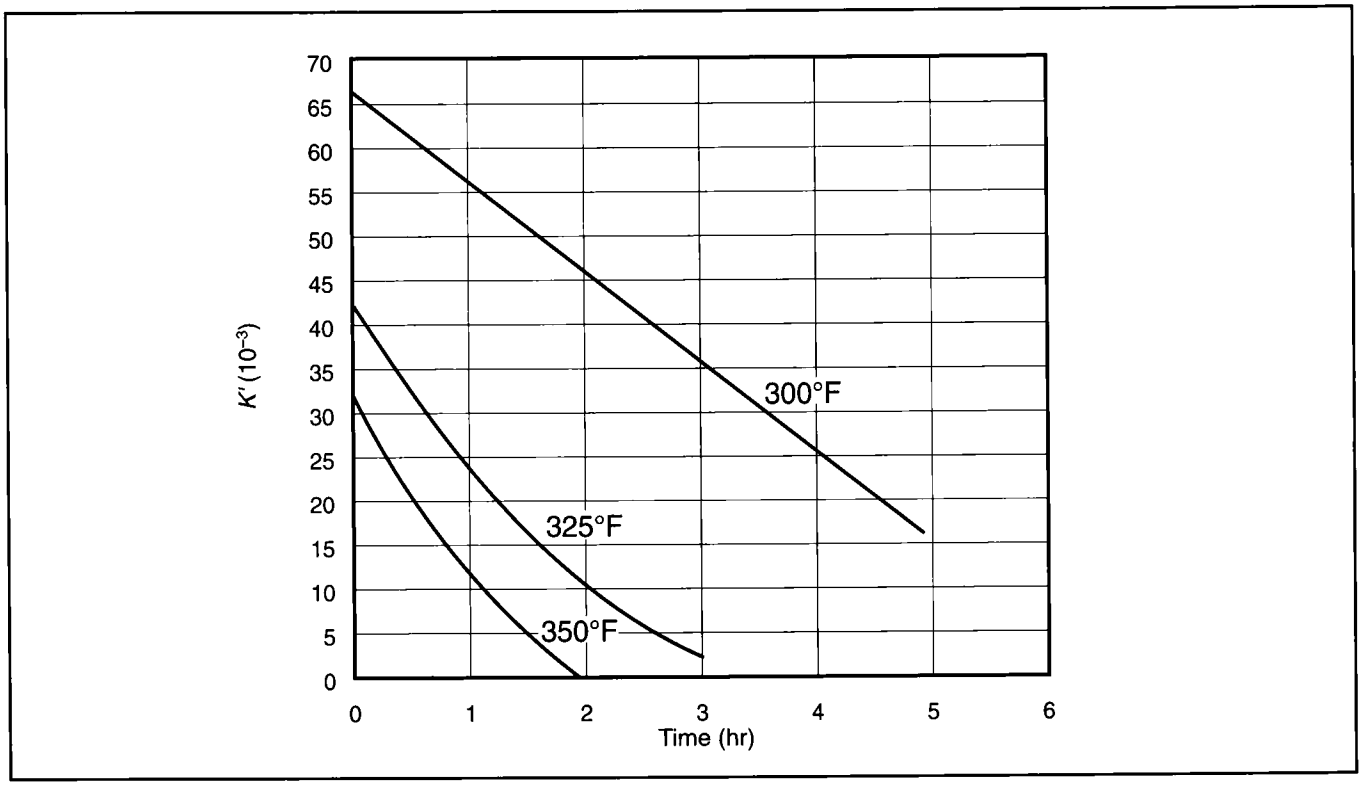

Figure P-18—*K'* for 60 lb/1000 gal zirconate-crosslinked fluid.

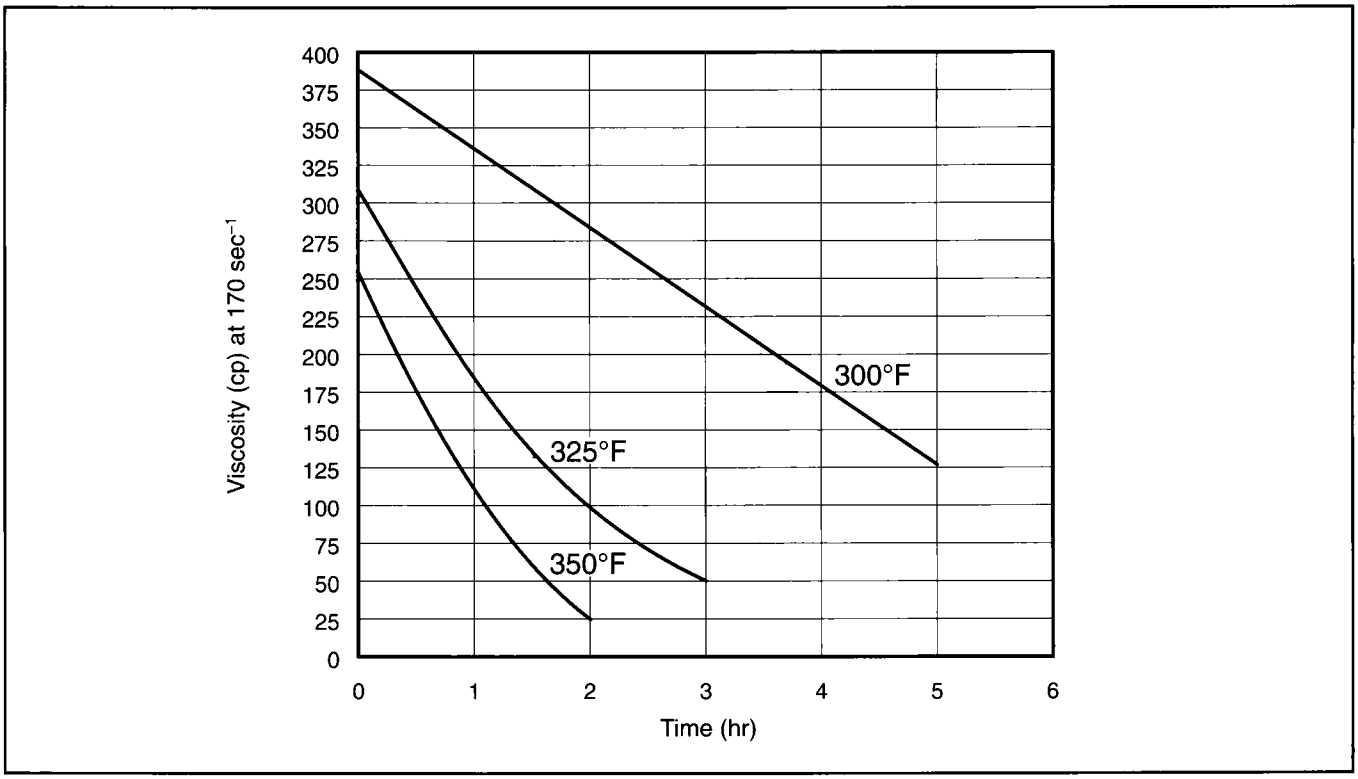

Figure P-19—Apparent viscosity at 170 sec^{-1} for 60 lb/1000 gal zirconate-crosslinked fluid.

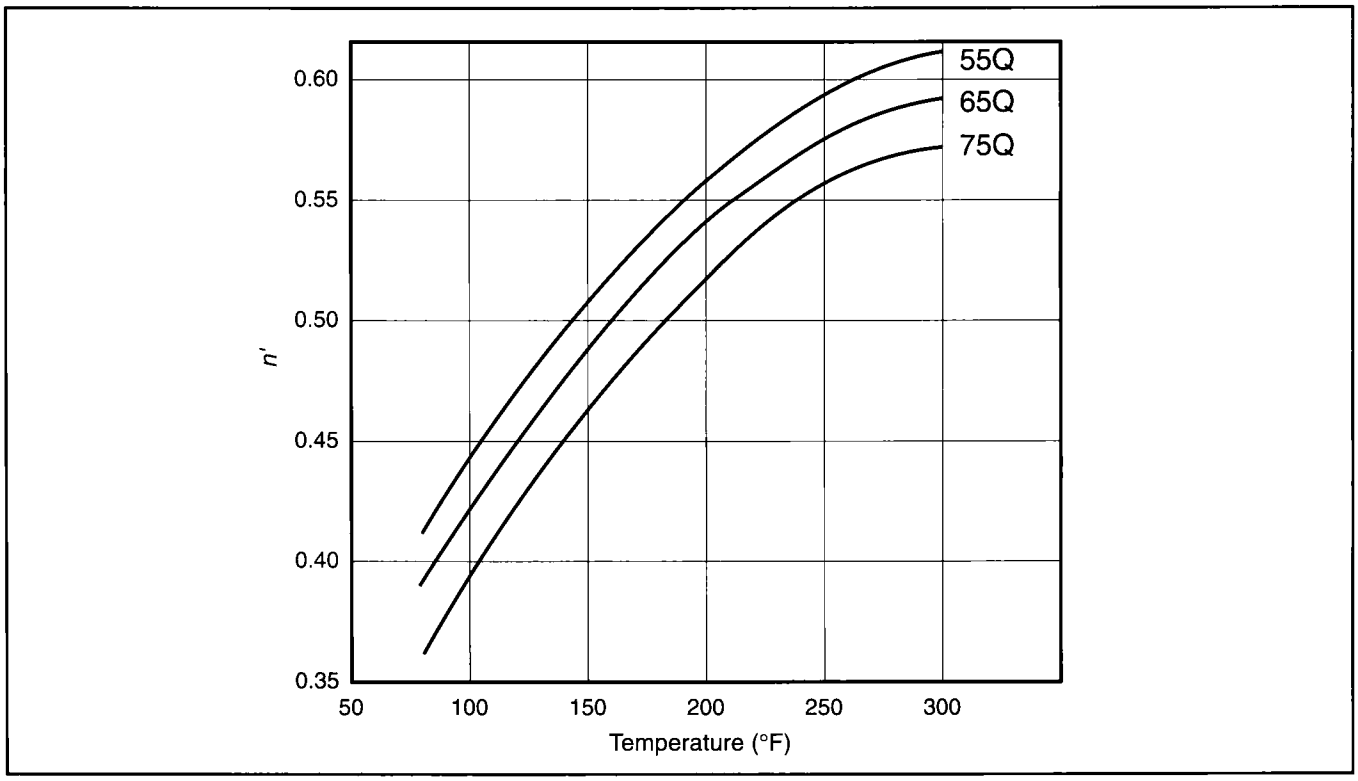

Figure P-20—*n'* for various quality foams with 30 lb/1000 gal polymer.

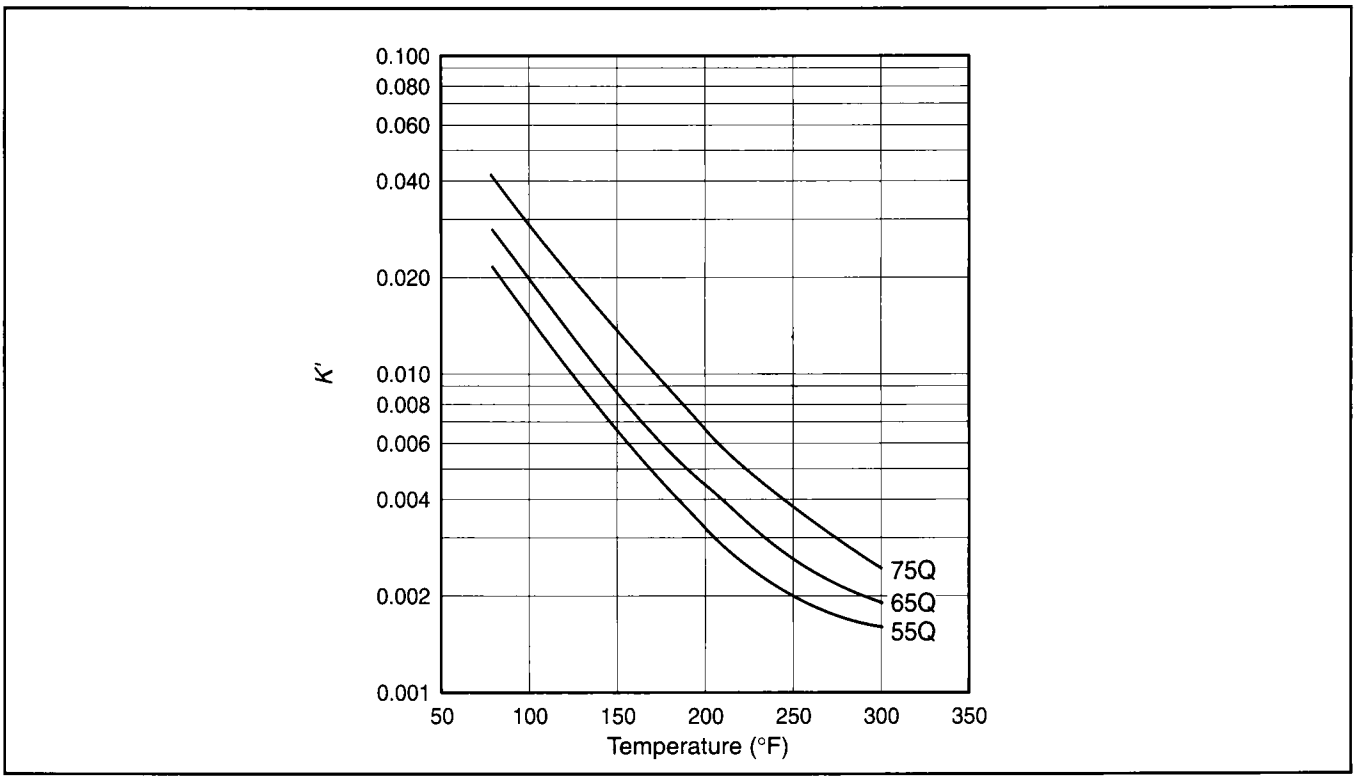

Figure P-21—K' for various quality foams with 30 lb/1000 gal polymer.

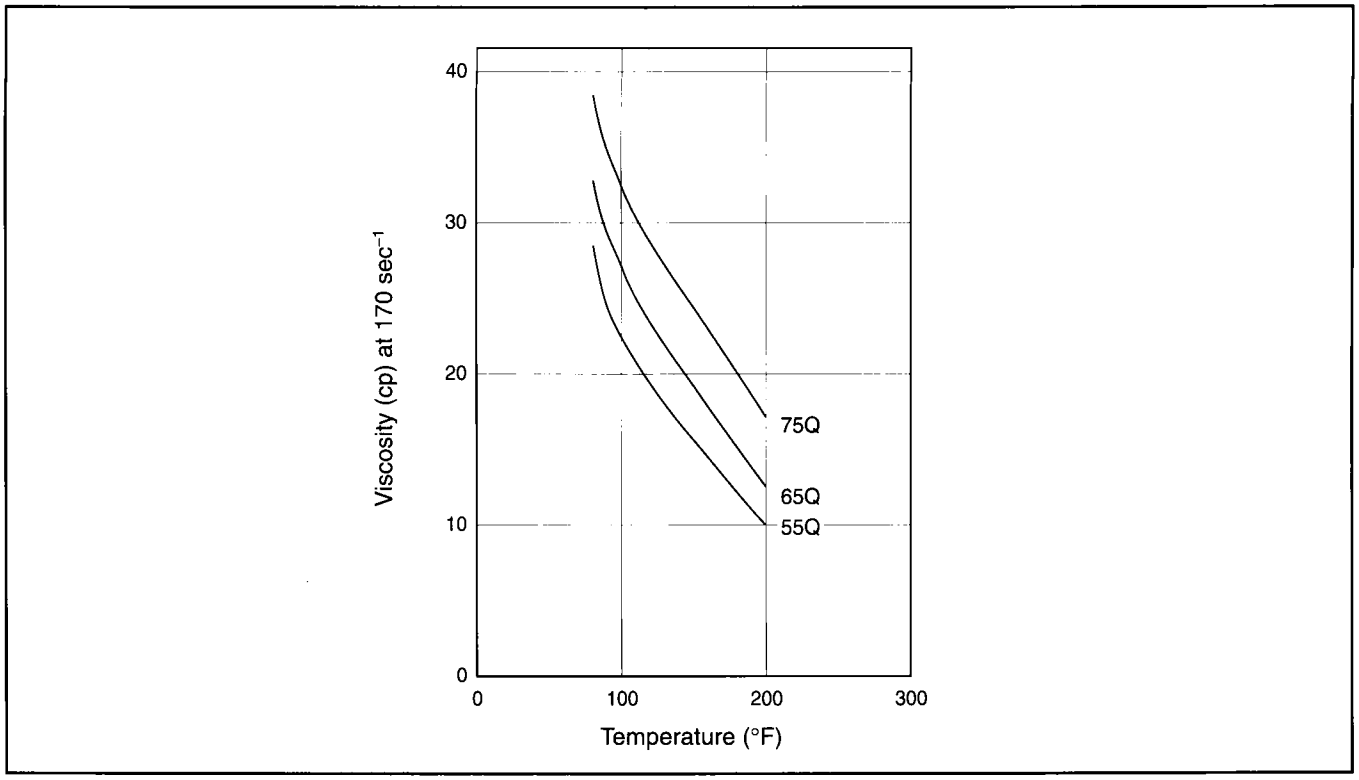

Figure P-22—Apparent viscosity of foams at 170 sec^{-1}.

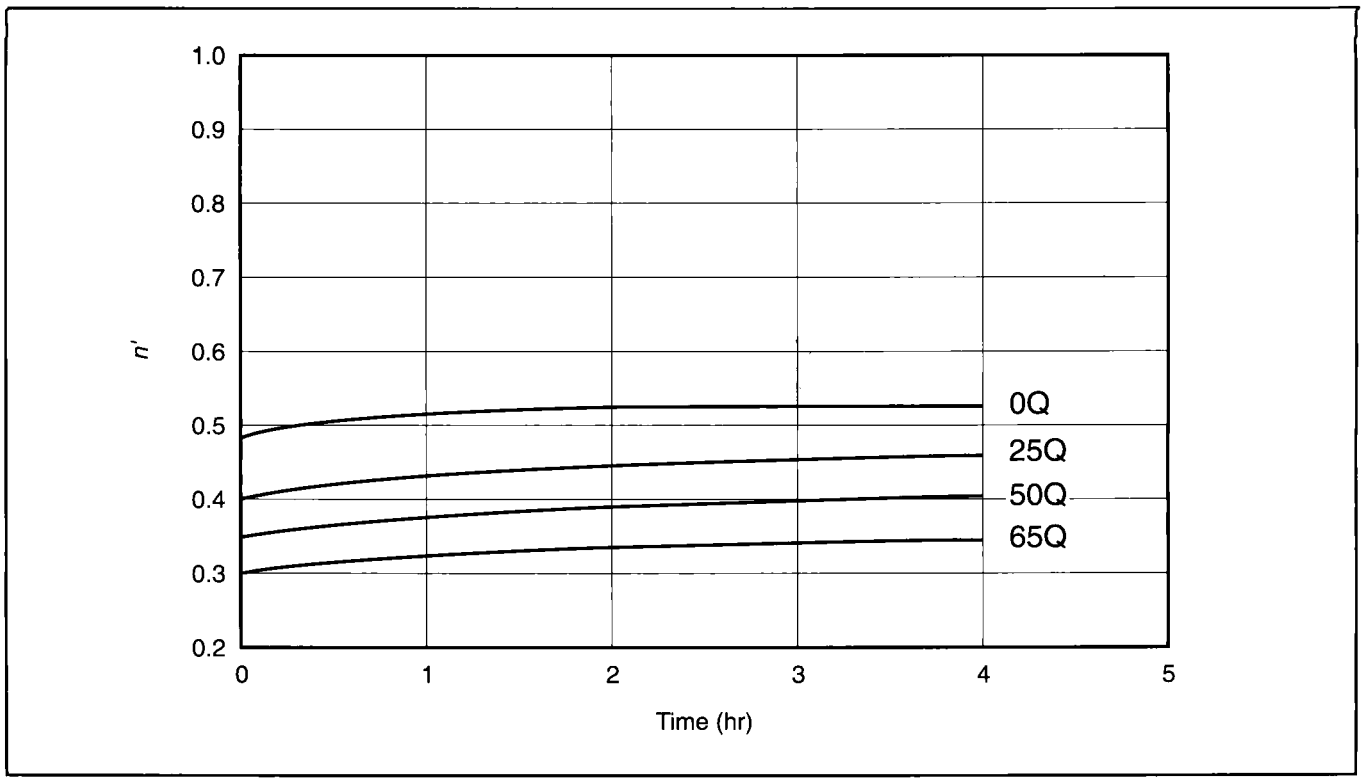

Figure P-23—*n'* for foams with crosslinked 40 lb/1000 gal fluid at 150°F.

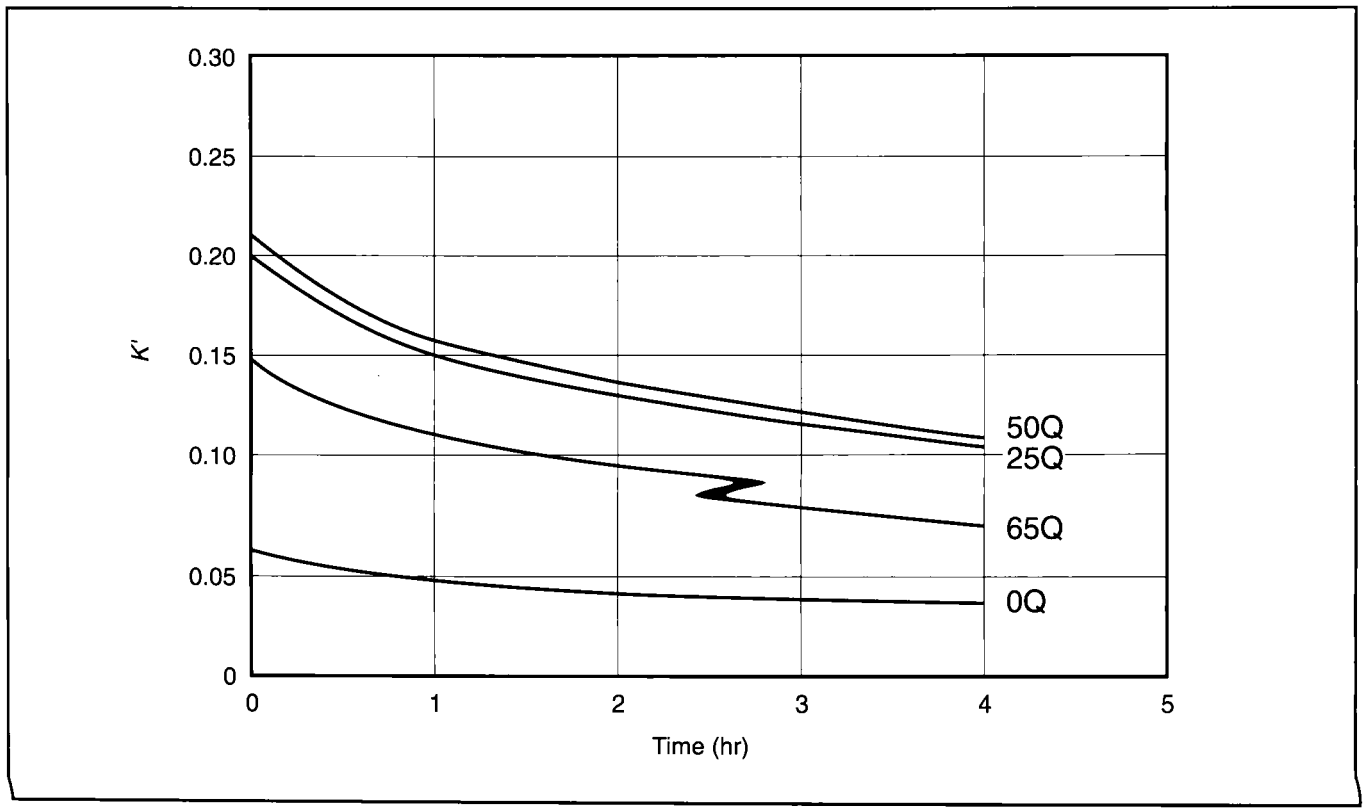

Figure P-24—*K'* for foams with crosslinked 40 lb/1000 gal fluid at 150°F.

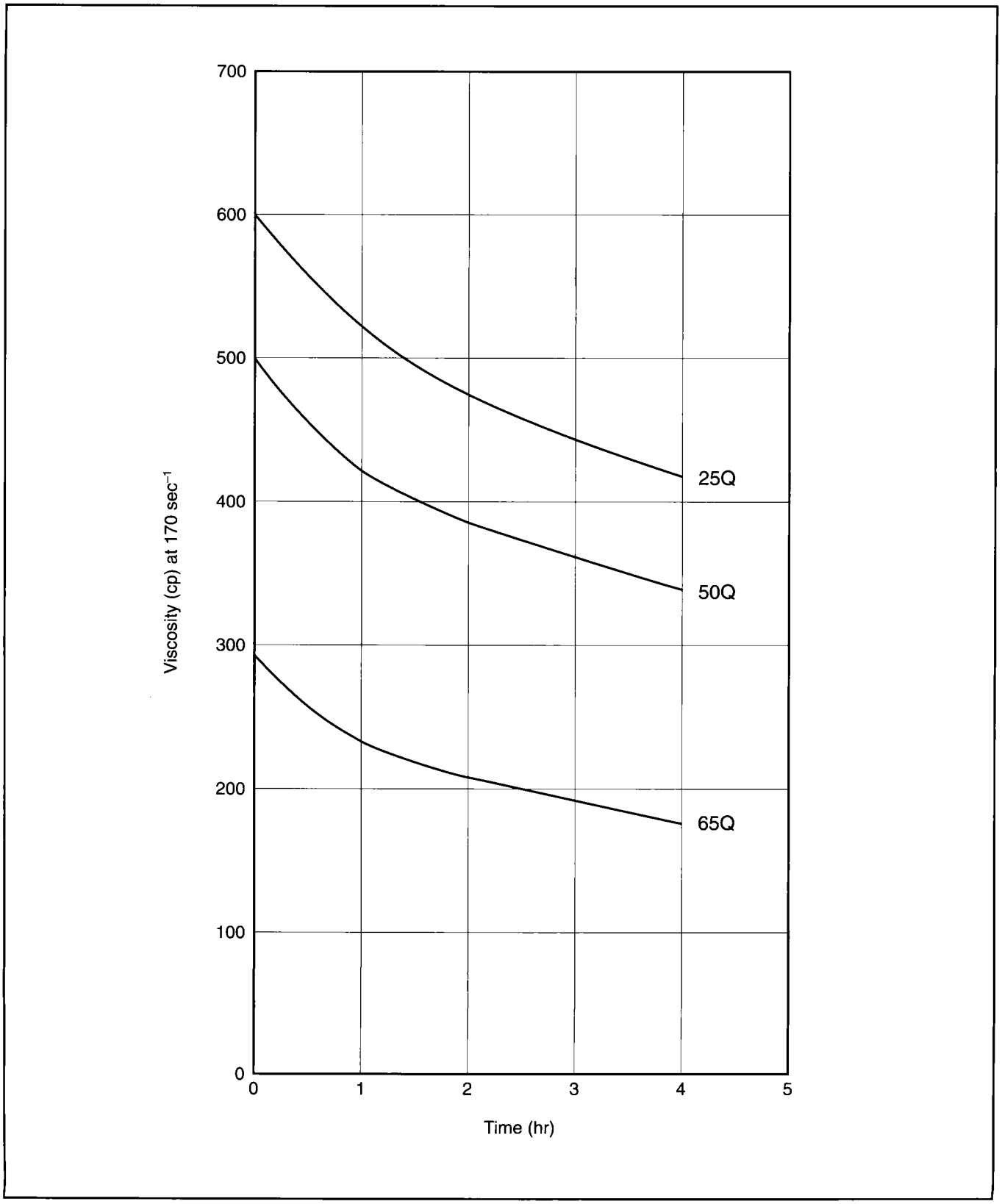

Figure P-25—Apparent viscosity for crosslinked 40 lb/1000 gal foams at 170 sec^{-1} and 150°F.

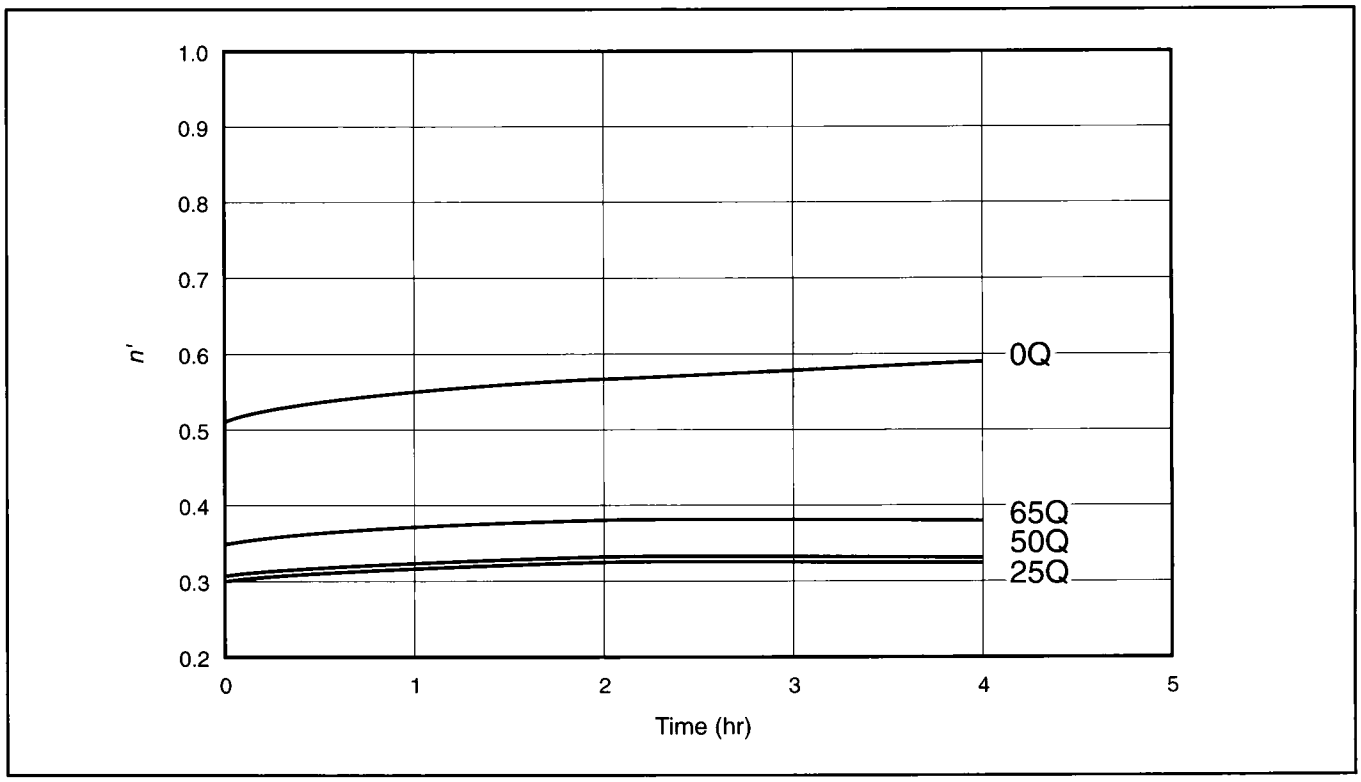

Figure P-26—*n'* for foams with crosslinked 40 lb/1000 gal fluid at 200°F.

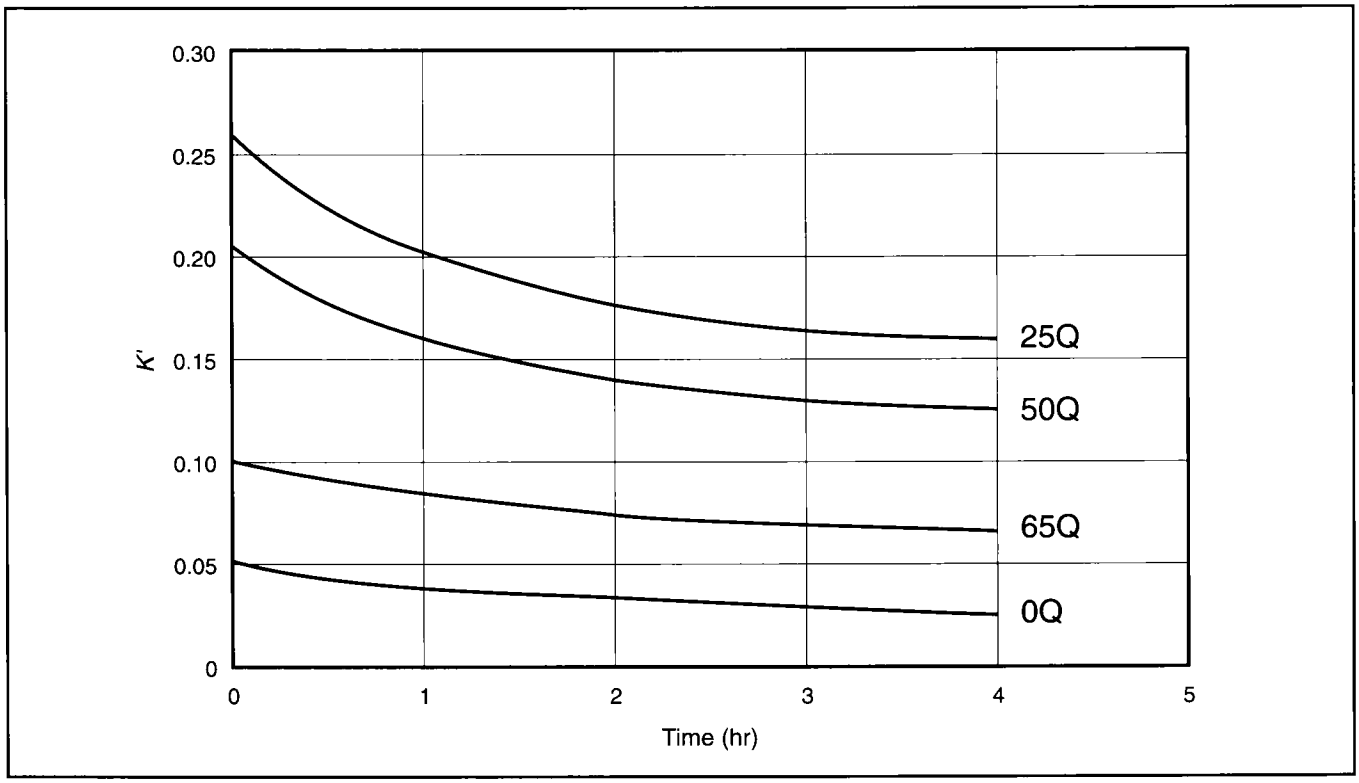

Figure P-27—*K'* for foams with crosslinked 40 lb/1000 gal fluid at 200°F.

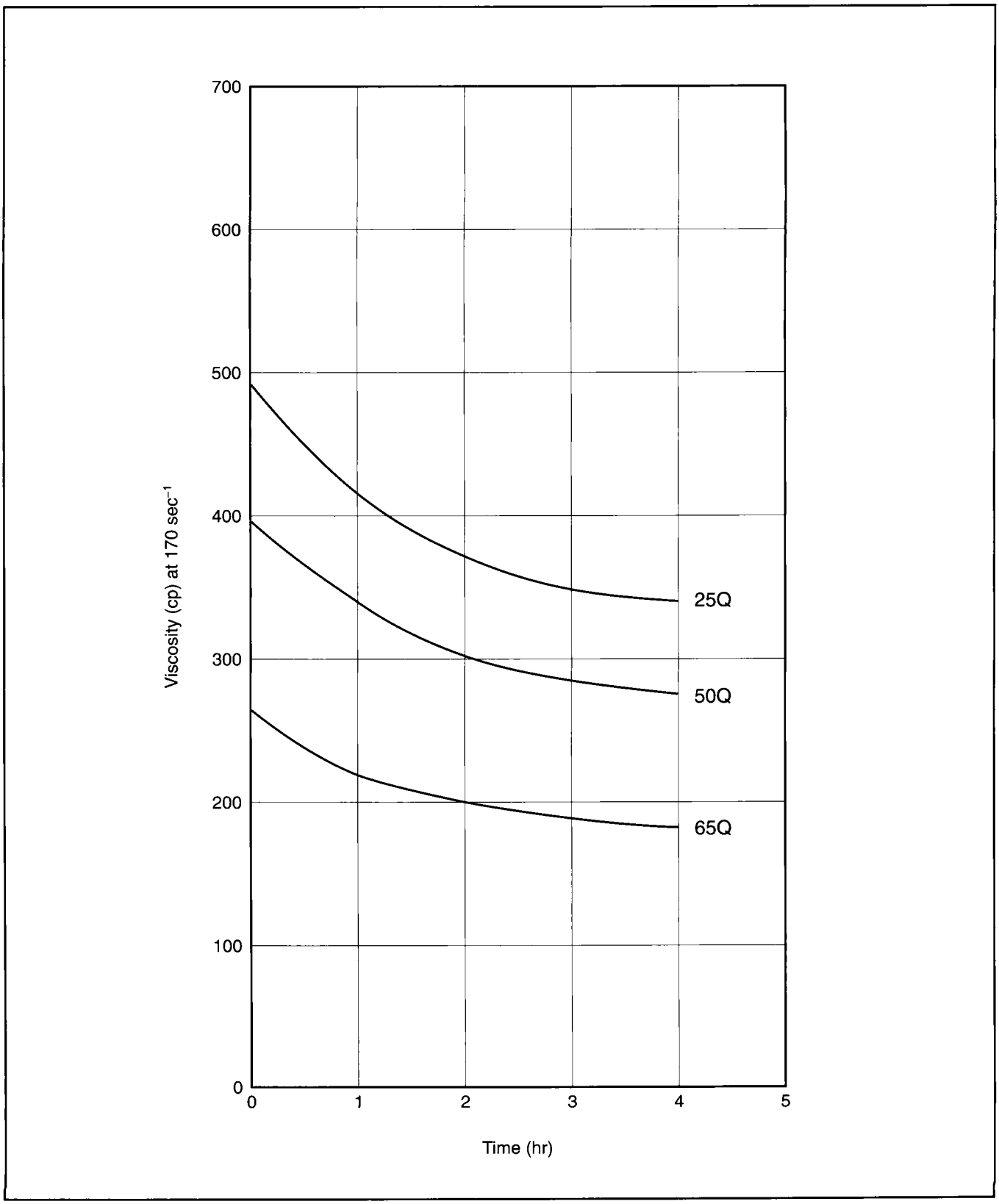

Figure P-28—Apparent viscosity for crosslinked 40 lb/1000 gal foams at 170 sec^{-1} and 200°F.

P-3.3: Friction Pressure Drop

The pumping of highly non-Newtonian viscoelastic fluids results in significant pressure drops through the treating tubulars. These pressure drops cannot be calculated readily through the classic Reynolds number/friction pressure drop methods. Thus, experimental data are necessary, especially in turbulent flow.

Figure P-29 provides the friction pressure for 30-lb borate-crosslinked fluid for various tubing sizes. The dashed lines are for completely delayed crosslinking, and the solid lines are for nondelayed polymers. The observed break in the curves corresponds to transition flow between laminar and turbulent flow.

For example, if 20 BPM are pumped down 2⅞-in. tubing, the friction pressure drop (Curve 2 in Fig. P-29) is equal to 320 psi/1000 ft. Figure P-30 contains the same data for 40-lb borate fluids.

To demonstrate the effect of the polymer load on friction pressure drop, the example above is repeated. At 20 BPM through 2⅞-in. tubing, the friction pressure drop is also 320 psi/1000 ft. Large differences will be observed at low flow rates in small-diameter tubings.

Figures P-31 through P-33 contain the friction pressure drop for 40-lb, 50-lb and 60-lb zirconates, respectively.

Figures P-34 through P-37 contain friction pressure drops for foams of various qualities in 2⅜-, 2⅞-, 4½- and 5½-in. tubings, respectively.

Friction pressure drops for foams are significantly larger than for crosslinked liquid fluids. For example, if 20 BPM of 70Q foam are pumped down 2⅞-in. tubing (Fig. P-35), the friction pressure drop would be 750 psi/1000 ft, which is significantly greater than the values for borate fluids.

Finally, Figs. P-38 and P-39 provide friction pressure drops for foams pumped down annuli.

It must be noted that the friction pressure drops for foams are only approximate; therefore, pumping down the annulus allows the direct measurement of pressure in the tubing by downhole measuring devices.

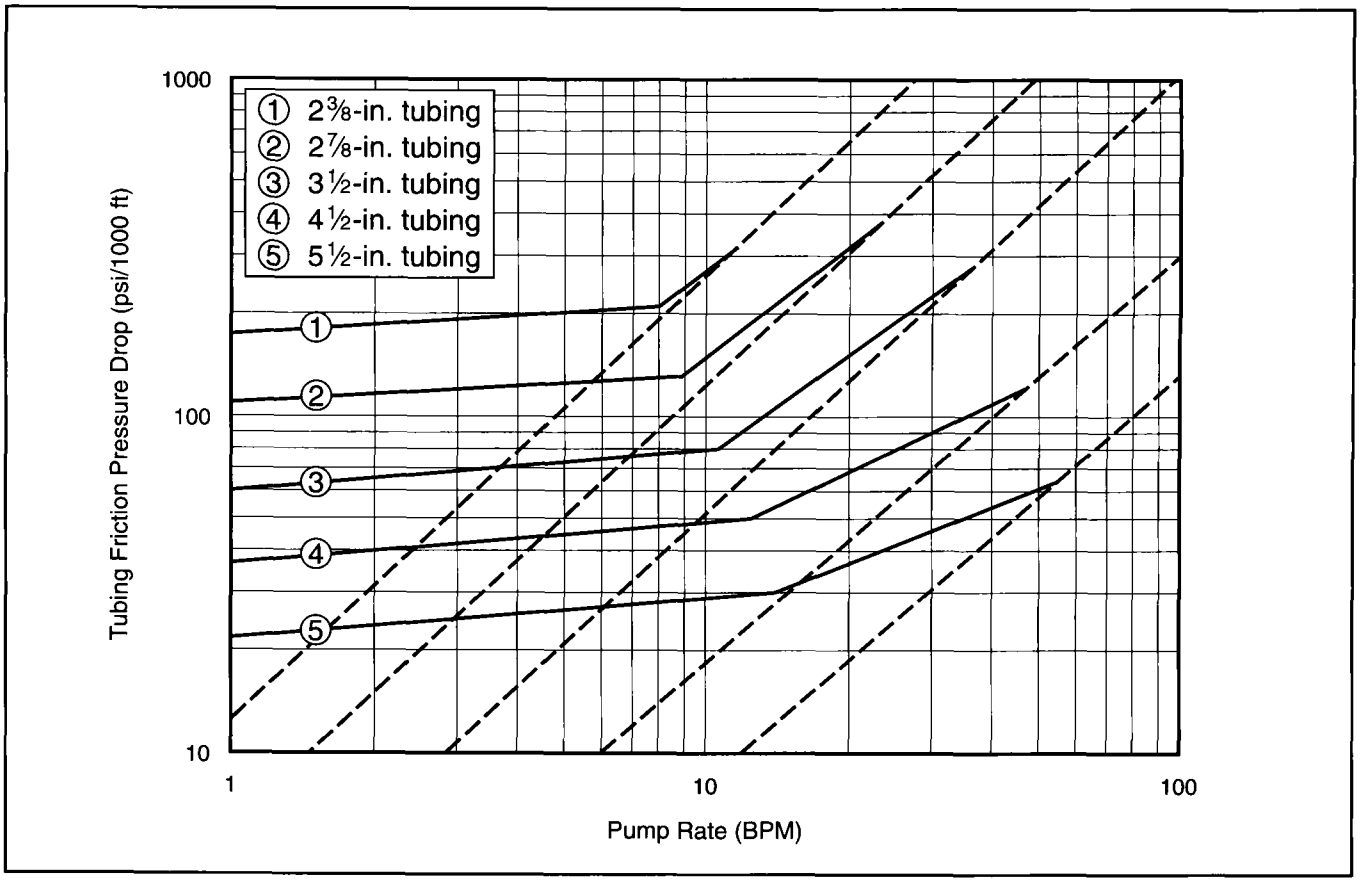

Figure P-29—Friction pressure drop in various tubing sizes for delayed (dashed lines) and nondelayed (solid lines) 30-lb borate fluids.

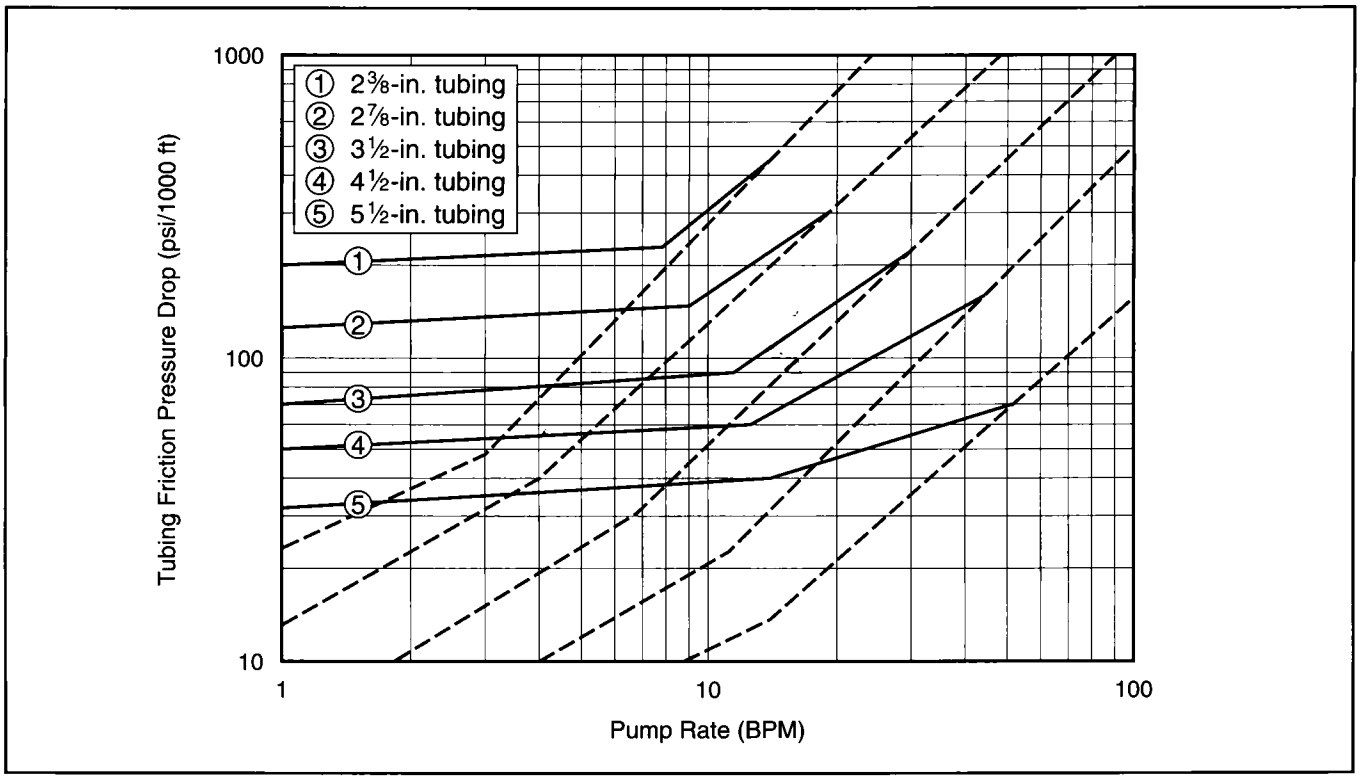

Figure P-30—Friction pressure drop in various tubing sizes for delayed (dashed lines) and nondelayed (solid lines) 40-lb borate fluids.

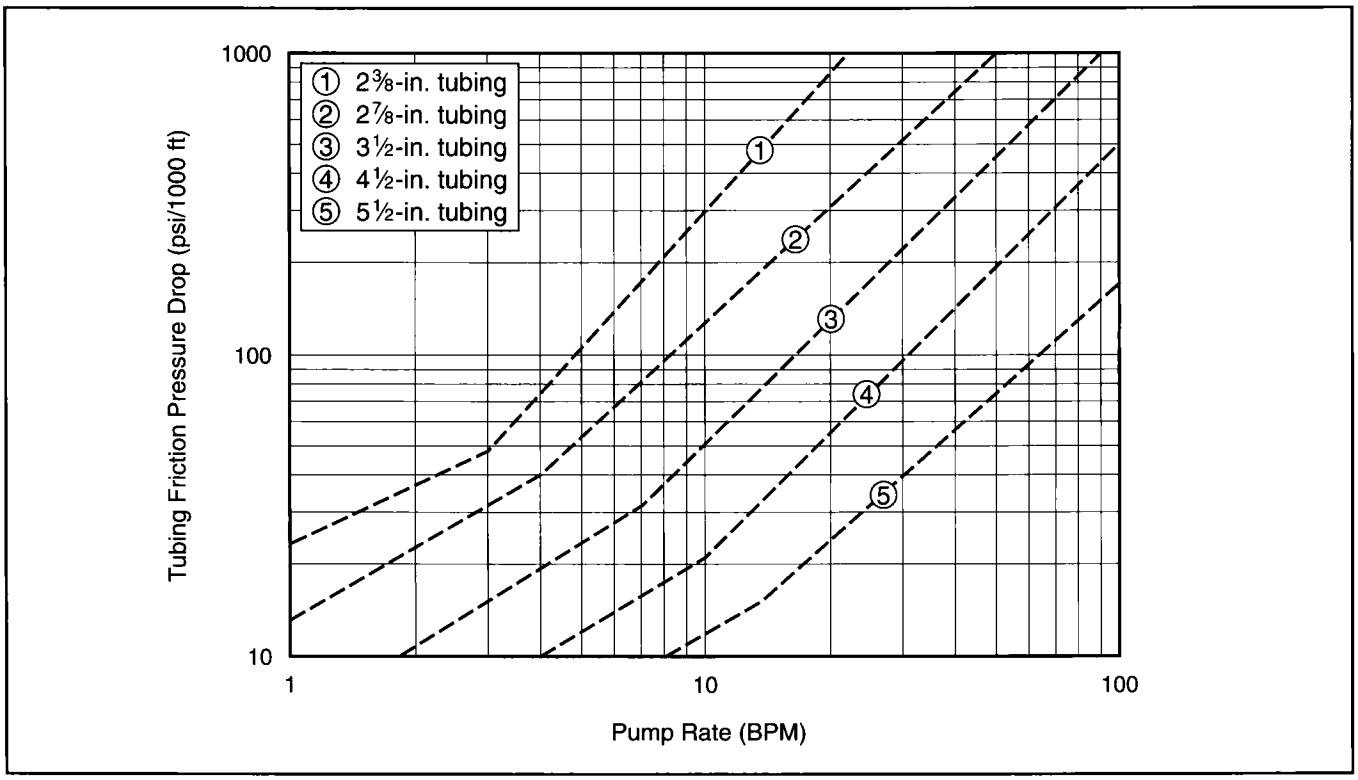

Figure P-31—Friction pressure drop for 40-lb zirconate fluids in various tubing sizes.

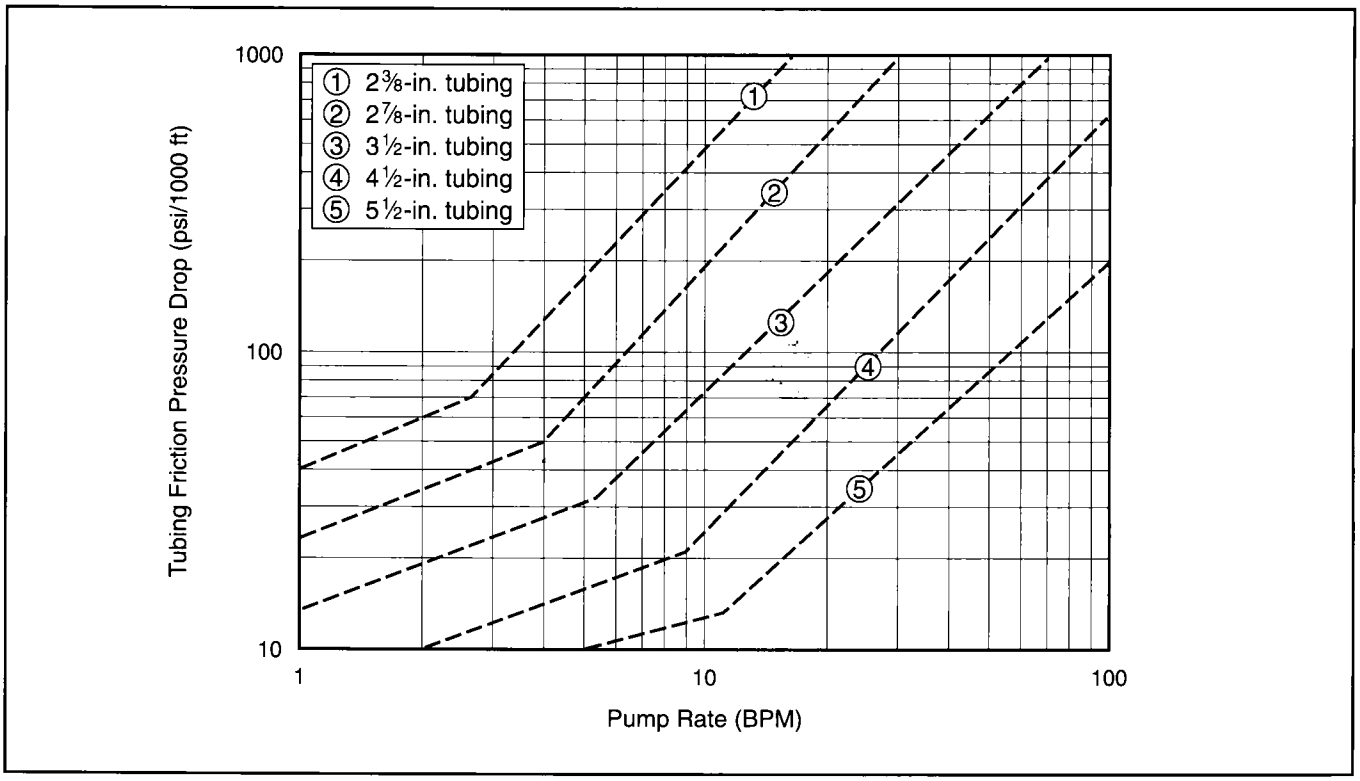

Figure P-32—Friction pressure drop for 50-lb zirconate fluids in various tubing sizes.

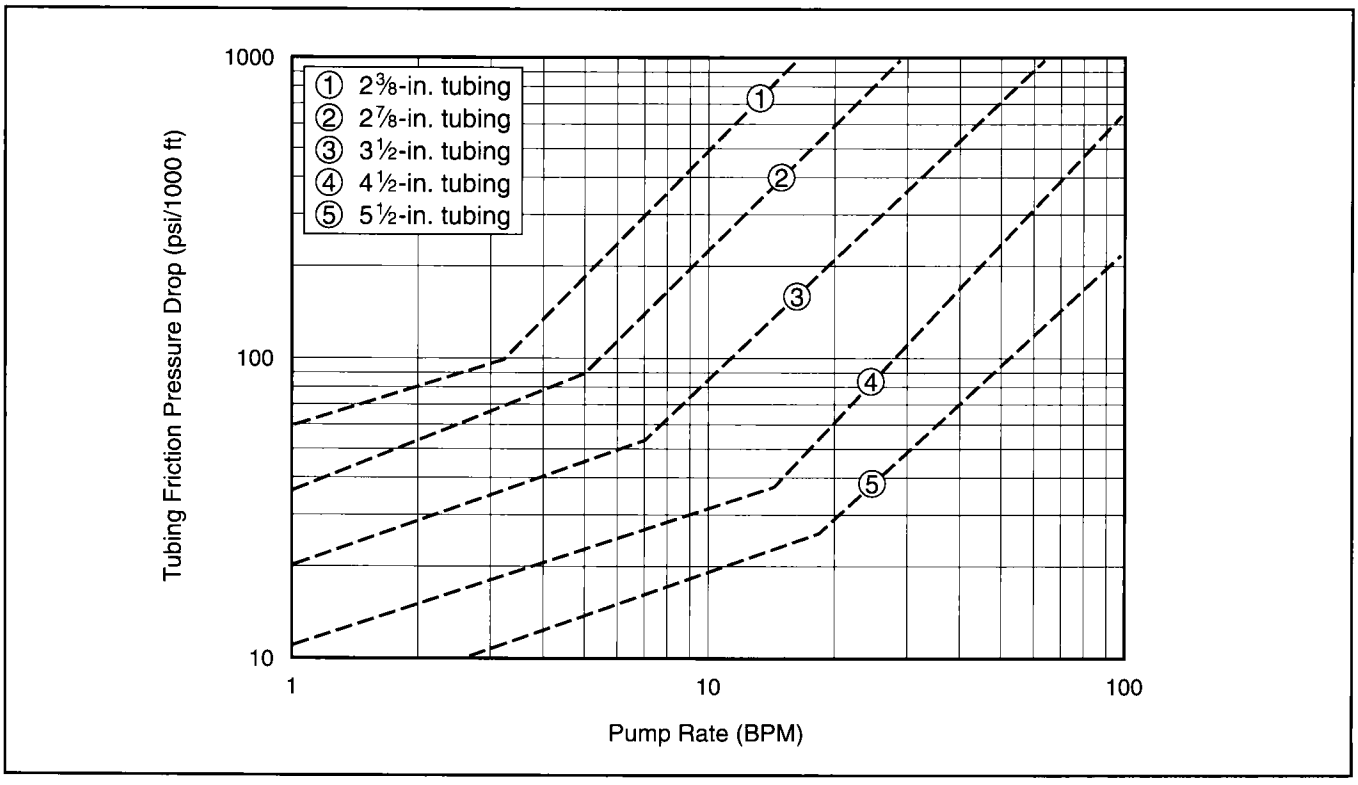

Figure P-33—Friction pressure drop for 60-lb zirconate fluids in various tubing sizes.

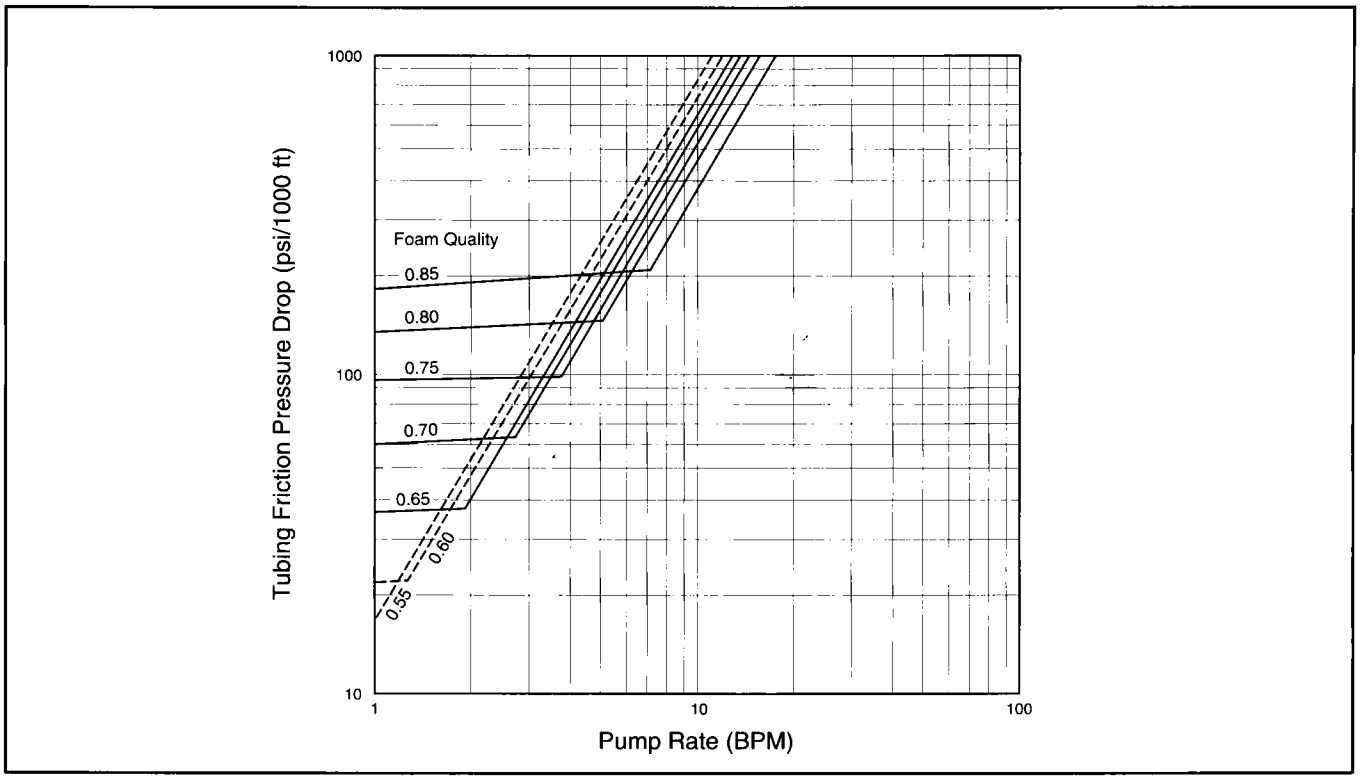

Figure P-34—Foam friction pressure drop in 2⅜-in. tubing.

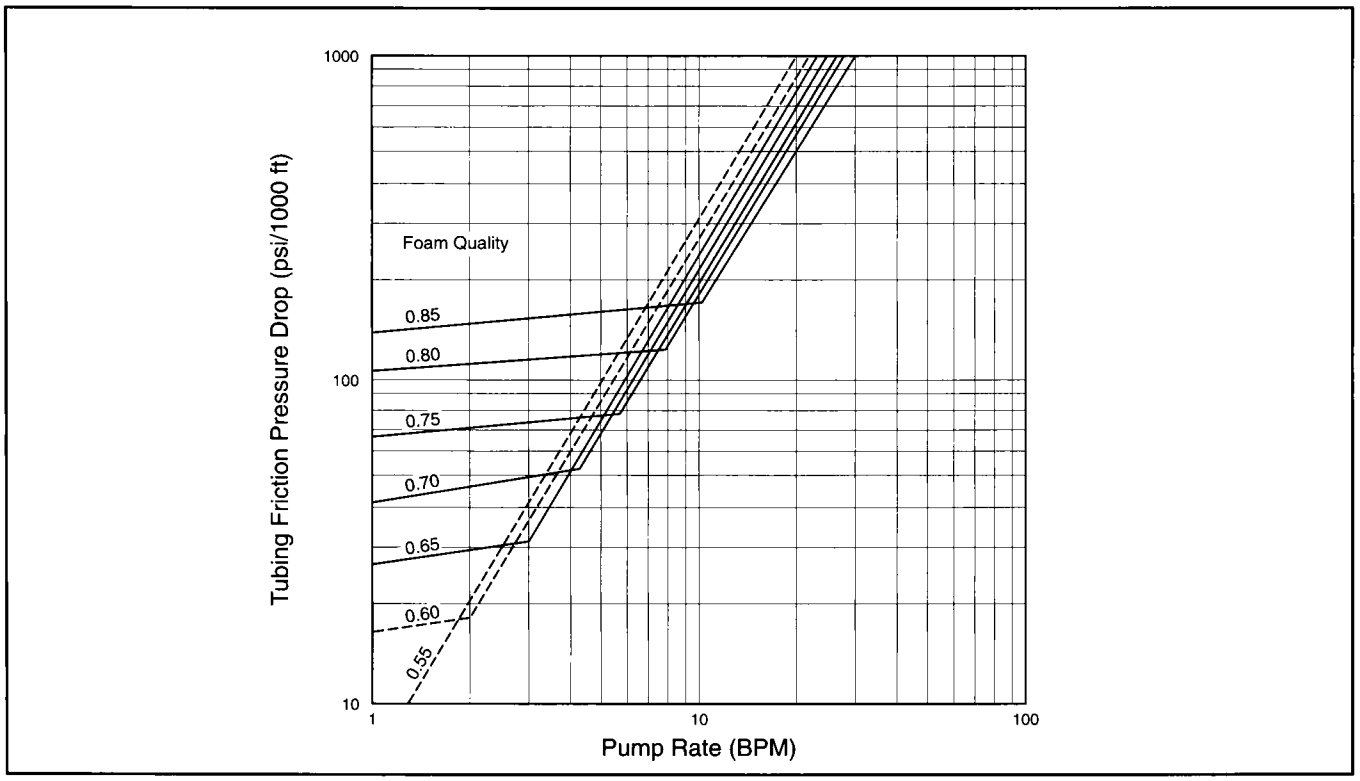

Figure P-35—Foam friction pressure drop in 2⅞-in. tubing.

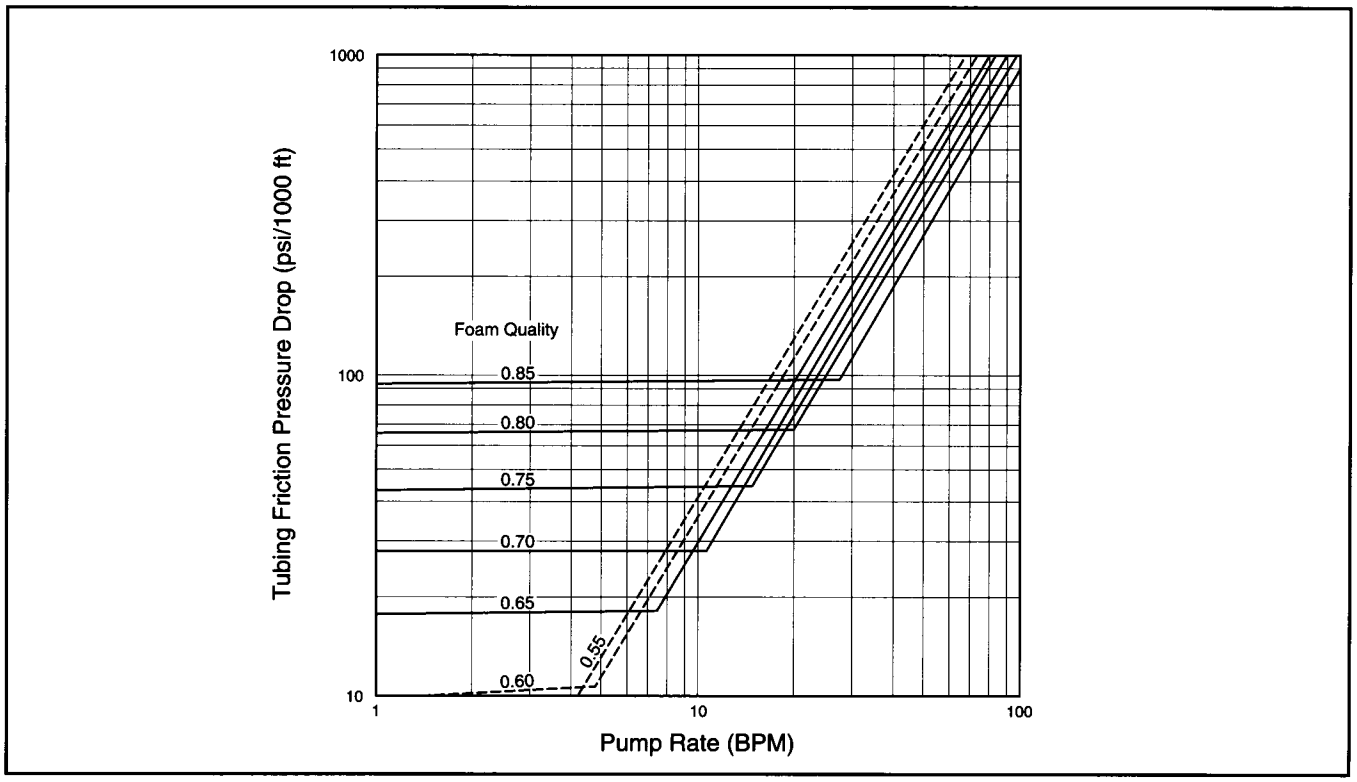

Figure P-36—Foam friction pressure drop in 4½-in. tubing.

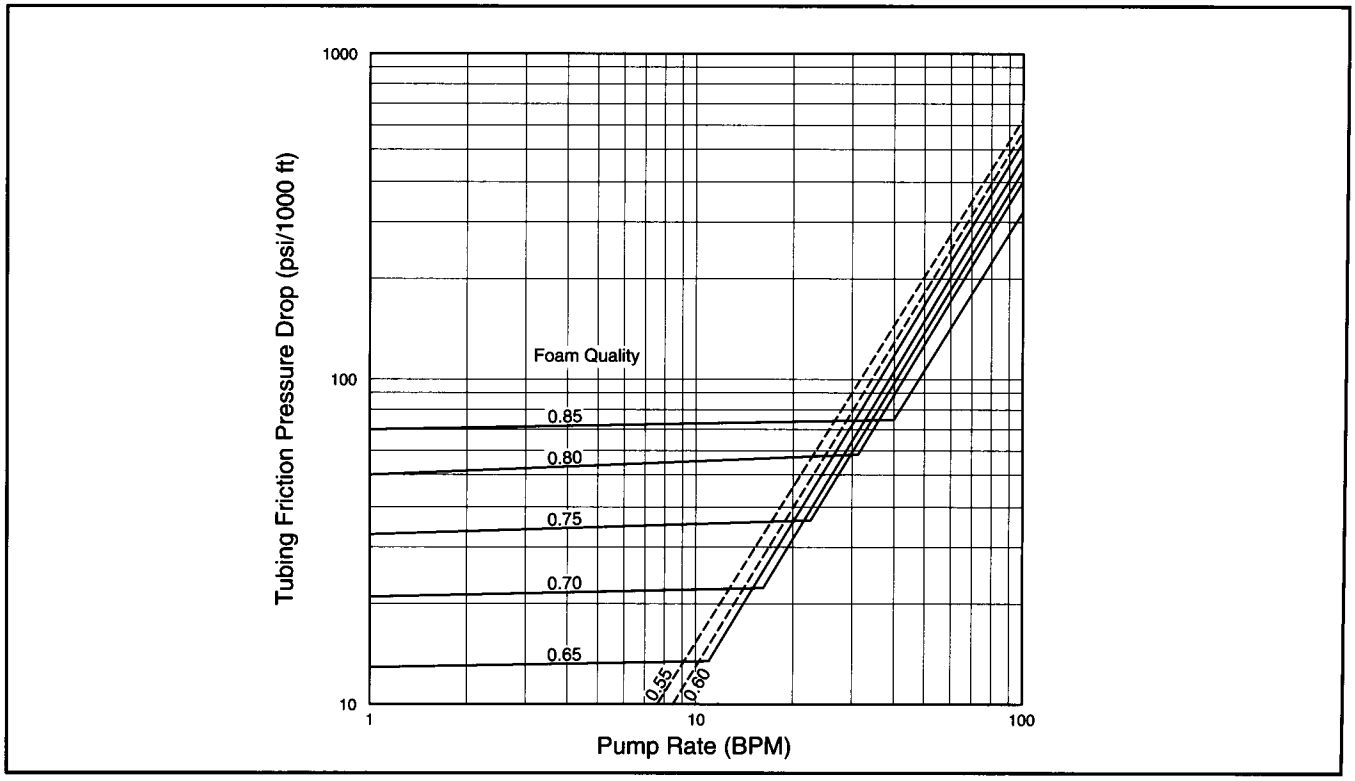

Figure P-37—Foam friction pressure drop in 5½-in. tubing.

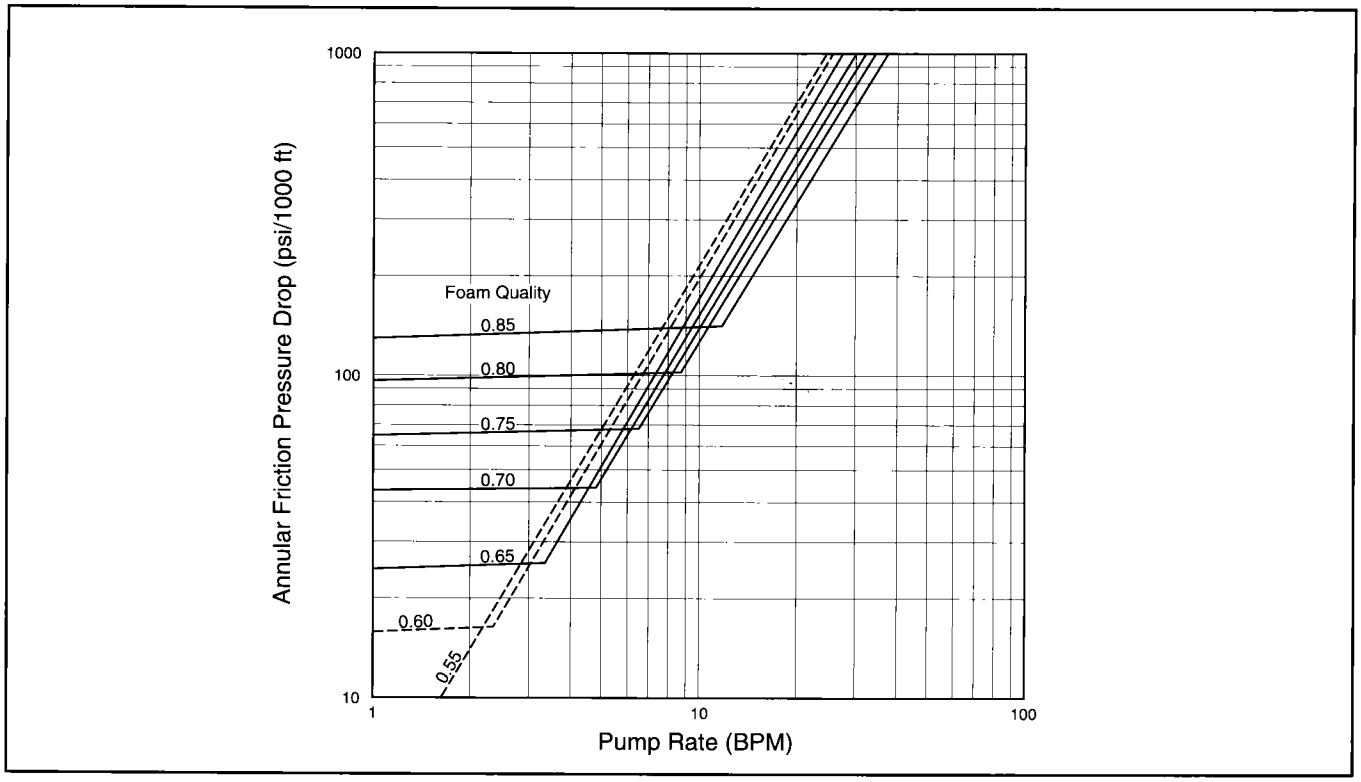

Figure P-38—Foam friction pressure drop in annulus of 4½-in. casing and 2⅜-in. tubing.

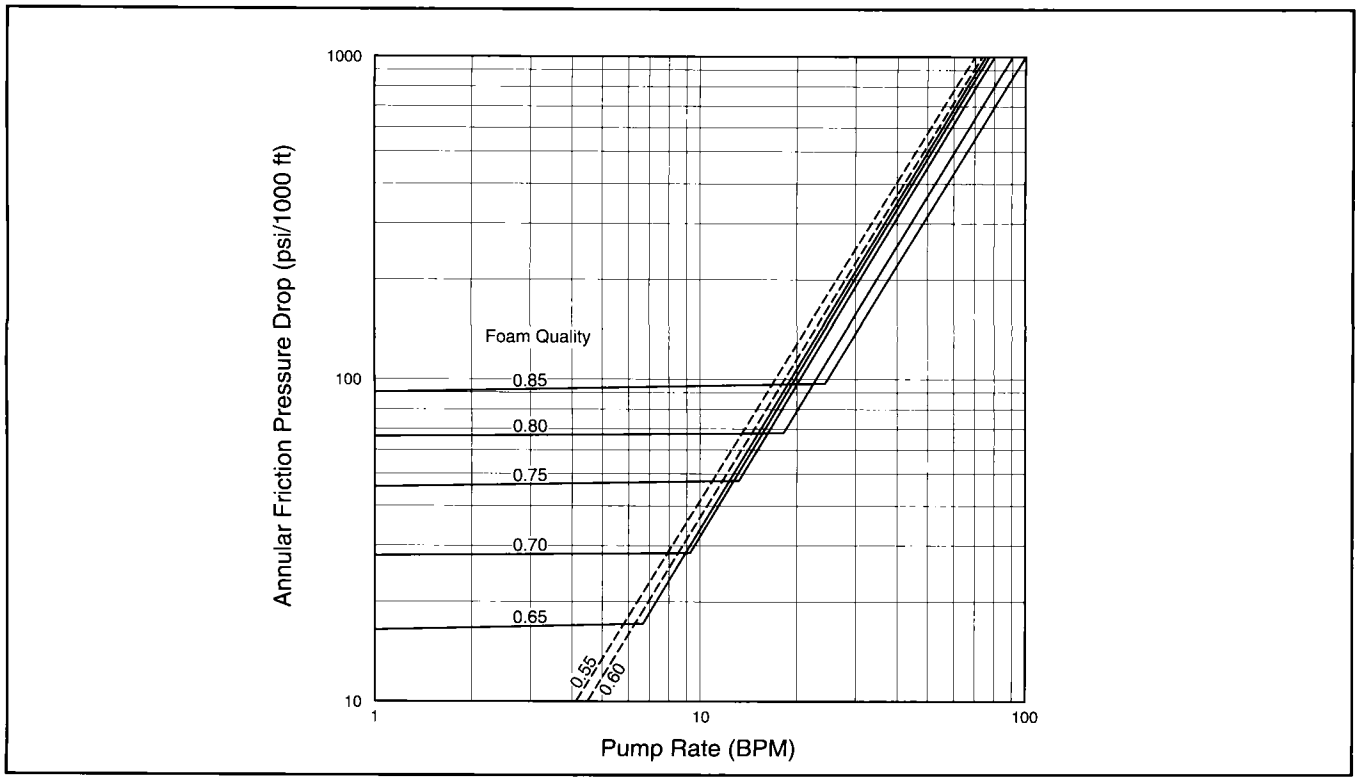

Figure P-39—Foam friction pressure drop in annulus of 5½-in. casing and 2⅜-in. tubing.

P-3.4: Conductivity Damage from Fracturing Fluids

Recent advances in testing the long-term conductivity characteristics of proppants have led to further investigations of the proppant-pack damage caused by various fracturing fluids. Conductivity tests similar to those described in Section P-2.2 are performed but with fracturing fluids used to place the proppant slurry into the test cell. The fluids are subsequently broken and allowed to clean up before permeability measurements are taken. Table P-5 shows a trend measured early, demonstrating that 1) the type of crosslinker used in a fracturing fluid can have major significance on its ability to clean up, and 2) higher polymer loadings damage conductivity more than lower polymer loadings. This second point is emphasized by the fact that foams of either N_2 or CO_2 clean up much better than standard water-base fracturing fluids. Table P-6 gives the results of similar tests performed at much lower temperatures. Even though the conductivity values vary slightly from the earlier tests, the relative damage caused by different crosslinkers remains the same. These data indicate that when a water-base fluid is used, borate-crosslinked fluids are best for wells with bottomhole temperatures of 200°F or less.

Type of Fluid	% Retained Permeability
70Q N_2 Foam (4000 psi, 175°F)	100
70Q CO_2 Foam (4000 psi, 175°F)	98
Gelled Oil (4000 psi, 175°F)	85
40-lb Guar + Borate (3000 psi, 150°F)	84
Emulsion (4000 psi, 175°F)	67
40-lb Guar + Titanate (3000 psi, 150°F)	55
40-lb HPG + Titanate (4000 psi, 175°F)	50
40-lb CMHPG + Aluminate (3000 psi, 150°F)	47

Table P-5—Proppant-pack permeability retention for various fracturing fluids, 2 lb/ft² proppant concentration (from STIMLAB, 1987).

Further work in this area has shown that polymer concentration and crosslinker type is even more important than polymer type when considering the effect of fracturing fluids on proppant conductivity. During the late 1970s, several investigators began to develop derivatives of base polymers in an attempt to make them "cleaner." Natural guars were derivitized with propylene oxide to create hydroxypropylguar (HPG). Later, HPG polymers were further derivitized to carboxymethylhydroxypropyl guar (CMHPG). However, the new testing procedures show little or no benefit in using these more costly polymers based on their proppant-pack permeability damage. Table P-7 shows virtually no conductivity difference between HPG and guar, yet Table P-5 shows a CMHPG fluid to be very damaging when crosslinked with an aluminate crosslinker.

Later studies indicate that fracturing fluid damage is even more significant than previous studies implied. The polymers used in fracturing fluids are far too large to enter the pore throats of most reservoir rocks and therefore become very concentrated as fluid leaks off and the fracture volume decreases during the closure period. The eventual concentration of the polymer far exceeds the mixing concentration of 40 to 60 lb/1000 gal. In many instances, the polymer concentration may be 10 to 15 times greater than the original polymer load. The effect of polymer concentration on retained permeability

Type of Fluid	Retained Permeability (%)	Proppant Permeability (darcies)	Conductivity (md-ft)
Borate-Crosslinked 30-lb HPG with Persulfate/Amine Breaker	95	227	2128
Borate-Crosslinked 40-lb HPG with Persulfate/Amine Breaker	88	212	1971
Borate-Crosslinked 40-lb HPG with Enzyme Breaker	68	162	1500
Titanate-Crosslinked 40-lb HPG (Low pH) with Enzyme Breaker	50	121	1115
Antimonate-Crosslinked 40-lb HPG (Low pH) with Enzyme Breaker	40	97	898
Titanate-Crosslinked 40-lb HPG (Neutral pH) with Enzyme Breaker	19	46	430

Table P-6—Long-term conductivity and permeability of 20/40 Jordan sand at 2000 psi closure stress, 100°F, and 1 lb/ft² as a function of placement fluid (from Thomas, R.L. and Brown, J.E., SPE paper 18862, 1989).

is shown in Fig. P-40. These tests confirm the earlier claims that guar is more damaging than HPG. However, the overall level of damage is significantly greater as polymer concentrations increase.

With a better understanding of fracturing fluid damage, it has become increasingly evident that higher breaker concentrations are necessary to overcome polymer damage. In the past, breaker concentrations have been determined based on the base polymer loading of the fracturing fluid. Since the base polymer loading is concentrated severalfold, conventional breaker concentrations are generally ineffective in minimizing polymer damage (Fig. P-41).

Type of Fluid	Retained Permeability (%)	Conductivity (md-ft)
30-lb Guar + Borate	100	2200
40-lb Guar + Borate	89	1950
30-lb HPG + Borate	95	2100
40-lb HPG + Borate	89	1950

Table P-7—Impact of base fluid on proppant-pack permeability, 1 lb/ft² (from Wine, J.D. et al., SPE paper 18969, 1989).

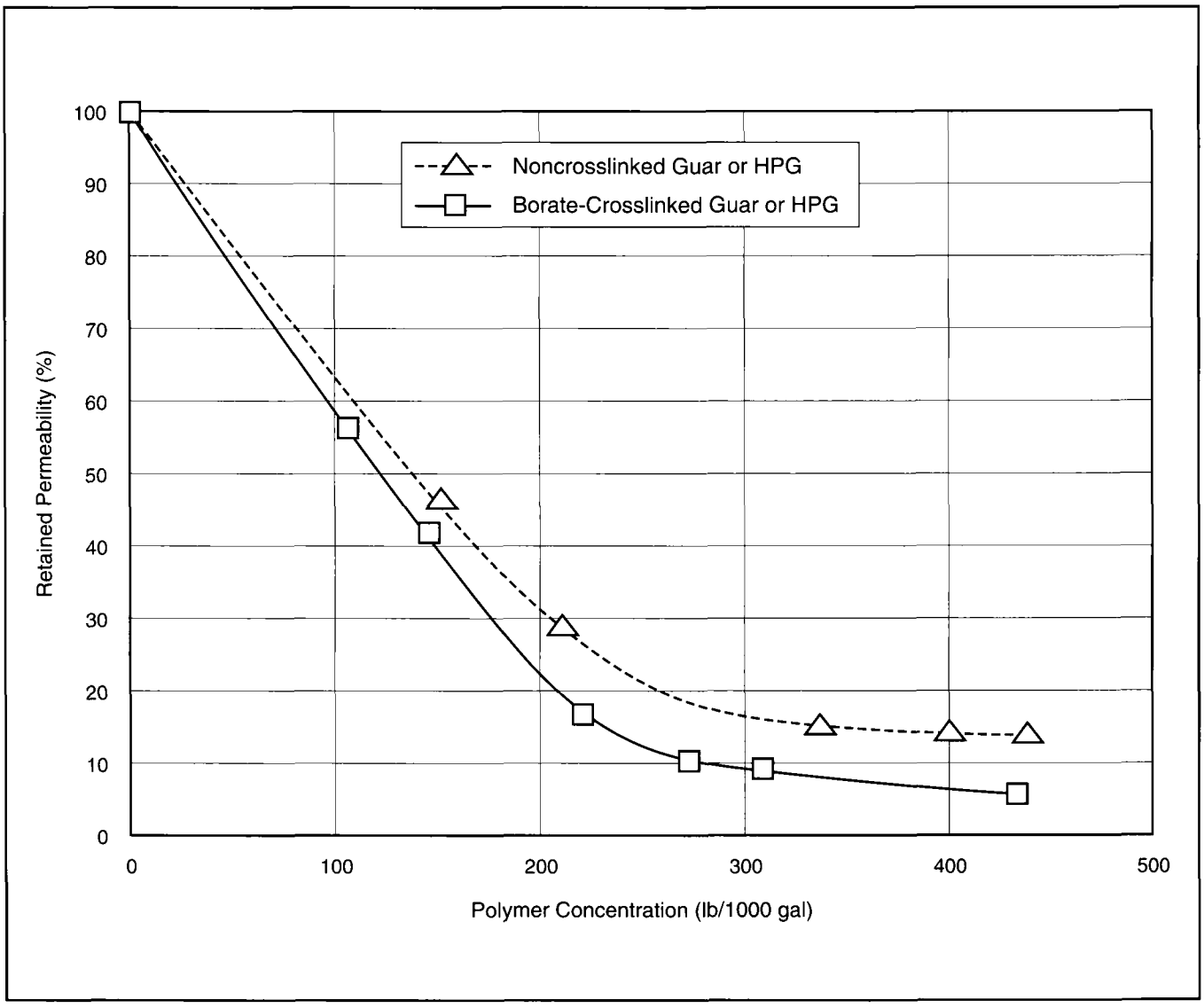

Figure P-40—Effect of polymer load on retained permeability of 20/40 northern white sand, 2 lb/ft², 160°F (from Brannon, H.D. and Pulsinelli, R.J., SPE paper 20135, 1990).

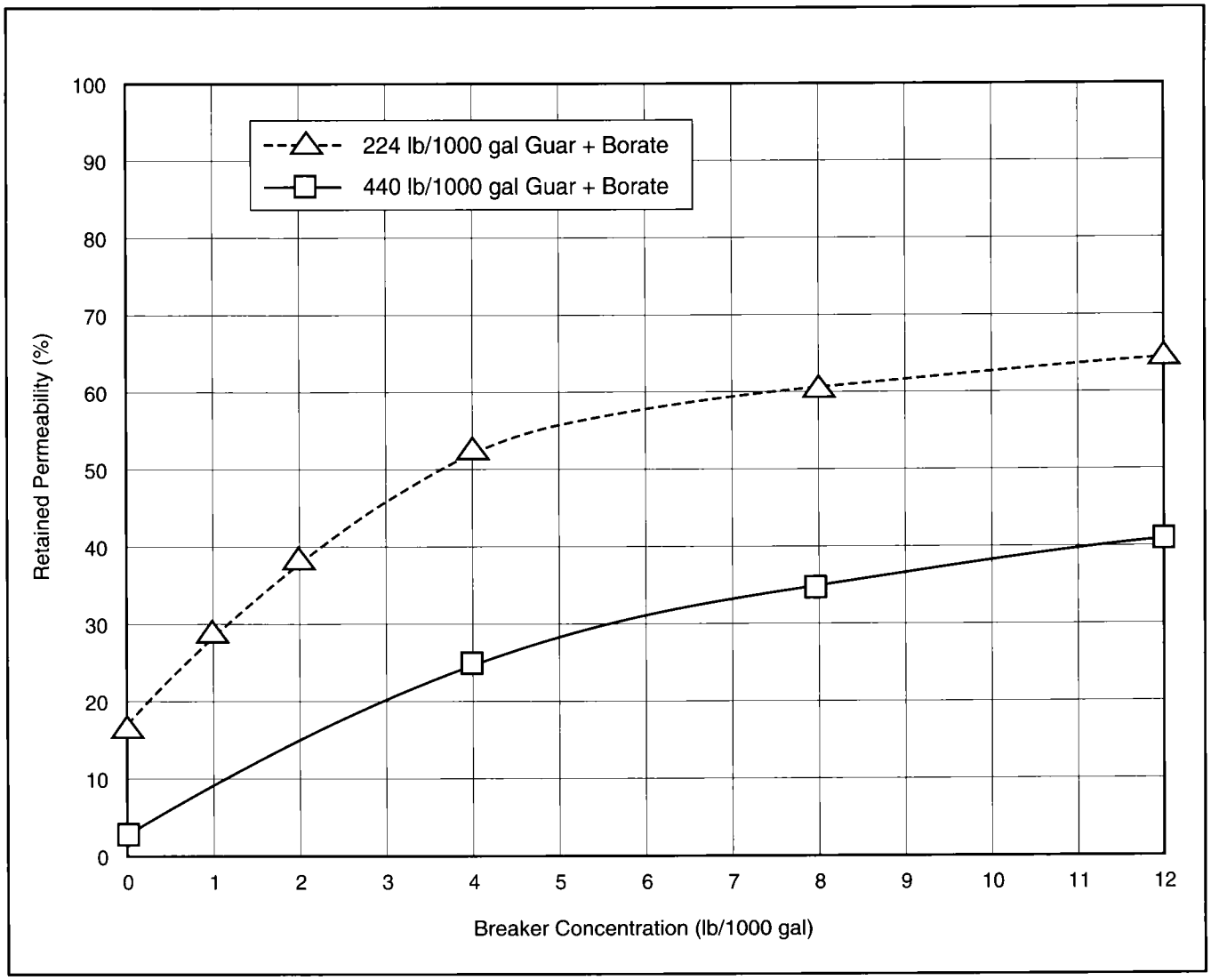

Figure P-41—Effect of breaker concentration on retained permeability of 20/40 northern white sand, 2 lb/ft^2, 160°F (from Brannon, H.D. and Pulsinelli, R.J., SPE paper 20135, 1990).

P-3.5: Viscosity Reduction from Breakers

Breakers are added to fracturing fluids for two reasons. First, the viscosity of the fluid must be reduced so that the fluid can be cleaned up quickly following a treatment. Second, as demonstrated in Section P-3.4, the breaker should also degrade the fluid and thus reduce proppant-conductivity damage. All common breakers perform both these tasks by attacking the backbone of the polymer and reducing its size. As the molecular weight of the polymers decreases, so does the fluid's viscosity.

Several systems are currently used to break water-base fracturing fluids. Table P-8 shows the concentration of conventional breaker systems needed to break linear fluids when the well can be shut in for 24 hr. Enzyme breakers can be effective over a relatively wide temperature range (70°F to 150°F) but are limited to a pH range between 3.5 and 8. The optimum pH for most enzyme breakers is 5. Oxidizing breakers are used in applications where the fluid is exposed to bottomhole temperatures between 125°F and 225°F. These breakers can be expanded into lower temperature applications (60°F to 125°F) if an amine is concurrently added to catalyze the reaction. These breakers are effective over a wide pH range (3 to 14) and demonstrate superior breaking properties based on observed proppant-permeability reduction. This is especially true when the oxidative breaker reaction is catalyzed by the amine (see Fig. P-42).

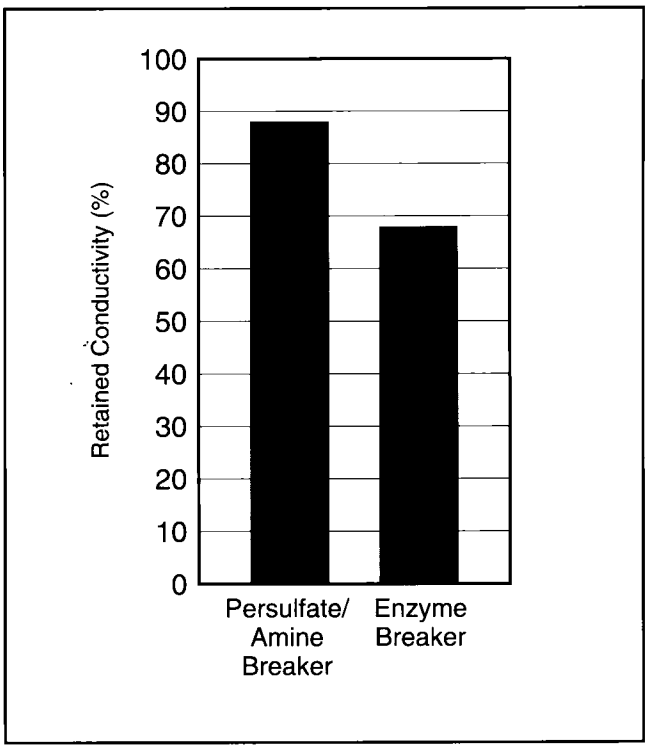

Figure P-42—Retained conductivity of a 40 lb/1000 gal borate-crosslinked fluid with two types of breakers (from STIMLAB, 1988).

Temperature	20 lb/1000 gal		40 lb/1000 gal		60 lb/1000 gal		80 lb/1000 gal	
(°F)	E*	O**	E	O	E	O	E	O
60	0.4		0.7		1.2		3.0	
80	0.1		0.2		0.4		1.0	
100	0.06		0.1		0.25		0.5	
120	0.06		0.1		0.175		0.3	
130	0.06	0.25		0.5	0.175	0.8	0.25	1.0
140	0.06	0.175	0.1	0.375	0.15	0.375	0.2	0.55
160	0.06	0.08	0.1	0.2	0.15	0.375	0.2	0.55
180		0.075		0.15		0.275		0.425
200		0.075		0.15		0.2		0.3

* E = enzyme
** O = oxidizer

Table P-8—Breaker concentrations (lb/1000 gal of fluid) for breaking a linear fluid in 24 hr. Data applicable for guar, HPG, HEC, CMC and CMHEC for the polymer loadings shown (from Gidley et al., *Recent Advances in Hydraulic Fracturing,* SPE Monograph Vol. 12, 1990).

Controlling the timing of the breaking process is critical to the success of the treatment. Once a breaker is added to a fracturing fluid, the degradation process immediately begins. Careful planning must go into the design of breaker schedules. If too much breaker is added early in the treatment, the viscosity required for fluid loss control and proppant transport may be prematurely lost, resulting in a screenout. If the breaker schedule is not ambitious enough, the molecular chains may not degrade sufficiently, causing the treatment to clean up slowly. Even worse, the fluid may not completely degrade without sufficient breaker quantities, limiting well production because of proppant-conductivity damage. This is particularly true at high polymer concentrations. As the polymer concentration increases, higher breaker concentrations must be maintained to sufficiently degrade the polymer and prevent proppant-permeability damage. It is now recognized that the in-situ polymer concentration in the fracture may increase more than tenfold (concentrations greater than 500 lb/1000 gal) because of fluid loss. The breaker level in this concentrated fracturing fluid decreases as the polymer concentration increases. The breaker is dissolved into the water portion of the slurry and is lost in the fluid leaking off as the fracturing fluid dehydrates. This can result in a damage to the proppant pack, which may exceed 90%.

Tapered breaker schedules allow much greater quantities of breaker to be added to the fluid while minimizing the risk of excessive degradation. To design the breaker schedule, the time of exposure to bottomhole temperature for each stage of the fracture treatment must be determined. From this, a maximum quantity of breaker can be calculated without risking premature loss of viscosity. This can best be demonstrated through the following example: Table P-9 gives viscosity data for a borate fracturing fluid with breaker included. The table shows how time, temperature and breaker concentration contribute to the viscosity degradation of a fluid. The temperature of the fracturing fluid along the fracture will vary significantly as a result of cool-down effects. Figure P-43 can be used to estimate the temperature of a fracturing fluid relative to its dimensionless position along the fracture, based on fluid efficiency. Time- and temperature-dependent viscosity values can then be applied to develop a breaker schedule that maximizes the amount of breaker used while never allowing the fracturing fluid to degrade below the critical viscosity of 100 cp 170 sec^{-1}. Table P-10 gives a hypothetical treatment schedule using a 40-lb borate-crosslinked fracturing fluid. The tapered breaker schedule was calculated based on a fluid surface temperature of 80°F and a bottomhole temperature of 150°F. The pad fluid will be exposed to bottomhole temperature for more than 1 hr so only a minimal amount of breaker can be added. The last proppant stage is exposed to bottomhole temperatures for less than 10 min, allowing the breaker concentration to be very aggressive for this one stage.

Breakers for oil-base gels operate much differently than their water-base counterparts. Most gelled oil breakers are slowly dissolving bases, such as lime or bicarbonate, and they are intended to reverse the crosslinking reaction. These systems work quite well at temperatures above 150°F, but large quantities of breaker are required at lower temperatures. The low-temperature break mechanism is not precise and is often expensive because of the quantity of breaker needed. Amine systems can also be used in gelled oil systems to aid in the break process at low temperatures.

Ideally, a breaker would not become active until after the treatment has finished and the formation has closed on the proppant. The ideal breaker would then completely degrade the polymer in a very short period of time, and the fracturing fluid could be produced back. Recent advances in encapsulation technology have allowed the development of breakers that perform in a similar manner. Even though the current techniques are not perfected, they do allow significantly higher concentrations of oxidative breaker to be placed into fracturing fluids without sacrificing viscosity (see Fig. P-44). These breakers also have the advantage of remaining with the polymer inside the fracture. Once encapsulated, the breaker is large enough that it will not be lost during fluid leakoff.

Temperature (°F)	Oxidative Breaker (lb/1000 gal)	Amine Catalyst (lb/1000 gal)	Time (hr)	Viscosity at 170 sec^{-1} (cp)
80	12.0	2.0	0.0 0.5 1.0 2.0 3.0 4.0 5.0 6.0	547 565 591 518 301 209 127 28
100	2.0	0.5	0.0 1.0 3.0 6.0	575 732 832 704
100	4.0	2.0	0.0 1.0 3.0 4.0	400 504 333 306
100	8.0	2.0	0.0 0.5 1.0 2.0 3.0	450 439 369 130 7
125	4.0		0.0 0.5 1.0 2.0	351 351 67 4
150	0.5		0.0 0.5 1.0 2.0	396 312 67 4
180	0.125		0.00 0.25 0.50 1.00	416 136 86 24
180	0.25		0.00 0.25 0.50	431 56 25

Table P-9—Breaker effects on the rheology of a 40 lb/1000 gal borate-crosslinked fluid.

Fluid = 40-lb crosslinked borate Rate = 35 BPM Fluid temperature = 80°F BHST = 150°F					
Stage	Volume (gal)	Dimensionless Fracture Position	Maximum Exposure Temperature (°F)	Exposure Time to BHST (min)	Oxidative Breaker Concentration (lb/1000 gal fluid)
Pad	30,000	1 (depleted)	150	68	0.1
2 PPA	10,000	0.9–1	150	49	0.5
4 PPA	15,000	0.65–0.7	150	41	0.5
6 PPA	20,000	0.35–0.65	150	29	2
8 PPA	25,000	0–0.35	150	7	4

Table P-10. Example treatment.

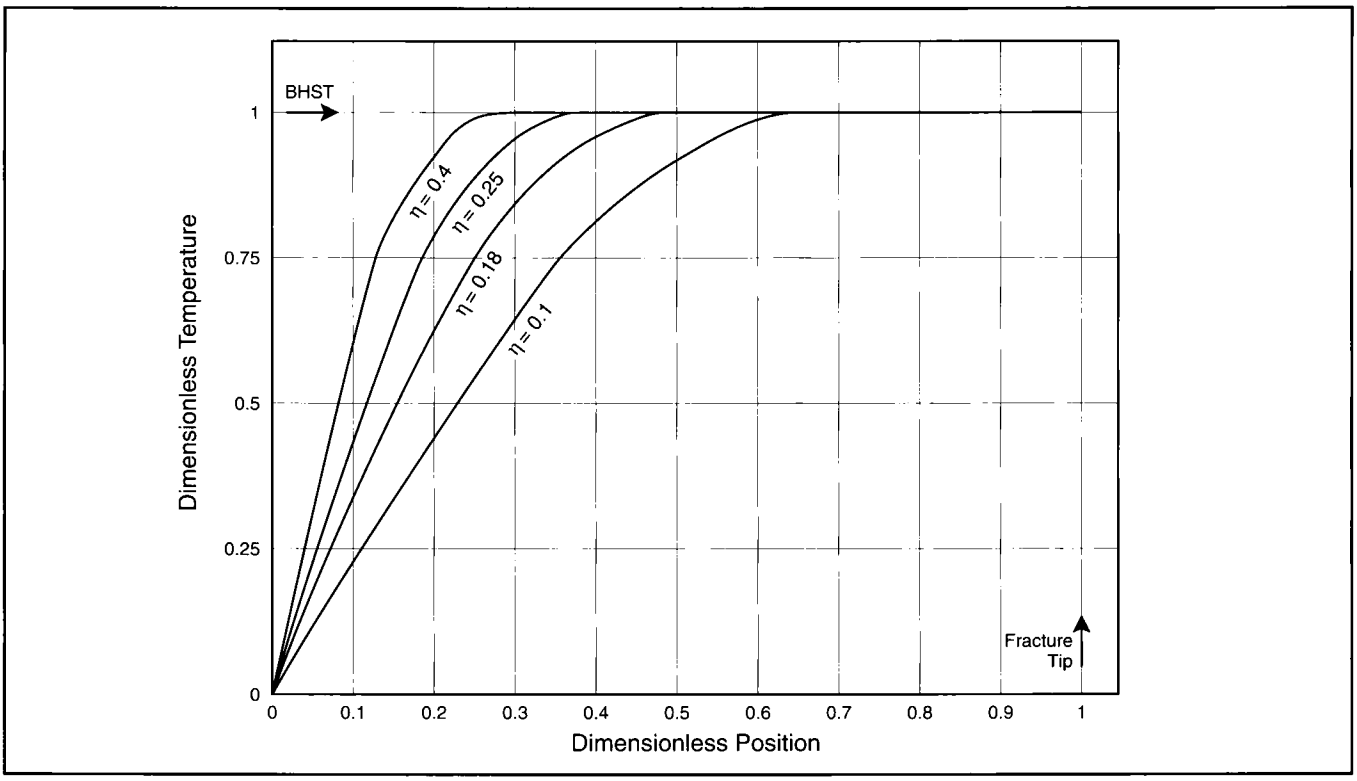

Figure P-43—Dimensionless temperature profiles for various efficiencies (PKN model).

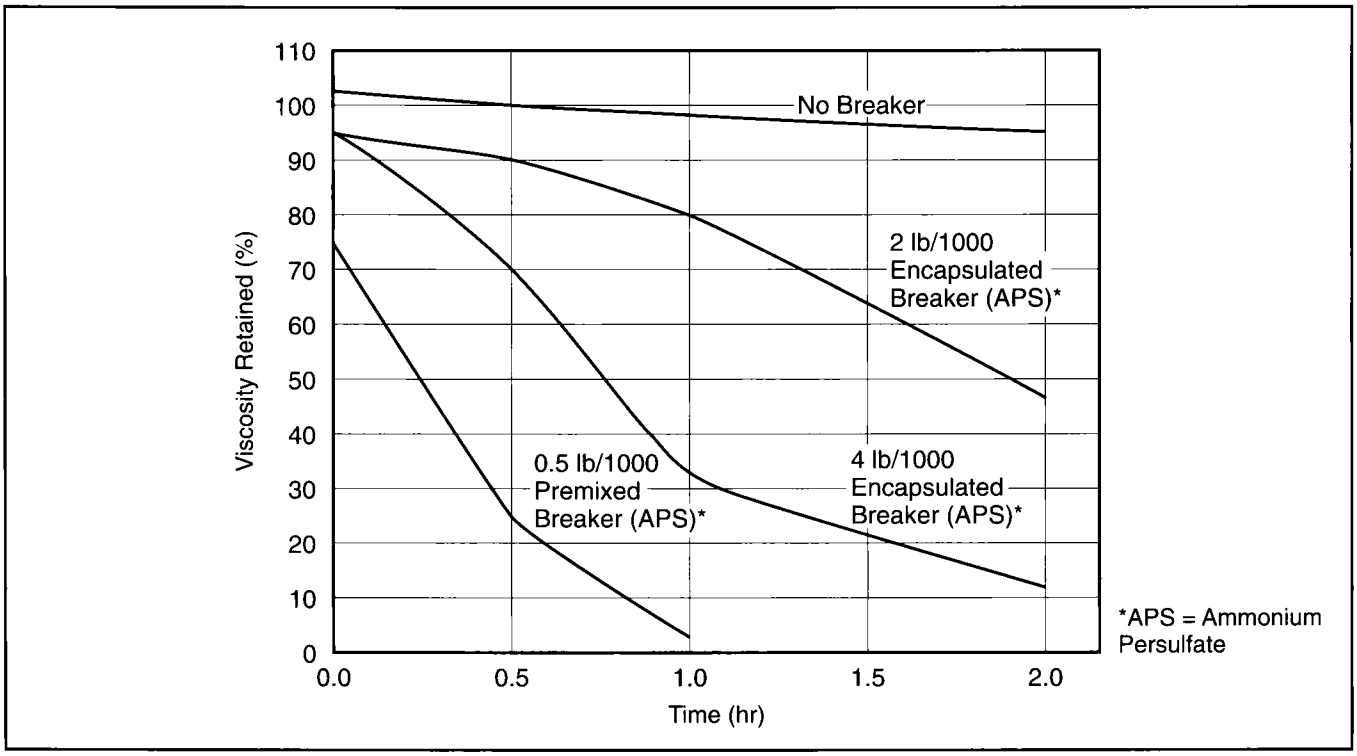

Figure P-44—Effects of breakers on viscosity of borate-crosslinked guar at 160°F (from Gulbis, J. et al., SPE paper 19433, 1990).

P-4

Treatment Sizing

P-4.1: Determination of Volumes of Fluids and Mass of Proppant

The optimum volume of fluid and proppant is best determined by following the methodology outlined in Chapter 8 in *Reservoir Stimulation.* That chapter explains the optimization of fracture length and conductivity based on the net present value (NPV) concept. The major parameters impacting the net present value of a fracture treatment are the reservoir permeability, fracture height, fluid efficiency and residual damage to the proppant conductivity.

Height containment is a major constraint in determining the volume of materials needed. Both fluid and proppant volumes will increase significantly as fracture height increases. Figure P-45 is an example comparing total slurry volumes needed to obtain a fracture half-length of 1000 ft when fracture height increases. As fracture height doubles from 20 ft to 40 ft, the volume of slurry increases from 22,000 gal to 66,000 gal. Before a treatment can be economically optimized, it is obvious that some knowledge about the anticipated gross fracture height is absolutely necessary.

A parametric study of this same example shows the net pressure generated within these fractures. Realizing that the net pressure is inversely proportional to fracture height helps explain the difficulty of containing fractures to very small zones. Large fracture heights are easier to confine because the net pressure generated over a larger interval is much smaller. Small stress contrasts (< 250 psi) between the pay zone and a barrier will almost never be sufficient for containment unless relatively large fracture heights are obtained. Figure P-46 shows that a barrier with a stress contrast of 3416 psi would be needed to contain a 1000-ft fracture with a gross height of 20 ft. Stress barriers of this magnitude do not generally exist. However, if the fracture height is increased to 160 ft, a barrier with a stress contrast of 554 psi may contain the fracture. A stress contrast of this magnitude is often found between sandstones and shales.

Fluid efficiency has a direct relationship on the volume of fluid needed to obtain a given fracture length. The parameter that best quantifies efficiency is the leakoff coefficient. Figure P-47 shows that subtle changes in this fluid property can have dramatic effects on the volume of fluid needed to obtain a given fracture length. By increasing the fluid loss coefficient from 0.001 ft/$\sqrt{\text{min}}$ to 0.003 ft/$\sqrt{\text{min}}$, the volume of fluid required to obtain a 1000-ft fracture half-length increases from 65,000 gal to 103,000 gal of slurry. Although fluid loss

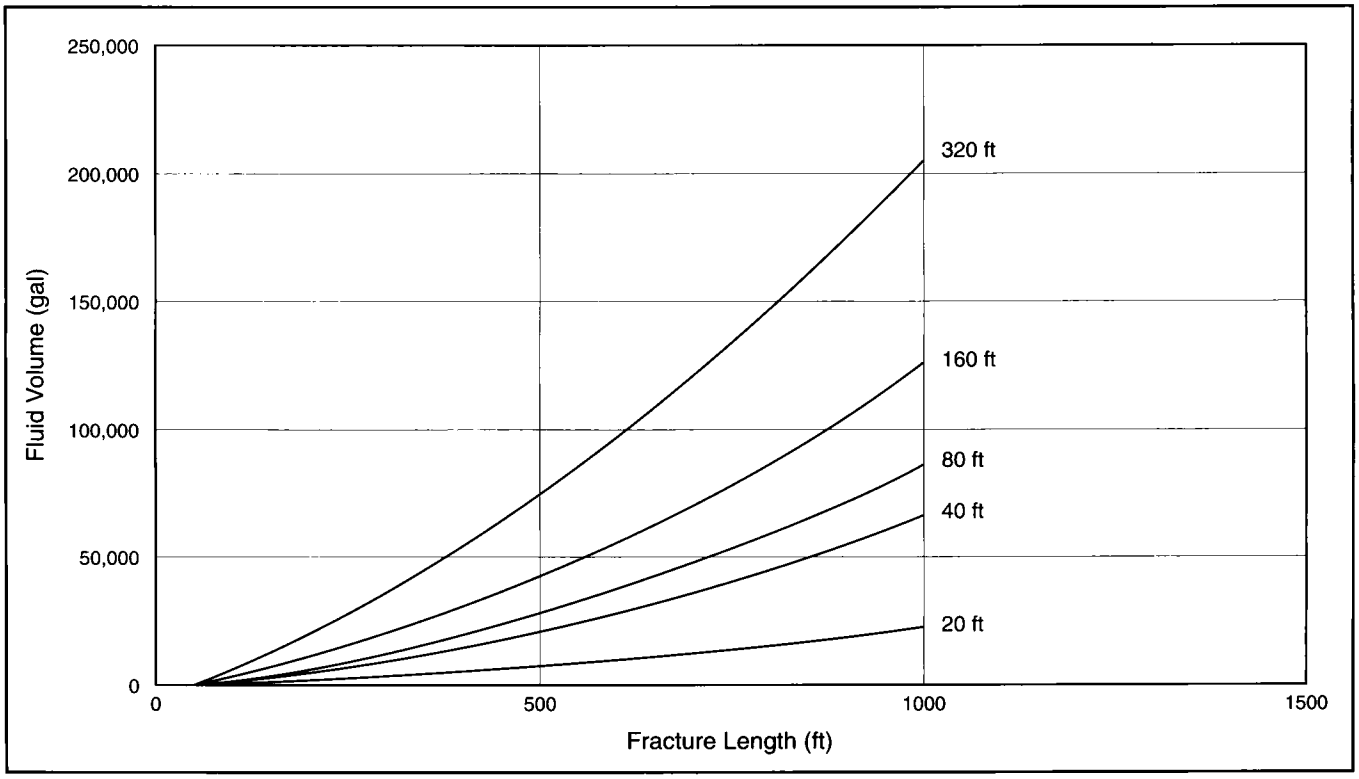

Figure P-45—Effect of fracture height on the fluid volume required to generate a given fracture length.

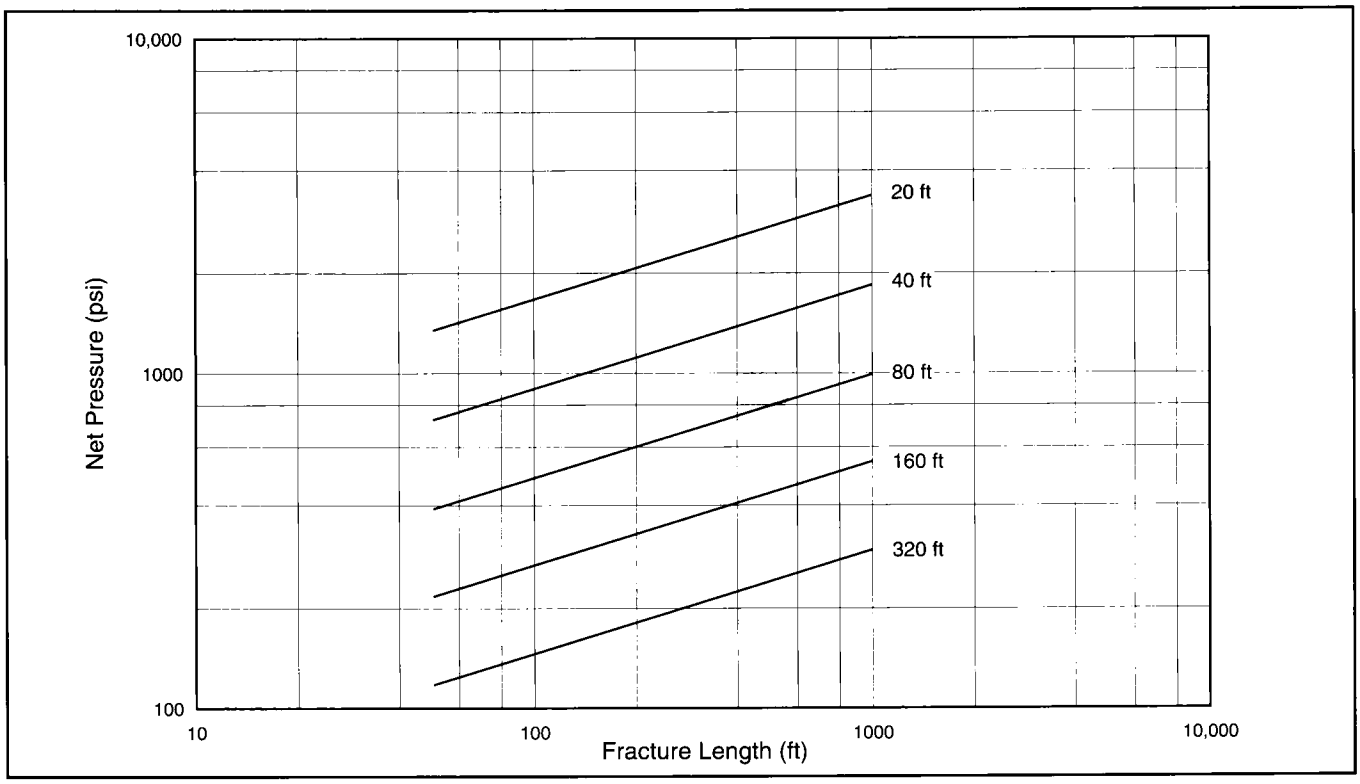

Figure P-46—Effect of fracture height on net pressure.

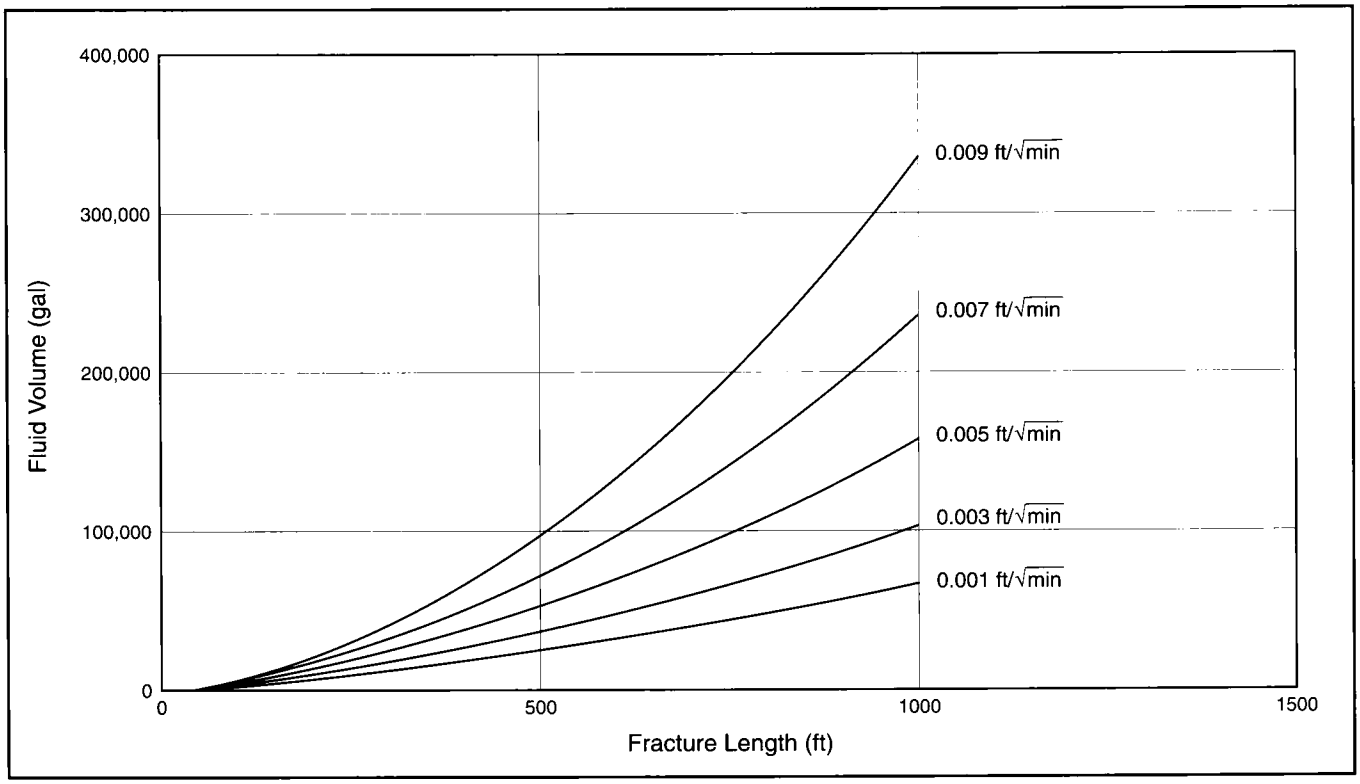

Figure P-47—Effect of fluid efficiency on the fluid volume required to generate a given fracture length.

coefficients are routinely calculated in the laboratory for various fluids, these values, for a variety of reasons, may not be effective in an actual treatment. The best method for quantifying an actual leakoff value is to follow the methodology outlined in Chapter 7 of *Reservoir Stimulation*. Pressure analysis has proved to be an invaluable tool in designing treatments.

P-4.2: Determining the Pump Rate

Pump rates are best determined by balancing the benefits of increasing rate to improve fluid efficiency and decreasing rate resulting from high friction. One of the best ways to improve the overall efficiency of a fracturing fluid is to simply pump faster as demonstrated in Fig. P-48. This figure clearly points out that considerable volumes of fracturing fluid can be conserved if a treatment can be pumped at a higher rate. Fluid loss is proportional to the square root of time; so, the benefits of increasing rate are greater for long fracture lengths or where initial designed rates are small. The main key is to minimize the time exposure of the fracturing fluid to leakoff.

However, higher rates result in higher wellhead treating pressures caused by the frictional pressure drop in the treating tubulars. Charges for pumping equipment are usually based on the amount of hydraulic horsepower the pump trucks develop. Therefore, higher pumping pressures increase the cost of a fracture treatment. Hydraulic horsepower can be calculated using the following expression:

$$\text{HHP} = \frac{q_i\, p}{40.8}, \qquad \text{(P-1)}$$

where q_i = pump rate (BPM) and p = pressure (psi). Price schedules generally increase as hydraulic horsepower increases; the price difference between a 20-BPM treatment and a 40-BPM treatment can be significant if the treatment must be pumped down 2⅞-in. tubing. Using the values for friction pressure drop on Fig. P-29, a standard nondelayed borate fluid will exhibit 310 psi of friction drop per 1000 ft at 20 BPM and 800 psi of friction pressure drop at 40 BPM. The same fluid pumped down 5½-in. casing will exhibit only 38 and 55 psi of friction, respectively. Therefore, rate will only impact the economics through hydraulic horsepower for certain tubular and fluid combinations. For cases where the friction of the fluid is not a major consideration, the increased rate will benefit the economics through improved fluid efficiency.

It becomes obvious that anticipated surface pressures must be calculated during the process of optimizing the pumping

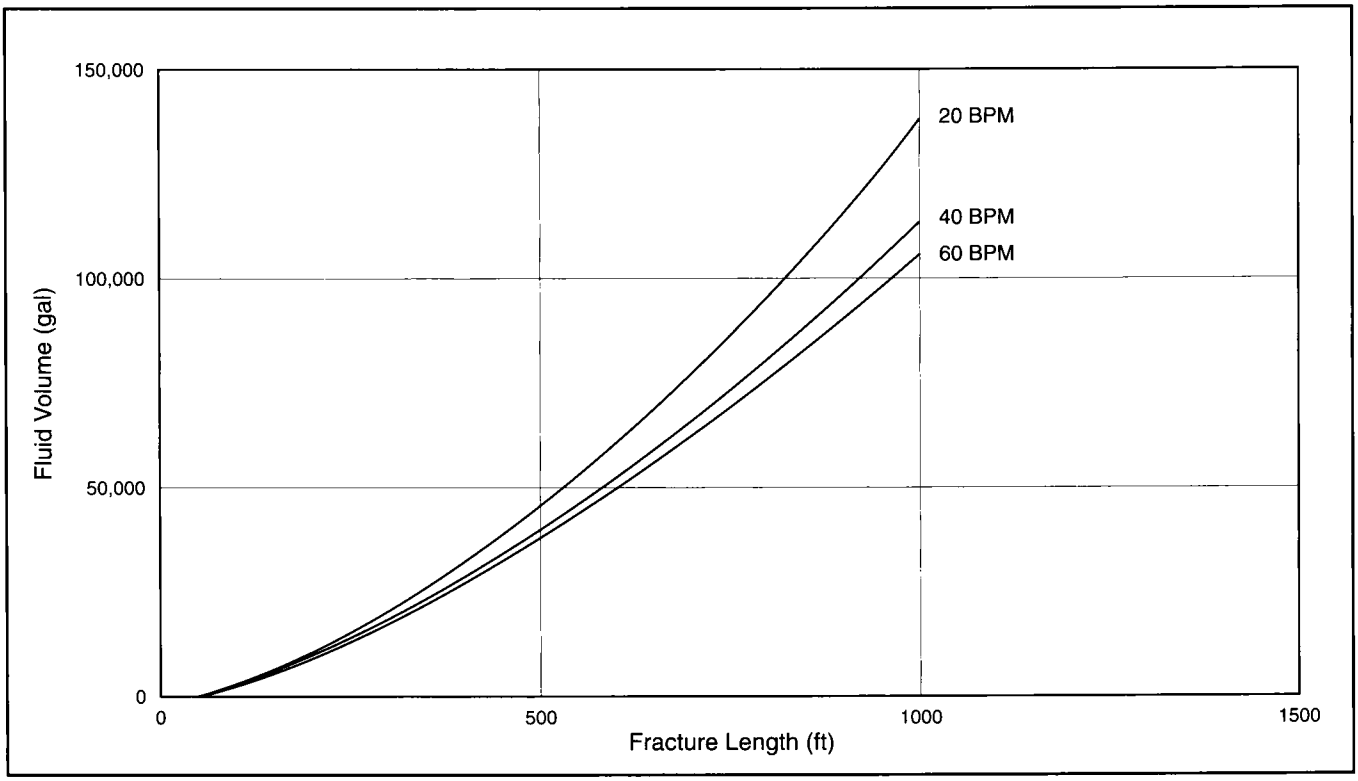

Figure P-48—Effect of pump rate on the fluid volume required to generate a given fracture length.

rate. The following expression can be used to calculate the expected surface pressure for a treatment:

$$\text{WHTP} = [(g_f)(H)] + \Delta p_{net} + \Delta p_{f_{PIPE}} + \Delta p_{f_{PERFS}} - p_H, \quad \text{(P-2)}$$

where WHTP is the wellhead treating pressure, the bottomhole fracturing pressure is estimated by multiplying a fracture gradient g_f by depth H, Δp_{net} is the net pressure within the fracture, Δp_{fPIPE} is the friction pressure drop of the fluid in the tubulars, Δp_{fPERFS} is the friction pressure drop across the perforations and p_H is the hydrostatic pressure. This same calculation is necessary early in the planning of the well when casing and tubular decisions are being made.

The surface pressures of a contained fracture treatment will be the highest at the end of the treatment. Pump rates are often limited in an attempt to contain the fracture to a given interval. By increasing the pump rate, the net pressure within the fracture increases and thereby the chances for fracturing through a stress barrier also increase. However, upon examining this methodology closely, it can be determined that it is almost impossible to control the fracture height growth by simply limiting the injection rate. Figure P-49 shows that even when the pump rate is doubled the net pressure only increases 13.7% from 531 psi to 604 psi. In reality, the stress contrast between the fracture interval and the barrier is rarely known within this level of accuracy.

P-4.3: Selection of High-Pressure Pumps

The rates and pressures of fracture-stimulation treatments can vary substantially from one treatment to the next. Treatments are routinely pumped from less than 10 to more than 100 BPM and pressures can vary from a few hundred psi to more than 20,000 psi. With this wide range of applications it is obvious that care must be taken in selecting the proper pump for a particular treatment. The standard high-pressure pumps used in well stimulation are single-acting positive displacement reciprocating pumps (Fig. P-50). These pumps are divided into two sections: the fluid end and the power end. The power end is connected directly to an engine/transmission power train and converts the rotating power into reciprocating power. The fluid end is the chamber and plunger of the pump. Suction and discharge valves allow fluid flow into and out of the chamber at the beginning and end of each plunger stroke, respectively. These pumps displace fluid out of the chamber only during a forward stroke of the plunger and fluid intake on the backstroke. There is no fluid bypass within a pump stroke (positive displacement); therefore, the pump efficiently moves fluid even under pressure. Most standard pumps have three cylinders (triplex pump, Fig. P-51), but some pumps have five cylinders (quintiplex pump, Fig. P-52).

A pumping unit must convert engine horsepower or brake horsepower into hydraulic horsepower to do the work of a fracturing treatment. Efficiency losses through the transmission and power end of the pump result in only 85 to 95% of the brake horsepower being converted to hydraulic horsepower. The average pumping unit in service today can supply about 1000 HHP. Some pump configurations will allow more than one pump to be mounted on a single truck to provide up to 2000 HHP from one truck.

The pressure limitations placed on a pump are determined by the design of both the fluid end and the power end. The power end moves the plunger against the pressure of the

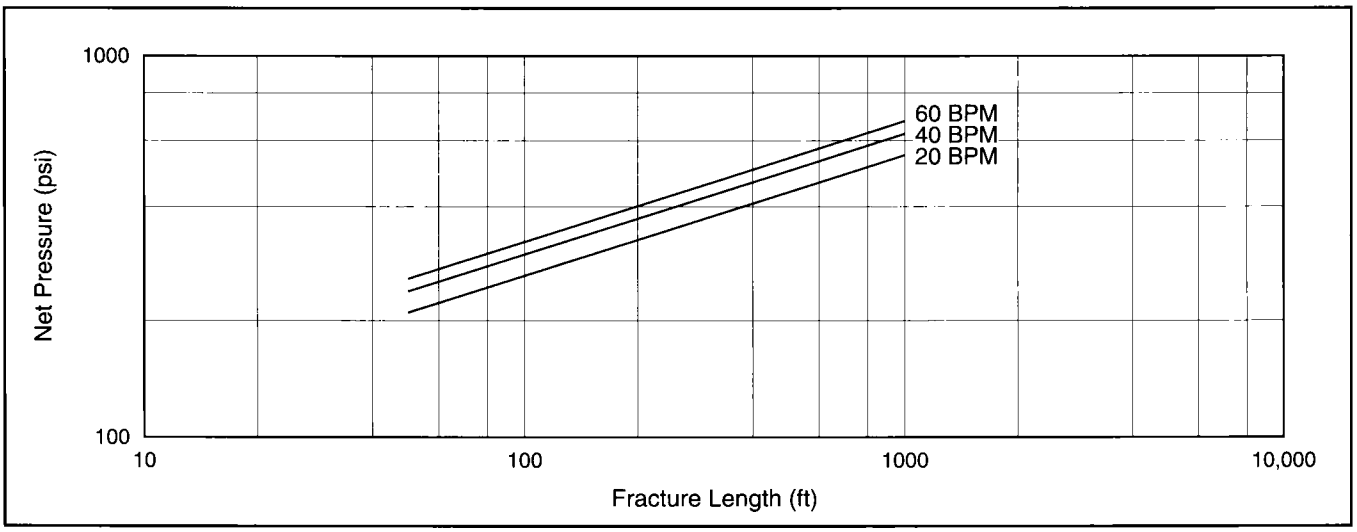

Figure P-49—Effect of pump rate on net pressure.

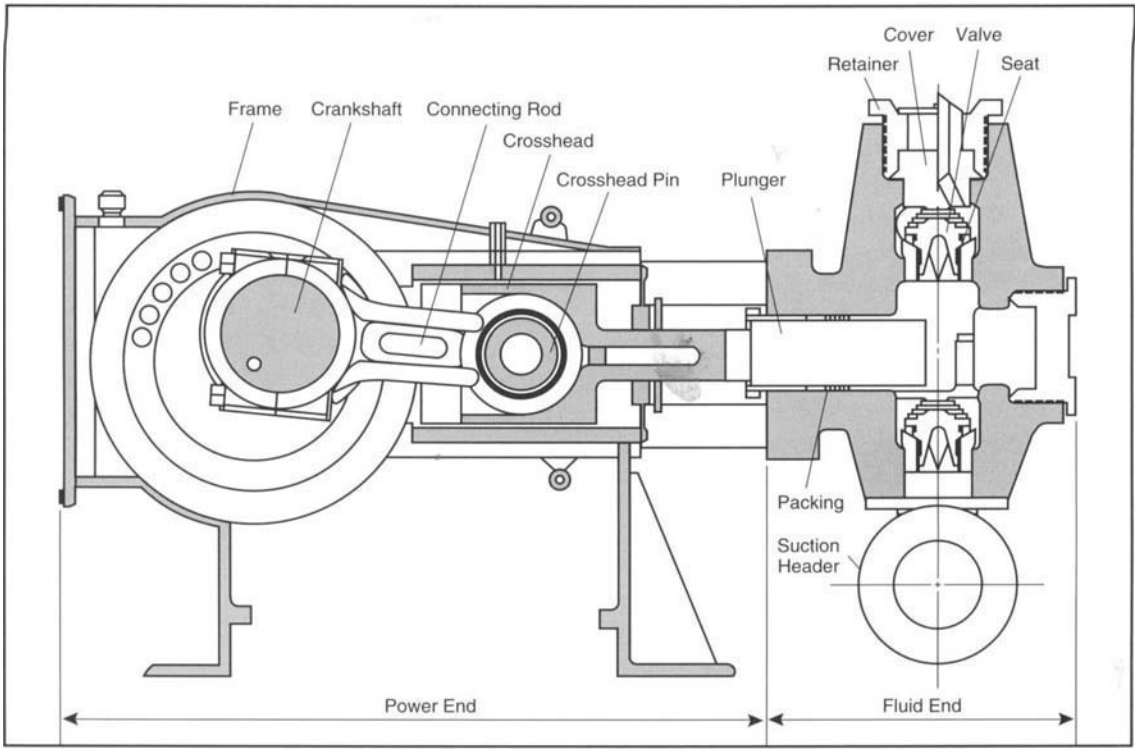

Figure P-50—Diagram of a typical high-pressure pump showing both the power end and the fluid end.

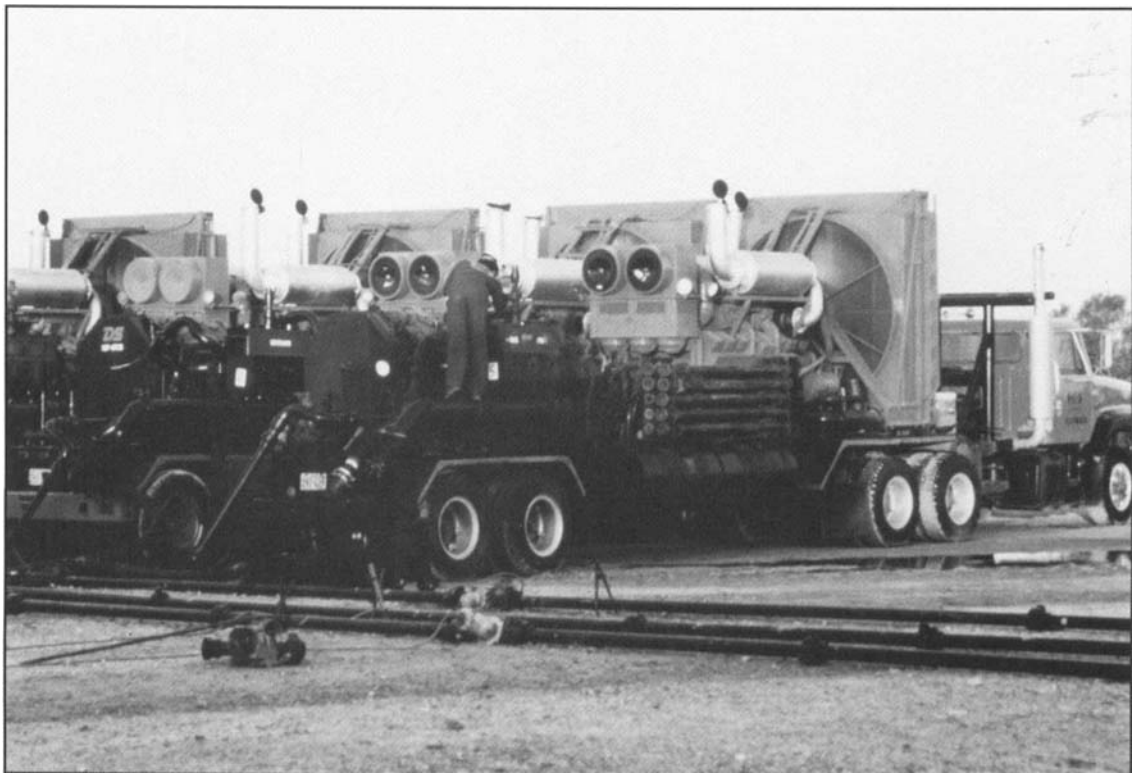

Figure P-51—Triplex pump truck.

treatment. The total force (lbf) felt by the power end is the rod load, RL, of the plunger

$$RL = p_{td}A, \quad \text{(P-3)}$$

where p_{td} = pressure differential between suction and discharge (psi), and A = cross-sectional area of the plunger (in.^{2}).

When larger plungers are used in the fluid end portion of the pump, the rod load against the power end increases for any given pressure. Therefore, different fluid ends with various plunger sizes are needed to cover a wide range of treating pressures. For a power end with a rod load rating of 200,000 psi, the maximum pressure rating would be 10,185 psi if the fluid end had 5-in. plungers. The same power end would have a pressure rating of 15,915 psi when using a 4-in. plunger.

The fluid end can be designed to withstand these pressures regardless of the size of the plunger. Rate is the main limiting factor for the fluid end portion of a high-pressure pump. As pump speed increases, it becomes increasingly difficult to keep the fluid end completely primed on each pump stroke. Several factors contribute to inefficiencies as the pump speed increases. The fluid frictional forces between the fluid end chamber and the valves increase. At the same time, the valve cycle time, or the time the valves stay open, decreases. Table P-11 gives the maximum rates and pressures for several different pump configurations. The maximum rate a pump is

Number Plunger	Maximum Rod Load (psi)	Plunger Size (in.)	Maximum Pressure (psi)	Maximum Rate (BPM)
3	120,000	2½	20,000	2.5
3	120,000	3	15,000	4.0
3	120,000	3¾	10,500	6.0
3	120,000	4½	7,500	8.5
3	120,000	5	6,000	10.5
3	120,000	5¾	4,500	14.0
3	120,000	6¾	3,500	19.0
3	120,000	7¾	2,500	25.0
3	195,000	3¾	17,000	7.0
3	195,000	4½	12,000	10.0
3	195,000	5	10,000	12.0
3	195,000	5½	8,000	14.5
3	195,000	6¾	5,500	22.0
5	160,000	3¾	15,000	11.0
5	160,000	4½	10,000	16.0
5	160,000	5½	7,000	24.0

Table P-11—Maximum rate and pressure for various pump configurations.

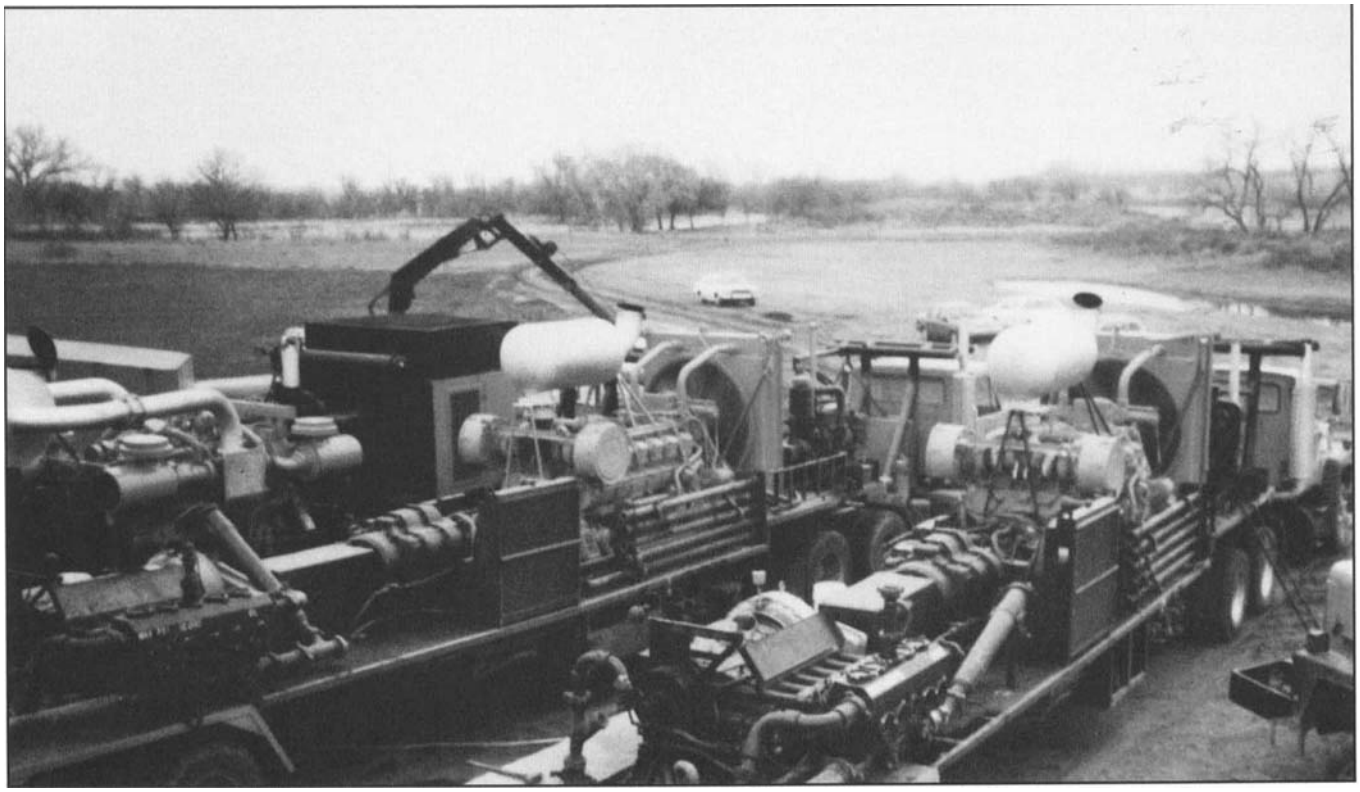

Figure P-52—Quintiplex pump trucks.

able to achieve at a given pressure is best determined on a pump performance curve. Each pump and power system will have a unique performance curve. An example is given in Fig. P-53.

P-4.4: Blending and Mixing Considerations

Material storage and deliverability may also be determining factors in sizing a fracture treatment. Fluid and proppant storage must be organized and laid out on location so that the pumping procedures of the treatment can be followed smoothly. For the fluid portion, a major consideration is deciding whether the fluids should be batch mixed or continuously mixed just prior to being pumped. Recent developments in hydration technology as well as new process control capabilities have made continuous mix treatments a viable alternative to batch mix operations (Fig. P-54). There are several advantages to performing a fracture treatment in a continuous mix mode. Environmental concerns are greatly reduced with only fresh water remaining in the frac tanks after a treatment. Besides eliminating the cost of gelled tank bottoms, no tank cleaning or disposal costs are incurred. At the same time, a more predictable and consistent viscosity is obtainable for very large treatments where bacteria can often degrade the gel viscosity of a batch-mixed fluid before pumping can begin. Also, manpower time and costs can be greatly reduced. The continuous mix process eliminates the need to have gelling crews precede fracturing operations. This results in a direct saving in time for both personnel and equipment. Finally, viscosities can be easily changed throughout the treatment. This allows the polymer loading to be tapered so that fluid damage to proppant conductivities can be minimized or net pressure limitation can be met.

To ensure that a continuous-mix operation goes smoothly several requirements must be observed. The polymers should be of a liquid or slurried variety to ensure that they can be added at precise concentrations. Liquid or slurried additives can be pumped and monitored much more accurately than dry, powdered materials. These polymers will show an improved and quicker hydration especially when mixed with new process controlled equipment (Fig. P-55). These specialized mixing and hydration units provide the metering capabilities, the proper shear environment and sufficient residence time for proper hydration. The hydration process related to time and shear has proved to be extremely impor-

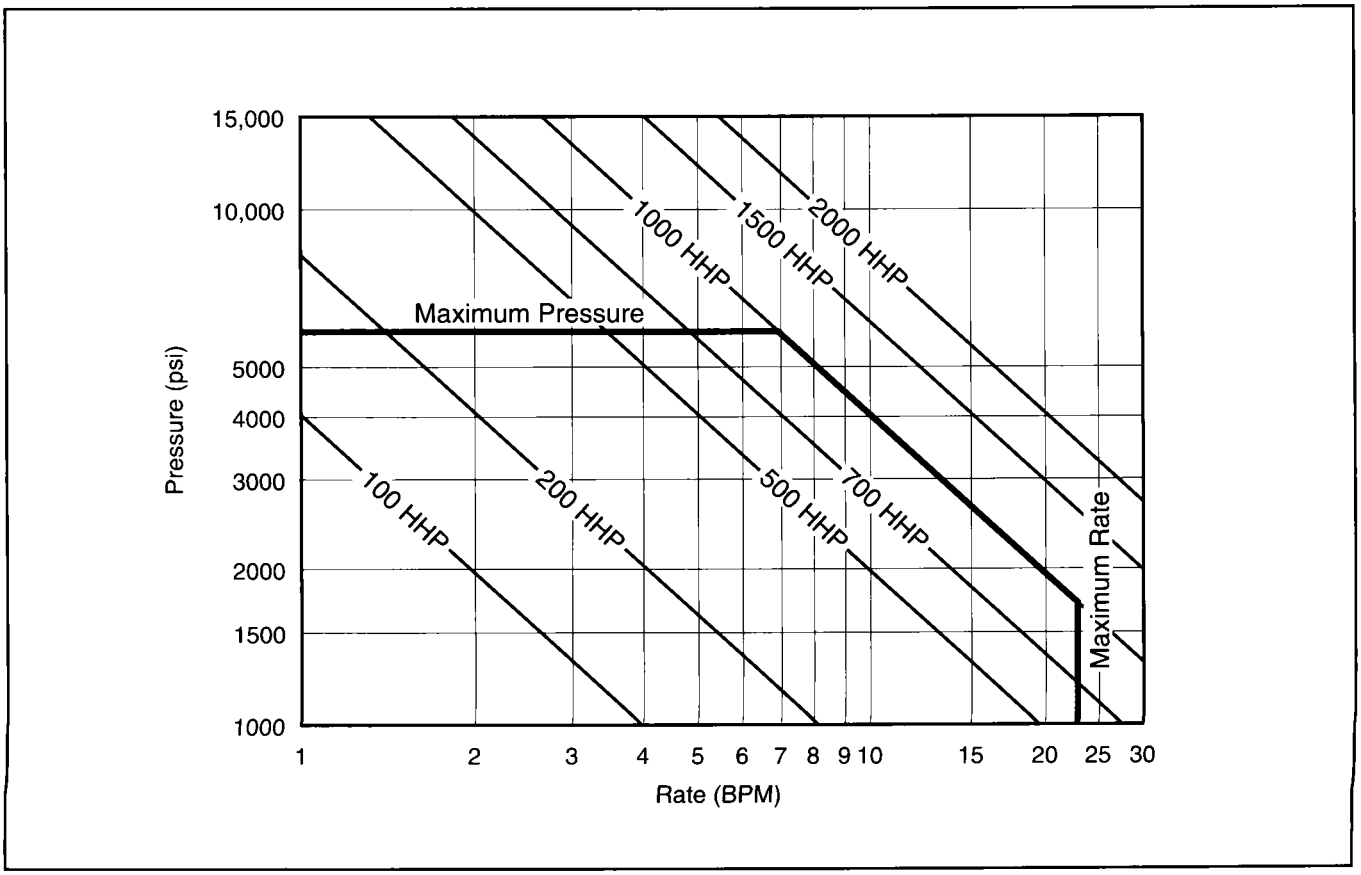

Figure P-53—Typical pump performance curve.

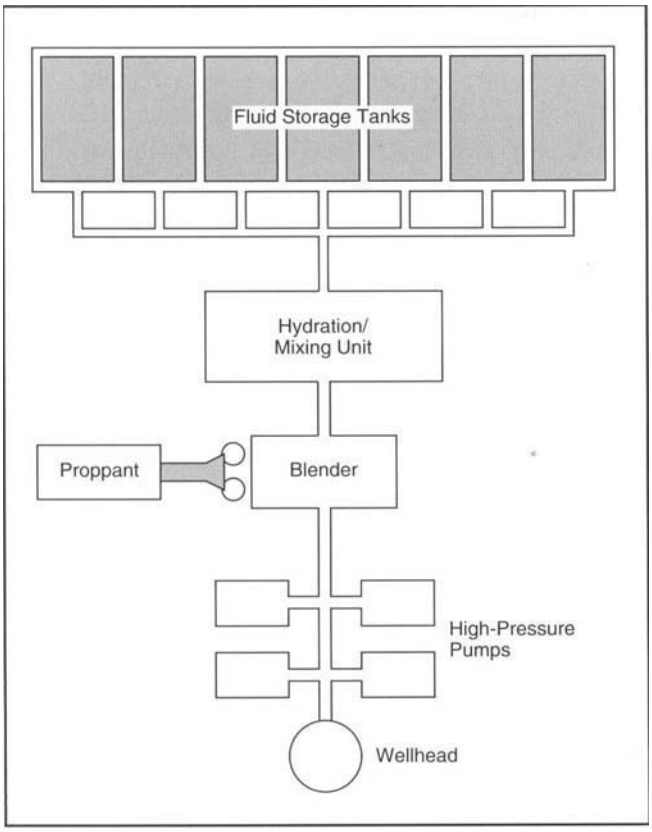

Figure P-54—Location schematic for continuous-mix fracturing treatment.

tant on continuous-mixed treatments. If the base fluid has not moved far enough along in the hydration process before the fluid is crosslinked, the fluid may experience stability problems.

The organization of tanks and equipment should allow easy transfer of fluid from storage to the mixing and blending equipment and then ultimately to the high-pressure pumps. When the size of the job is large enough to require several tanks, the tanks should be linked together with a common manifold. The transfer of fluid is usually done with centrifugal pumps. The hoses or manifolding coming from the tanks must be large enough not to impede the flow to the pump. A good policy is to limit suction hose flow rates to less than 8 ft/sec (8 ft/sec ≈ 8 BPM in a 4-in. hose). If the rate exceeds 8 ft/sec, more hoses should be added.

Proppant storage must also be planned and laid out with equipment limitations in mind. Most treatments use proppant storage vessels with bottom conveyor systems to handle proppant on location (Fig. P-56). These units can generally move proppant at about 10,000 lb per minute. If treatments are designed at very high rates or requiring high proppant concentrations, several of these units may need to operate simultaneously to maintain the proper addition rate. On very large jobs a central conveyor system may be required with multiple storage units feeding it. Some smaller treatments use hydraulic pumps to haul and add proppants. These units must be fully raised to ensure that proppant will flow out of them at sufficient rates.

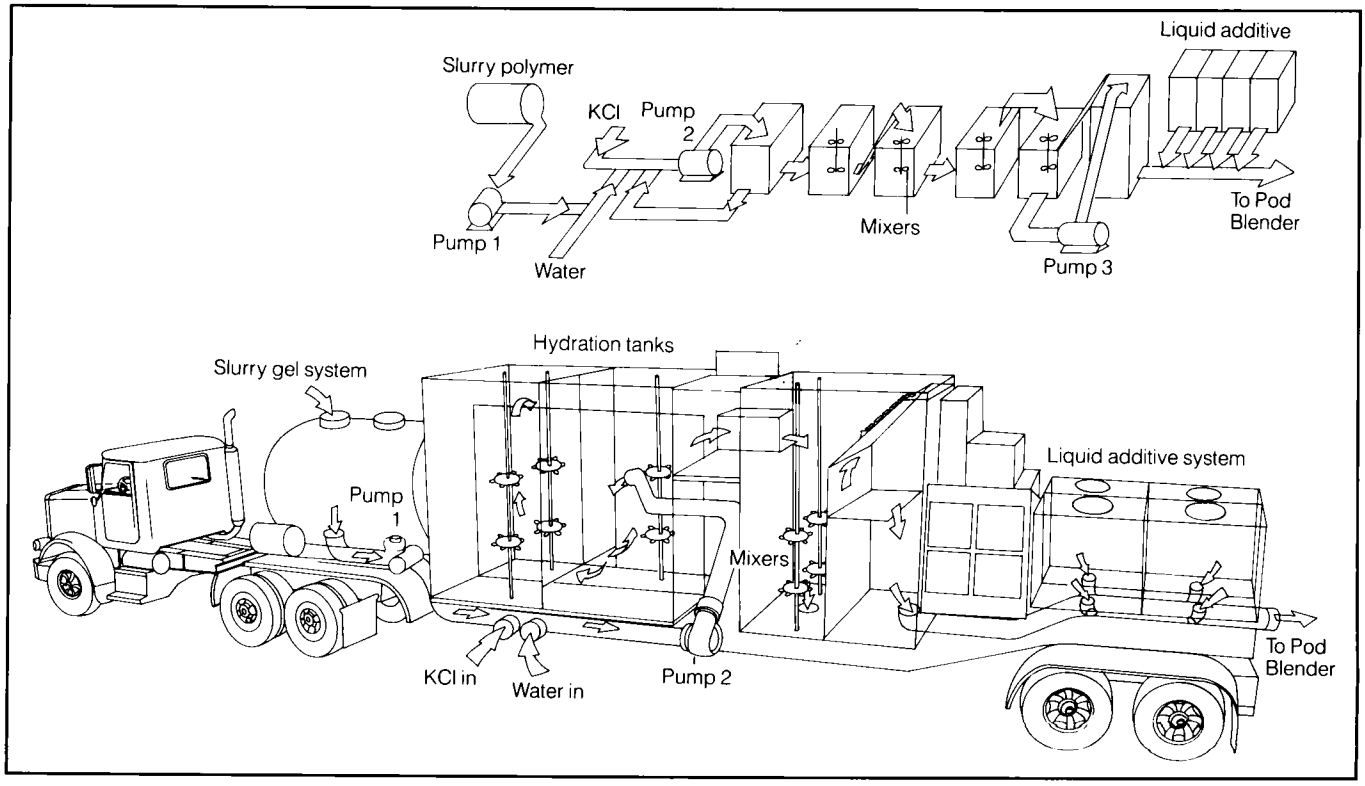

Figure P-55—Continuous-mix hydration unit.

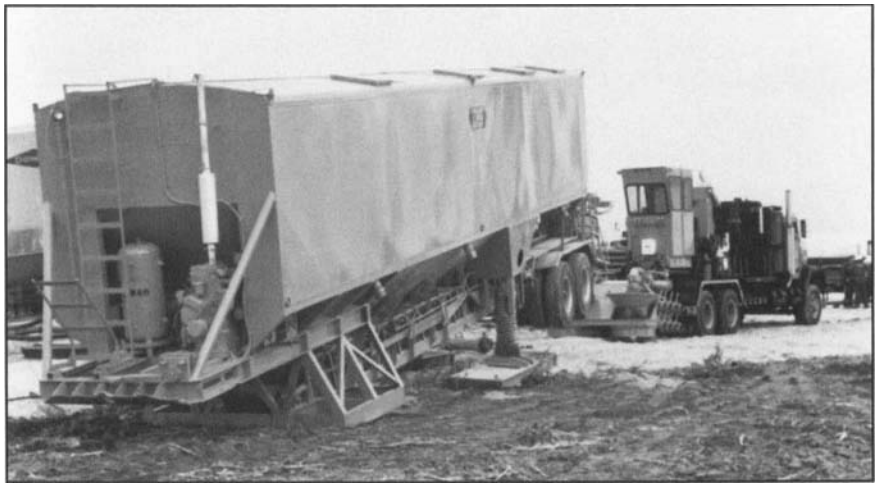

Figure P-56—Proppant storage with bottom conveyor system.

P-5

Effects of Perforations

Perforations are the communication link between the producing reservoir and the wellbore. The number of perforations required to perform this function is determined by two factors. First, the producing capability of the well should be considered. A mechanical skin can be created if too much production is forced through a limited number of perforations, thereby reducing the productivity of the formation. The other factor controlling the number of required perforations is the rate at which the stimulation treatment is to be pumped. Frictional pressure drop through perforations becomes significant once the fluid rate through a given perforation exceeds 0.5 BPM. Therefore, to avoid excessive pressure drop and the resulting high treating pressure, at least two effective perforations are needed for each BPM planned for the treatment.

P-5.1: Calculation of Number of Effective Perforations

The following procedure can be used to calculate the number of effective perforations. The total frictional pressure loss is estimated by shutting down the pumping units and measuring an ISIP (instantaneous shut-in pressure). The pressure drop at the wellhead can be accounted for by the loss of friction in both the casing and through the perforations. To separate these values, the friction pressure drop of the fracturing fluid must first be estimated as discussed in Section P-3.5. This value is subtracted from the total friction loss, leaving the remaining friction to be accounted for by perforational friction drop.

$$\Delta p_{f_{perf}} = \text{WHTP} - \text{ISIP} - \Delta p_{f_{pipe}}. \qquad \text{(P-4)}$$

The remaining frictional losses can be attributed to perforation friction drop. The number of effective perforations can then be calculated using the following equation:

$$n = \sqrt{\frac{q_i^2 \rho}{\Delta p_{f_{perf}} d_{perf}^4 (0.323)}}, \qquad \text{(P-5)}$$

where q_i is the pump rate (BPM), ρ is the density of the fracturing fluid (g/cm^3), n is the number of perforations, and d_{perf} is the diameter of the perforations (in.). For quick reference, this equation is often used in nomograph form and is shown in Fig. P-57.

This method of estimating the number of perforations is of limited use if proppant-laden fluid has been pumped through the perforations. Data show that after only 10,000 lb of proppant, the perforation face can become significantly eroded. As the perforation face becomes rounded, the choke effect of the perforation changes, making this type of calculation very difficult, if not meaningless (see Fig. 9-15 in *Well Cementing*, Prentice Hall, 1990).

P-5.2: Breakdown of Perforations

Wells are often "broken down" after perforating and prior to pumping the fracturing treatment. These treatments are often performed several days before the actual fracture treatment to allow testing of the formation. They are performed in cased wells to ensure that the perforations have been effectively shot through the casing and are "open," creating a communication path between the reservoir and the wellbore. Even if holes have been shot through the casing, it is very common for the perforation tunnel to be extensively damaged, especially when wells are perforated in an overbalanced condition (i.e., the hydrostatic pressure of the well is greater than the reservoir pressure). This damage is often severe enough to prevent the flow of stimulation fluids from adequately entering the formation. A proper breakdown procedure effectively removes perforation debris and eliminates most of the damage. At the same time, this small treatment can confirm whether it is possible to pump into the formation without excess pressure before an entire stimulation crew is mobilized to the wellsite.

This is also a very convenient time to ensure that the fracture gradient used in the hydraulic fracture design is accurate. If the estimation is in gross error, the fracture treatment can be redesigned so that surface pressure limitations are not exceeded. The fracture gradient can be estimated by taking an ISIP and applying the following equation:

$$g_f = \frac{\text{ISIP} + p_H}{H}, \qquad \text{(P-6)}$$

where p_H is the hydrostatic pressure.

Performing a breakdown treatment is very important when the interval has been shot with a limited number of perforations or when perforations are spread over an interval exceeding 100 ft. If a limited number of perforations have been shot and a breakdown has not been performed, excessive treating pressures may be encountered because of an insufficient number of perforations accepting fluid. When a large interval has been perforated, some of the perforations may not accept fluid and that part of the interval may not be adequately treated.

However, when a relatively small interval has been shot with a high perforation density (four shots per foot over ≈ 25 ft), there may be no advantage in performing a separate breakdown treatment. In this case, enough perforations are present so that a fracture treatment can be started without experiencing excessive pressures.

When a breakdown treatment is pumped, ball sealers are required to divert the breakdown fluid into all the perforations. It is common practice to use at least 50 to 100% more

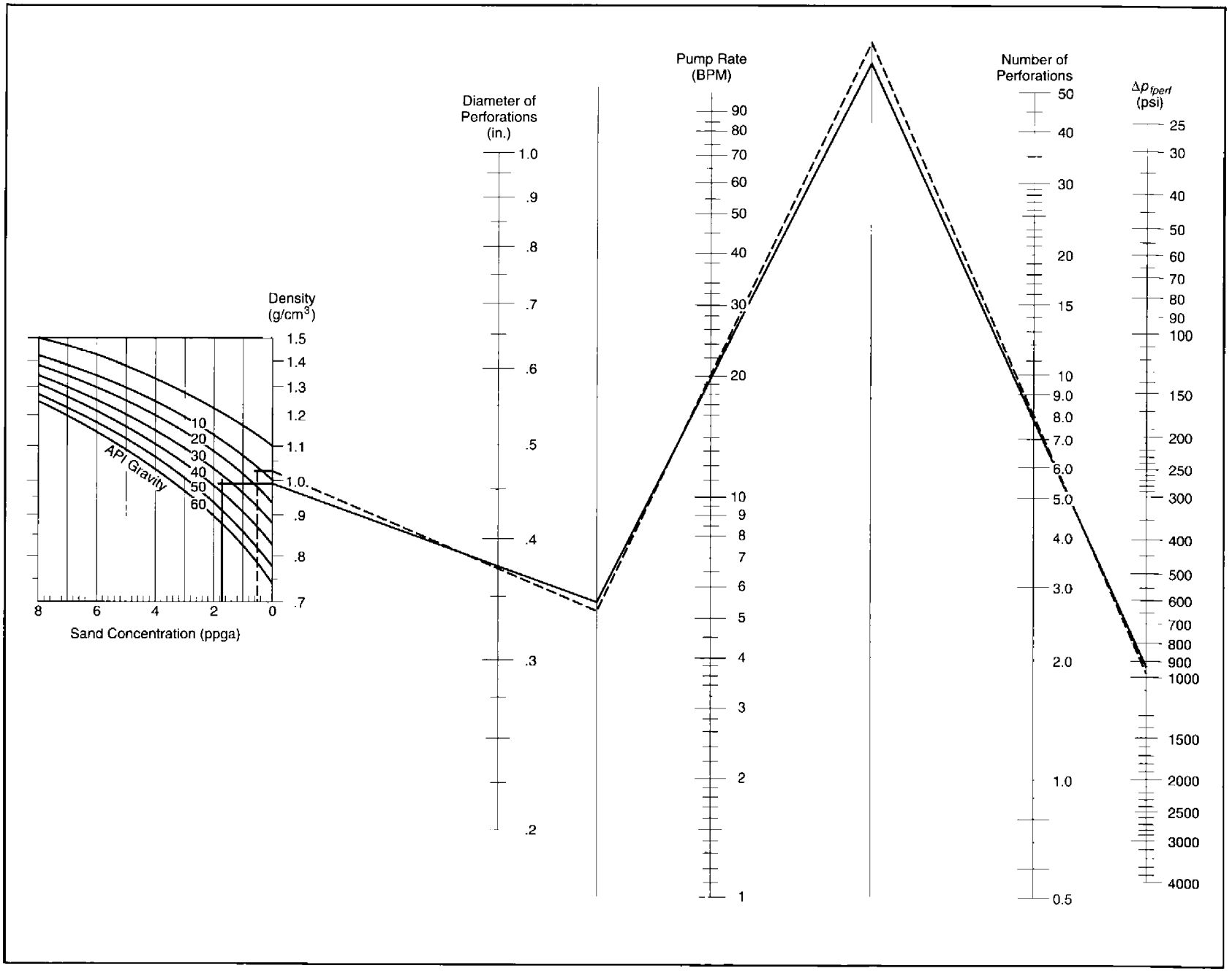

Figure P-57—Nomograph for friction loss across perforations (courtesy of Conoco).

ball sealers than there are perforations. The excess balls must be pumped because of ball seating inefficiencies and placement timing. Breakdown treatments usually consist of only a few thousand gallons of fluid, and all the ball sealers must therefore be injected in a short period of time. Some balls may be rendered ineffective because they are already below a perforation when it opens and begins accepting fluid. The seating efficiency is dependent on the density of the ball sealer and its velocity, which results from the pump rate. Figure P-58 shows the required pump rate to efficiently seat ball sealers of varying densities in various size tubulars.

Ball sealers having a higher density than the fluid with which they are pumped have a lower seating efficiency but will fall into the rathole after the treatment and will therefore not affect subsequent treatments. Lightweight ball sealers will be more efficient at seating but must be circulated out of the hole before the hydraulic fracturing treatment. If a lightweight ball sealer is left in the hole, it can float in the wellbore fluids and reseat once the fracturing treatment begins. It is a good practice to run tubulars past the entire perforated interval to physically knock off any remaining ball sealers before fracturing operations.

P-5.3: Choice of Breakdown Fluids

Even though production will not be significantly affected by near-wellbore damage once a fracture has been placed, a nondamaging fluid should be chosen as a breakdown fluid. The fluid design should take into consideration emulsions, water blocks, wettability and destabilization of clays.

Any time water and oil are mixed together the possibility of an emulsion exists. Special nonemulsifying surfactants can usually eliminate this problem. Pretreatment compatibility testing between well fluids and breakdown fluids should be conducted to identify the most effective nonemulsifier. This type of testing will also reveal any tendency for the well fluids to drop out paraffins or asphaltenes.

In dry gas wells emulsions are not a problem. However, these formations often tend to retain water because of relative permeability and capillary pressure effects. Breakdown fluids used in these formations should incorporate surfactants that are efficient in lowering the interfacial tension properties of the fluid. To further minimize the potential for a water block, breakdown fluids in tight gas reservoirs may benefit from pumping an energized fluid to reduce the amount of water put in the formation. Either CO_2 or N_2 can be used as the gas phase. The fluid phase can be a weak acid, water or a water and methanol blend.

Clay problems can be minimized by using an organic polymer clay stabilizer in addition to 2% KCl water. Energized or foamed fluids may also help minimize the effects of water on the clay particles.

Weak acids (7.5% HCl) have long been accepted as common breakdown fluids. These fluids are most appropriate in carbonate reservoirs where the acid can actually react with the formation. In sandstone formations the acid may not have any material with which to react. A blend of 2% KCl water and methanol incorporating a surfactant package has proved to be at least as effective as acid. In sandstone formations having carbonaceous cement, an acidic fluid may actually destabilize the formation and allow the perforations to collapse. If acid is used as the breakdown fluid, reducing agents and/or chelants should be added to the fluid to prevent iron precipitation damage.

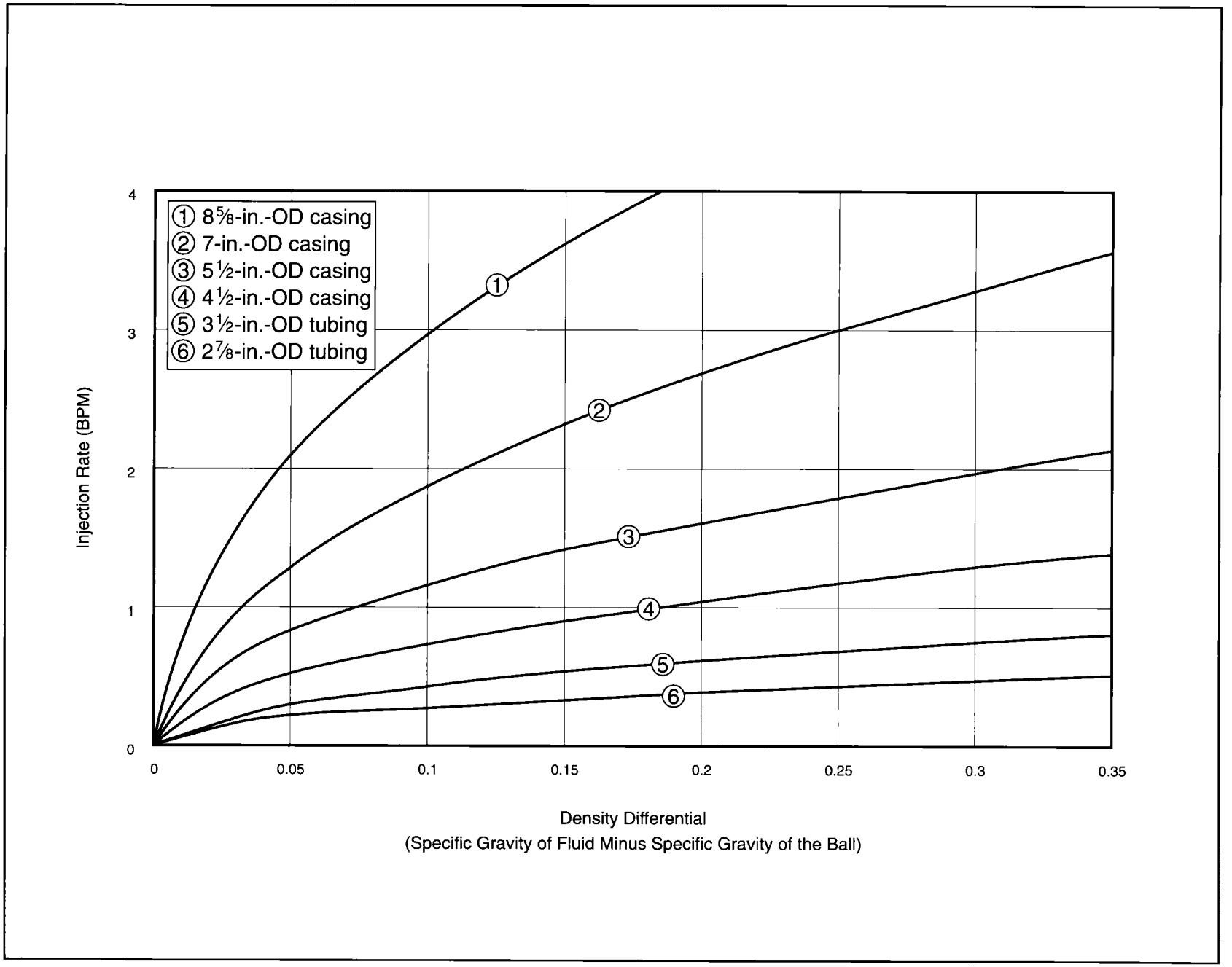

Figure P-58—Injection rate required to balance buoyant ball sealers.

P-6

Zonal Isolation

There are often several potential producing zones penetrated by a wellbore that must be hydraulically fractured. To ensure each zone is stimulated effectively, these intervals must be isolated from one another, and individual treatments must be designed and pumped for each one. Several isolation methods have proved to be effective. These methods can be used only when the various formations and intervals are isolated from each other behind the casing by cement.

P-6.1: Importance of the Cement Sheath

The cement sheath must provide zonal isolation during both production and stimulation operations. For a producing well, the cement seal between pipe and formation must be relatively tight to prevent fluids from flowing through the annular area. The permeability of a set Portland cement of normal density is in the low microdarcy range. However, if the cement does not bond perfectly to either the pipe or formation and a small channel remains, the effective cement permeability can be drastically increased. However, very large permeabilities may result from channel widths that are quite small (see Chapter 1 in *Well Cementing*, Prentice Hall, 1990). For example, a channel width of only 1.4×10^{-4} in. is sufficient to create an effective cement permeability of 1000 md. Channel permeabilities of this order may allow significant crossflow between zones.

However, during hydraulic fracturing these small channels, or microannuli, are relatively insignificant. The effective cement permeability, given above, does not create a high leakoff risk for the fracturing fluid within the annulus. A leakoff rate for this channel is less than 1 gal/min. As long as major channels within the cement can be avoided, containment of a fracturing treatment should be possible.

The effects of fracturing pressures on the adhesion tension between cement and casing or cement and formation are not clearly understood. Data on this phenomenon are lacking. Consequently, the resulting condition of the cement sheath following hydraulic fracturing is difficult to predict. Sonic logs run after fracturing treatments often indicate that the cement bond across the fractured interval is destroyed, but the bond further uphole remains intact. The loss of cement bond across the fractured interval probably does not affect the placement or containment of the fracturing treatment. Cement of relatively low compressive strength should prevent the fracture from migrating between the casing and the formation. However, the alteration of the bond may occur after the treatment. Any small loss of adhesion may result in a microannulus that would lead to crossflow of reservoir fluids.

P-6.2: Controlling Fracture Placement

The most reliable method of controlling the placement of fracturing fluids is to limit perforations to a single zone. When several zones of a well are to be stimulated, the individual zones must be isolated from one another during pumping. This is best accomplished through progressive perforation and stimulation. After a fracturing treatment has been placed in the first zone, it is isolated, and another zone of interest is perforated and treated in another single stage. Of course, this methodology works best when the deepest zone is completed first and subsequent zones are individually stimulated by working uphole.

P-6.2.1: Mechanical Bridge Plugs

Several mechanical methods are available to provide adequate isolation. The most reliable method is the use of mechanical bridge plugs. The bridge plug can be run on tubulars or on a wireline. Bridge plugs that are run on tubulars are retrievable and can be moved and reset several times. Wireline bridge plugs cannot be moved once set and generally need to be milled out after the treatment. Wireline bridge plugs are often used when several treatments are attempted in one day or when a rig is not scheduled to be over the hole during the treatment. They can be run in the hole very quickly, and cleanout trips are not required between stages. The retrievable bridge plugs are used when zones are individually tested before another zone is opened. Any excess proppant must be circulated out of the hole before the tool is moved in order to prevent the proppant from sticking the tool.

A typical treatment would involve perforation of the bottom zone, a hydraulic fracture treatment and a zonal isolation by setting a bridge plug immediately above the perforated interval. The next zone would then be perforated and fracture stimulated. Subsequent zones would be stimulated following the same procedure (Fig. P-59).

P-6.2.2: Sand Plugs

A similar method of isolation can be achieved by using sand plugs after the fracturing treatment. The volume of sand necessary to cover the perforated interval is added to the casing. The sand plug is then tested by pressuring up on the casing. The next zone is then perforated and stimulated. Once all zones have been fracture stimulated, the sand can be circulated out of the wellbore by using either conventional or coiled tubing. The amount of sand needed above the top perforations is generally quite small and can be calculated by applying Darcy's law to linear flow:

$$q_i = \frac{1622.88 A k \Delta p}{\mu L}, \qquad \text{(P-7)}$$

where q_i is the rate in BPM, A is area in ft^2, k is permeability in darcies, Δp is the pressure drop in psi, μ is viscosity in cp, and L is the length in ft. Using this expression, 10 ft of 20-40 sand in 5½-in. casing will create more than 6000 psi of pressure drop for a linear gel of 40 cp leaking through the sand pack at 0.5 BPM. A mixture of sand meshes can be used if the permeability of the sandpack must be reduced to prevent flow through the pack.

P-6.2.3: Frac Baffles

Mechanical diversion can also be accomplished by using frac baffles. These baffles are run as part of the casing string and are placed between individual producing zones. After the lowest interval is perforated and fractured, a ball is dropped down the casing. This ball seats on the baffle and prevents fluid flow below this point. The next zone can then be perforated and fracture stimulated. When multiple zones are isolated with baffles, care must be taken to taper the baffle openings. The first ball must be allowed to pass through the upper baffles and still seat in the bottom baffle (Fig. P-60).

P-6.2.4: Bridge Plugs and Packers

When completion practices do not allow the progressive order of fracturing to proceed from the lower zone of interest up to higher intervals, bridge plugs must be used in conjunction with packers. Using a combination of bridge plugs and packers to straddle an interval provides an extremely reliable method of isolation. These retrievable tools can easily be moved to cover any interval, provided the unperforated casing is sufficient to provide a packer seat. However, caution should be taken when open perforations are present above a packer. This leads to the possibility of proppant entering into the annular area if the fracture reaches the open perforations. Very small quantities of proppant on top of a retrievable packer can stick the tool string.

P-6.2.5: Diversion

At times, diversion is used to control the placement of fluid and slurry into the zones of interest. This type of treatment is advantageous over separately isolating individual zones because all treatments can be pumped continually and are therefore both economical and time efficient. Although initially attractive, controlling placement through diversion carries many inherent risks.

The use of bridging materials, such as rock salt and benzoic acid flakes, as the diverting medium will usually result in an overflushed fracture. Some of the bridging material will enter the fracture and displace the near-wellbore proppant before diversion is achieved at the perforations. Conductivity near the wellbore will be destroyed, resulting in a choked fracture with limited production capabilities.

This problem is pronounced when high-viscosity, crosslinked fluids are used for fracturing. These fluids are very efficient at proppant transport and will carry the proppant away from the perforations as they are displaced by the diverter slurry. The diverter overflush may not be a significant

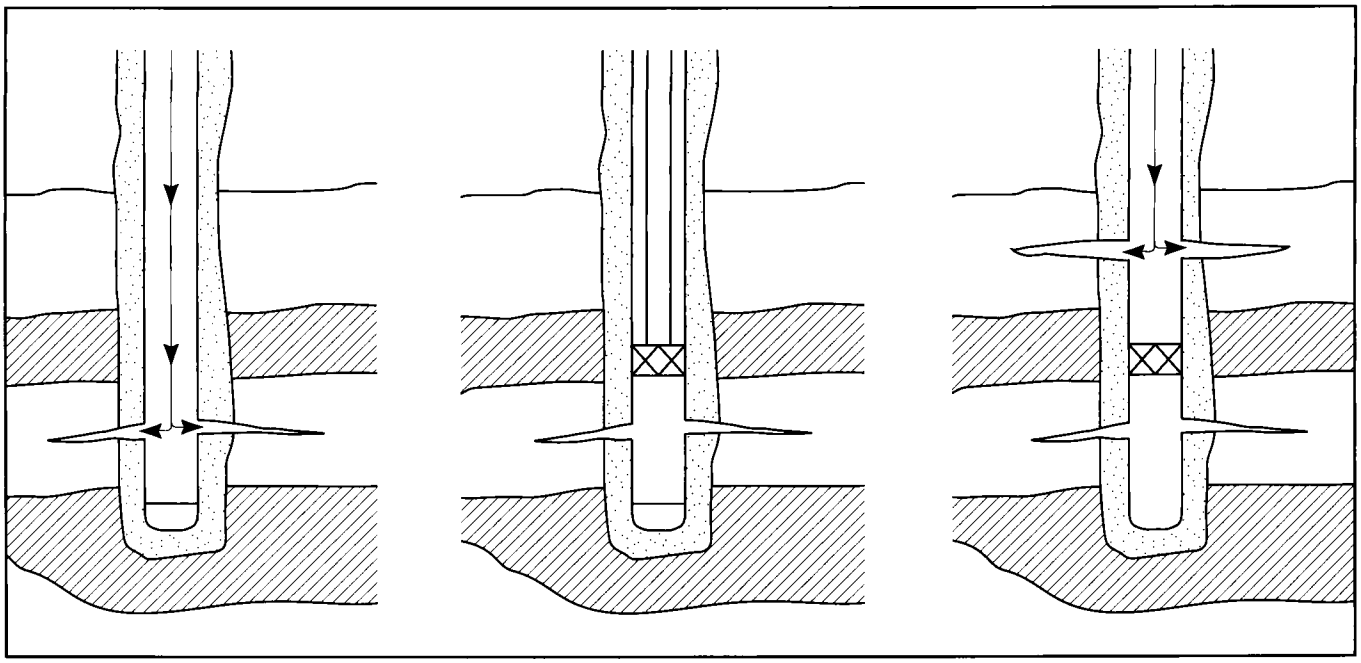

Figure P-59—Diversion of fracturing treatments into individual zones using bridge plugs.

problem if the fluids used in the treatment are of low viscosity and create an equilibrium proppant bank. With this type of proppant transport, the proppant bank will not be destroyed during the overflush of the diverter.

Using conventional ball sealers to divert fracturing stages has many of the same inadequacies as bridging materials. It is extremely difficult to predict the seating efficiency of ball sealers. This problem is even more difficult after proppant has eroded the perforations. Also, the ball sealers must be introduced into the fluid while proppant is being added. The presence of proppant will reduce the seating efficiencies, but it is impossible to predict by how much. If the ball sealers are dropped in a clean fluid stage immediately following the proppant stages, the clean fluid will overflush proppant away from the perforations until the balls finally seat.

Designing a schedule that assures precise proppant placement into multiple zones by using diverter stages is almost impossible. When several zones are open to the wellbore it is extremely difficult to calculate which zone will fracture first. The zones will almost surely be different in size and will have slightly different rock properties. Since it is not practically possible to know which zone will fracture at a given time, most hydraulic fracturing schedules using diverters are simply broken up into even stages. The uneven in-situ parameters will cause slurry placement in the separate zones to create fractures of uneven geometries and conductivities.

It is also very difficult to design and size the diverter stage so that all perforations in the zone being fractured become plugged and the other zones remain unaffected by the diverter. A diverter stage that is too large may plug the unfractured intervals before the fracturing slurry designed for that stage has been pumped. If the diverter stage is too small, the first zone may not be adequately plugged and the original fracture may continue to accept fluid. Portions of the pad fluid intended for the second interval will overflush the proppant pack away from the immediate wellbore. At the same time, the second zone is losing critical volumes of pad fluid, which may result in an early screenout.

There is also no assurance that the rock properties vary enough to prevent zones from accepting fluid simultaneously. Even if one zone initially accepts all the fluid, a second zone may begin to accept a portion of the treatment later in the procedure. As net pressure in the fracture increases so does the pressure in the wellbore. At some point the net pressure

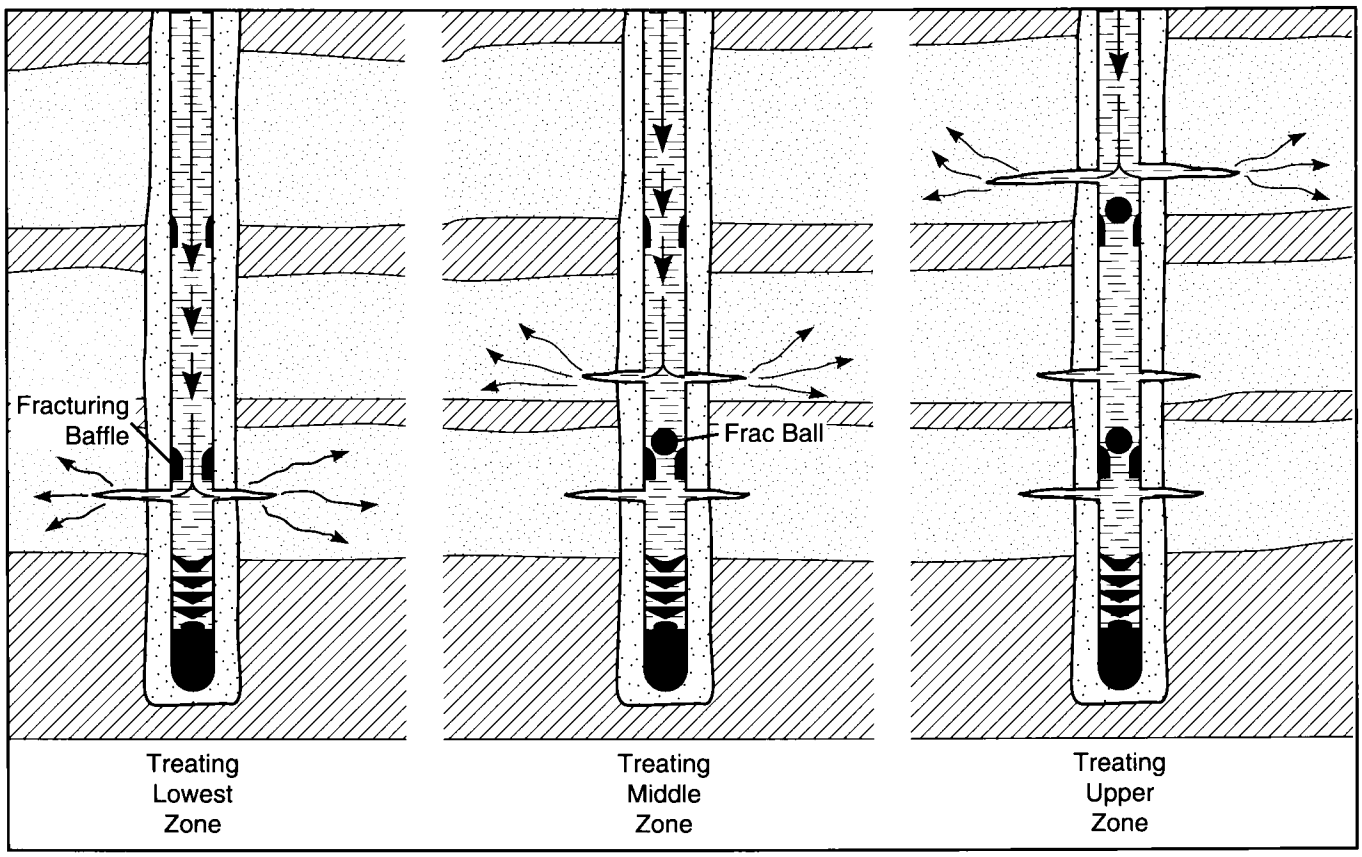

Figure P-60—Diversion of fracturing treatments into individual zones using frac balls and baffles.

becomes high enough to allow a second fracture system to accept fluid. If this scenario happens during a pad stage, the proppant placement may be unsuccessful because of insufficient pad. If a second zone opens during the proppant stages, the second zone will quickly screen out. Fracture initiation in the screened-out second zone may not happen even when a new pad fluid is started after the diverter stage.

Using diverter stages to control placement of fracturing fluids will usually result in uneven fracture geometries, poor conductivities near the wellbore and overall poor well performance. Relying on diverters to place multiple fracturing stages should be avoided unless no other isolation methods are practically feasible.

P-6.2.6: Limited Entry

Limited-entry treatments are designed to place fracturing fluids into multiple zones simultaneously. The limited-entry technique uses the pressure drop created across the perforations during pumping to divert the fracturing fluid into several different perforated intervals. Generally, a 500- to 1000-psi pressure differential is considered necessary to provide adequate control over fluid placement. Equation P-2 can be used to calculate the differential pressure across the perforations. The total flow of fluid entering into a given zone is restricted by controlling the size and number of perforations in that interval. The high pressure drop at the perforations forces fluid to go to another zone. This diversion technique has proved popular because of its simplicity and economics. The diversion does not require expensive tools; it does not require the running and retrieving of tools or making cleanout trips. The only cost for applying this type of diversion is the excess HHP needed to pump the treatment at higher pressure.

However, if this treatment is not applied correctly, each producing zone may not receive adequate treatment. Several factors must be considered when designing a limited-entry treatment. The number and size of perforations are calculated to divert the pad fluid. Smaller zones will not need as much fluid or proppant and therefore require fewer perforations. Some zones may require less than five perforations to control flow into that section. With a limited number of perforations available, the importance of the breakdown procedure becomes obvious. The loss of one or two perforations can significantly alter the flow distribution into all the zones.

Introducing sand into the fracturing fluid quickly erodes the perforations and changes the corresonding flow coefficient of each perforation. After only 10,000 lb of proppant, the pressure drop across the perforations will be drastically reduced. Therefore, diversion of the pad fluids may be successful, but diversion of the proppant-laden stages may be unsuccessful. After the perforations have been eroded, one zone is likely to accept most of the fluid.

An accurate stress profile of the wellbore is necessary to design a successful limited-entry treatment. Each zone will have a different fracture gradient and therefore will break down and fracture at different pressures. If great contrast exists between the fracture gradient of individual zones, the perforation scheme must be designed to reflect this difference.

Limited-entry designs often do not consider the net pressure effects of the fracture. It is not uncommon for a fracturing treatment to create more than 500 psi in net pressure. An imbalance in net pressures between zones can effectively negate the perforation pressure drop. Fracture height and Young's modulus are two parameters having a major effect on net pressure. Both parameters should be closely evaluated prior to the design of a limited-entry treatment.

The net pressure in the fracture is inversely proportional to the gross fracture height. Large zones will have smaller net pressures and therefore tend to accept a disproportionate amount of fracturing fluid. Very small zones will most likely remain unstimulated because they rapidly build very high net pressures and do not accept significant volumes of fracturing fluids. The global Young's modulus of the zone has a similar effect: The larger the Young's modulus, the narrower the fracture and the higher the net pressure.

One final parameter having significant impact on the successful placement of fractures via the limited-entry technique is fluid leakoff. The size of the zone and the rate the fluid is pumped into the zone directly impact the leakoff volume. With several zones accepting fluid at one time, the total pump rate into any one interval may be quite low. Zones with the lowest pump rates will generally have poor fluid efficiency, which may result in an early screenout.

Accurately placing proppant into multiple zones by using limited entry is extremely difficult. Fracture penetration and width will most likely be very irregular between zones. Smaller zones may not accept any fluid. The increased producing capabilities of several stimulated zones should be carefully examined and weighed against the economic advantages of a limited-entry treatment before this fracture procedure is used.

P-7

Equipment Hookup

Assembling the equipment in a safe, organized and efficient manner is extremely important for the success of a fracturing treatment. Thorough pretreatment planning is essential to the organizational process of coordinating equipment hookup. An inspection of the location prior to the actual treatment allows diagrams to be made that can optimize the use of available space.

Many steps of the organizational procedures are driven by common sense. Yet, small problems can easily be overlooked in the rush to get things ready. Pretreatment planning can eliminate many small problems that have the potential to develop into problems which may ultimately jeopardize the success of the treatment.

P-7.1: Safety Considerations

At no time should the safety aspects of a treatment be compromised. Safety guidelines have been developed from experiences derived from previous incidents. Many of these incidents have had great potential to seriously injure personnel or destroy valuable equipment. The inherent risks of dealing with high pressures can be greatly minimized by following simple safety procedures. Hydraulic fracture treatments can never be considered a success if an accident results in destruction of equipment or injury to personnel.

P-7.1.1: Safety Meeting

The pretreatment safety meeting ensures that all personnel on location are aware of specific dangers and required procedures relative to the treatment. Each person on location should clearly understand his or her role during the treatment as well as his or her responsibility during emergency situations. A head count must be taken to account for everyone on location. An escape route and meeting place should be agreed upon where all personnel will gather in the event of an emergency situation. Personnel who are not directly involved in the treatment should have limited location access during the actual pumping operations.

Everyone should be aware of the unique dangers of each treatment. Some locations may be in an area of H_2S, or possibly the fluids being pumped are highly flammable. As many of the possible safety problems or concerns as possible should be brought to the attention of everyone.

Maximum pressure limits should be set at this time, and every high-pressure pump operator must be aware of this limit. Instructions for pressure testing the treating iron will also be covered. The high-pressure treating line, up to the wellhead valve, should be tested to slightly above the anticipated fracturing pressure. A properly tested line will test each pump in addition to the main treating line. The pressure rating of the wellhead should be checked to make sure it exceeds the treating pressure. If the wellhead has a lower pressure rating than the anticipated treating pressure, a tree saver will be necessary to isolate the wellhead from this pressure level.

The pretreatment safety meeting is the principal means of communication where final instructions to all personnel can be given. A well-organized safety meeting helps ensure the treatment is an operational success without being a threat to human safety.

P-7.1.2: Controlling Wellhead Pressure

To ensure that well control is always maintained, the valve arrangement at the wellhead should consist of at least two valves. A "frac" valve or "master" valve should be installed above the main wellhead valve. If one valve fails to hold the pressure, the other valve can quickly be closed to control the well. It is preferable to have the main wellhead valve flanged to the casing head, rather than having a threaded connection. If a threaded connection is necessary, the condition of the threads must be thoroughly inspected for thread wear and proper taper.

P-7.1.2.1: Tree Saver

Specialized isolation tools, or tree savers, can protect a Christmas tree from damage and possible failure that results from exposure to high pressure, corrosive fluids or abrasive proppant-laden fluids. Often, the pressure rating of a wellhead is less than the pressure required to pump a stimulation treatment. Replacing the existing tree with one having a higher pressure rating is expensive and requires killing the well with potentially damaging fluids. Even if the existing tree has a sufficient pressure rating, exposure to high pressures and the treating fluids may leave it in an unsafe condition.

The tree saver can be mounted on the existing Christmas tree. A mandrel is then extended through the valves on the tree and into the tubing. The mandrel has a rubber cup assembly that seals to the walls of the tubing and prevents fluid or pressure from directly reaching the tree. Once set, the tree saver can extend the working pressure of the wellhead up to 20,000 psi. Figure P-61 shows the tree saver mandrel set in the tubing. Once the stimulation treatment is completed, the mandrel is pumped back out of the Christmas tree, and the wellhead valves can be closed.

P-7.1.2.2: Check Valves

A check valve should be placed in the treating line, on the ground, as close to the wellhead as practical. This valve allows flow in one direction; therefore, it can be pumped through but automatically closes once pumping stops. This isolates well pressures to the closed side of the check valve and prevents flow of well fluids. This type of valve is essential

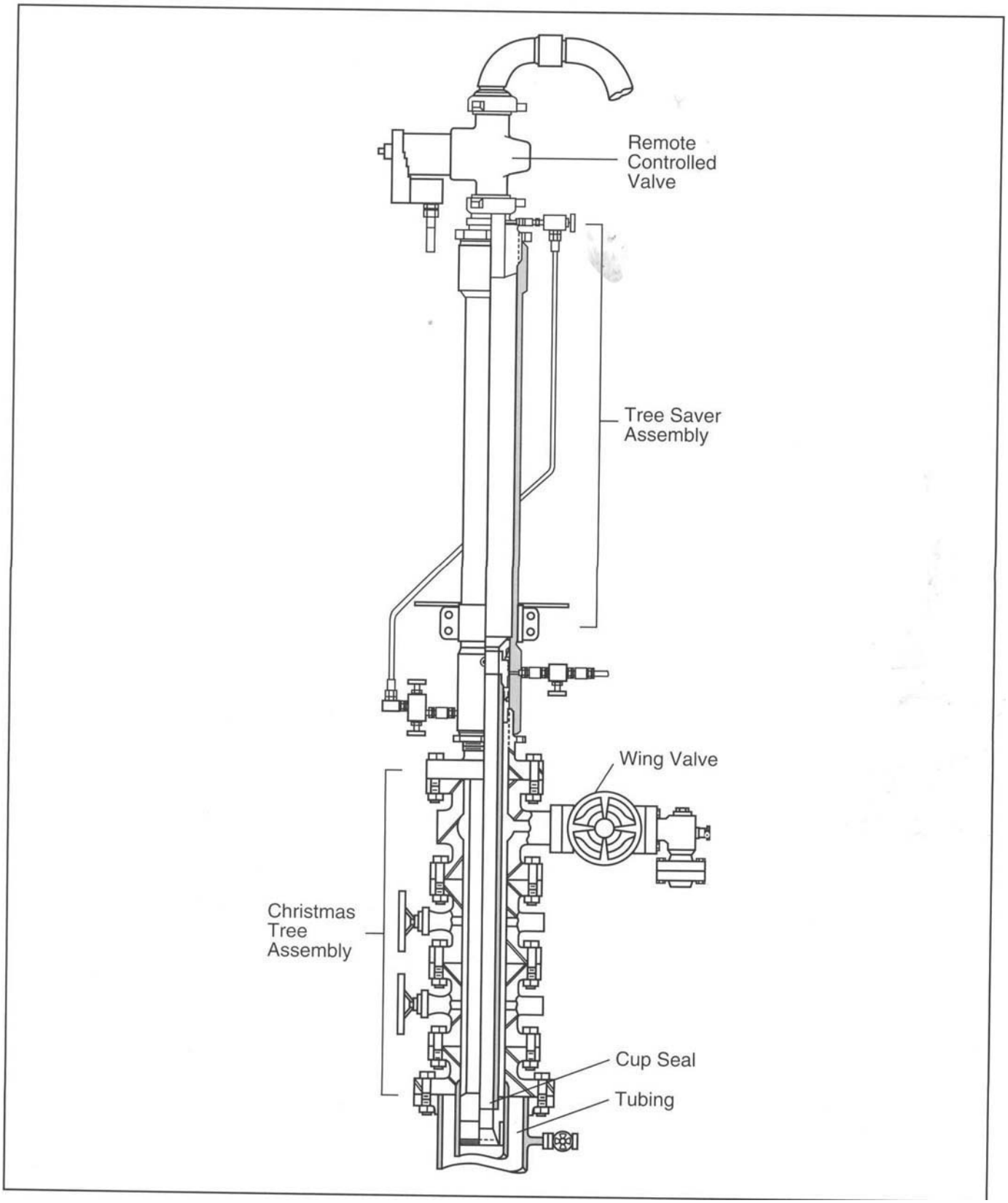

Figure P-61—Diagram of a tree saver, flanged in place with the mandrel set.

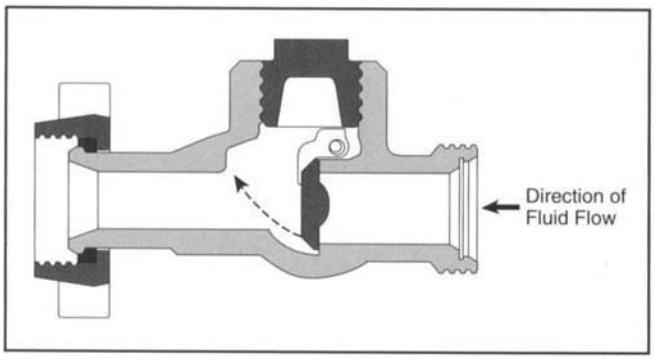

Figure P-62—Flapper-style check valve in the closed position.

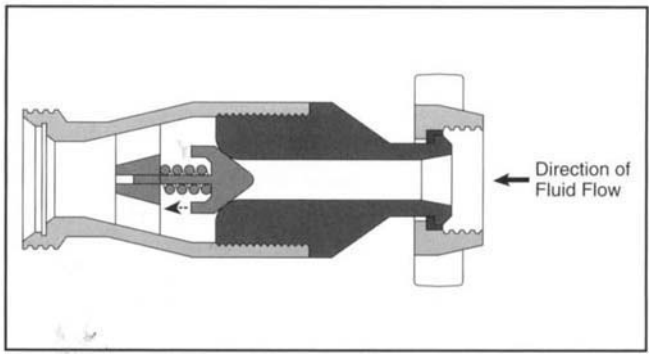

Figure P-63—Dart-style check valve in the closed position.

for controlling the well when there is a sudden loss of pump pressure, such as when a treating line fails. In these emergency situations there is no time to physically close the wellhead valves, but the check valve can automatically close almost instantaneously.

Two common types of check valves are used in high-pressure treating lines. Flapper-type check valves (Fig. P-62) are usually used in the main treating line. Proppants, solid diverting agents and ball sealers can all be pumped through this style of valve without fear of plugging or destroying its reliability. Dart check valves (Fig. P-63) are used in nitrogen and CO_2 treating lines. These valves use a spring to seat a dart and close the valve when injection stops. The dart check valve is easily cut by proppants and plugged by diverting agents; it is not recommended for use in the main treating line.

P-7.1.3: Bleedoff Lines

A bleedoff line is used to relieve pressure from the system of high-pressure treating lines once the wellhead valves have been closed. This line is not intended for extended flowback of well fluids. A permanent flowback line should be laid for long-term flow of well fluids. This line should be placed between the check valve and the wellhead control valve. If the bleedoff arrangement is misplaced, pressure will be trapped between the wellhead and the check valve, and a pressure hazard will result when the treating line is rigged down.

A choke and double-valve arrangement should be "teed" off of the main treating line to start the bleed line. One valve serves as a master valve that is always fully open or fully closed and is opened first and closed last. The second valve is slowly opened and closed to control the flow of fluid. Swivel joints should be avoided in a bleed line. When a turn in the line is necessary, teed connections should be used. This line must be restrained every 15 ft to 20 ft to prevent it from moving. Care should be taken when flowing back fluids that could potentially be carrying ball sealers. A ball sealer flow diverter can be included on the wellhead side of the choke to catch the balls and prevent them from interfering with the bleedoff procedure. The bleed line should tee off of the main treating line and be staked (Fig. P-64). Lateral, or "Y," connections should be avoided when laying the bleed line. A bleed line using a lateral is difficult to stake in place and may move when the bleed valves are opened and there is high pressure at the wellhead.

P-7.1.4: Measuring Pressure

It is imperative that the treating pressures be accurately known during a treatment. The main sensor used to measure the pressure should be placed as near to the wellhead as practically possible. Care should be taken to locate the pressure sensor on the wellhead side of the check valve to ensure that an accurate pressure is available even after the pumping operations have stopped. Should the transducer inadvertently be placed on the upstream side of the check valve, pressure readings could indicate that pressures have bled off while actual wellhead pressures remain dangerously high.

Generally, there will be several pressure sensors available for monitoring purposes in addition to the primary transducer at the wellhead. A second transducer should be identified and calibrated to the primary sensor. Pressure measurements from this transducer should be used if the primary sensor fails during the treatment. All pump trucks should have a transducer on each high-pressure pump. However, these sensors should not be used as the backup to the primary pressure transducer. The pumps may need to be shut in and isolated during the treatment, which will result in a loss of pressure measurements. The pump sensors may be used to indicate problems associated with each unit. A pressure that deviates significantly from the other sensors indicates that a pump needs to be shut in and isolated. Once the source of the abnormal pressure is located and repaired, the pump may be brought back on line.

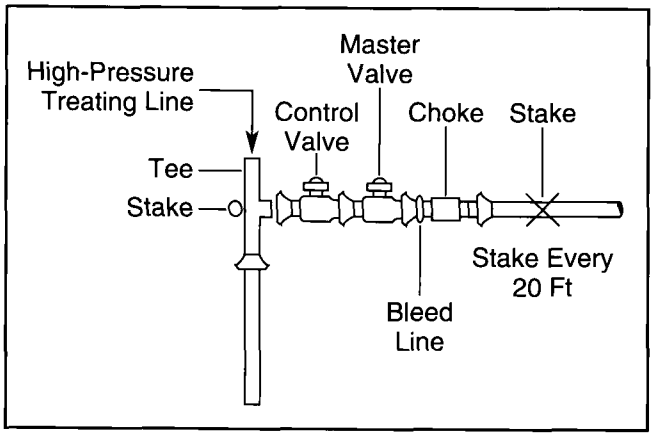

Figure P-64—Diagram of a proper bleed line hookup.

Treating Pipe Nominal OD (in.)	ID (in.)	Maximum Working Pressure (psi)	Maximum Rate (BPM)
1½	1.30	15,000	4.5
2	1.30	20,000	4.5
2	1.80	15,000	8.5
2½	2.51	4,000	16.5
3	2.75	15,000	20.0
4	3.83	6,000	40.0
5½	5.00	6,500	60.0
6⅝	6.00	6,500	100.0

Table P-12—Maximum recommended pumping rate through treating lines.

P-7.1.5: Treating Iron

The size of the high-pressure treating iron used on a given treatment will be dictated by both the anticipated rates and pressures. The smaller lines will have a higher maximum treating pressure limitation than the larger sizes. The velocity of the fluid should be limited to 45 ft/sec to minimize excessive wear of the iron. Pumping above these rates for any prolonged period of time can erode the treating iron and thereby lower the effective working pressure that the iron could be exposed to before a catastrophic failure would occur. If the designed treating rates exceed the rate limits of a given size of iron, then either a larger iron must be used or multiple lines must be laid to the wellhead. Table P-12 gives the rate and pressure limitations for the common sizes of treating iron.

The treating iron should not have welded seams or exposed threaded connections. To eliminate these seams and exposed threads, the iron and associated connections should be machined from single pieces of metal. The connections between two pieces of treating iron should have nonpressure unions (Fig. P-65). This style of connection prevents the threaded portion of the connection from being exposed to the treating pressures.

During pumping operations the treating iron will tend to slightly move and vibrate. To prevent the iron from being exposed to stress from this movement, the line is laid to provide some flexibility. Swivel joints or Chiksans allow the iron some freedom of movement. These same connections also provide a means for the iron to make corners and change directions. To ensure that straight sections of iron are completely free to move, it is recommended to have three Chiksans between any two fixed points in the line. A Chiksan will be required at each end of the straight section, plus another three-way Chiksan (the connection swivels in the center plus each end is free to rotate) is needed at one of the ends.

P-7.1.6: Spotting Equipment

Several considerations must be made when planning the spotting of the pumping equipment. Equipment should be spotted upwind at least 50 ft from the wellhead. If a service rig is on location, equipment should be spotted out of the fall line of the rig mast. Care should also be taken to spot the high-pressure pump trucks where personnel will not be exposed to the fluid end portion of the pump. If the equipment on location is to be operated from a remote site, personnel should set up in an area protected from potential high-pressure line problems (Fig. P-66). If CO_2 or N_2 equipment is present on location, it should be spotted at least 60 ft from other equipment and the wellhead.

P-7.1.7: Precautions for Flammable Fluids

Oil-base fluids should be tested for volatility before they are accepted as a fracturing fluid. The oil is generally considered safe to pump if it has a Reid vapor pressure less than 1, an API gravity less than 50° and an open cup flash point of 10°F. However, even if the fluid is considered safe to pump, several additional safety rules should be followed when pumping an oil.

Storage tanks for flammable fluids should be diked and spotted at least 150 ft from the wellhead. Spotting the fluids in this manner will help minimize exposing the wellhead to fire if problems occur during pumping. Also, all low-pressure

hoses should be enclosed in a hose cover to prevent the oil from spraying on hot engine components of the trucks, should the hose ever leak.

Care must be taken to ensure that there is no smoking on location. It is a good idea to have all personnel check matches and lighters when they arrive on location to prevent them from unintentionally lighting a match. Finally, it is a good idea to have fire-fighting equipment on location and ready to operate. In this way, a small fire may be contained before it has a chance to spread and become a major disaster.

P-7.1.8: Safety Equipment

Each person on location should wear proper safety equipment to minimize the risk of personal injury. Hard hats, hard-toed shoes and safety glasses should be the minimum level of safety equipment worn on location. Other equipment such as hearing protection, goggles, fire-retardant fabrics and filter masks should be worn if exposure to their respective conditions is a possibility. Wearing the proper safety equipment is a simple step that can be taken to create a positive safety atmosphere on location.

Additional specific safety considerations are discussed in the following sections.

P-7.2: Backside Organization

Fracturing treatments are generally organized in an orderly fashion from fluid storage (frac tanks) to the wellhead. The frac tanks must be spotted so that the remaining equipment can also fit on location. Special attention should be given to the type of equipment on location during the treatment. Often, other contractors (workover rigs, logging trucks, etc.) will be on location, and allowances for the positioning of this additional equipment must also be made. Water haulers must have access to the tanks so they can be quickly and easily filled.

Care should be taken to always spot tanks on high ground. Blending equipment is required to suck the fluid from these tanks at high rates. By placing the tanks on high ground, the net positive suction head (npsh) is increased, and the odds of losing prime on the blender are reduced. Tanks should never be spotted below the level of other equipment where the centrifugal pumps of the blender would have to lift fluid against gravity. Such placement compromises the performance of the blender, especially as fluid is drawn down and the tank nears empty.

Also, to improve fluid flow and the suction properties of the blender, a common manifold should be used to connect all the frac tanks together. In some geographical areas the frac tanks will be equipped with this type of manifold as a permanent connection. These tanks are connected with a section of flexible 8-in. hose. In other areas it may be necessary to lay a portable manifold in front of the tanks so that all the frac tanks can be tied together.

The quality and condition of frac tanks directly impact the

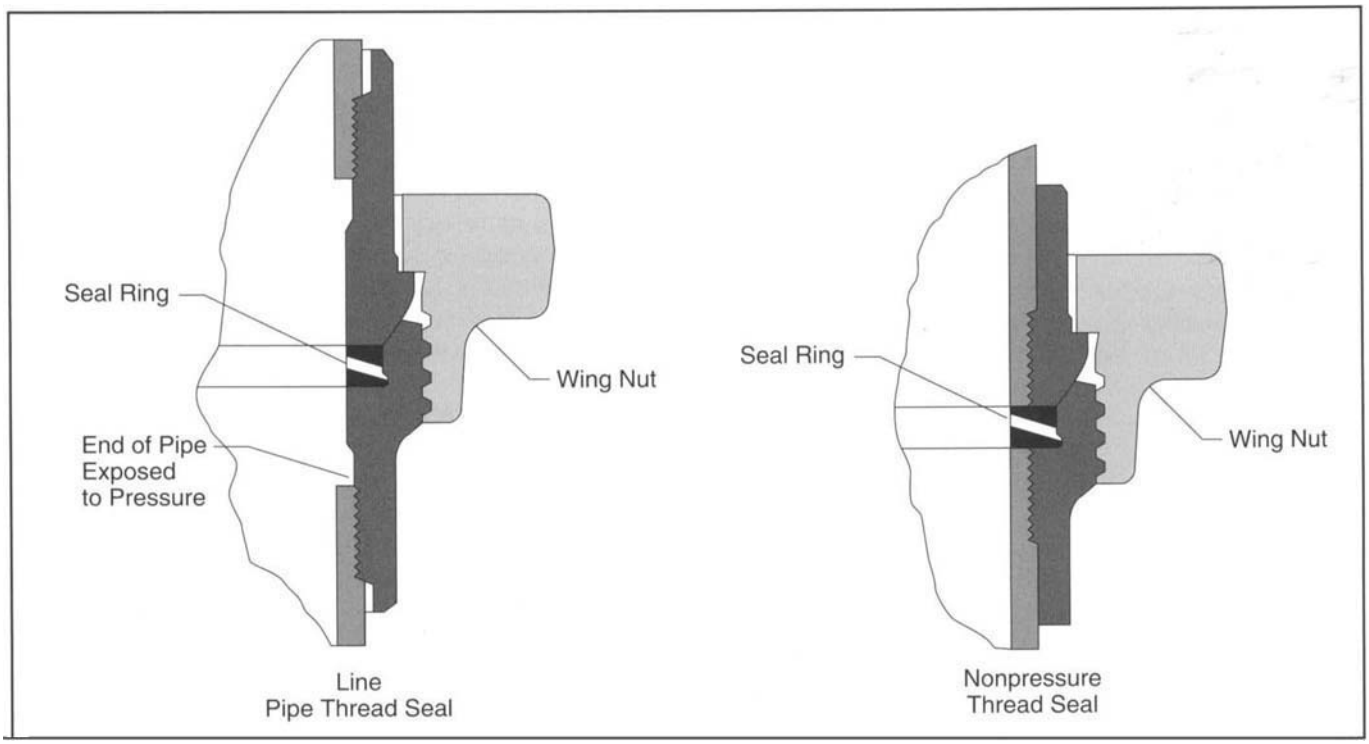

Figure P-65—Diagram showing the differences between ordinary line pipe thread seal and a nonpressure thread seal.

ultimate success of the treatment. All tanks must be emptied and cleaned after each treatment and before they are refilled for subsequent jobs. If not removed during cleaning operations, contaminants from previous use can undermine the fluid quality.

Lined tanks help to ensure the fluid quality after fluid has been added to the tank. The lining prevents oxidation byproducts from contaminating the fluids. Excessive metal ions can aggravate break and crosslink problems of standard fracturing fluids. The lining itself should be periodically examined to ensure that holes are not present. Once holes have developed, fluid can get between the lining and the tank wall. Water that has penetrated the lining may become a source of bacteria or oxidation since it is never completely drained from the tank.

All valves must be checked to ensure they are in working order. Frac tanks with bull plugs covering a valve should never be used since it is impossible to determine if the valve is either leaking or missing. If the bull plug is removed after the tank is filled, significant amounts of fluid may spill before another connection can be made to control the flow. A frac tank spill is potentially disastrous when oil-base fluids are pumped. Many of the worst location fires involving stimulation treatments have been linked to frac tank leaks and faulty valves. Even when the fluids are water base, bull plugs should not be removed from the frac tank. Large amounts of water, expensive premixed chemicals and time may be lost.

In different regionalized areas the style of the "standard" frac tank will vary significantly. Some of the most common tank styles in use today are rectangular flat bottom, rectangular V-bottom, horizontal cylindrical and upright cylindrical. The shape of the rectangular V-bottom and the horizontal cylindrical tanks helps minimize the amount of fluid left in the tank bottoms. These styles can generally be very nearly emptied, leaving only a few barrels of fluid, before blender suction is lost. The amount of fluid left in the tanks is

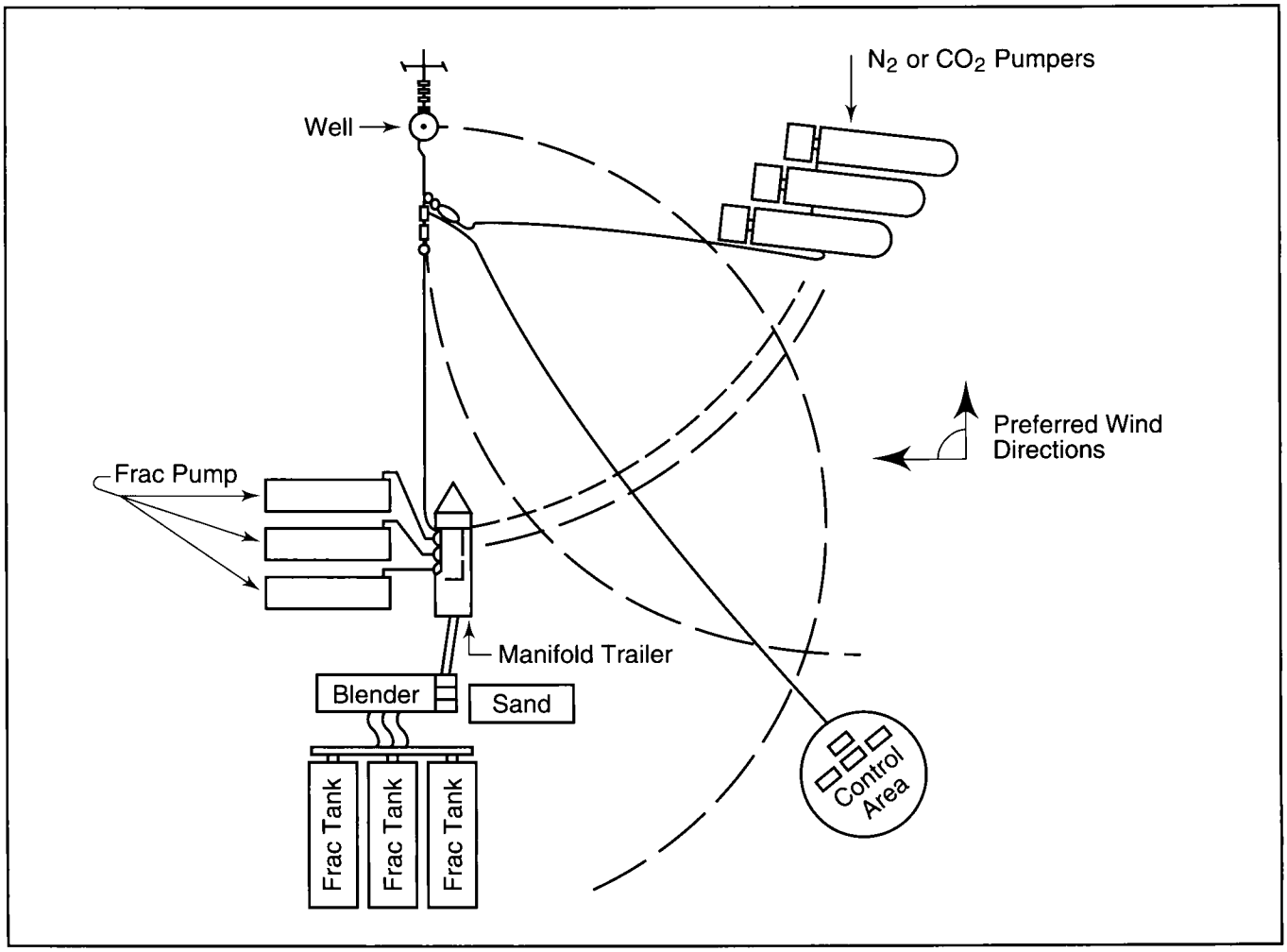

Figure P-66—Location schematic showing safe spotting distances.

becoming a larger concern as environmental issues become more prominent.

It is important to be able to quickly determine the volume of fluid in a frac tank. The fluid volume may be determined by using strap charts that display a volume in accordance to a measured level of fluid. Strap charts for the standard types of frac tanks currently in use are shown in Tables P-13 through P-16.

P-7.3: Proppant Storage and Delivery

The total volume of proppant, the rate of proppant delivery and the number of different proppants to be used in the treatment must be considered when choosing the proper vessel for storing proppant on location. Small treatments may only require dump trucks to deliver the proppant to the blender. Bobtail dumps and trailer dumps are routinely used throughout the industry. These units are spotted directly over the blender hopper and gravity feed the proppant at a controlled rate through a chute. Care should be taken to ensure that the hydraulic lift mechanism is in good working order, allowing the dump to be completely raised. If the dump is not completely raised, the proppant delivery rate may not be sufficient, especially as the dump nears empty. This can be very critical at high proppant concentrations where the delivery rate needs to be the highest. To prevent problems with the proppant delivery rate, it is a good idea to bring out extra proppant if capacities allow. Bobtailed units will generally haul between 250 ft^3 and 450 ft^3 of proppant, and trailer units will haul up to 600 ft^3. The maximum delivery rate of these units depends on the chute size and placement but is generally between 3000 lb/min and 7000 lb/min of proppant.

Moving proppant dumps during a treatment should be

Inside Diameter (ft)	Inside Diameter (in)	Capacity per ft of Depth (bbl)	Inside Diameter (ft)	Inside Diameter (in)	Capacity per ft of Depth (bbl)	Inside Diameter (ft)	Inside Diameter (in)	Capacity per ft of Depth (bbl)	Inside Diameter (ft)	Inside Diameter (in)	Capacity per ft of Depth (bbl)
2	0	0.560	4	0	2.238	8	0	8.952	14	0	27.418
	1	0.607		1	2.332		3	9.521		3	28.405
	2	0.657		2	2.429		6	10.107		6	29.411
	3	0.708		3	2.527		9	10.710		9	20.434
	4	0.762		4	2.627	9	0	11.331	15	0	31.474
	5	0.817		5	2.729		3	11.969		4⅝	33.151
	6	0.874		6	2.822		6	12.625		6	33.607
	7	0.934		7	2.939		9	13.298	16	0	35.811
	8	0.995		8	3.046	10	0	13.989		6	38.084
	9	1.058		9	3.156		3	14.697	17	0	40.427
	10	1.123		10	3.268		6	15.422		6	42.840
	11	1.190		11	3.382		9	16.166	18	0	45.323
3	0	1.259	5	0	3.497	11	0	16.926		6	47.875
	1	1.330		3	3.856		3	17.704	19	0	50.499
	2	1.403		6	4.232		6	18.500		6	53.191
	3	1.478		9	4.625		9	19.320	20	0	55.954
	4	1.554	6	0	5.036	12	0	20.143		6	58.787
	5	1.633		3	5.464		3	20.991	21	0	61.690
	6	1.714		6	5.900		6	21.857		6½	64.916
	7	1.807		9	6.374		9	22.740	22	0	67.705
	8	1.881	7	0	6.854	13	0	23.641			
	9	1.967		3	7.353		3	24.559			
	10	2.056		6	7.869		6	25.494			
	11	2.146		9	8.402		9	26.447			

Table P-13—Capacity of vertical cylindrical tanks.

minimized. Even with good operators, it takes 3 to 5 min to move a dump into place and raise it to allow proppant delivery. Excessive movement of proppant dumps increases the chance of not pumping the proper proppant concentration. If a treatment is designed with large proppant volumes requiring the movement of the dump trucks during pumping procedures, other proppant storage equipment should be considered.

Upright storage silos can hold up to 4000 ft^3 of proppant. These silos rely on gravity to feed the blender and do not require hydraulic power to operate. This type of storage eliminates the need for moving trucks around during most treatments because of the quantity of proppant they hold. However, use of this type proppant storage requires considerable preplanning since the units are not mobile once they are spotted. Specialized cranes are required to raise these units into place and to lower them for transportation.

The conveyored sand bin is the most common unit used to deliver proppants to the blender. These units have several compartments for storing proppant. Each compartment has a set of hydraulically controlled doors at the bottom. When these doors are opened, proppant falls from the container onto a conveyor belt that leads to the blender. Storage capacity of these units ranges between 2500 ft^3 and 4000 ft^3. Hydraulically powered conveyors can unload these units at proppant delivery rates approaching 25,000 lb/min. When

Depth (in.)	Volume (bbl)	Depth (in.)	Volume (bbl)	Depth (in.)	Volume (bbl)	Depth (in.)	Volume (bbl)	Depth (in.)	Volume (bbl)
1	0.5	26	73.2	51	186.7	76	304.9	101	418.2
2	1.6	27	77.3	52	191.6	77	309.7	102	422.1
3	3.0	28	81.4	53	196.5	78	314.6	103	426.0
4	4.6	29	85.5	54	201.4	79	319.3	104	429.9
5	6.5	30	89.8	55	206.3	80	324.2	105	433.7
6	8.5	31	94.9	56	211.3	81	329.0	106	437.4
7	10.7	32	98.3	57	216.2	82	333.7	107	441.1
8	13.0	33	102.7	58	221.2	83	338.4	108	445.2
9	15.6	34	107.1	59	225.1	84	343.1	109	448.0
10	18.2	35	111.5	60	231.0	85	347.8	110	451.5
11	21.0	36	116.0	61	236.1	86	352.4	111	454.8
12	23.8	37	120.5	62	241.0	87	347.8	112	458.0
13	26.8	38	125.0	63	244.7	88	361.7	113	461.1
14	29.9	39	129.7	64	246.0	89	366.2	114	464.2
15	33.0	40	134.3	65	250.9	90	370.7	115	467.1
16	36.3	41	138.9	66	255.7	91	375.2	116	469.9
17	39.7	42	143.6	67	260.6	92	379.6	117	472.5
18	43.1	43	148.3	68	265.6	93	384.0	118	475.1
19	46.6	44	153.0	69	270.5	94	388.4	119	477.6
20	50.2	45	157.8	70	275.5	95	392.7	120	479.8
21	53.9	46	162.5	71	280.4	96	397.0	121	482.0
22	57.6	47	167.4	72	285.3	97	401.7	122	484.0
23	61.5	48	172.1	73	290.2	98	406.0	123	485.7
24	65.4	49	177.0	74	295.1	99	410.1	124	487.2
25	69.3	50	181.9	75	300.0	100	414.2	125	488.5
								126	489.2
								127.5 (full)	489.5

Table P-14—Gauge chart for horizontal cylindrical tank, 500-bbl capacity.

Depth (ft)	Depth (in)	Volume (bbl)	Depth (ft)	Depth (in)	Volume (bbl)	Depth (ft)	Depth (in)	Volume (bbl)	Depth (ft)	Depth (in)	Volume (bbl)
			3	0	125.0	6	0	267.5	9	0	413.5
0	1	3.5		1	129.5		1	271.5		1	417.0
	2	7.0		2	133.7		2	275.5		2	420.0
	3	10.4		3	136.1		3	279.5		3	423.0
	4	13.8		4	138.8		4	283.5		4	426.2
	5	17.3		5	143.0		5	287.5		5	429.5
	6	20.8		6	146.8		6	291.5		6	432.7
	7	24.4		7	150.5		7	295.5		7	436.0
	8	27.8		8	154.5		8	299.5		8	439.0
	9	31.2		9	158.2		9	303.0		9	442.0
	10	34.8		10	162.2		10	307.5		10	445.0
	11	38.4		11	166.2		11	312.0		11	448.0
1	0	41.8	4	0	170.2	7	0	316.0	10	0	450.5
	1	45.0		1	174.2		1	320.0		1	453.0
	2	48.3		2	178.2		2	324.0		2	455.5
	3	52.0		3	182.5		3	328.0		3	458.0
	4	55.5		4	186.5		4	332.2		4	460.5
	5	59.1		5	190.5		5	336.0		5	463.0
	6	62.6		6	194.5		6	340.2		6	465.5
	7	66.0		7	198.5		7	344.0		7	468.0
	8	69.5		8	202.5		8	348.2		8	470.0
	9	73.1		9	206.5		9	352.5		9	472.0
	10	77.0		10	210.7		10	356.0		10	474.0
	11	80.5		11	214.5		11	360.5		11	475.8
2	0	83.6	5	0	218.7	8	0	364.5	11	0	477.5
	1	87.0		1	222.9		1	368.5		1	479.3
	2	90.5		2	227.0		2	372.5		2	481.0
	3	94.0		3	231.0		3	376.5		3	482.5
	4	97.5		4	235.0		4	380.8		4	484.0
	5	100.5		5	239.0		5	385.0		5	485.5
	6	104.0		6	243.2		6	389.0		6	486.6
	7	107.5		7	247.2		7	393.0		7	487.8
	8	111.0		8	251.5		8	397.0		8	488.9
	9	114.5		9	255.5		9	401.0		9	490.0
	10	118.0		10	259.5		10	405.0		10	491.0
	11	122.5		11	263.5		11	409.0		11	492.0
									12	0	492.9
										1	493.7
										2	494.5
										3	495.2

Table P-15—Gauge chart for flat-bottom tanks, 500-bbl capacity.

Depth (ft)	Depth (in)	Volume (bbl)	Depth (ft)	Depth (in)	Volume (bbl)	Depth (ft)	Depth (in)	Volume (bbl)	Depth (ft)	Depth (in)	Volume (bbl)
			3	0	124.8	6	0	272.9	9	0	422.7
0	1	0.5		1	128.4		1	277.1		1	426.4
	2	1.9		2	132.2		2	281.3		2	430.0
	3	4.1		3	136.0		3	285.5		3	433.6
	4	7.4		4	139.8		4	298.7		4	437.1
	5	11.1		5	143.7		5	293.9		5	440.5
	6	14.7		6	146.7		6	298.1		6	443.8
	7	18.4		7	151.7		7	302.2		7	447.0
	8	22.1		8	155.8		8	306.4		8	450.1
	9	25.7		9	159.9		9	310.6		9	453.1
	10	29.4		10	164.1		10	314.8		10	456.0
	11	33.1		11	168.3		11	319.0		11	458.9
1	0	36.7	4	0	172.5	7	0	323.2	10	0	461.7
	1	40.4		1	176.6		1	327.4		1	464.3
	2	44.1		2	180.8		2	331.5		2	466.9
	3	47.7		3	185.0		3	335.7		3	469.4
	4	51.4		4	189.2		4	340.0		4	471.9
	5	55.1		5	193.4		5	344.1		5	474.2
	6	58.8		6	197.6		6	348.3		6	476.4
	7	62.4		7	201.8		7	352.5		7	478.6
	8	66.1		8	205.9		8	356.7		8	480.4
	9	69.8		9	210.1		9	360.9		9	482.6
	10	73.4		10	214.3		10	365.0		10	484.5
	11	77.1		11	218.5		11	369.2		11	486.3
2	0	80.8	5	0	222.7	8	0	373.4	11	0	488.0
	1	84.4		1	226.9		1	377.6		1	498.7
	2	88.1		2	231.1		2	381.8		2	491.2
	3	91.8		3	235.3		3	386.0		3	492.7
	4	95.4		4	239.4		4	390.2		4	494.1
	5	99.1		5	243.6		5	394.3		5	495.3
	6	102.8		6	247.8		6	398.5		6	496.5
	7	106.4		7	252.0		7	402.8		7	497.6
	8	110.1		8	256.2		8	406.9		8	498.7
	9	113.8		9	260.4		9	411.0		9	499.6
	10	117.4		10	264.6		10	415.0		10	500.0
	11	121.1		11	268.7		11	418.9			

Table P-16—Gauge chart for V-bottom frac tanks, 500-bbl capacity.

extremely large volumes of proppant are required for a treatment, conveyored sand bins can be positioned to offload their proppant onto a second conveyor that feeds the blender. Spotting sand bins in this arrangement allows millions of pounds of proppant to be easily stored and pumped.

Regardless of the type bulk proppant storage used, great care and planning must go into treatments where proppant types will be changed during the treatment. Often, several different mesh sizes of proppant are used, and it is becoming increasingly common to tail in fracture treatments with resin-coated proppants to eliminate proppant flowback. The time and procedures required to change proppant types during the treatment must be considered in the pretreatment planning.

P-7.4: High-Pressure Pumps

High-pressure pumps should be spotted close enough to the blender so that the centifugal pumps of the blender can easily feed slurry at a high enough net positive suction head to the intake manifolds on the pumps. On large treatments with many pumps, a manifold trailer (Fig. P-67) may be used to consolidate the hookup. The manifold trailer helps organize both the low-pressure suction hookup and the high-pressure discharge hookup.

The number of suction hoses between the blender and the pumps is determined by the pumping rate. Standard 4-in. suction hoses of 25-ft length or less will allow roughly 12 BPM of fluid flow to the pump. If higher rates are attempted through one hose, insufficient net positive suction head may result and cause the pump to cavitate and run roughly. If rates by one pump are expected to exceed 12 BPM, another suction hose should be used to provide fluid to the intake manifold.

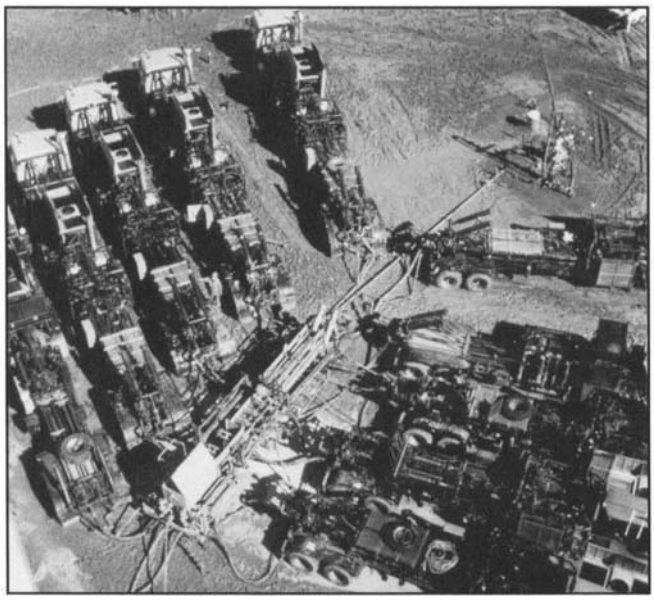

Figure P-67—High-pressure pump trucks around the manifold trailer.

On low-rate treatments, the hose diameter may have to be decreased to maintain a high enough fluid velocity inside the hose, especially on high proppant concentration treatments such as a foam frac. If the pump rate is 5 BPM or less, a 3-in. hose may be required to prevent proppant from settling out in the hose. If the fluid velocity in a hose drops to a point where proppant settling is severe, the hose may actually plug off and starve the pump for fluid.

Each pump truck should have an isolation valve where it is tied into the main treating line to allow minor repairs during pumping operations. Without this valve the pump would always be exposed to the treating pressure. Behind the isolation valve a bleedoff valve should be present so that the pressure on the pump can be safely bled off any time the pump is brought off line.

The iron on the pump should be of a size that is compatible with the rate and pressure capabilities of the pump. If the pump and iron are not performance matched, the effective efficiency of the pump will be minimized.

Recirculation lines between the blender and the suction manifold of the high-pressure pump may be needed when high proppant concentrations are pumped. At high concentrations the proppant may settle out of the slurry within this manifold. Settling problems are more likely to occur at low pump rates and in low-viscosity fluids. The recirculation line keeps fluid moving within the suction manifold and prevents proppant from settling out. Fracturing treatments using foamed fluids often require a recirculation line.

P-7.5: Treatment Monitoring

Monitoring of hydraulic fracture treatments has evolved from simple pressure strip charts to sophisticated computer recording and display. The information displayed by these instruments provides the supervising engineers with diagnostics on how the treatment is proceeding. Real-time execution decisions are made during the treatment based on this information.

P-7.5.2: Computer Monitors

As treatments have become more complex, the amount of information required to adequately control the job has greatly increased. Computerized monitoring systems can track and record numerous sensor inputs, making them ideal for monitoring complex treatments. These systems can also use data to create a presentation that makes interpretation easy. Examples of the simple calculations routinely performed by the computer monitors are:

- Several individual pump rates can be added together to show the total pump rate.
- Time scales can be easily changed so that data are plotted against a log of time or square root of time rather than linear time.
- Surface pressures, fluid frictions and fluid densities are combined to calculate bottomhole pressures.

The real-time treatment of data has proved to be invaluable when monitoring complex treatments.

In some cases these same computers not only monitor but also control additive rates based on a predetermined schedule. Process control of blending and pumping operations is proving to be a major advancement in treatment execution. Proppant schedules are now ramped rather than added in stages. The field computer uses input from density sensors to control the amount of proppant added at the blender. Very small but precise changes can be made in the proppant addition, providing the accuracy needed for the always increasing ramped schedule. Viscosities of fracturing fluids may also be changed by process control. Polymer loadings are tailored throughout the job to deliver the desired fluid properties. The computer-controlled execution helps eliminate human-induced errors that can be detrimental to the treatment (Fig. P-68).

Figure P-68—Computer system with multiple processors capable of simultaneous monitoring, control and simulation.

P-7.5.2: Sensors

Sensors acquire input data so the numerous operations taking place on location can be tracked and accounted for. Most any parameter needed for evaluating a fracturing treatment can be followed with sensors. Pressure, rate, density, temperature, pH and viscosity are some of the most common parameters requiring sensor output.

Two basic types of signals are sent by most sensors to the data-acquisition device. Frequency sensors deliver a pulsed signal. This type of sensor is often used in rate measurements where the frequency of these pulses is directly proportional to the rotational speed of a pump. Analog sensors deliver a current signal with a defined range. Common signal ranges are 0-20 milliamp or 4-20 milliamp. The sensor is then calibrated to give minimum and maximum values based on the signal range.

P-7.5.2.1: Pressure Sensors

Pressure transducers measure the deformation of a sensing material to provide a pressure reading. Specially designed strain gauges are bonded to precision-machined metals that subtly deform as they are exposed to pressure. The quality of pressure transducers varies both in accuracy and resolution. The accuracy of a gauge is determined by how closely it measures pressures over an entire pressure span. The resolution indicates the size of pressure increment needed to affect the measurement.

Earlier pressure transducers used a hydraulic separator hose between the high-pressure connection and the sensor electronics. The pressure actually moved a pressure indicator in a sight glass, and electronics measured the movement of the pressure indicator. This type of sensor was very reliable but did not provide the accuracy or resolution required for detailed evaluation.

P-7.5.2.2: Density Sensors

For years radioactive densitometers have been used to measure density. This technique provides a nonintrusive, continuous density measurement for any fluid flowing in a pipe. The technique is based on the absorption of gamma rays by the measured fluid.

The densitometer consists of:

- A radioactive source on one side of a pipe.
- A gamma ray detector on the other side of the pipe.
- An electronic panel to provide a signal reading.

As fluid passes through the pipe, gamma rays emitted by the source are attenuated in proportion to the fluid density. The detector senses the gamma rays transmitted through the fluid and converts this signal into an electrical signal (Fig. P-69). The electronic panel processes the electric signal into a density indication. A denser material absorbs more radiation, resulting in the detection of fewer gamma rays. Thus, the signal output of the detector varies inversely with respect to density.

Most densitometers use a radioactive isotope with an extended half-life. A densitometer using cesium 137 can

function accurately for nearly 30 years if the electronics are properly maintained.

Care should be taken to ensure that density measurements are always taken under pressure. Air can become entrained in a slurry when proppant is added. This air has the effect of increasing the volume of the slurry without a substantial increase in mass. Figure P-70 shows that nearly 100 psi of pressure is necessary to eliminate most of the effects of air entrainment.

A good densitometer will be accurate to within 0.1 ppg over a density range of 8.0 to 25 ppg. This remarkable accuracy can still lead to errors, especially when using a densitometer to detect proppant totals when treatments go to high proppant concentrations. If the fluid and proppant densities vary by 0.1 ppg and the densitometer has an accuracy level of 0.1 ppga, an error of nearly 10% can occur at proppant concentrations above 10 ppga because the densitometer is actually measuring radioactive adsorption, which is proportional to density. The value of pounds per gallon must be calculated from the density reading. This calculation at higher densities is less accurate because a small change in absolute density means a larger change in pounds per gallon. As an example, the density reading comparing no proppant to 3 ppga sand is 8.43 lb/gal and 10.06 lb/gal, respectively (a change in density of 1.63 lb/gal). However, a similar change in density (1.52 lb/gal) from 13.96 lb/gal to 15.48 lb/gal corresponds to a change from 15.0 to 23.5 ppga.

P-7.5.2.3: Rate Sensors

Several styles of rate sensors are used for monitoring high-pressure treatments. Some of the common rate sensors include pump stroke counters, turbine flowmeters, magnetic flowmeters and venturi flowmeters for gaseous fluids. Pump stroke counters generally measure the rotational speed of the pump. Each full rotation of the pump moves the pump plunger through one complete cycle. By knowing the volume of each pump stroke, the number of pump strokes and the pump's efficiency, a rate can be easily calculated. This type measurement is advantageous for high-pressure pumps that are pumping high volumes of solids, as is the case in pumping proppants during a fracturing treatment. The presence of solids or varying fluid rheology does not affect this type of measurement. However, if the pumps are not fully primed the actual rate may be significantly lower than the stroke counters indicate.

Turbine flowmeters are designed primarily for measuring clean fluids. As fluid is pumped through the flowmeter housing, turbine blades are forced to rotate. Each of the blades on

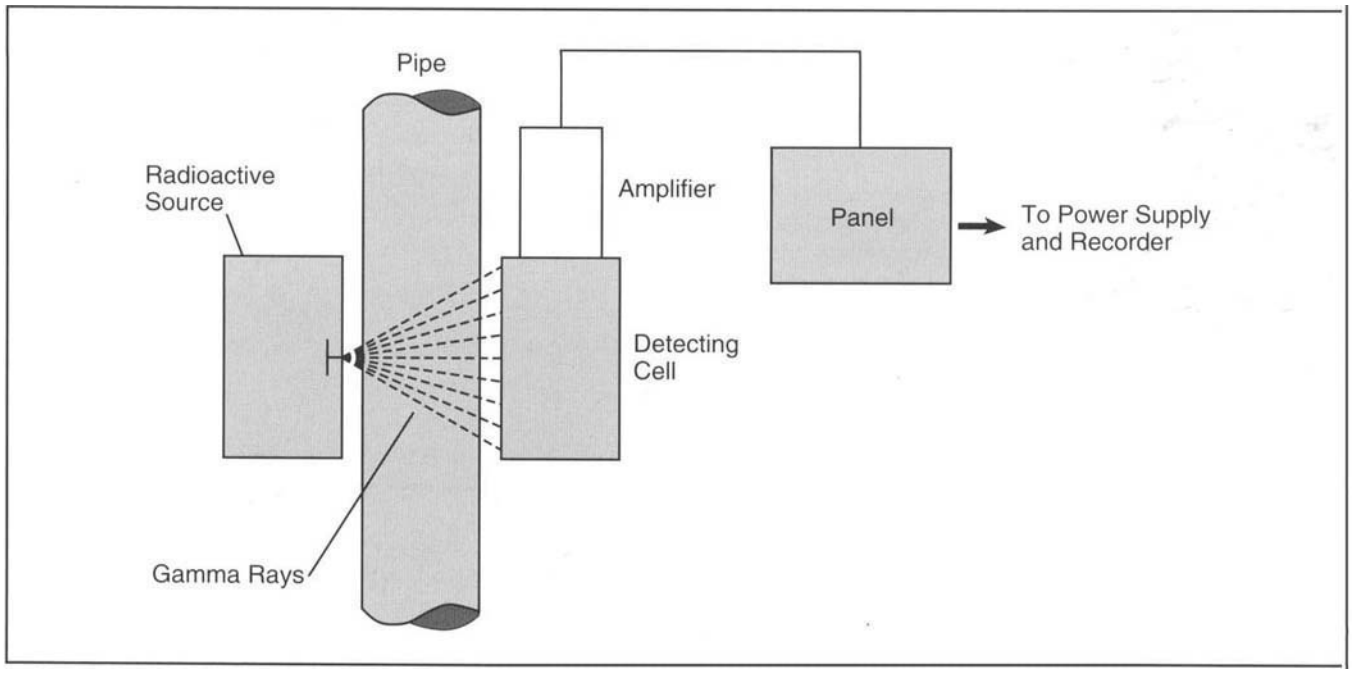

Figure P-69—Principle of radioactive densitometers.

the rotor creates a small pulse as it passes beneath a magnetic pickup. Each revolution of the rotor generates a distinct pattern of pulses equal to the number of turbine blades. The rotational speed of the rotor defines the flow rate, while each pulse defines a volume of liquid passing through the meter. Most turbine meters are calibrated with fresh water. As the viscosity of the measured fluid increases, the rotor speed decreases proportionally. Therefore, the turbine flowmeter should be calibrated with the actual fluid to be measured to ensure accuracy. These meters are useful for measuring liquid additive rates but have limited value when used in proppant slurries. Fracturing fluid viscosities often vary throughout a treatment, especially when proppant is introduced. The proppant also tends to erode the turbine blades, further reducing the accuracy of the flow measurement.

Magnetic flowmeters are becoming more popular for measuring treating fluid rates. These flowmeters measure the rate of fluid flow in a line, similarly to a turbine flowmeter, but they do not have any intruding parts that can be affected by the changing viscosities or proppant addition. The electromagnetic flowmeter operates on Faraday's law of electromagnetic induction. When a conductor is moved across a magnetic field, an electromagnetic force is induced in the conductor. The electromagnetic force is orthogonal to both the direction of movement and to the magnetic field itself. The electromagnetic flowmeter uses a pair of coils mounted on the outside of a nonmagnetic pipe. An electrical current flows through the coils to produce the magnetic field. The electromagnetic force is created when fluid (a conductive material) passes through the coils. The biggest limitation of the electromagnetic flowmeter is that it cannot be used with oil-base fluids.

To accurately measure nitrogen or carbon dioxide rates, a venturi flowmeter should be used. The velocity of the gas through the venturi is determined by measuring the pressure drop across a reduced area (Fig. P-71). The line pressure and temperature must also be measured to compensate for any change in density.

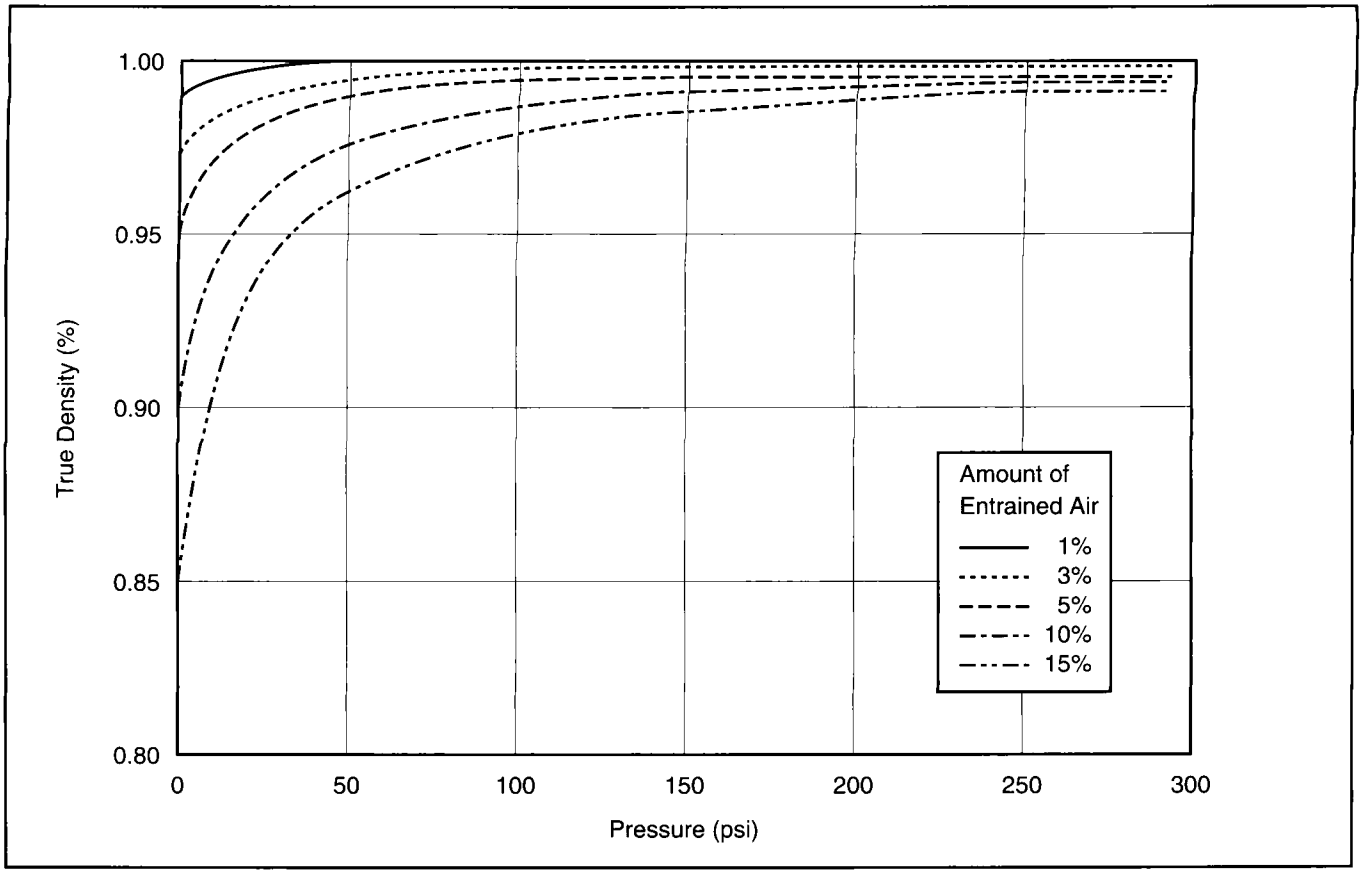

Figure P-70—Effect of entrained air on slurry density.

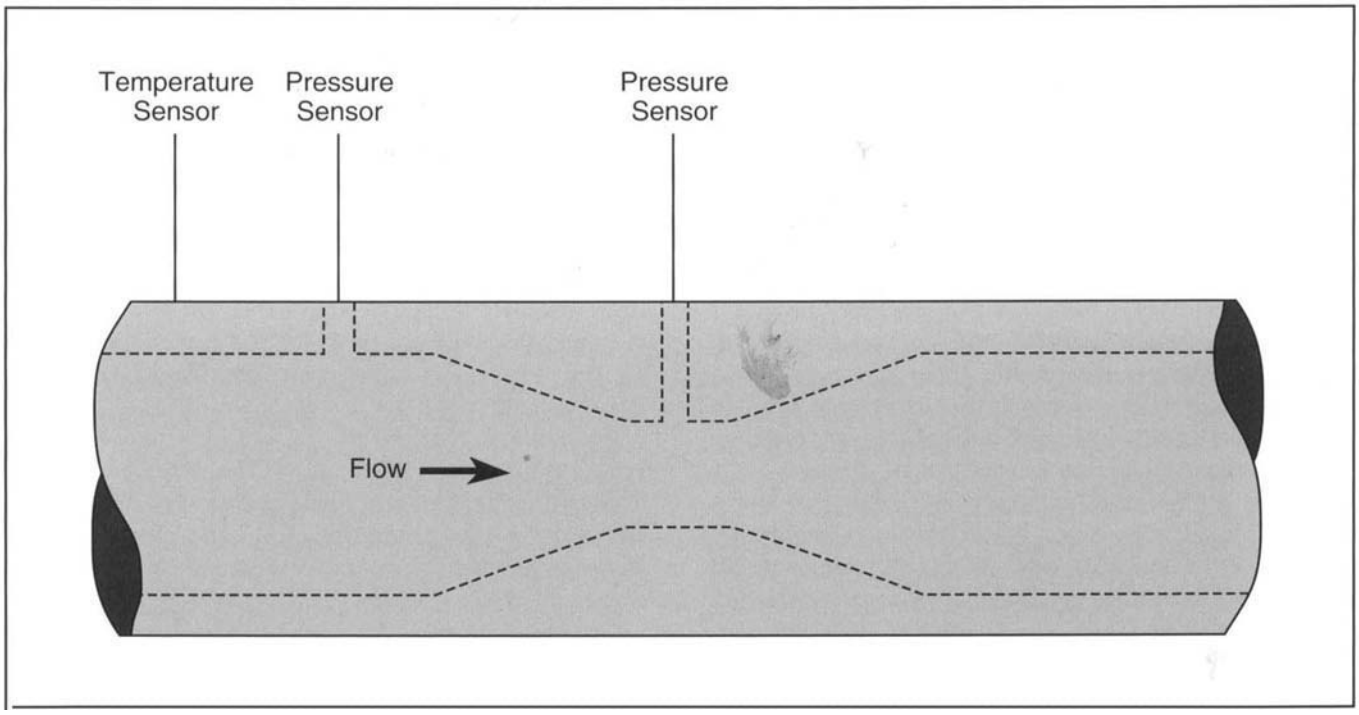

Figure P-71—Principle of venturi flowmeter.

P-8

Location Quality Assurance

A significant effort is made in the design process to determine an optimum fracturing treatment. An equal effort toward quality assurance ensures that the treatment is executed as designed. Simple quality assurance steps can greatly increase the odds of success for a hydraulic fracturing treatment.

P-8.1: Fluids

The fracturing fluid must hydraulically create the fracture and transport the proppant to make an effective conduit for production. If the fluid does not have the rheological or leakoff properties used in the design process, the ultimate well performance will suffer. Great care must be taken to ensure that the fluid performs as designed. Several simple tests performed on location can detect problems before pumping operations begin. At this time, steps can be taken to correct any deficiencies, ensuring that the rheological properties of the fluid are adequate.

P-8.1.1: Initial Water Quality

Water used for the fracturing treatment must meet certain standards before the fracturing fluids are prepared. Meeting these standards greatly increases the odds that the fluids will perform as designed. The temperature of the mix water should be between 50°F and 100°F for proper hydration. Certain polymers may hydrate at temperatures lower than 40°F if they are treated with buffer packages. However, mixing fluids at low temperatures may result in low viscosities because some of the polymer may not completely hydrate before settling out. At temperatures above 100°F, hydration may occur so quickly that the individual powdered polymer crystals do not have sufficient time to disperse. If the polymer crystals are not well separated, the gel will develop lumps, or "fish eyes." Low viscosities result from the unhydrated polymer on the inside of the fish eye.

The rate of hydration for polymers is very pH sensitive. The time needed to hydrate a guar is seen in Fig. P-72. In general, the pH of the water should be between 6 and 8 to ensure proper hydration of a guar or derivitized guar polymer. A pH greater than 8 retards the hydration development of some polymers and can completely stop the hydration of others. A pH less than 6 may result in lumping of the gel. The viscosity of the gelled fluid may prematurely degrade if the pH is lower than 4.

A simple chlorides test indicates if the proper amount of KCl has been added to the water. However, this test cannot distinguish between KCl, NaCl, $CaCl_2$ or other common chlorides. Table P-17 shows the amount of chloride present in various concentrations of KCl and NaCl waters.

High levels of bicarbonate ions may cause poor hydration of the gelling agent and may interfere with the crosslinking chemistry of many fluids. Levels of bicarbonate can be changed by altering the pH of the fluid (Fig. P-73). There is always a balance between the different CO_2-related ions in solution with the various amounts of carbonate, bicarbonate and CO_2 gas. An accurate understanding of bicarbonates must also be accompanied with a pH measurement. When bicarbonates are measured on fluids that are to be crosslinked, the fluid must be tested at the full pH range between hydration and crosslinking.

The iron content should be less than 25 mg/liter. Excess iron accelerates the development of free radicals from the polymer molecules. These free radicals increase the degradation process of the polymer, especially at temperatures above 200°F. If an oxidizer has been premixed in metal frac tanks, the tanks undergo an oxidation reduction reaction. Part of the oxidizing breaker spends itself in this reaction, resulting in a lower total breaker amount that produces unpredictable break times once the fracturing fluid is pumped.

Additives remaining from previous treatments in the frac tank can be detrimental to fracturing fluid quality. Surfactants can create foaming problems during the mixing procedure. If the foam problem becomes severe, circulation rates will be reduced as the mixing pumps lose prime, leading to excessive additions of gelling material and lumping of the base gel. The presence of reducing agents can interfere with the crosslinking process or alter the break time. To test for reducing agents, add 2 drops of a 1% potassium permanganate solution to 500 ml of water having a pH between 5.5 and 7. A white precipitate forms if reducing agents are present; otherwise, the water turns light pink.

P-8.1.2: Base Fluid Viscosity

The ultimate viscosity of a crosslinked fluid depends on the base viscosity of the linear gel. Figures P-74 through P-77 can be used to check the base fluid viscosity for various polymer loadings. For Figs. P-74 and P-75, the viscosity must

Chloride Content (ppm)	KCl (%)*	NaCl (%)*	$CaCl_2$ (%)*
5,000	0.82	1.05	0.78
10,000	1.64	2.10	1.56
15,000	2.47	3.15	2.35
20,000	3.29	4.20	3.13
25,000	4.12	6.14	3.91
*If all chlorides are exclusively from this compound.			

Table P-17—Salt concentrations for various chloride levels.

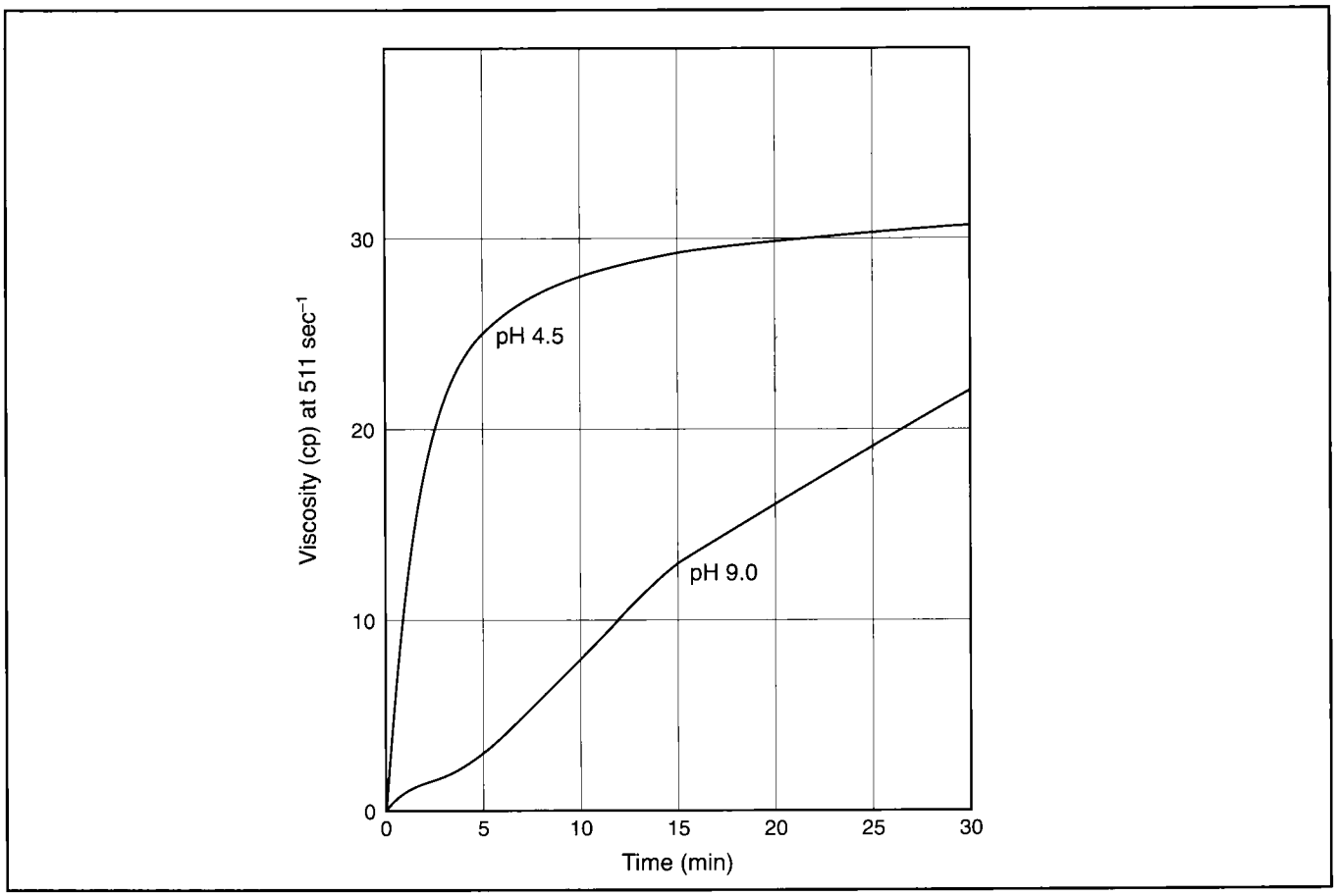

Figure P-72—pH effect on the viscosity development of HPG (from Brown, J. E. et al., Southwestern Petroleum Short Course paper, 1988).

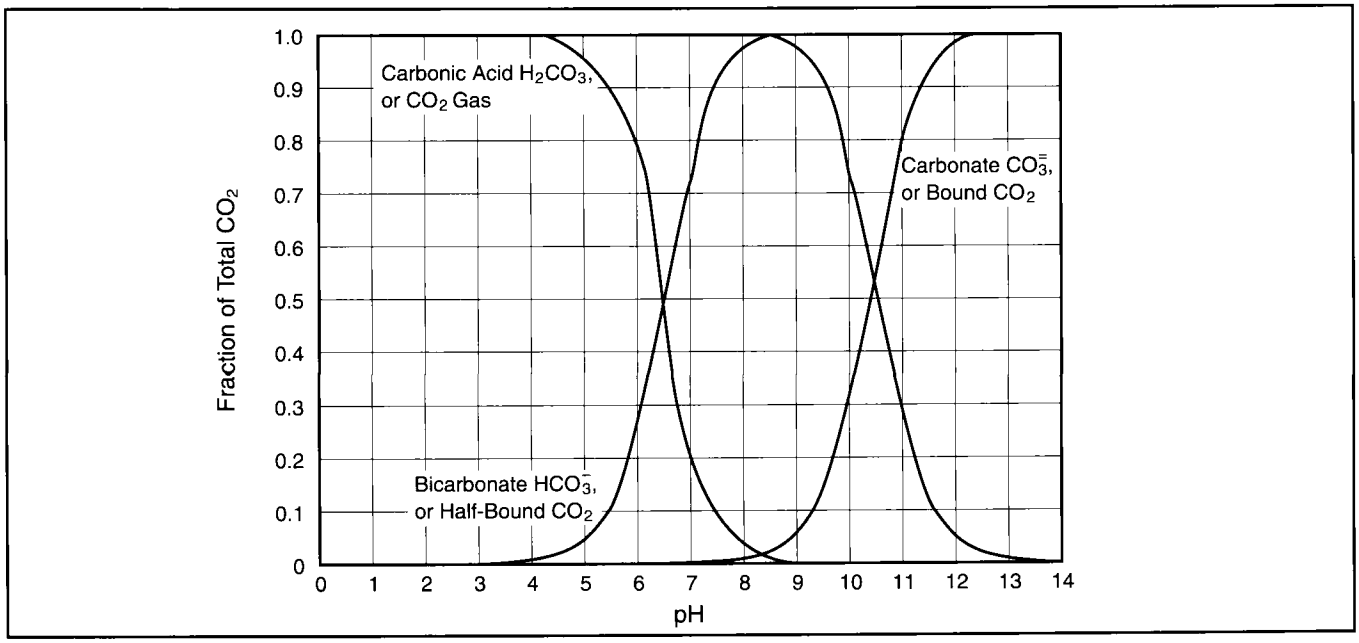

Figure P-73—Effect of changing pH on distribution of different CO_2-related ions in solution.

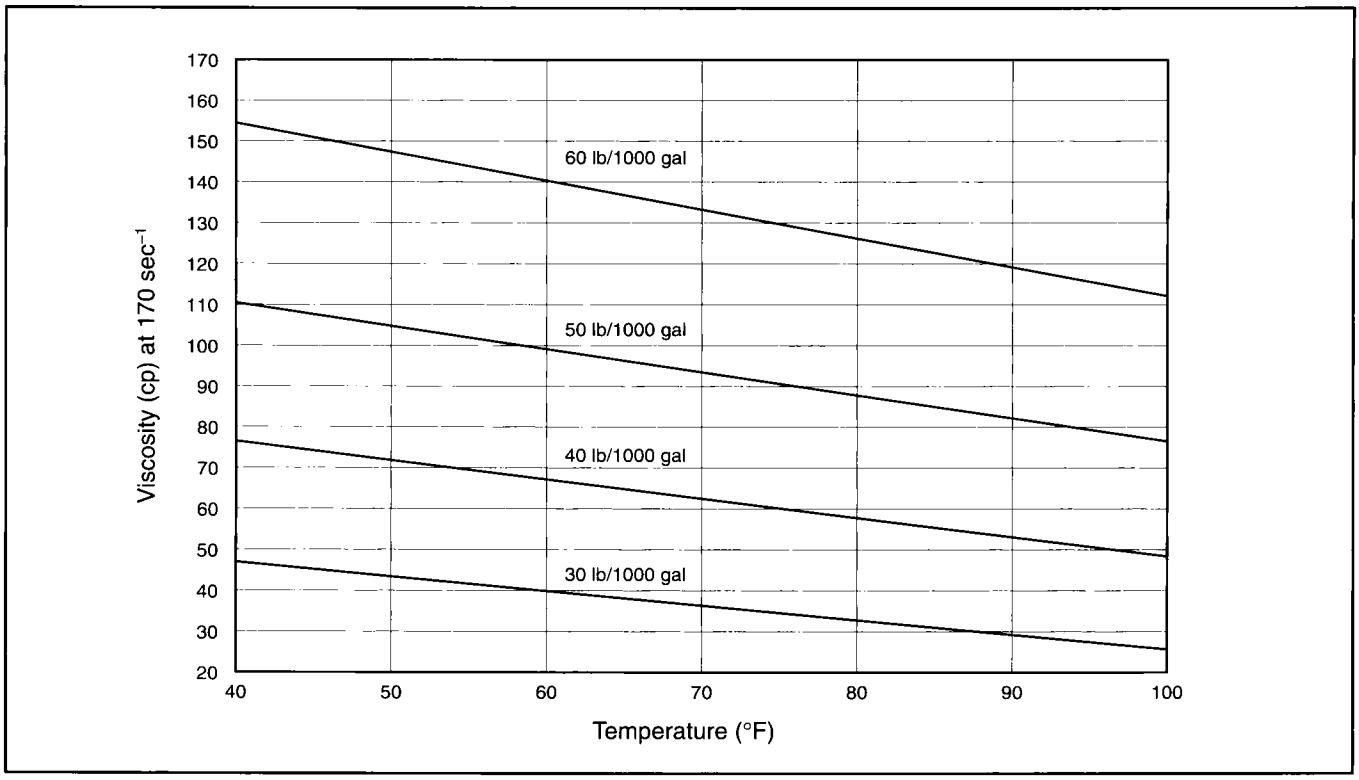

Figure P-74—Typical guar viscosity, polymer loading vs. temperature.

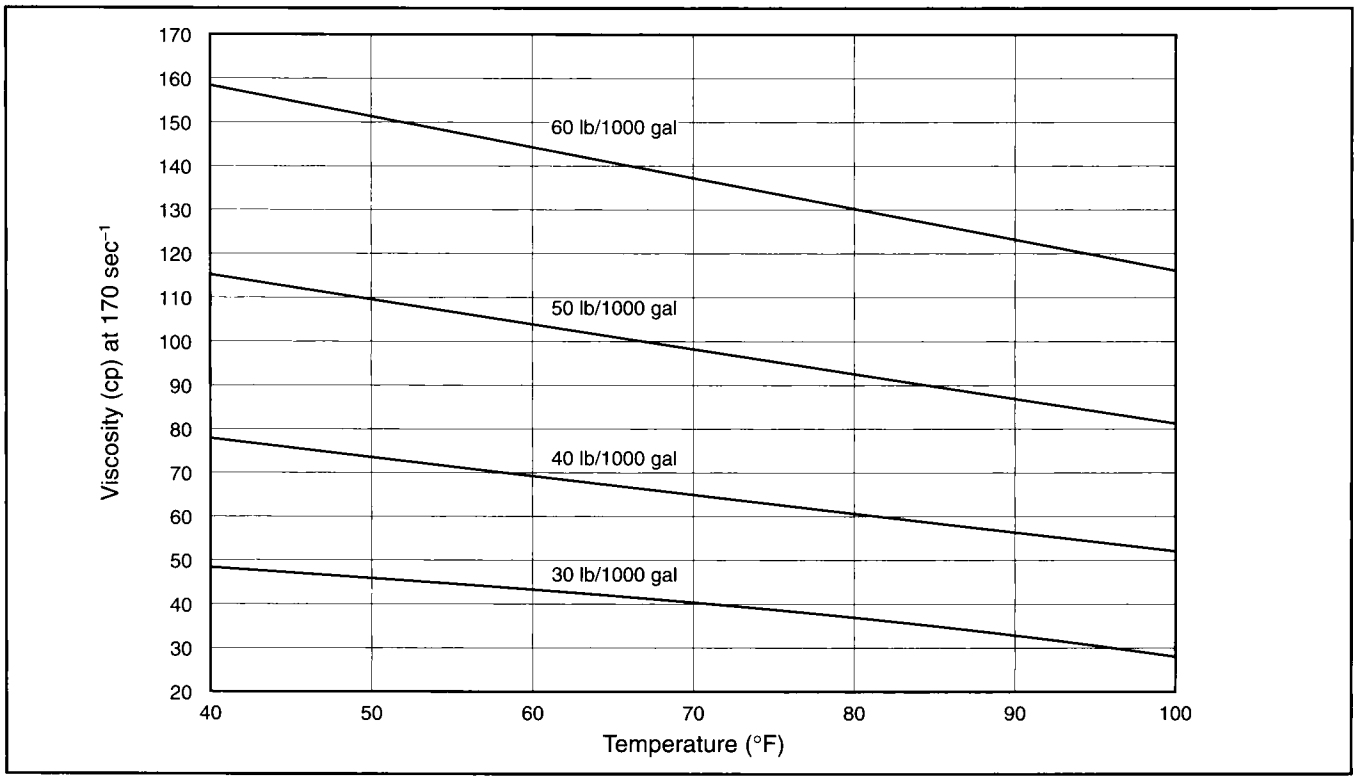

Figure P-75—Typical HPG viscosity, polymer loading vs. temperature.

be measured with a rotational viscometer such as a Fann-35. Figures P-76 and P-77 use marsh funnel times to calculate viscosities. Whenever possible, a rotational viscometer should be used to check viscosities.

P-8.1.3: Crosslinked Fluids

The crosslink time of a fracturing fluid must be adjusted to prevent shear degradation and excess friction. The ultimate viscosity of a crosslinked fluid, made from organometallic crosslinkers, depends on the exposure of the fluid to shear. Figure P-78 shows the effect of shear on an organometallic fluid. The viscosity of the fluid not exposed to shear is several times higher than the fluid exposed to high shear during the crosslink process. Borate-crosslinked fluids are not shear sensitive. They can recrosslink after being exposed to shear and therefore do not have to be delayed to ensure proper rheological properties.

The ultimate viscosity degradation of an organometallic fluid is a function of both shear rate and time exposed to shear. To prevent the shear degradation of these fluids, their crosslink must be delayed. However, precise control of the crosslink time is not required to ensure optimum fluid performance for most applications. A window can be established to prevent the shear degradation while minimizing friction. The crosslink process does not have to be extended past the perforations. The shear at the perforations is extremely high but lasts for such a short time that the fluid will not be adversely affected. Hodge and Baranet have shown that delaying the crosslink for as little as 1 min is adequate for preventing shear degradation (Fig. P-79). Each of these fluids was subjected to 5 min of shear history at 1350 sec^{-1} (13 BPM down 2⅞-in. tubing). The amount of shear a fluid experiences at different rates in different tubing sizes can be found on Fig. P-80.

Delaying the crosslink time also lowers the friction pressure drop of a crosslinked fluid. Experience has shown that delaying the crosslink time to a point where the fluid will be two-thirds down the tubulars usually controls excess friction. This delay eliminates high friction from most of the tubing, yet allows the fluid to maintain adequate viscosity for transporting proppant as it enters the formation. Both organometallic and borate crosslinkers can be delayed to minimize the amount of frictional pressure drop they create.

Several methods of checking crosslink times can be used on location. A long-time standard test requires checking the time a fluid needs to develop a "floppy lip." The fluid is considered crosslinked once it forms a rigid structure that will hang from the lip of a cup rather than pouring out completely. A vortex closure test has become popular in recent years. In this test, a gelled fluid is stirred in a blender at a rate just high enough to create a vortex. The crosslink time is determined by monitoring the time for the vortex to close after the crosslinker has been added. Some crosslinked fluids require temperature in addition to time to crosslink. For these fluids, the vortex closure must be tested in a cup that can be heated with a thermocouple or in a water bath. Another test checks the crosslink time in a falling ball viscometer. The crosslinked fluid is added to the viscometer, and the time for the ball to fall is recorded. This type of viscometer can be made from a 50-cm^3 syringe and a 1.9 specific gravity ⅞-in. ball sealer. The fluid is considered crosslinked when the ball takes 7 sec to fall from one end to the other. The apparent viscosity of the fluid can be calculated using Fig. P-81. The floppy lip method of checking crosslink time should be avoided if possible. This method does not adequately simulate the shear conditions a fluid experiences during pumping. The viscosity of a fluid crosslinked under shear conditions is very different from viscosity development under static conditions. The super-high viscosity of a floppy gel never forms during pumping.

Crosslinking requires the precise addition of a crosslinker solution to a gelled fluid. Varying the concentration of this solution has significant effects on the stability and rheological performance capabilities of the fracturing fluid. Some crosslink solutions have a limited shelf life and may degrade when exposed to air or water. Therefore, large treatments may require mixing several crosslink solutions throughout the job. If several batches of crosslink solution are required for the treatment, each batch should be tested for crosslink performance prior to pumping.

P-8.1.4: Gelled Oil

The quality of a gelled oil depends not only on the proper additive chemistry but also on the quality of the crude used as the fluid base. Crudes that are high in either asphaltenes or paraffins cannot be used to create a gelled fluid. For this reason, gelled oils are often prepared from diesel or kerosene rather than crude. Even these refined products should be tested in the laboratory to ensure they can be gelled. Other chemicals added to these refined oils may interfere with viscosity development. Antigelling additives added to diesel in cold climates often deteriorate the long-term performance of gelled oils. Care should also be taken to prevent contamination of the oil with common polar species such as water, acid, bases or salts. These polar species often destroy the association between the aluminum ions and phosphate ester groups. Water usually makes the gel structure more rigid at surface temperatures but greatly reduces gel stability at elevated temperatures. Figure P-82 shows the effect of water on the surface viscosity of a typical gelled oil based on a marsh funnel time. From this chart, it is evident that 10 gal to 20 gal of water in a standard frac tank can affect the quality of

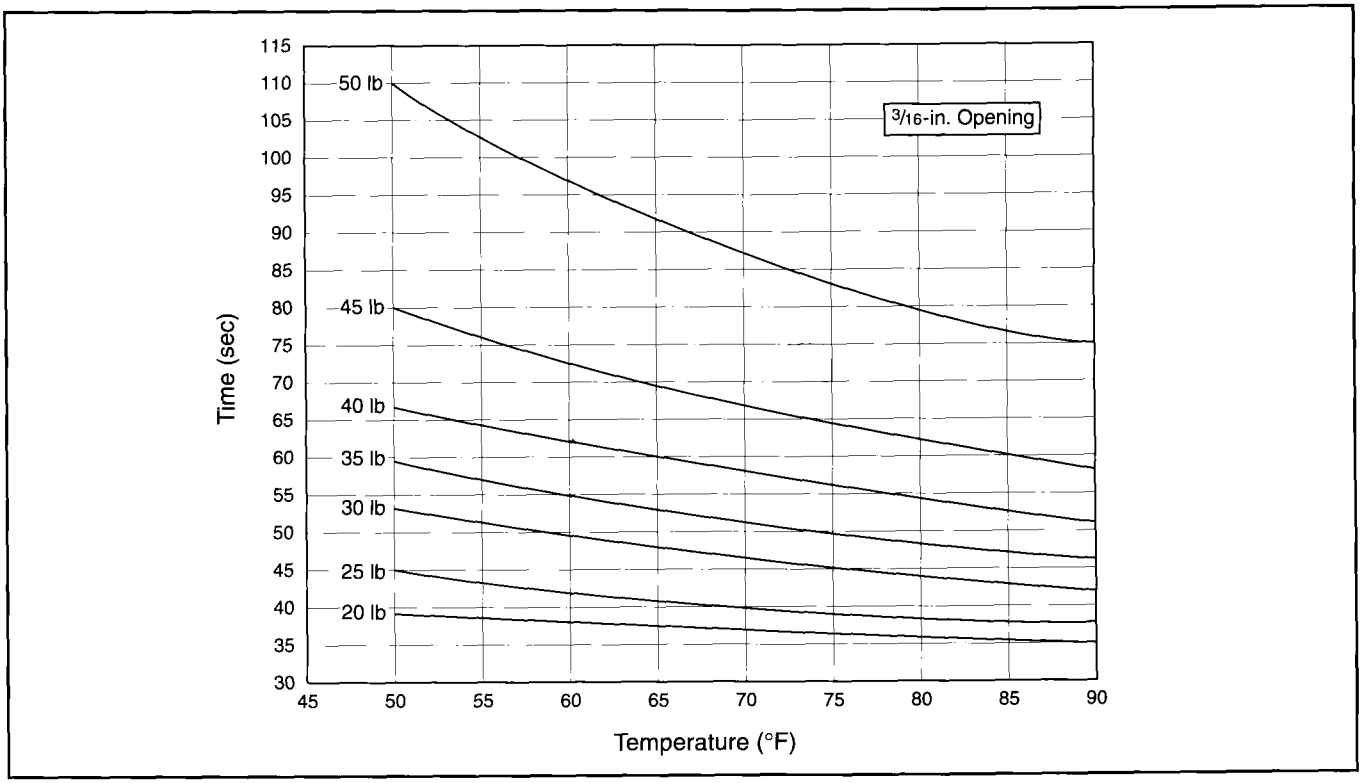

Figure P-76—Marsh funnel times for checking viscosities of guar fluids.

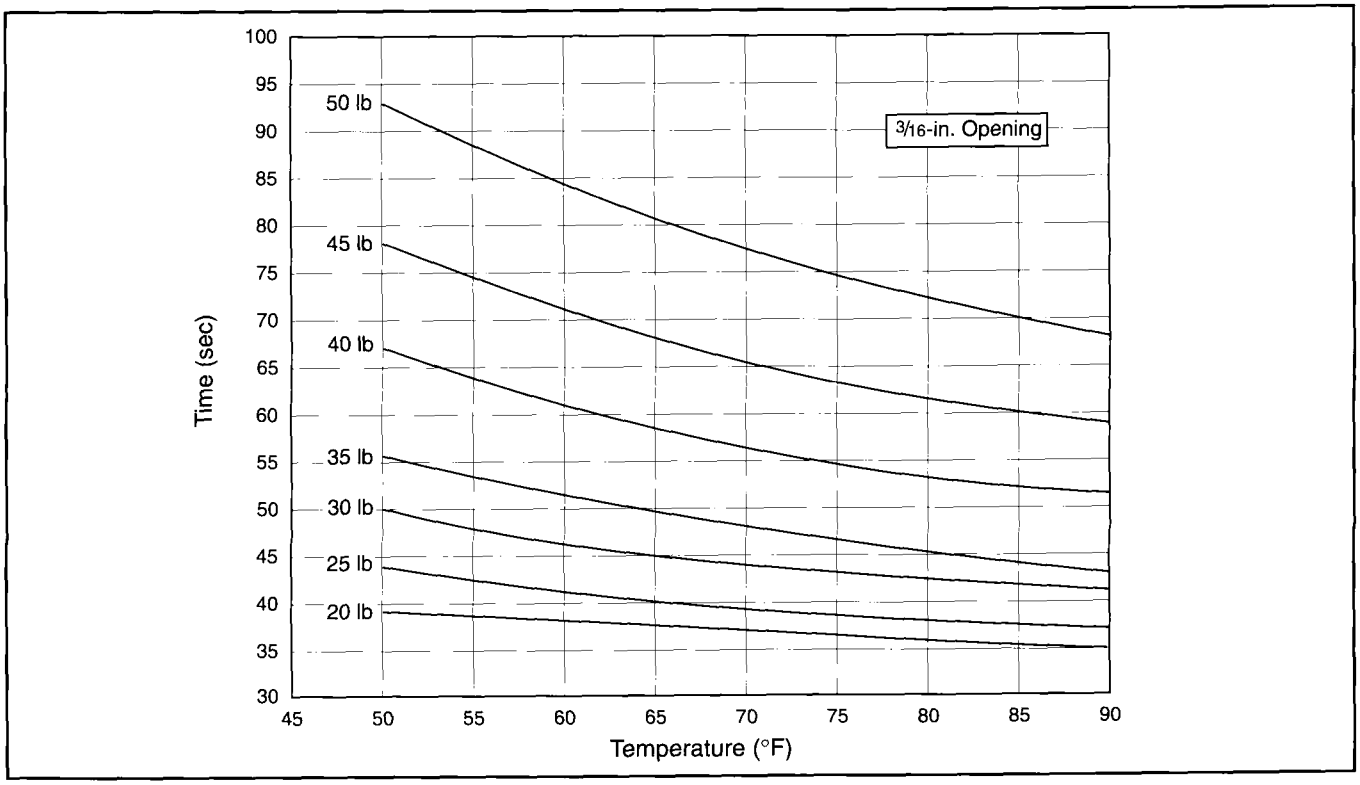

Figure P-77—Marsh funnel times for checking viscosities of HPG fluids.

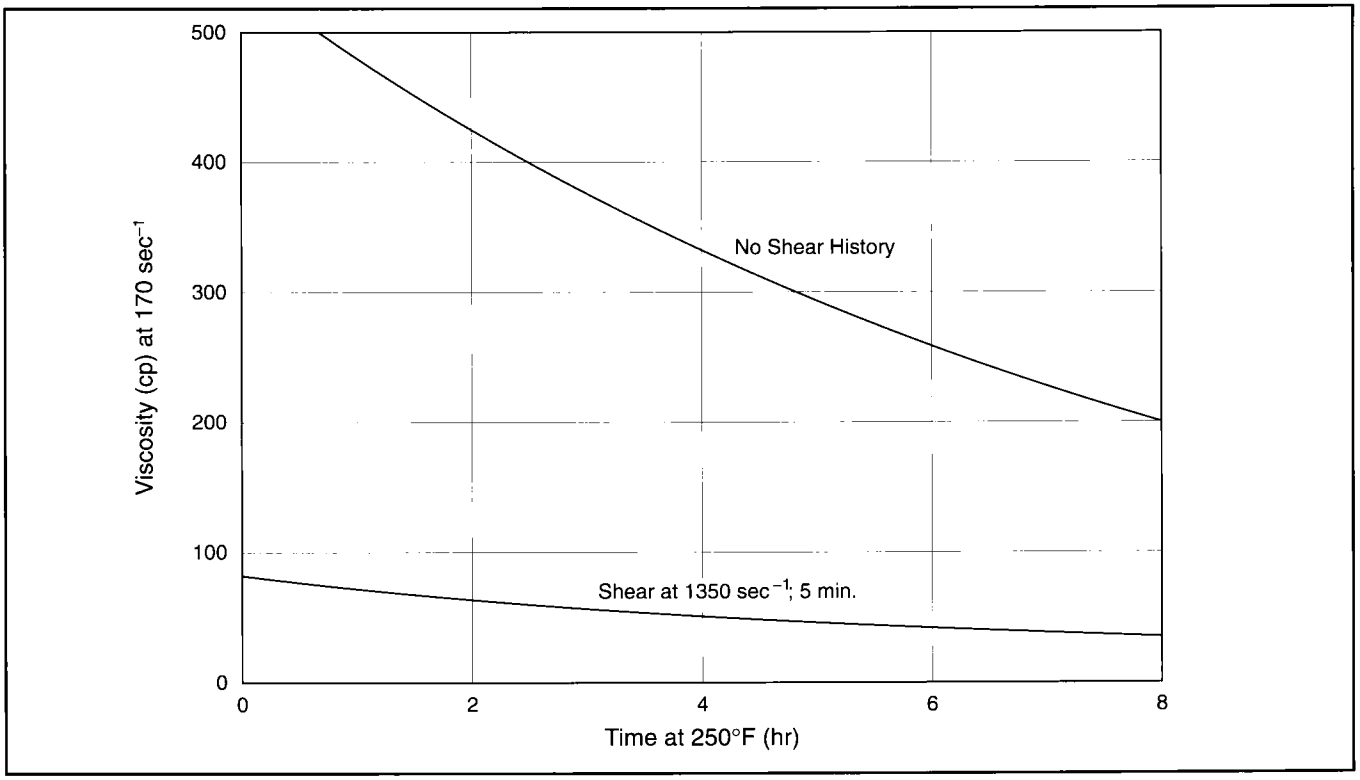

Figure P-78—Shear effects on the viscosity of an organometallic crosslinked fluid (from Craigie, L.J., SPE paper 11635, 1983).

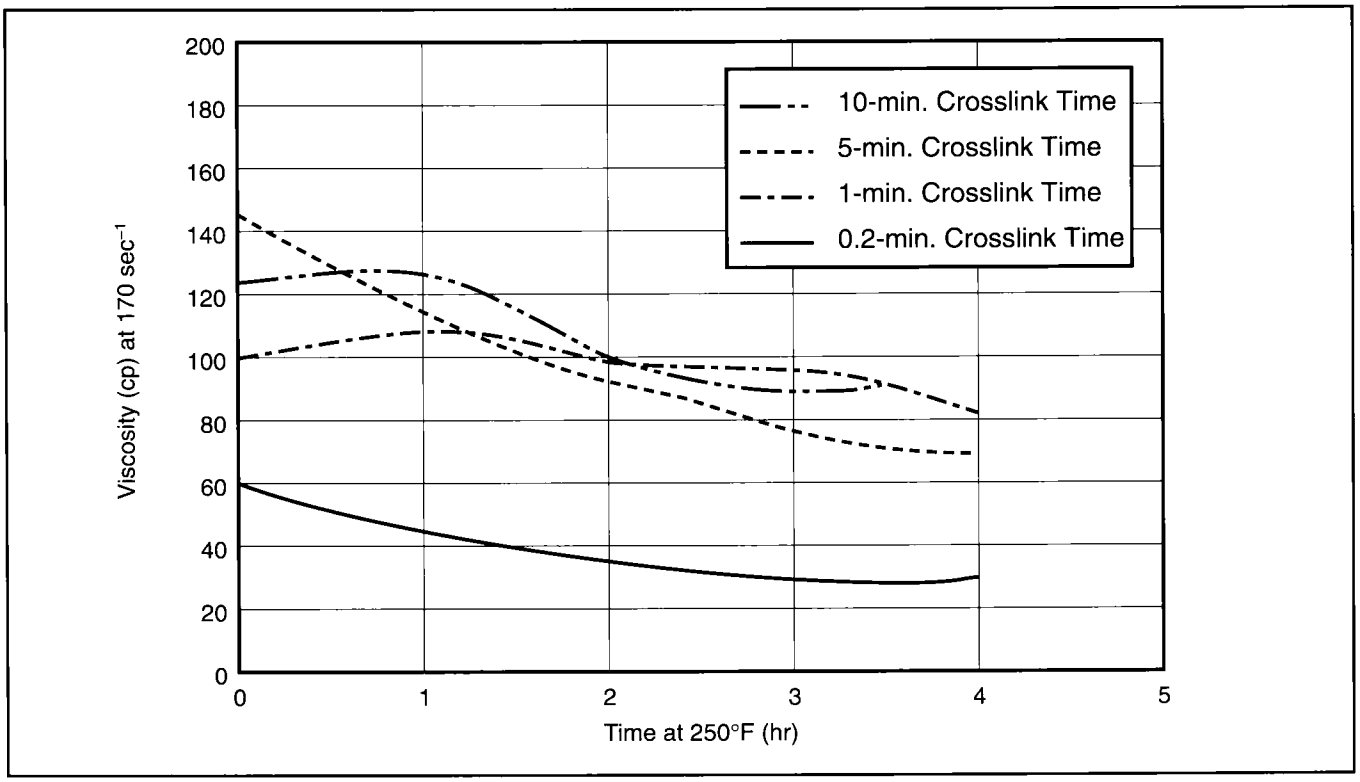

Figure P-79—Effect of crosslink time on fluid performance (from Hodge, R.M. and Baranet, S.E., SPE paper 16249, 1987).

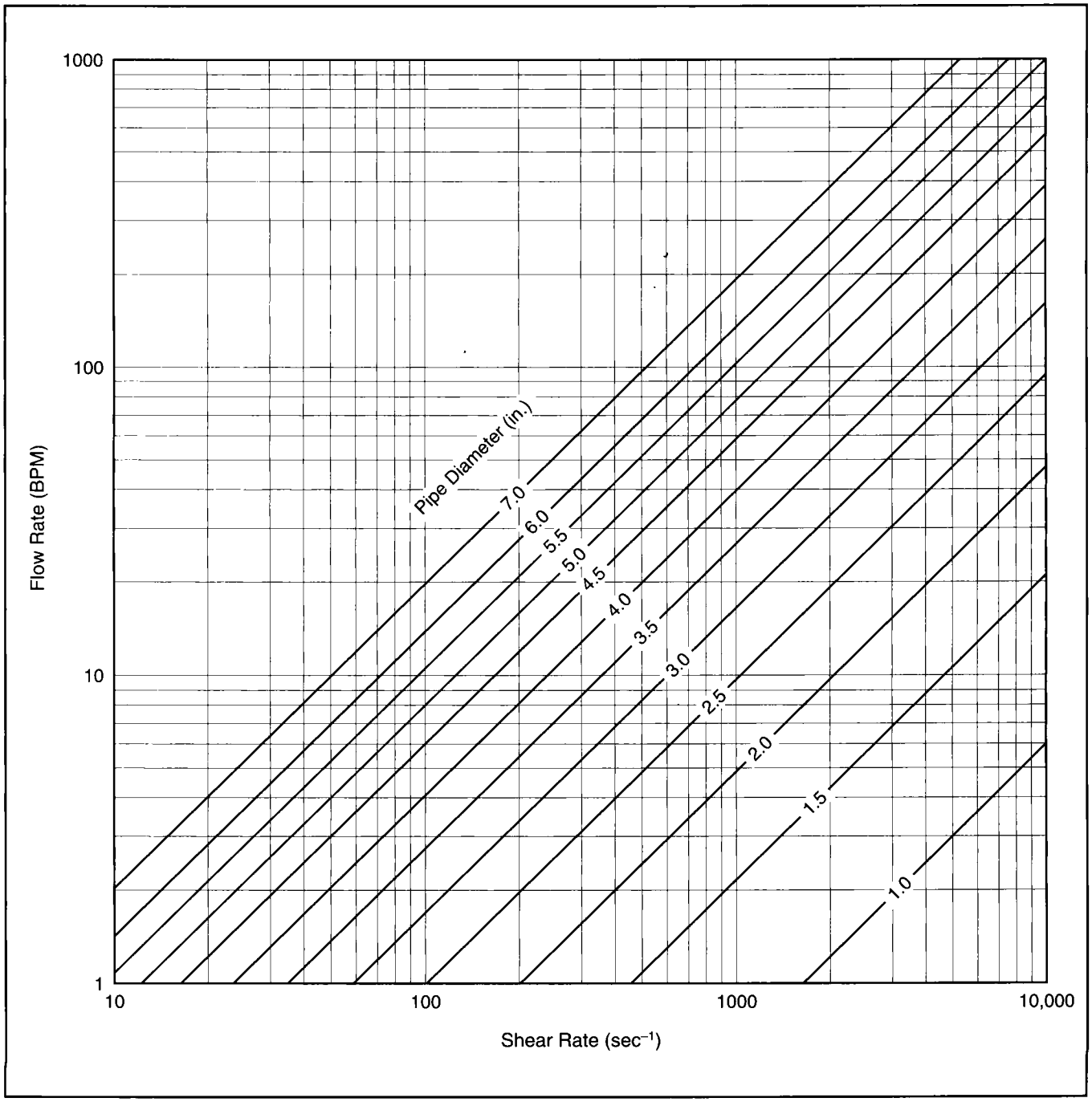

Figure P-80—Flow rate versus shear rate through pipe.

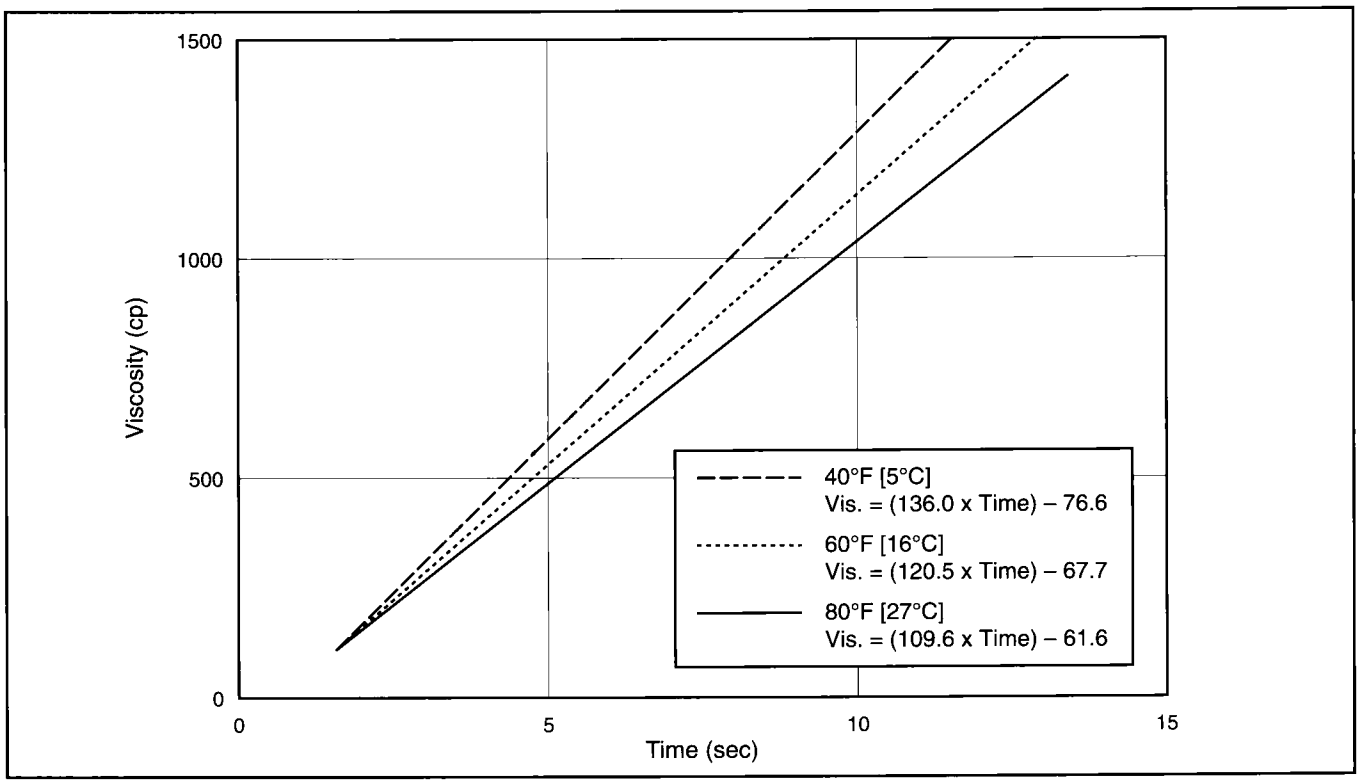

Figure P-81—Viscosity determination from a falling ball viscometer.

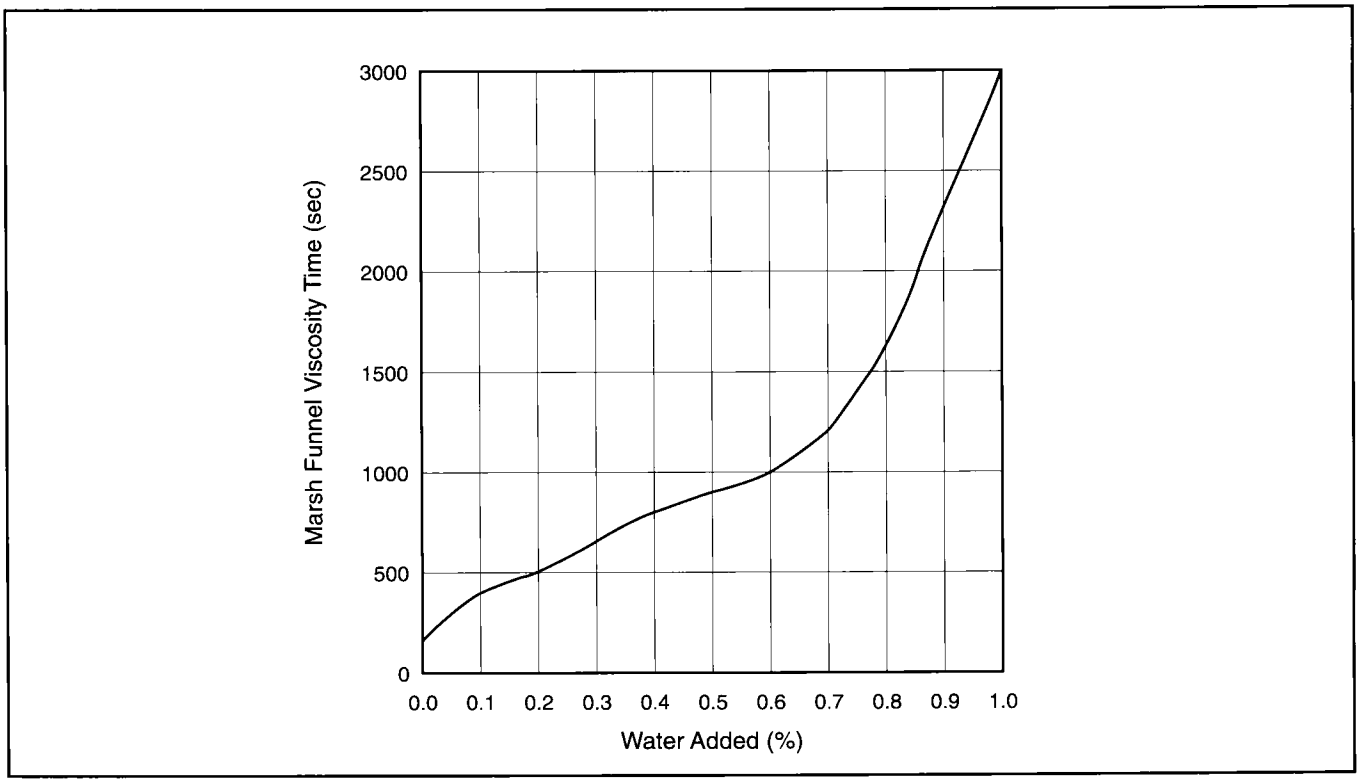

Figure P-82—Effect of water contamination on viscosity of gelled oils.

the gel. Weak acids and bases are used by design to break gelled oils. It is therefore imperative that these species do not contaminate the gelled oil.

Care must be taken to add the phosphate ester gelling agent and the aluminate crosslinker at the proper concentration and ratios. An overactivated gelled oil initially becomes highly viscous but quickly reaches a point where the gel breaks out and viscosity is lost. Materials must be added in the proper sequence for most gelled oils. The two materials can be added simultaneously during the mixing procedure, but directly mixing together the gelling agent and activator must be avoided. After the gel structure begins to form, viscosity measurements should be taken to ensure the fluid has the correct rheological properties. Very small amounts (less than 1 gal when mixing 500-bbl frac tanks) of either activator or gelling agent can be added to create a fluid with the proper viscosity. If the viscosity of the fluid is low, then additional activator is probably needed. If the viscosity is high, then more phosphate gelling agent should be added.

Often, these fluids slowly build viscosity for several hours after mixing. Slow viscosity development can lead to very high static viscosities that cause fluid transfer problems. To prevent this, the concentration of the aluminate activator may be deliberately kept low. Small amounts of the activator can then be added until the desired fluid properties are reached.

Recent developments in continuous-mix technology have made new gelled oil fluids practical. These fluids exhibit lower friction pressures while providing adequate viscosities. As with any continuous mix procedure, all additive rates must be closely monitored to ensure the desired fluid is being created.

Breaker tests should be run on all gelled oil fluids before they are pumped. Each different oil displays a characteristic break. Using a standard breaker concentration based only on temperature and gel loading must be avoided.

P-8.1.5: Foamed Fluids

Using nitrogen or carbon dioxide as part of the fracturing fluid requires extra effort to ensure proper execution. The compressibility and solubility of these fluids must be accounted for based on downhole conditions. An error in the compressibility calculations can significantly change both the rheological properties and the overall volume of the fracturing fluid.

Foams are usually characterized by quality. The quality of a foam, Q, is defined as the ratio of gas volume to the total liquid and gas volume:

$$Q = \frac{V_g}{V_g + V_l}, \tag{P-8}$$

where V_g and V_l are the volumes of gas and liquid, respectively. The liquid ratio of the total foam is then $1 - Q$.

Proppant is added only to the liquid portion. Therefore, the proppant concentration at the blender must take into account the dilution of the gas. The required concentration can be calculated by:

$$\text{Blender Proppant Concentration} = \frac{\text{Foam Proppant Concentration}}{1 - Q}. \tag{P-9}$$

The downhole volume of these fluids can be calculated by using standard gas calculations. The formation volume factor, B (SCF/bbl), is defined as

$$B = \frac{Volume_{Reservoir\ Conditions}}{Volume_{Standard\ Conditions}}, \tag{P-10}$$

where

$$PV_{Reservoir} = (ZnRT)_{Reservoir} \tag{P-11}$$

and

$$PV_{Standard\ Conditions} = (ZnRT)_{Standard\ Conditions}. \tag{P-12}$$

Therefore,

$$B = \left(\frac{TZ}{P}\right)_{Res}\left(\frac{P}{TZ}\right)_{sc}. \tag{P-13}$$

With standard conditions of 60°F [620°R], pressure of 14.7 psia and a Z factor of 1; reservoir conditions of 180°F, fracture pressure of 5000 psi and a Z factor of 1.2, the B is 7.7×10^{-4} bbl/SCF, or 1299 SCF/bbl. Z factors for N_2 and CO_2 can be found in Figs. P-83 and P-84, respectively. A quick estimation of the volume factor can be obtained from Figs. P-85 and P-86.

These two gases are also soluble in the base fluid. The amount of gas lost to solution should be accounted for. Figures P-87 and P-88 show the varying solubilities of N_2 and CO_2, respectively. The total downhole volume of gas needed for the quality calculation is the sum of the compressibility volume factor and the solubility.

It is critical to know the accurate fracture gradient before attempting a treatment with either CO_2 or N_2. All the compressibility calculations are based on this value. These gases occupy a different amount of space for any given pressure. The volume of these gases must be calculated at fracturing pressures. Changing the amount of gas pumped based on surface pressures during a treatment will almost always lead to an error in the downhole foam quality.

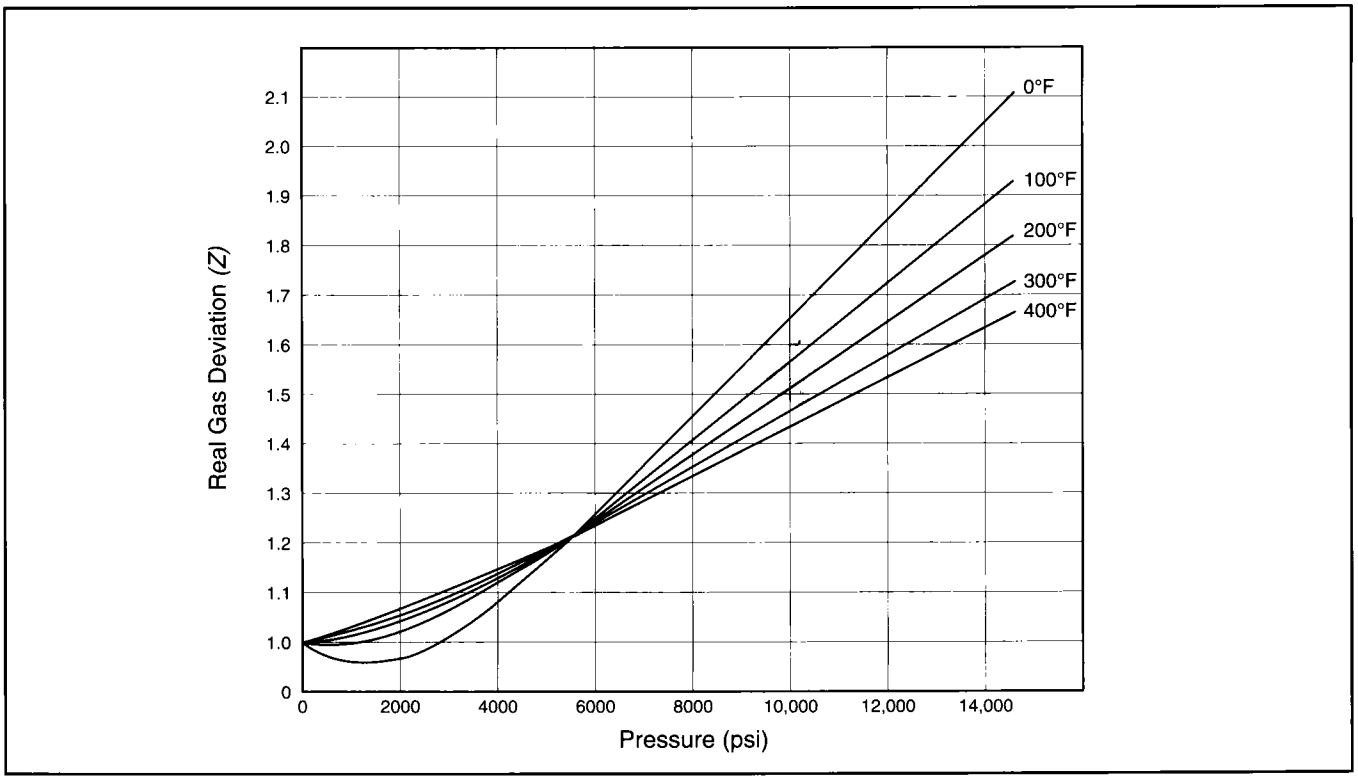

Figure P-83—N_2 real gas deviation factor, *Z*.

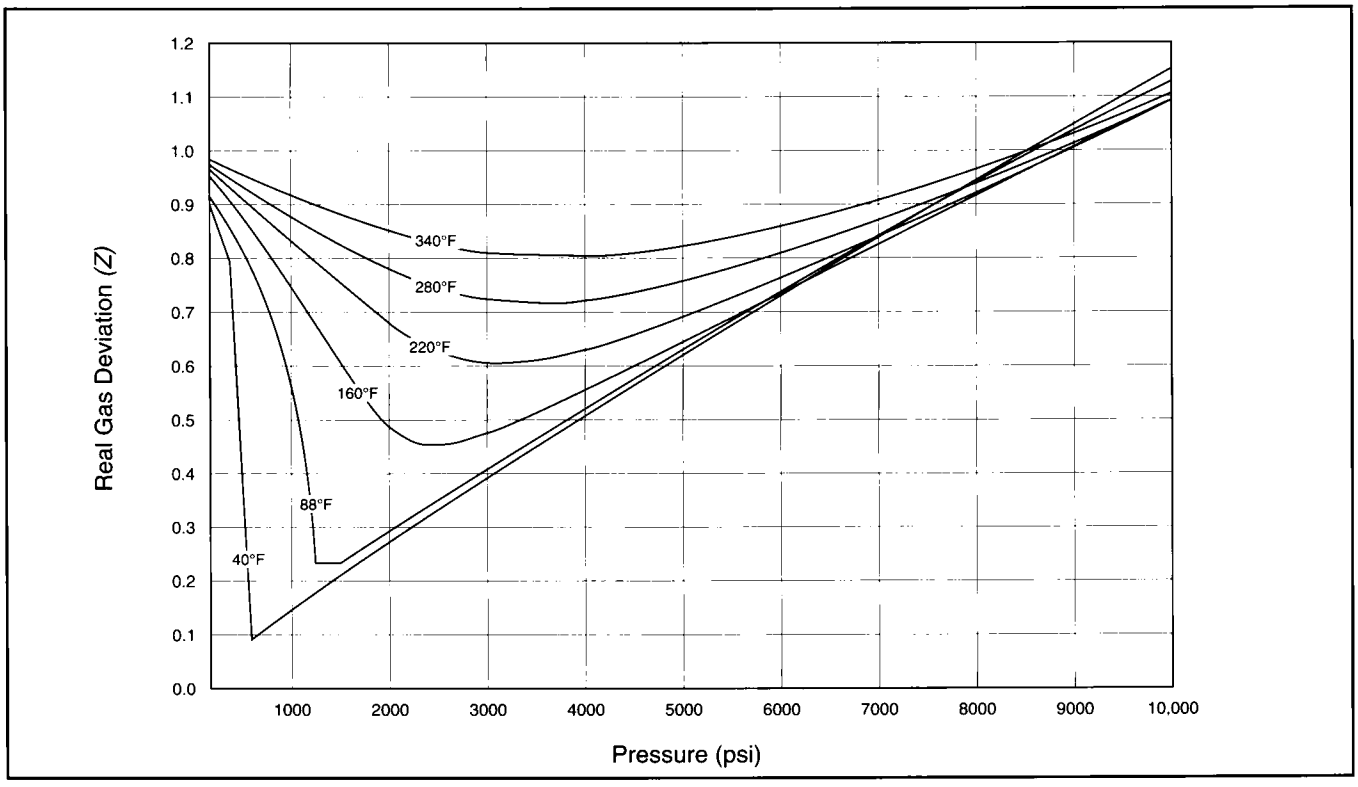

Figure P-84—CO_2 real gas deviation factor, *Z*.

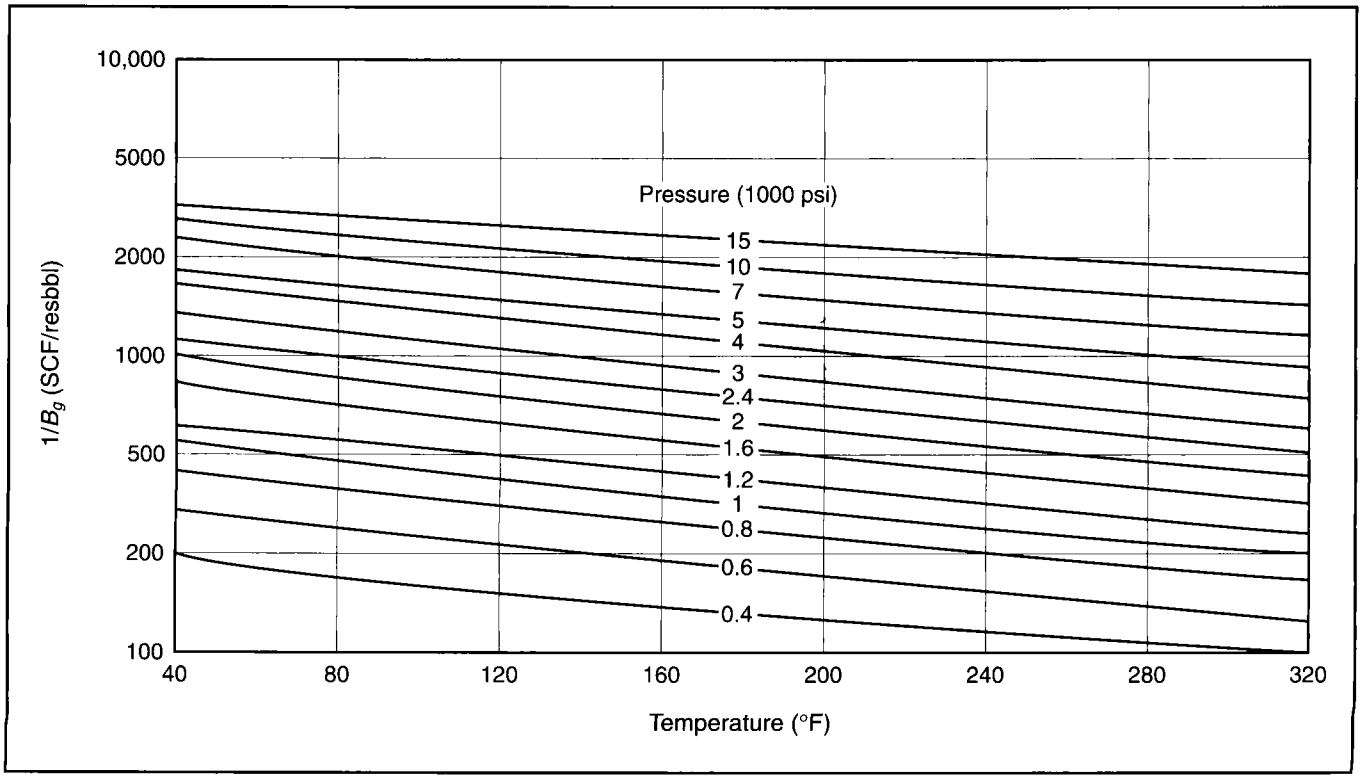

Figure P-85—Nitrogen gas formation volume factor.

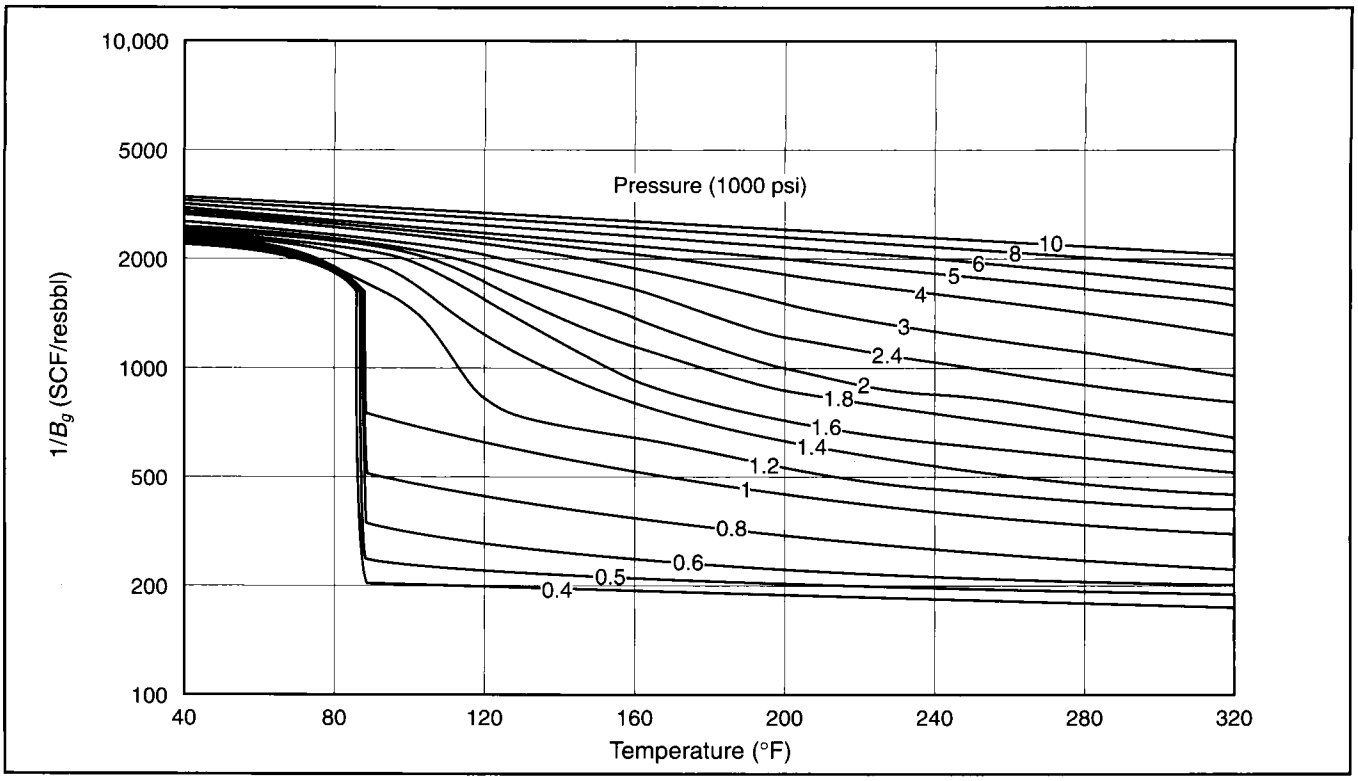

Figure P-86—Carbon dioxide gas formation volume factor.

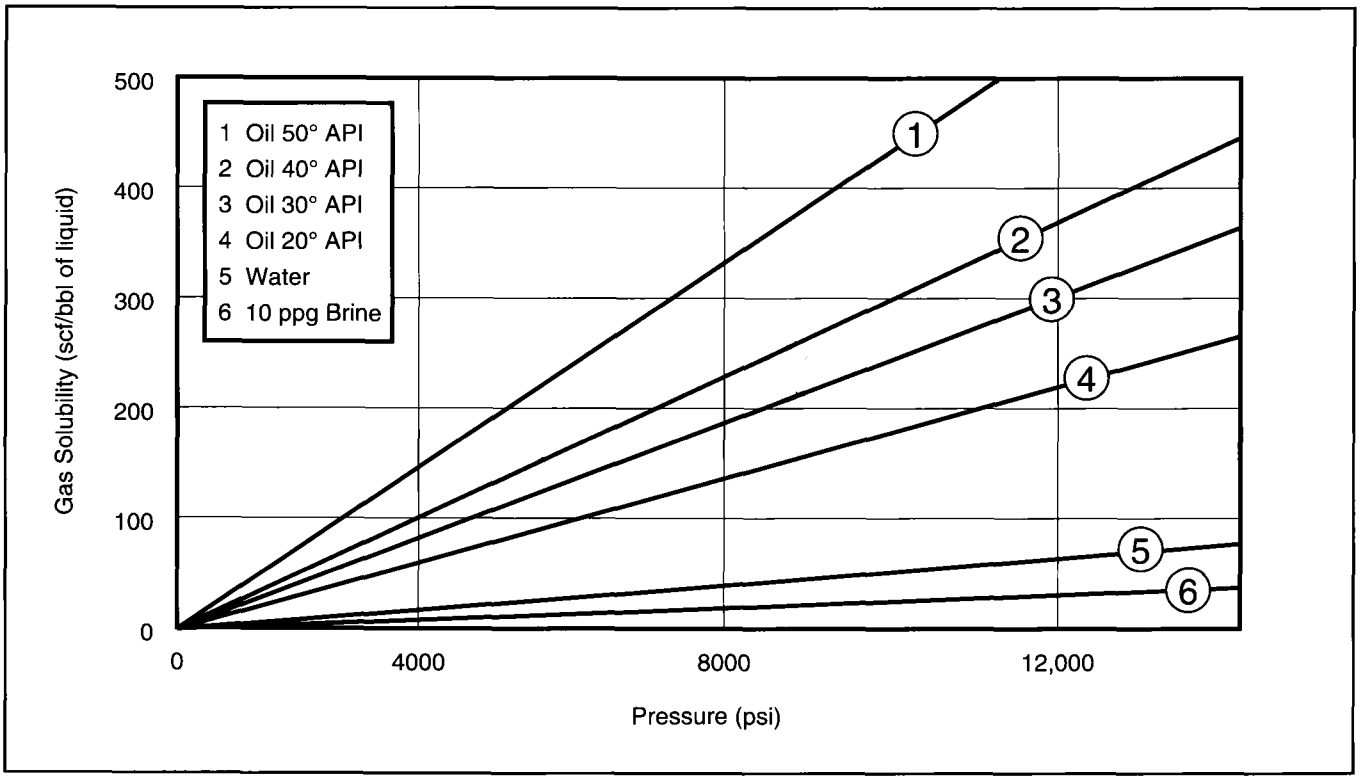

Figure P-87—Solubility of nitrogen in crude oil and water.

P-8.2: Proppants

The quality of the proppant used has a direct impact on the conductivity of the fracture. One of the most difficult problems in checking the quality of a proppant is obtaining a good representative sample. The sample should be provided on location, compiled from a flowing stream of proppant rather than a sample from the storage vessels. Therefore, the sand is sampled as it is loaded into storage. The top of the proppant siting storage will almost surely contain a much higher volume of fines than the rest of the proppant. The sampling procedure outlined in the *API Recommended Practices for Testing Sand Used in Hydraulic Fracturing Operations* should be followed.

The proppant should be sieved to ensure that the correct size proppant is used. Some artificial proppants may have a much narrower range of proppant sizes because of the controls used during manufacturing. The API lists a given set of sieve sizes that are to be used for each proppant mesh size. Ninety percent of the sample should fall between the largest and the smallest sieve size of the proppant (between the 20 and 40 mesh screens for a 20/40 proppant). In addition, less than 0.1% of the total sample should remain on the largest sieve, and less than 1% should fall through to the pan. Table P-18 gives the API-recommended sieves for testing various proppant sizes.

The proppant should have a roundness and a sphericity value of 0.6 or greater, an arbitrary measurement where proppant grains are examined at low magnification and compared to the roundness and sphericity chart developed by Krumbein and Sloss, 1963 (Fig. 5-29, *Reservoir Stimulation*).

To ensure the proppant is low in contaminants, a solubility test in 12-3 hydrochloric-hydrofluoric acid should be performed. Sand often contains contaminants such as feldspars or clay, which will be soluble in this acid. Pure quartz sand is not affected by this acid. In this test, as described by the API, 5 g of sand are placed in 100 ml of acid, heated to 150°F for 30 min, and then filtered and dried. The amount of mass lost to the test is then measured. The maximum solubility for 6/12 through 30/50 mesh sands is 2% and 3% for 40/70 through 70/140 mesh. This test should be conducted before moving the proppant to location.

A simple turbidity test providing similar information can be performed on location. Proppant is poured to the 20-ml mark on a standard 4-oz. prescription bottle, and then distilled water is added to the 100-ml mark on the bottle. A black

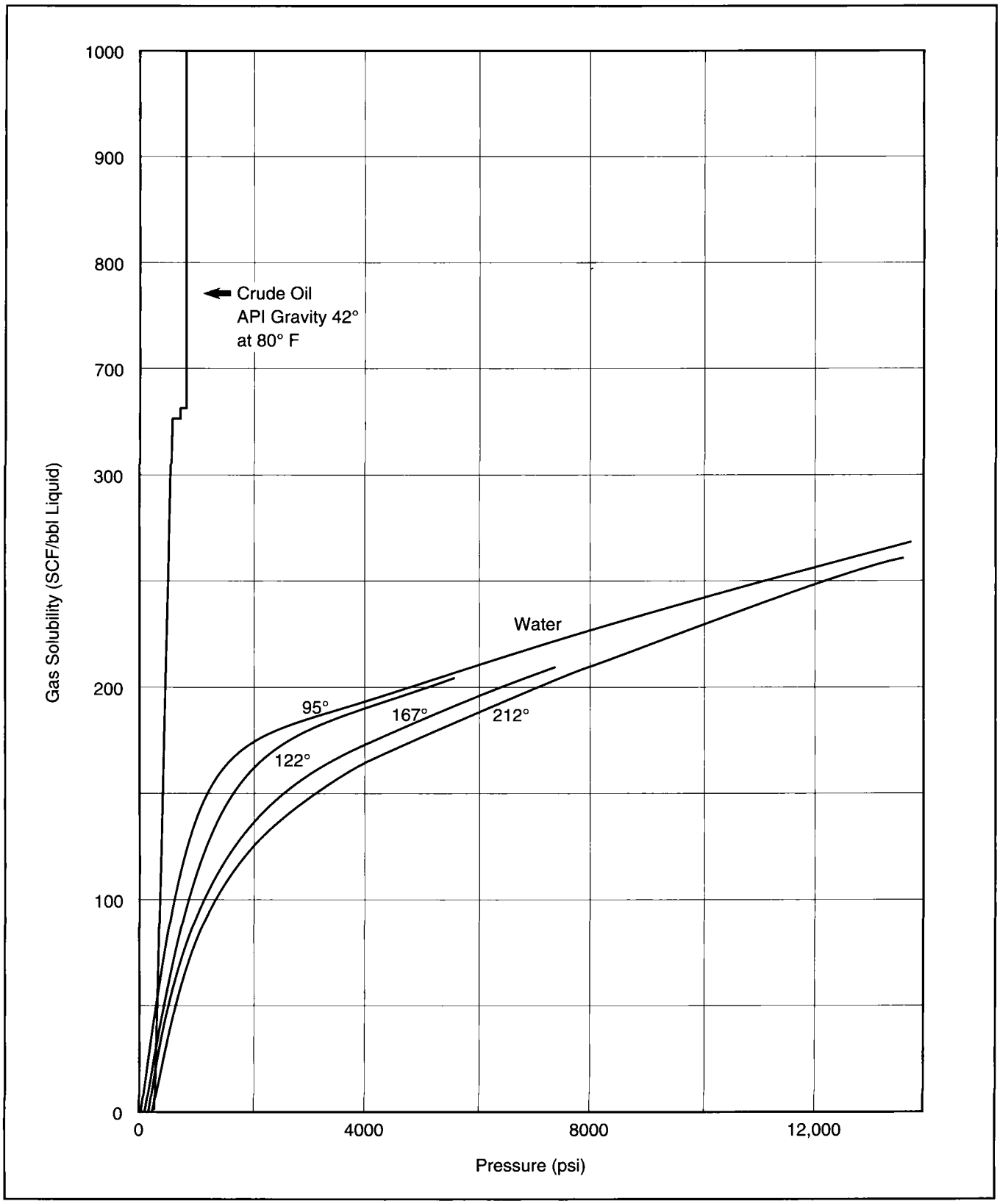

Figure P-88—Solubility of CO_2 in crude oil and water.

felt-tip marker is used to make a distinguishing character approximately ½-in. high on the flat side of the bottle. The bottle is then shaken for 10 sec. The character on the bottle should be distinguishable at arm's length when looking through the bottle.

P-8.3: Material Balance

Preplanning the material balance of the treatment is one of the most critical steps toward precise execution. The supervisor in charge of pumping operations must know exactly how much material is needed, how much has already been pumped and how much remains on location. This dynamic problem must be closely followed throughout the treatment. First, the treatment must be outlined into various stages. These stages often follow the proppant stages, but for very large jobs may also have to be shortened into timed stages. All additives should be cross checked in approximately 15-min intervals throughout a treatment. Each fluid and additive on location should be accounted for at every timed step. Figure P-89 is an example of a useful format for tracking the progress of a treatment. During the treatment, adjustments should be made for any deviation from the plan.

Proppant stages are based on adding a volume of proppant to a gallon of fluid; therefore, the terms "pounds of proppant added" (ppga) or "pounds per gallon" (ppg) are used to designate these stages. The ppga term is preferred since ppg connotates a true density, which is not true in this case. All additives are calculated on the basis of clean fluid volume. Once proppant is added to the fluid, only a portion of the rate is fluid. Compensations must be made to the additive rates to account for the amount of proppant in the slurry. Tables P-19 through P-21 can be used to find the volume of fluid and the volume of proppant for various proppant concentrations.

The densitometers used to calculate proppant density measure the true density of the fluid and then calculate the pounds of proppant added per gallon. The following equation can be used to validate the proppant concentration based on the slurry density:

$$\rho = \frac{\text{Mass}}{\text{Volume}}. \qquad \text{(P-14)}$$

Therefore,

$$\rho = \frac{\text{weight of base fluid} + \text{weight of proppant}}{\text{volume of base fluid} + \text{volume of proppant}}. \qquad \text{(P-15)}$$

and

$$\rho = \frac{\text{weight of base fluid} + \text{ppga}}{1 \text{ gal} + \frac{\text{ppga}}{\rho \text{ of proppant}}}. \qquad \text{(P-16)}$$

For a base fluid density of 8.4 ppg, sand with a density of 22.1 ppg and a proppant stage of 3 ppga, the densitometer should read 10.4 ppg.

Sieve Opening Sizes (Micrometers)	3350/1700	2360/1180	1700/850	1180/600	850/425	600/300	425/212	212/106
Frac Sand Size Designations	6/12	8/16	12/20	16/30	20/40	30/50	40/70	70/140
Nest of Sieves Recommended for Testing*	4	6	8	12	16	20	30	50
	6	8	12	16	20	30	40	70
	8	12	16	20	30	40	50	100
	10	14	18	25	35	45	60	120
	12	16	20	30	40	50	70	140
	16	20	30	40	50	70	100	200
	Pan	Pan	Pan	Pan	Pan	Pan	Pan	Pan
*From API RP56								

Table P-18—Fracturing sand sizes.

Proppant Concentration (lb of proppant added per gal of fluid) (ppga)	Slurry Density (ppg)	Clean Fluid Volume (gal of fluid per gal of slurry) (gal)	Proppant Mass (lb of proppant per gal of slurry) (lb)	Slurry Yield (gal)
0.00	8.43	1.000	0.00	1.000
0.50	8.79	0.984	0.49	1.016
1.00	9.13	0.969	0.97	1.032
1.50	9.47	0.954	1.43	1.049
2.00	9.80	0.939	1.88	1.065
2.50	10.11	0.925	2.31	1.081
3.00	10.42	0.911	2.73	1.097
3.50	10.72	0.898	3.14	1.113
4.00	11.00	0.885	3.54	1.130
4.50	11.29	0.873	3.93	1.146
5.00	11.56	0.861	4.30	1.162
5.50	11.82	0.849	4.67	1.178
6.00	12.08	0.837	5.02	1.194
6.50	12.33	0.826	5.37	1.211
7.00	12.58	0.815	5.71	1.227
7.50	12.82	0.805	6.03	1.243
8.00	13.05	0.794	6.35	1.259
8.50	13.28	0.784	6.67	1.295
9.00	13.50	0.774	6.97	1.291
9.50	13.71	0.765	7.26	1.303
10.00	13.92	0.755	7.55	1.324
11.00	14.33	0.737	8.11	1.356
12.00	14.71	0.720	8.64	1.389
13.00	15.08	0.704	9.15	1.421
14.00	15.43	0.688	9.63	1.453
15.00	15.77	0.673	10.10	1.486

Table P-19—Slurry table for bauxite in a water-base fluid (based on sand specific gravity= 3.7 and fluid specific gravity= 1.011).

Proppant Concentration (lb of proppant added per gal of fluid) (ppga)	Slurry Density (ppg)	Clean Fluid Volume (gal of fluid per gal of slurry) (gal)	Proppant Mass (lb of proppant per gal of slurry) (lb)	Slurry Yield (gal)
0.00	6.80	1.000	0.00	1.000
1.00	7.46	0.957	0.96	1.045
2.00	8.07	0.917	1.83	1.090
3.00	8.63	0.881	2.64	1.136
4.00	9.15	0.847	3.39	1.181
5.00	9.62	0.816	4.08	1.226
6.00	10.07	0.787	4.72	1.271
7.00	10.48	0.760	5.32	1.317
8.00	10.87	0.734	5.87	1.362
9.00	11.23	0.711	6.40	1.407
10.00	11.57	0.689	6.89	1.452
11.00	11.89	0.668	7.35	1.497
12.00	12.19	0.648	7.78	1.543
13.00	12.47	0.630	8.19	1.588
14.00	12.74	0.612	8.57	1.633
15.00	12.99	0.596	8.94	1.678
16.00	13.23	0.580	9.28	1.724
17.00	13.46	0.565	9.61	1.769
18.00	13.67	0.551	9.92	1.814
19.00	13.88	0.538	10.22	1.859
20.00	14.07	0.525	10.50	1.904
21.00	14.26	0.513	10.77	1.950
22.00	14.44	0.501	11.03	1.995
23.00	14.61	0.490	11.27	2.040
24.00	14.77	0.480	11.51	2.085
25.00	14.93	0.469	11.73	2.130

Table P-20—Slurry table for sand in a diesel-base fluid (based on sand specific gravity = 2.65 and fluid specific gravity = 0.815).

Proppant Concentration (lb of proppant added per gal of fluid) (ppga)	Slurry Density (ppg)	Clean Fluid Volume (gal of fluid per gal of slurry) (gal)	Proppant Mass (lb of proppant per gal of slurry) (lb)	Slurry Yield (gal)
0.00	8.43	1.000	0.00	1.000
0.50	8.73	0.978	0.49	1.023
1.00	9.02	0.957	0.96	1.045
1.50	9.30	0.936	1.40	1.068
2.00	9.56	0.917	1.83	1.090
2.50	9.82	0.898	2.25	1.113
3.00	10.06	0.881	2.64	1.136
3.50	10.30	0.863	3.02	1.158
4.00	10.53	0.847	3.39	1.181
4.50	10.75	0.831	3.74	1.203
5.00	10.95	0.816	4.08	1.226
5.50	11.16	0.801	4.40	1.249
6.00	11.35	0.787	4.72	1.271
6.50	11.54	0.773	5.02	1.294
7.00	11.72	0.760	5.32	1.317
7.50	11.90	0.747	5.60	1.339
8.00	12.07	0.734	5.87	1.362
8.50	12.23	0.722	6.14	1.384
9.00	12.39	0.711	6.40	1.407
9.50	12.54	0.700	6.65	1.430
10.00	12.67	0.689	6.89	1.452
11.00	12.98	0.668	7.35	1.497
12.00	13.24	0.648	7.78	1.543
13.00	13.50	0.630	8.19	1.588
14.00	13.73	0.612	8.57	1.633
15.00	13.96	0.596	8.94	1.678
16.00	14.17	0.580	9.28	1.724
17.00	14.38	0.565	9.61	1.769
18.00	14.57	0.551	9.92	1.814
19.00	14.75	0.538	10.22	1.859
20.00	14.93	0.525	10.50	1.904
21.00	15.10	0.513	10.77	1.950
22.00	15.25	0.501	11.03	1.995
23.00	15.41	0.490	11.27	2.040
24.00	15.55	0.480	11.51	2.085
25.00	15.69	0.469	11.73	2.130

Table P-21—Slurry table for sand in a water-base fluid (based on sand specific gravity = 2.65 and fluid specific gravity = 1.011).

		Prop					Base Fluid				Additive I				Additive II (low/high)				Energized			Wellhead Total		
Stage Number	Stage Prop	Prop Type	Prop Conc	Prop Rate (min)	Stage (lb)	Cum (lb)	Type	Rate (BPM)	Stage Vol	Cum Vol	Type	Rate (BPM)	Stage Vol	Cum Vol	Type	Rate (BPM)	Stage Vol	Cum Vol	Type	Stage Vol	Cum Vol	Rate	Stage Total	Cum Total
P																								
A																								
P																								
A																								
P																								
A																								
P																								
A																								
P																								
A																								
P																								
A																								
P																								
A																								
P																								
A																								
P																								
A																								
P																								
A																								
P																								
A																								
P																								
A																								
P																								
A																								
P																								
A																								
P = Planned; A = Actual																								

Figure P-89—Treatment schedule/material balance worksheet.

Nomenclature

a = Prats' relative capacity parameter (Ch. 11)

a = Ellipse axis, ft, m (Ch. 19)

a = Viscosity degradation coefficient

A_f = Fracture area, ft^2, m^2

A_l = Cross-sectional area of longitudinal fracture, ft^2, m^2

A_p = Fracture area during pumping, ft^2, m^2

A_t = Cross-sectional area of transverse fracture, ft^2, m^2

Ac = Acid capacity number

b = Ellipse axis, ft, m

b_x = Width of fracture face damage, ft, m

B = Formation volume factor, resbbl/STB, $resft^3/SCF$, $resm^3/m^3$

B_o = Oil formation volume factor, resbbl/STB, $resm^3/m^3$

B_g = Gas formation volume factor, $resft^3/SCF$, $resm^3/m^3$

c = Compressibility, psi^{-1}, bar^{-1}

c_f = Compressibility of fissures, psi^{-1}, bar^{-1} (Ch. 1)

c_f = Concentration of proppant in fracture, ppg, kg/m^3 (Ch. 8)

c_f = Fracture compliance

c_o = Compressibility of oil, psi^{-1}, bar^{-1}

c_p = Compressibility of rock, psi^{-1}, bar^{-1}

c_p = Proppant concentration, ppg, kg/m^3 (Ch. 8)

c_p = Heat capacity, BTU/lb, J/kg (Ch. 3)

c_p = Average proppant concentration, ppg, kg/m^3

c_p = Slurry concentration, ppga, kg/m^3

c_t = Total compressibility, psi^{-1}, bar^{-1}

c_w = Compressibility of water, psi^{-1}, bar^{-1}

C = Wellbore storage, bbl/psi, m^3/bar

C = Chemical concentration, mole/lit (Ch. 13 and Ch. 18)

C_c = Compressibility control leakoff coefficient, $ft/min^{1/2}$, $m/s^{1/2}$

C_D = Dimensionless wellbore storage constant

C_{Df} = Fracture storage coefficient

C_{div} = Diverter concentration, lb/gal, kg/m^3

C_L = Leakoff coefficient, $ft/min^{1/2}$, $m/s^{1/2}$

C_p = Proppant concentration per fracture area, lb/ft^2, kg/m^2

C_v = Viscosity control leakoff coefficient, $ft/min^{1/2}$, $m/s^{1/2}$

C_w = Fluid loss coefficient through wall filter cake, $ft/min^{1/2}$, $m/s^{1/2}$

d = Diameter, in., m

d_p = Proppant diameter, in., m

d_{tbg} = Tubing diameter, ft, m

D = Molecular diffusion constant, cm^2/s (Ch. 13)

D_{eff} = Effective acid diffusion coefficient, ft^2/s, m^2/s

E = Young's Modulus, psi, bar

E' = Plane-strain modulus, psi, bar

f = Fanning friction factor

f_g = Geometric factor for fracture shape

F_{CD} = Dimensionless fracture conductivity

g = Acceleration of gravity, ft/s^2, m/s^2

g_f = Fracturing gradient, psi/ft, Pa/m

G = Elastic shear modulus, psi, bar

G_p = Gas cumulative production, SCF, m^3

h = Reservoir thickness, ft, m

h_d = Downward fracture height, ft, m

h_f = Fracture height, ft, m

h_p = Permeable (net) height, ft, m

h_u = Upward fracture height, ft, m

H = Tubing vertical depth, ft, m

k = Permeability, md

k_f = Fracture permeability, md

k_H = Horizontal permeability, md (Ch. 19)

k_s = Damaged permeability, md

k_v = Vertical permeability, md (Ch. 19)

K = Bulk modulus, psi

K' = Consistency coefficient in power law fluids, lbf-$sec^{n'}/ft^2$

K_{IC} = Critical stress intensity factor, $psi/in.^{1/2}$, $bar/m^{1/2}$

l_p = Perforation channel length, ft, m

L = Tubing length, ft, m

L = Horizontal well length, ft, m

m = Slope on semilogarithmic straight line, psi/cycle (oil), psi^2/cycle (gas), or psi^2/cp/cycle (gas)

M_p = Mass of proppant, lb, kg

n = Number of moles (Ch. 1)

n' = Power law exponent

N_p = Oil cumulative production, bbl, m^3

N_{Pe} = Peclet number

N_{perf} = Number of perforations

N_{Re} = Reynolds number

N_{Re} = Reynolds number, dimensionless

p = pressure, psi, bar

p = Average reservoir pressure, psi, bar

p_b = Bubblepoint pressure, psi, bar (Ch. 8)

p_D = Dimensionless pressure

p_e = Constant outer reservoir pressure, psi, bar

p_h = Hydrostatic pressure head, psi, Pa

p_i = Initial reservoir pressure, psi, bar

p_{iw} = Bottomhole injection pressure, psi, bar

p_{sc} = Standard pressure, psi, bar

p_{wf} = Bottomhole flowing pressure, psi, bar

p_{1hr} = Pressure on extension of semilogarithmic straight line at t = 1 hr

PI = Productivity index, bbl/d/psi, MSCF/d/psi, m^3/d/bar

q = Flow rate, STB/d (oil), MSCF/d (gas), m^3/d

q_b = Flow rate above bubblepoint, bbl/d, m^3/d

q_i = Injection rate, bbl/d, BPM, m^3/d, m^3/s

q_{imax} = Maximum injection rate, BPM, m^3/s

q_{ing} = Injection rate, MMSCF/d, m^3/s

Q_D = Dimensionless cumulative production

r_b = Acid bank radius, ft, m

r_e = Reservoir radius, ft, m

r_{eH} = Drainage radius, ft, m

r_p = Ratio of permeability to fracture height

r_{perf} = Perforation radius, in., m

r_w = Well radius, ft, m

r'_w = Effective well radius, ft, m

r'_{wD} = Dimensionless effective well radius

R_{cake} = Diverter cake resistance (Eq. 15-1)

RL = Rod load, lbf, Nt

s = Skin effect, dimensionless

$s_{c+\theta}$ = Skin due to partial penetration and slant

s_{cake} = Temporary skin due to diverter cake

s_{fs} = Fracture face skin effect, dimensionless

s_p = Skin due to perforations

S_g = Gas saturation, fraction

S_o = Oil saturation, fraction

S_w = Water saturation, fraction

t = Time, hr

t_D = Dimensionless time

t_{Dxf} = Dimensionless fracture time

$t_{e.w.b.}$ = Time to end of wellbore storage effects, hr, s

t_i = Injection time, hr

t_p = Producing time, hr (Ch. 1)

t_p = Pumping time, hr

t_{pad} = Time for pad injection, hr

T = Absolute temperature, °R, °K

T_{sc} = Standard temperature

u = Velocity, ft/s, cm/s

u_t = Terminal settling velocity, ft/s, m/s (Ch. 5)

u_s = Slurry velocity, ft/s, m/s

v_p = Proppant specific volume, dimensionless

v_t = Total specific volume, dimensionless

V = Volume, ft^3, m^3

V_i = Total volume of fluid injected, bbl, gal, m^3

V_{Lp} = Leaked off volume during pumping, bbl, m^3

V_{Ls} = Leaked off volume during shut-in, bbl, m^3

V_p = Pore volume, ft^3, m^3

V_w = Well volume, bbl, m^3

w = Fracture width, in., ft, m

w = Average fracture width, in., ft, m

w_p = Propped fracture width, ft, m

x_f = Fracture length, ft, m

x_{fa} = Acid fracture length, ft, m

y = Linear distance, ft, m

Z = Gas deviation factor, dimensionless

Z_{sc} = Gas deviation factor at standard conditions

Symbols

α = Poroelastic constant (Ch. 2)

α_g = Gas specific gravity (to air)

β = Permeability anisotropy ratio, $\sqrt{k_H/k_v}$

γ = Euler's constant (Ch. 1)

γ = Shear strain (Ch. 2)

γ = Surface energy, BTU/ft^2, J/m^2 (Ch. 3)

γ = Fracture shape factor (Ch. 8)

γ = Specific gravity (Ch. 9)

γ = Shear rate, s^{-1}

γ_g = Gas specific gravity (to air)

Γ = Fracture shape factors (Ch. 3)

Δp = Pressure difference, psi

Δp_f = Excess fracture pressure, psi, bar (Ch. 8)

Δt = Time difference, hr

ε = Longitudinal strain

η = Coefficient of internal friction (Ch. 2)

η = Fluid efficiency

θ = Angle

μ = Viscosity, cp

μ_d = Apparent viscosity, cp

ρ = Density, lb/ft^3, g/cc

ρ_A = Diverter cake mass per unit sandface area, lb/ft^2, kg/m^2

ρ_p = Proppant density, lb/ft^3, g/cc

ρ_{prop} = Proppant density, lb/ft^3, kg/m^3

σ = Stress, psi, bar

σ' = Effective stress, psi, bar

σ_c = Critical load, psi, Nt

$\sigma_{H,max}$ = Maximum horizontal stress, psi, bar

$\sigma_{H,min}$ = Minimum horizontal stress, psi, bar

σ_v = Vertical stress, psi, bar

τ = Shear stress, psi, bar

τ_w = Wall shear stress, lb/ft^2, kP_a, bar

ϕ = Porosity, fraction

ϕ_p = Proppant pack porosity, fraction

This Page Intentionally Left Blank

Errata

A Practical Companion to Reservoir Stimulation

Page	*Error*
A-12	In Table A-7, μ should be 0.7 instead of 0.8.
B-7	In Table B-2, σ_c should be 5300 psi instead of 5900 psi.
C-5	The last sentence of the first paragraph should read, "Use the data for the *gas* well only."
C-6	The result of Eq. C-20 should be 38.1 ft/sec instead of 3.81 ft/sec.
F-6	Replace Eq. F-28 with the following:

$$k_f w = \left[\frac{(44.1)(375)(1.1)(1.2)}{(53)(249)}\right]^2 \left[\frac{1}{(0.12)(1.2)(9\times 10^{-6})(2)}\right]^{0.5}$$
$$= 1700 \text{ md-ft.}$$

Replace Eq. F-29 with the following:

$$F_{CD} = \frac{1700}{(2)(700)} = 1.2$$

This Page Intentionally Left Blank